The Effect of Topography on Thermohaline Adjustment

Thesis submitted in accordance with the requirements of
the University of Liverpool for the degree of Doctor in Philosophy
by
Eleanor Anne O'Rourke

March 2009

Abstract

The signals of high-latitude forcing in the North Atlantic can be communicated to the rest of the ocean basin in two ways: the advective route proposed by Marotzke and Klinger (2000); or a much more rapid coastal trapped wave response, as suggested by Johnson and Marshall (2002), in the form of baroclinic Kelvin waves. The Johnson and Marshall (2002) study has important implications for the rapid climate change question; however, their reduced-gravity, vertical sidewalls model did not address the effect of topography or allow for the barotropic mode. Therefore this thesis aims to determine which of the advective or coastal trapped responses is the main rate-setting adjustment process, and then to address the effect of including topography on the coastal trapped response, and subsequent adjustment pattern of the Atlantic Ocean.

Detailed wave mode calculations allowed us to identify three main wave modes: a very fast mode 0 deep ocean or double Kelvin wave propagates around the basin within days, initiating westwards propagating barotropic Rossby waves from the eastern boundary and, thus, provides a very fast full ocean response; a fast coastal Kelvin wave-like mode 1; and a slower slope-trapped mode 2 wave. The effect of stratification, in speeding up the waves, was dominated by the effect of a decreasing f parameter, which slows the mode 1 and mode 2 waves as they approach the equator.

Idealised modelling using the MIT General Circulation Model revealed that the most important effect of topography was to (i) alter wave speeds and (ii) alter the pattern of flow and sea level in the western boundary region of the North Atlantic, with coastal sea level changing quite markedly between the various cases. A JEBAR theory of barotropic adjustment explained the basic mechanism for the response to forcing; rapid propagation away from the forcing region was only apparent when forcing occurred over a slope region.

We conclude that the coastal trapped response is clearly the most important adjustment process in response to high-latitude forcing. The fundamental dynamical rapid response of Johnson and Marshall (2002) remains largely valid for a topographic ocean. However, the inclusion of topography results in a number of wave modes being supported which travel considerably faster than the baroclinic Kelvin wave leading to an even more rapid

response along the western boundary, although it is not clear whether propagation as far as the eastern boundary will also be enhanced.

Additionally, the location of the forcing region, the form of the topography and frictional influences have a significant impact on the sea level at the western boundary. This may have implications for the use of western boundary sea level as a proxy for strength of the Meridional Overturning Circulation.

Contents

Acknowledgement

I would like to firstly thank my supervisors Prof. Chris Hughes of the Proudman Oceanographic Laboratory and Prof. Ric Williams of the Department of Earth and Ocean Sciences at the University of Liverpool. Chris had endless patience in helping me understand the problem I was addressing and was never without ideas and enthusiasm for the project. Ric always managed to boost my confidence when I really needed it and provided expert guidance throughout the writing process.

For his many hours helping me set up the MITgcm and numerous Grads and Fortran queries, I would like to thank Dr Vassil Roussenov, also of the Department of Earth and Ocean Sciences at the University of Liverpool. Many other people within the Proudman Oceanographic Laboratory also deserve my thanks for their help and support during my time there.

I do not think I could have made it to submission without a number of people who I wish to mention: Mark for hours of chatting, gossiping, dancing until the cleaners came and cooking me offal; Rob for making a disproportionate amount of tea, endless Matlab help and putting up with me complaining about the cold and; Craig, Dave and Rich who all managed to brighten my day whenever I saw them.

This Ph.D. was funded by the Natural Environment Research Council studentship no. NER/S/S/2005/13793. An additional three month Parliamentary Fellowship at the Parliamentary Office for Science and Technology was also funded by NERC.

Chapter 1

Theoretical Review

1.1 Introduction

The question of rapid climate change in the ocean due to the effects of a changing climate prompted the UK Natural Environment Research Council (NERC) to launch the £20 million six-year RAPID Climate Change programme. The aims of the programme were to investigate and understand the causes of rapid climate change with a focus on the Atlantic Thermohaline Circulation (THC).

How we are able to detect changes to the driving forces of the Atlantic THC is vital to addressing the question. This thesis examines how topography affects the response of the ocean to such a change in forcing. This chapter starts with a description of the Thermohaline Circulation (Section 1.2) and potential signals of a change (Section 1.3) which include a coastal trapped wave response. The theoretical background of coastal trapped waves will then be outlined (Section 1.4) followed by an evaluation of their forcing effects (Section 1.5) and boundary conditions (Section 1.6). Section 1.7 will then provide a summary of the key points of the chapter before the aims of the thesis are outlined in Section 1.8.

1.2 The Thermohaline Circulation

The THC is the conveyor belt of warm and cold currents within the ocean which is effectively driven by the high-latitude cooling in the North Atlantic (Fig 1.1). The deep outflow of the North Atlantic Deep Water (NADW) is matched by a warm northward surface flow which transports heat into the North Atlantic where it is released into the atmosphere, intensifying the jet stream, and moderating the climate of northwestern Europe (Vellinga and Wood, 2002).

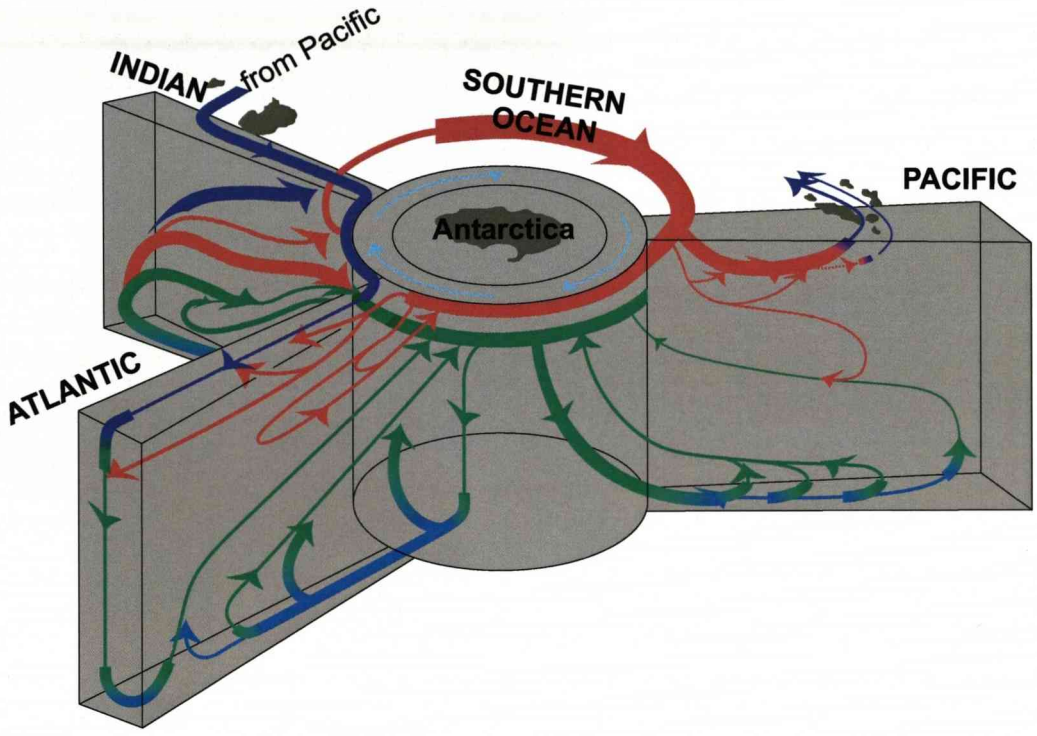

Figure 1.1: A three dimensional diagram of the global Thermohaline Circulation (Schmitz, 1996) showing the deep water formation in the North Atlantic that is not observed in the other ocean basins.

There is no deep water convection in the Pacific as it has much greater freshwater input in comparison to evaporation from the surface. This is due to the tropical Trade winds dumping moisture from the Atlantic Ocean into the Pacific. The resulting cooler sea surface temperatures reduces the overlying atmosphere's ability to hold moisture therefore reducing the evaporation rates and salinity of the ocean (Rahmstorf, 1995). In the North Atlantic the freshwater input is almost matched by the evaporation rates, which are heightened by the warmed atmosphere. As a result the Atlantic is significantly more saline driving an enhanced deep water convection.

1.2.1 Predictions for the future THC

C^{14} and $\partial^{18}O$ studies including Broecker (1995) and Keigwin et al. (1991) have argued that a weakened or shut-down THC may have been responsible for cold periods throughout history, including the 1200 year Younger Dryas cold period (Broecker, 1998), and therefore it is possible such events could occur again. Concern has been heightened as to whether anthropogenically induced global warming may force the THC into an altered state or, indeed, a complete shut down.

It is, however, a very complicated system with a large number of positive and negative feedbacks to any forcing, either by heat or freshwater forcing. Schiller et al. (1997) found that a reduction in the Atlantic overturning results in longer residence times of surface water at high latitudes. The resulting accumulation of precipitation and run off lead to a more stably stratified North Atlantic. This is further amplified by an enhanced northward atmospheric water vapour transport increasing the freshwater input. The reduced northward oceanic heat transport leads to colder sea surface temperatures and intensification of the atmospheric cyclonic circulation over the Norwegian Sea. The associated Ekman transports then cause increased upwelling and increased freshwater export within the East Greenland current. The wind stress feedback seen here acts to destabilise modes without deep water formation in the North Atlantic suggesting the conveyor belt type THC is much more stable than previously thought.

Model predictions vary from no change at all to the system (Gent, 2001) to a total conveyor shut-down for CO_2 quadrupling (Manabe and Stouffer, 1993); however, it should be noted that very different forcing scenarios were used in these two model studies. In all models the THC weakening is affected to a greater extent by changes in surface heat flux than changes in the surface water flux (Gregory et al., 2005).

The existence of bifurcation points has been indicated by Bigg et al. (2003) and Rahmstorf (1995). Typical threshold values for a complete collapse of the present day THC are in the range $0.1 - 0.4\ Sv$ for anomalous freshwater input into the North Atlantic (Latif et al., 2000). This is a large volume of freshwater input; $0.1\ Sv$ is equivalent to

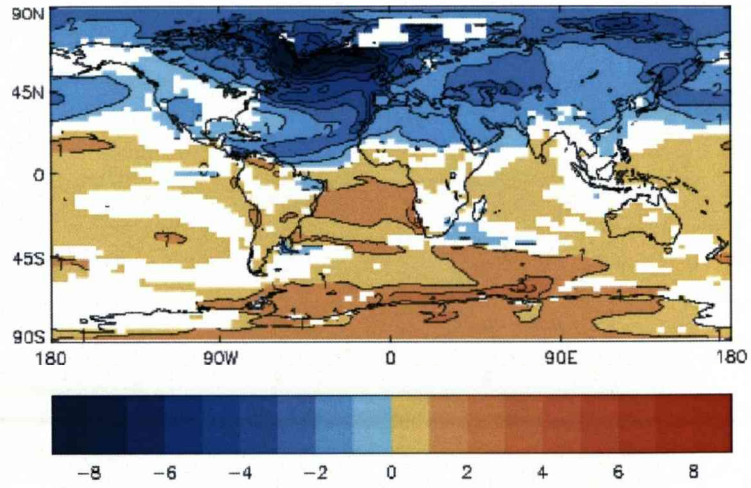

Figure 1.2: Changes in annual temperature 30 years after a THC collapse in comparison to pre-industrial levels (Vellinga and Wood, 2002)

a sea level rise of 8.7 $mmyr^{-1}$, the current rate is around 3.1 $mmyr^{-1}$ from all sources (Bindoff et al., 2007).

Vellinga and Wood (2007) suggest that a large, and possibly complete, THC shutdown in the 21st century cannot be completely ruled out. Studies including Latif et al. (2000) and Schmittner et al. (2000) propose that the relationship between the El Niño Southern Oscillation (ENSO), the Atlantic freshwater budget and the THC should be considered as a potentially important mechanism. Indeed Latif et al. (2000) found that a strengthened ENSO resulting in a -0.2 Sv freshwater change induced an increase in the THC, which balanced the thermally induced THC weakening.

1.2.2 Implications

The implications of such a shutdown would be at the most simple level a dramatic drop in the temperature of the North Atlantic. Vellinga and Wood (2002) found that within 20 years of the shutdown of the THC persistent temperature anomalies, lasting two or more decades, will cover most of the Northern Hemisphere. A maximum cooling of up to $8°C$ over the northwest Atlantic was observed, with Europe experiencing a cooling of 1 to $3°C$ in the third decade after a collapse of the THC (Fig 1.2), compared to pre-industrial temperatures.

A more recent HadCM3 study (Vellinga and Wood, 2007) improved upon their earlier study by taking account of greenhouse gas concentrations at levels according to the IS92a emissions scenario. Here the model simulated a cooling of the Northern hemi-

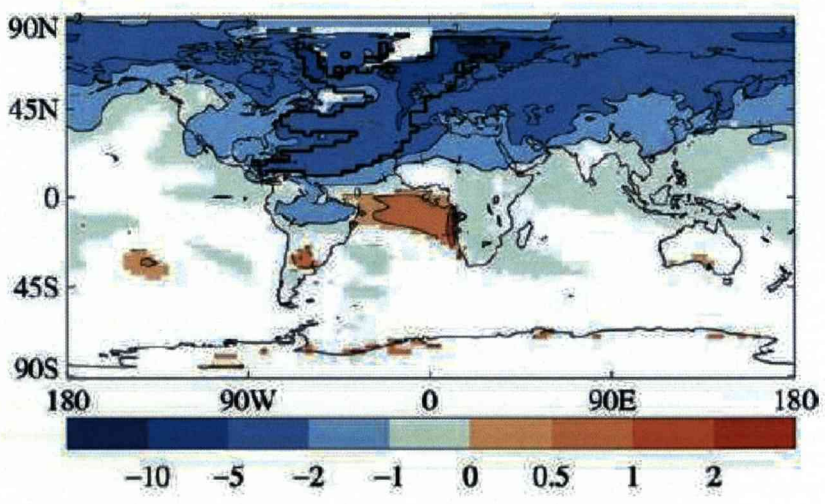

Figure 1.3: Difference in surface air temperature between experiments PG and G in the years 2049 to 2059. This difference is therefore the temperature change that a sudden THC shutdown would cause relative to an IS92a global warming scenario in 2049 to 2059. The area where cooling causes temperature to fall below pre-industrial conditions is outlined by the heavy solid line, areas where the difference is not significant have been masked (Vellinga and Wood, 2007)

sphere of $-1.7°C$, with stronger cooling locally. Over western Europe the cooling was strong enough to return to pre-industrial conditions, with a significant increase in frost and snow cover. The precipitation change induced by a THC shut-down was opposite to that caused by global warming except over western and southern Europe where an exacerbation of summer drying was seen. Sea level change along Atlantic coasts was found to be acting in the same direction as that induced by global warming and to be of the order of 25 cm.

Stocker and Schmittner (1997) concluded that a strong reduction of ventilation would lead to reduced transport of excess carbon and heat into the deep ocean and enhanced warming of the upper layers of the ocean resulting in decreased CO_2 solubility. The resulting increase of atmospheric CO_2 would compound the effects of greenhouse gas warming and would, almost certainly, not be limited to the North Atlantic region.

1.3 Detection of a change to the THC

1.3.1 The signals

Although a slowdown or collapse of the THC is, on the balance of evidence, a low risk event the potential catastrophic effects mean it is important to learn more about the

rate of deep water formation and of the signals that will transport information about any change.

The change in the temperature and salinity of the North Atlantic would eventually be advected; however, this would be on a decadal time scale. Observational studies such as Bryden et al. (2005) have detected a weakening of the Atlantic THC, or Meridional Overturning Circulation (MOC), which is closely related to the THC, over interannual timescales. However, due to poor temporal resolution of measurements the uncertainty of such results remains high. Indeed the seasonal variability has now been found to be as large as the interannual variability (Church, 2007). Furthermore work by Bingham et al. (2007) suggests that a single overturning cell is misleading over decadal timescales; they found variability above $40°N$ had a strong decadal component while to the south the variability was of a higher frequency.

Additionally the freshening seen in the deep Atlantic over the last forty years, such as that south of the Greenland-Scotland ridge (Dickson et al., 2002), is pervaded by an amplified North Atlantic Oscillation (NAO). Whether the phase of the NAO is driven by global change remains unresolved increasing further the uncertainty in hydrographic results.

An alternative signal has been suggested of a coastal trapped wave travelling down the western boundary of the North Atlantic. An altimetric study by Hughes and Meredith (2006) found a coherent signal in sub-surface pressure over long distances along the continental slope. Altimetry does not allow the modal structure of the signal to be examined and local wind driven dynamics can mask the signal meaning it is difficult to determine the propagation speed amongst the background noise.

Bingham and Hughes (2009) found a similar topography-following signal along the east coast of North America in response to MOC variability in the Atlantic which matches the propagation pathway of coastal trapped waves further supporting this theory. Therefore North American sea level, which in turn is closely related to western boundary bottom pressure, could prove a useful indicator of MOC variability. Indeed the model study of Bingham and Hughes (2008) found that for periods of greater than one year 90% of the variability of the main overturning cell at $42°N$ can be recovered using only the western boundary bottom pressure signal, provided the depth-averaged boundary pressure signal is removed. They did warn that this assertion may only be relevant to interannual timescales and at longer timescales may not remain a sound assumption.

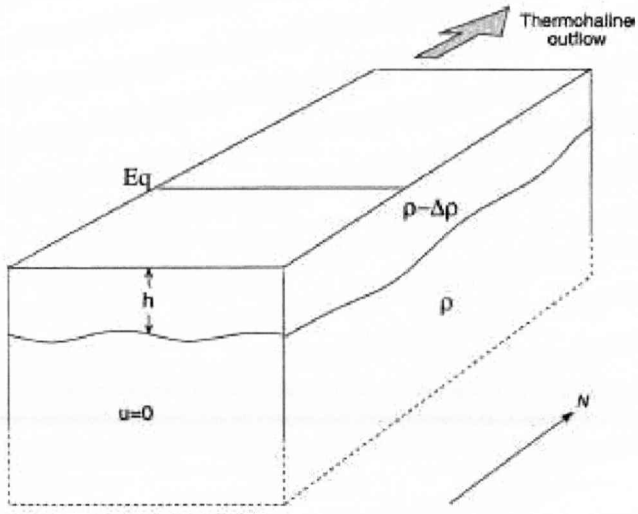

Figure 1.4: Shallow-water model with moving surface layer and infinitely deep, motionless layer. Thermohaline overturning is represented by a prescribed outflow from the surface layer on the northern boundary. Model domain extends from $45°S$ to $65°N$ (JM02)

1.3.2 The findings of Johnson and Marshall (2002)

Johnson and Marshall (2002), hereafter refered to as JM02, found the coastal trapped wave, in the form of a baroclinic Kelvin wave, was the major, and most importantly rapid, adjustment process in their idealised model study. In their problem setup JM02 first suppose that the rate of deep water formation in the North Atlantic is suddenly perturbed. They used a reduced gravity model (Fig 1.4) that represents only the upper, warm limb of the thermohaline circulation. Deep water formation is represented by a prescribed outflow from the surface layer on the northern boundary with the sinking assumed to take place outside of the model domain.

The standard non-linear shallow water equations were discretised on a C grid, with a resolution of 0.25°;

$$\frac{\partial \mathbf{u}}{\partial t} + (f + \zeta)\mathbf{k} \times \mathbf{u} + \nabla B = A\nabla^2 \mathbf{u}$$

$$\frac{\partial h}{\partial t} + (h\mathbf{u}) = 0$$

where

$$\frac{\partial v}{\partial x} - \frac{\partial u}{\partial y} = \zeta$$

with $B = g'h + \frac{(u^2+v^2)}{2}$, ζ representing vorticity and A representing the lateral friction coefficient.

Propagation pathway

A thermohaline outflow of 10 Sv at time $t = 0$ was turned on in the north west corner of the domain. An initial Kelvin wave signal on the western boundary reaches the Tropics in a timescale of around one month (Fig 1.5). Mass continuity therefore leads to a meridional velocity in the surface layers of the ocean on the western boundary in geostrophic balance with an anomaly in pressure, which then propagates southward along the western boundary as a Kelvin wave at a speed, c_g, of order 1 ms^{-1}.

$$\mathbf{u} = \frac{1}{\rho f}\mathbf{k} \times \nabla p$$

where $\mathbf{u}$ is the velocity, ρ is the density, $f = 2\Omega sin\phi$ is the Coriolis parameter, p is the pressure and $\mathbf{k}$ is the unit vertical vector. This is essentially the surface equivalent of the response shown for the deep ocean shown by Kawase (1987).

As latitude decreases, a smaller pressure gradient is required to support a given transport anomaly and the pressure anomaly reduces in amplitude and is small at the equator. This small signal is then transmitted across the domain by equatorial Kelvin waves. The meridional pressure gradient cannot be maintained along the eastern boundary as to balance it a Coriolis force would require a velocity across the coastline, and all other terms in the momentum equation are small. The eastern boundary signal is prevented from re-amplifying by the radiation of westward-propagating Rossby waves.

On a C grid the Kelvin wave speed is unaffected by spatial resolution although the wave structure and damping are altered (Hsieh et al., 1983).

The JM02 model results indicate that the Kelvin wave signal would be a very useful and most importantly, rapid indication of a change in deep water formation. However, it should be noted that their model;

1. neglects wind driven dynamics - they found their results were unaffected by the presence of mean wind driven gyres.

2. sets diapycnal upwelling to zero - this was to avoid the debate concerning the location of the upwelling required to balance the deep water formation at high latitudes and is seen as reasonable as the Atlantic only represents a small fraction of the global ocean.

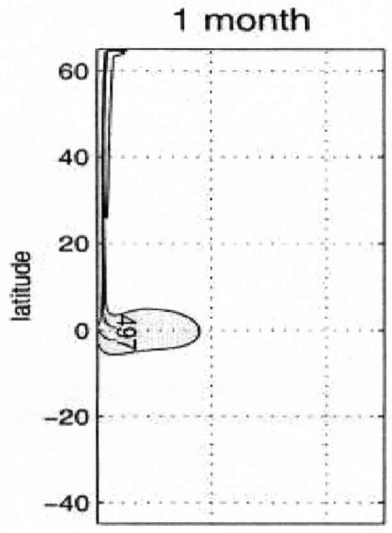

Figure 1.5: Surface layer thickness after a thermohaline overturning of 10 Sv has been turned on at time t=0 in the northwest corner of an ocean initially at rest (JM02)

3. is an idealised sector ocean 40° wide, stretching from 45°S to 65°N with vertical sidewalls and no bottom topography.

If the conclusions reached in JM02 remain true for the topographic and stratification conditions of the realistic ocean this would have important consequences for the rapid climate change and as such further investigation is certainly merited.

1.3.3 Studies in accord with JM02

We shall now review a number of other studies whose results support the JM02 theory. Kawase (1987) and the follow up by Cane (1989), looked at the spinup of the deep ocean using a linear, one-and-a-half layer model representing the thermocline and the deep layers. They concluded that the flow was first set up by a Kelvin wave along the western boundary on time-scales of less than a year. Yang (1999) later showed the time lag between the Labrador Sea Water and the tropical SST was primarily set up by coastal trapped waves indicating a similar response in the surface ocean on comparable time-scales.

Wajsowicz and Gill (1986) examined the spin up of the ocean under buoyancy forces (neglecting wind stress which is unrealistic but beneficial in determining the effects of buoyancy forcing). They found the main adjustment in the first few months, due to the density gradient representative of that observed in the North Atlantic, was by coastal

Kelvin waves with the first baroclinic mode containing most of the energy. Due to the compromises required to run the ocean General Circulation Model (GCM) in question they warn that the wave speed of the coastal Kelvin wave is greatly reduced and the attenuation rate greatly enhanced. In Wajsowicz (1986), the follow up to Wajsowicz and Gill (1986), the third stage of the adjustment shows that the first baroclinic mode Kelvin wave propagation no longer plays a significant role in the adjustment as the initial longshore gradient in the middle levels have been wiped out.

Roussenov et al. (2008) used an isopycnic model and found very similar results to JM02 despite the inclusion of wind driven circulation, background overturning and realistic topography. Topography was seen to have an effect, however, with rougher topography attenuating the wave communication. Rapid adjustment was also detected in the southern hemisphere suggesting that there may also be a role for the barotropic mode in the Atlantic adjustment process. It was therefore vital for further work to consider not just the impact of a more realistic ocean, in terms of topography and stratification, on the adjustment pattern but also the influence of the barotropic mode. Indeed Anderson and Killworth (1977) found that the dominant frequencies observed in the spin up of a baroclinic ocean are almost exactly the same as those of the purely barotropic basin modes.

The barotropic response to any forcing is rapid with the main adjustment taking place within days. Anderson et al. (1979) found that the introduction of stratification allows for a much slower baroclinic response and also for a slower barotropic response. The barotropic mode will respond to topography on its own rapid time scale but will also change on the longer time scale of the baroclinic mode. In this experiment, the baroclinic mode responds only on its own time scale. Anderson et al. (1979) concluded that the interaction of the baroclinic field with topography has an important effect on the barotropic mode resulting in the barotropic mode having a slow adjustment on the baroclinic time scale. This means that the barotropic mode becomes established with a flow comparable to that of a homogenous ocean with topography but then, over some years, this alters as the baroclinic mode becomes increasingly established and becomes more like the flow seen in a flat-bottomed ocean.

The Anderson and Killworth (1977) study of the spin-up of stratified flow found that the effects of topography were largely felt by the barotropic mode and it was only when the topography approached the interface, or as the gradient increased, that the effects on the baroclinic modes became evident. The long term effect of stratification was to filter out the effects of topography as a motionless bottom layer acts as a buffer between the flow and topography. This is due to the baroclinic Rossby waves carrying information about the eastern boundary condition to the interior, and so cutting off the flow in unforced layers.

In JM02 we saw that the inverse relationship of amplitude to f seen on the western boundary does not exist on the eastern side of the domain due to the westwards propagation of Rossby waves. These westwards propagating Rossby waves then set up the longer scale adjustment process. Any waves travelling from the western boundary with eastward group velocity are much shorter and slower and as a result most of the ocean is modified by the westward propagating Rossby waves only (Davey, 1983).

The behaviour of the anomaly as it reaches the eastern boundary is dependent on its frequency; for an incident wave of a fixed frequency a critical latitude, at which $f = f_c$, exists such that when f is less than f_c the result is offshore propagating Rossby waves whereas for $|f|$ is greater than f_c the waves are coastally trapped (Grimshaw and Allen, 1988). The critical latitude is a function of f and the angle of the coastline. Allen and Romea (1980) found that coastal trapped baroclinic waves will transform into barotropic shelf waves at f values close to f_c and then continue to propagate polewards.

Therefore the degree of offshore propagation is likely to alter as we move from a vertical sidewalls basin, as in JM02, to one with topography. Calculation of the wave modes supported by a sloping boundary (Chapter 2) will help us to predict the likely behaviour along a sloping eastern boundary which can then be tested in an idealised ocean model (Chapter 4).

1.3.4 Contradictions to JM02

Although the JM02 theory of rapid adjustment by coastal trapped waves is supported by a number of studies, as outlined in the previous section, some contradictory studies do exist.

Marotzke and Klinger (2000) used a two hemisphere, single basin, idealised GCM driven only by buoyancy forcing and found that the adjustment takes place via a propagating signal that travels along the same Kelvin wave pathway as JM02. However, the timescale of evolution of this model is not consistent with the propagation speed of Kelvin waves, at around 30 years for the signal to reach the Tropics (Fig 1.6). Other GCM studies, such as McDermott (1996) and Suginohara and Fukasawa (1988), also identify Kelvin waves during the spin up of the thermohaline circulation with adjustment taking place over a timescale of decades to centuries again disagreeing with the JM02 and Kawase (1987) results for a rapid initial adjustment.

The Marotzke and Klinger (2000) model was run at a coarse resolution on a B grid which slows the Kelvin wave speed considerably but the numerical effects of this coarse resolution cannot account for the difference seen in the results. They repeated the spin-up using asynchronous integration which would be expected to slow the Kelvin waves

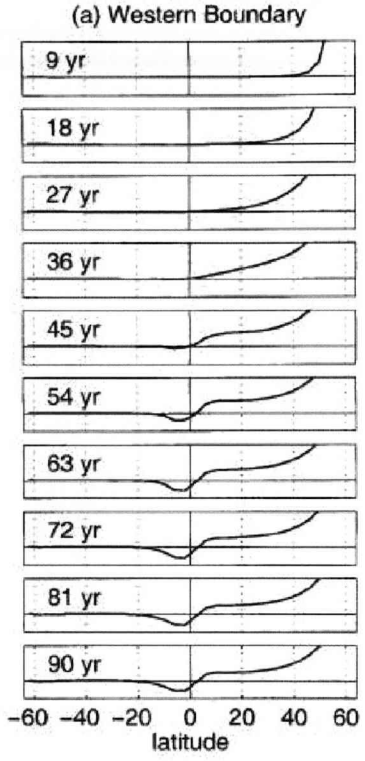

Figure 1.6: Spin up of the ocean in Marotzke and Klinger (2000) showing the 30 year propagation speed of their signal, represented by the vertically-integrated vertical velocity, which is incompatible with theoretical Kelvin wave propagation speeds.

by a factor of eight. However, the results were largely indistinguishable leading them to conclude that Kelvin waves were not the rate-setting adjustment process involved in their experiment.

They also suggest that the convective mixing used by Kawase (1987) and the deep downwelling used by themselves are fundamentally different processes and therefore can quite plausibly lead to very different dynamical responses. JM02 were unable to resolve the issue of these differences.

1.4 Coastal trapped waves: Theory and Model Studies

The vertical sidewalls topography of the JM02 model basin only allowed for a single coastal trapped wave mode, the baroclinic Kelvin wave. We will now consider the effects of including sloping topography, which will support a number of wave modes. This section examines the theory and properties of these coastal trapped waves and reviews a number of observational and modelling studies.

Coastal trapped waves (CTW) describe three types of wave; the edge wave, the Kelvin wave and the shelf wave, which is a form of the topographic Rossby wave (Fig 1.7). Edge waves can be thought of as long gravity waves over a sloping beach that are trapped by refraction. Unlike edge waves, Kelvin waves and shelf waves depend crucially upon the Earth's rotation (Mysak, 1980).

Shelf waves also differ fundamentally from edge waves as;

1. The decay of shelf wave amplitude occurs in the deep sea region.
2. In a specified hemisphere, the waves can travel in only one direction (the same is true of Kelvin waves).
3. The long waves are non-dispersive and have a very low frequency, considerably less than the Coriolis parameter (Mysak, 1967).

Continental shelf waves are a subset of topographic Rossby waves when there is no stratification present (Fig 1.7).

When looking at CTW it is useful to start with the most basic model ocean; a flat bottomed ocean with a vertical wall. Only one barotropic mode is compatible with the condition of no normal motion across a straight boundary, the Kelvin wave.

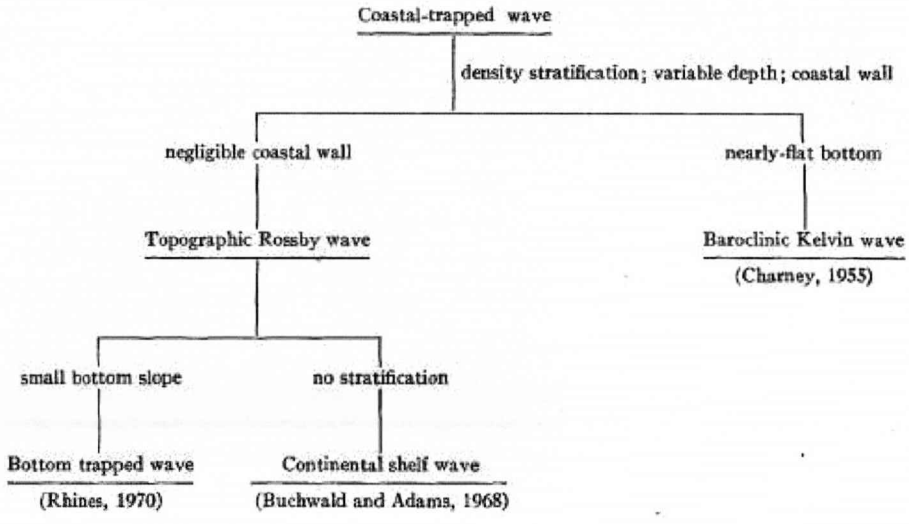

Figure 1.7: Classification of coastal trapped waves (Wang and Mooers, 1976)

1.4.1 The Kelvin wave

Barotropic Kelvin wave

Variation with x is exponential so if u vanishes on one line x =constant (boundary), it must vanish for other values of x as well. Hence the barotropic Kelvin wave solution can be found by putting $u = 0$ in the equations;

$$\frac{\partial v}{\partial t} = -g\frac{\partial \eta}{\partial y}$$

$$\frac{\partial \eta}{\partial t} + H\frac{\partial v}{\partial y} = 0$$

which determine η, the sea level, and v variations on any line x =constant and contains no Coriolis terms, that is identical to equations for non-rotating shallow water motion when $u = 0$. H is the constant ocean depth.

The complete Kelvin wave solution (Gill, 1982) is;

$$\eta = \eta_0 e^{\frac{-x}{R_0}} \cos(ly + \omega t)$$

$$v = -(\frac{g}{H})^{\frac{1}{2}} \eta_0 e^{\frac{-x}{R_0}} \cos(ly + \omega t)$$

where the dispersion relation between ω, the wave frequency, and l, the wavenumber, is $\omega = lc$. Kelvin waves are fundamentally maintained by an exact balance between

the Coriolis force and a pressure gradient normal to the wall (Mysak, 1980) and are non-dispersive.

In its simplest form, in water of uniform depth against a straight coast, the barotropic Kelvin wave progresses with the speed of long gravity waves, decaying seawards exponentially (Huthnance, 1975). In the barotropic ocean they travel at a phase speed of $c = (gH)^{\frac{1}{2}}$ where H is the total depth (Miles, 1972). For any one mode, the decay scale is the Rossby radius of deformation, $R_0 = \frac{(gH)^{\frac{1}{2}}}{f}$ (LeBlond and Mysak, 1978). Kelvin waves are right bounded in the Northern Hemisphere so travel southward on the western boundary and northward on the eastern boundary.

The wave speed of a barotropic Kelvin wave is equal to $\sqrt{gH}$ where H is the total water depth. For example in an ocean where $H = 3000\ m$ we would expect a deep ocean barotropic Kelvin wave to travel at 171.55 ms^{-1}. Over a shelf of 100 m depth we would find a coastal barotropic Kelvin wave with a propagating speed of 31.32 ms^{-1}.

Baroclinic Kelvin wave

Where stratification exists the baroclinic Kelvin wave is present and travels at $c = (g'H_e)^{\frac{1}{2}}$ where, for a two-layer case, g' is the reduced gravity given by;

$$g' = \frac{g(\rho_2 - \rho_1)}{\rho}$$

and H_e is the equivalent depth defined as;

$$H_e = \frac{(h_1.h_2)}{(h_1 + h_2)}$$

As $g' << g$ then the wave speeds are considerably slower for the baroclinic mode than the barotropic mode (Gill, 1982). For example in a two-layer ocean with a top layer of 1000 m and a deep layer of 2000 m a propagation speed of 3.48 ms^{-1} is calculated for the baroclinic Kelvin wave where $\frac{(\rho_2 - \rho_1)}{\rho} = 1.85 \times 10^{-3}$ leading to $g' = 0.018\ ms^{-2}$. In a two-layer baroclinic ocean we would expect only one baroclinic Kelvin wave mode travelling along the interface; however, in a continuously stratified ocean multiple wave modes would be found.

The boundary wave seen in JM02 is a pure baroclinic Kelvin wave, however, its structure and behaviour is likely to change once realistic stratification and topography are introduced.

Equatorial Kelvin wave

There also exists an equatorial Kelvin wave which is similar to the coastal Kelvin wave, having the same solution and dispersion relation $\omega = kc$, but is instead trapped within the equatorial zone as a result of the change in sign of f due to latitude. They are also uni-directional, travelling eastwards without dispersion (Gill, 1982) and their speed can be calculated in the same way as the Kelvin waves described above.

Double Kelvin waves

A further subset of the CTW family is the double Kelvin wave (DKW) which has properties which distinguish it from other CSW being sub-inertial but with similar longshelf and cross-shelf scales of variability (Wright and Xu, 2004). They generally occur in areas with a step-like topography.

The DKW mode occurs when the shelf width is wide compared to the local external Rossby radius and at large wavenumbers. Decreasing wavenumber results in a transformation into the first mode Continental Shelf Wave (CSW).

1.4.2 Continental shelf waves

When the effect of a sloping boundary at the coast is included a new form of waves exist even in the absence of stratification, the barotropic CSW. If we consider a simple case (Gill, 1982) where the depth increases exponentially with distance from the coast;

$$h(x) = h_0 e^{2bx}$$

where h_0 is the depth at $x = 0$ and b is the inverse topographic length scale. The dispersion relation is;

$$\omega = \frac{2fkb}{k^2 + m^2 + b^2}$$

where f is the Coriolis parameter, ω is the wave frequency, k is the wavenumber and m is the mode number (full derivation of the CSW dispersion relation may be found in Gill (1982). This dispersion relation is valid when the depth either continues to increase indefinitely, or when the exponential slope is bounded by two vertical walls.

The direction of travel depends on the sign of f and is the same as that of a Kelvin wave assuming depth increases with distance offshore. All studies of continental shelf

waves in the Northern Hemisphere have concluded that they always progress left as viewed from the deep sea (Huthnance, 1975).

The shelf wave's existence is very much related to the conservation of potential vorticity and they are highly rotational (Mysak, 1980). Potential vorticity is given by $\frac{(f+\zeta)}{h}$ and therefore as particles move into shallower water they aquire anticyclonic relative vorticity. Those moving into deeper water aquire cyclonic relative vorticity resulting in the wave moving along with the boundary on it's right (Gill, 1982) in agreement with earlier statements.

The variability these waves introduce in coastal currents is predominantly barotropic and typically have time-scales of the order of several days to a week (Hsueh, 1980).

Buchwald and Adams (1968) found a propagation speed of around 2.8 ms^{-1} for continental shelf waves over an idealised topography comparable to the continental shelf off New South Wales using an analytical solution of the rigid lid, barotropic equations.

1.4.3 Bottom-trapped waves

When stratification is included, and also if the bottom slope is small, another form of wave is possible; bottom-trapped waves. Rhines (1970) results derived from the 'small' slope case shows a tendency for bottom trapping of quasi-geostrophic waves with increasing density stratification (Fig 1.8). With strong stratification the baroclinic mode becomes significant. Furthermore, contributions from the baroclinic and barotropic modes are out of phase in the upper layer and in phase in the lower layer and therefore the quasi-geostrophic waves are bottom trapped (Wang, 1975).

For large stratification, Huthnance (1978) noted that the nodal lines became almost horizontal, corresponding to the inhibition of vertical motion and almost vertical wavenumber imposed on internal waves (Fig 1.8). Thus, the sloping sea floor is then seen approximately as a side wall such that the trapped modes approximate internal Kelvin waves which are trapped in the same sense.

Huthnance (1978) also concluded that the large longshore wavenumber modes took the form of Rhines (1970) waves. Wang and Mooers (1976) found that large wavenumber waves are strongly trapped even under intermediate density due to: the amplitude of the small scale wave motion decaying away from the shelf break and; the small scale wave motion has a smaller offshore length scale and thus, it is subject to a relatively stronger bottom trapping for the same baroclinic radius of deformation.

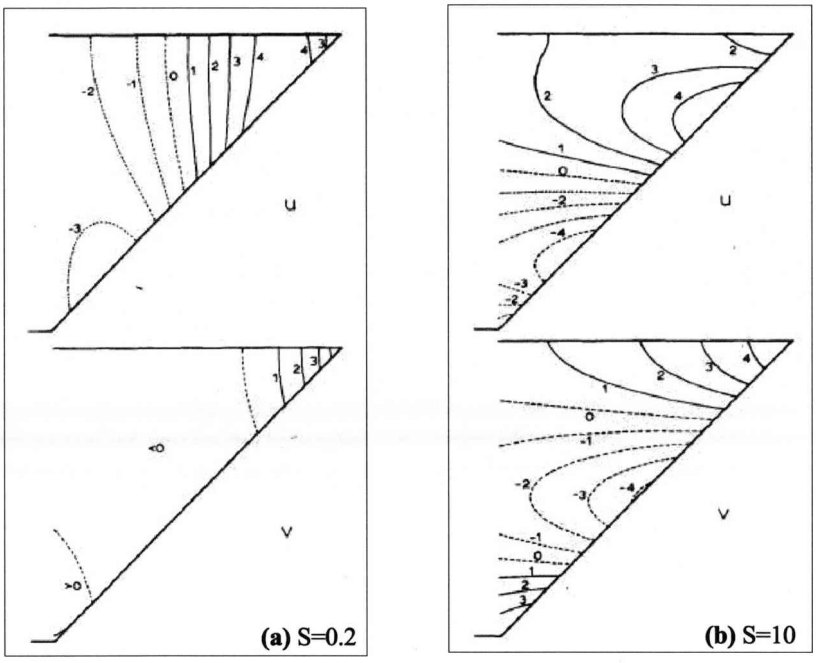

Figure 1.8: Velocity components u and v for a mode 2 wave with stratification parameter of (a) S=0.2 and (b) S=10 from Huthnance (1978).

1.4.4 Hybrid waves

Where a bottom slope is present, and not necessarily small, in a stratified ocean the wave modes cannot be easily broken down into the strict classifications above. In these conditions hybrid coastal trapped waves are found and these waves have been the subject of many model studies.

Mysak (1967) included a two layer density structure into his model, but with only the upper layer extending over the shelf, and found internal Kelvin waves against the vertical continental slope and continental shelf wave modes with phase speeds greater than in a homogenous ocean. Gill and Clarke (1974) found similar results using a comparable model set up.

Two layer models were also utilised by Kaijura (1974), Wang (1975) and Allen (1975), however, their models included both layers extending over the shelf (Fig 1.9) allowing for baroclinic modes in this region. Kaijura (1974) found four wave modes:

1. One with the largest phase velocity approximated to the barotropic shelf wave mode.

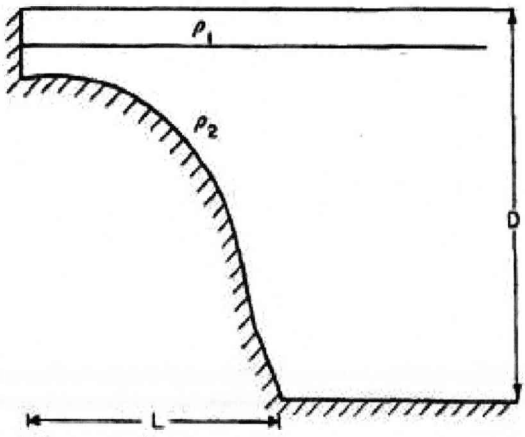

Figure 1.9: Two layer density structure model with both layers extending over the shelf (Wang, 1975)

2. The barotropic shelf wave mode is then modified by the baroclinic motions significantly.

3. The two remaining modes are dominated by baroclinic motions with significant contributions from barotropic motions.

The existence of rapid variation of depth at the shelf break is considered to be an essential factor causing the coupling of the barotropic and baroclinic motions only seen at the shelf break. Anderson and Killworth (1977) found there was indeed interaction between the barotropic and baroclinic modes in regions of non-zero topography caused by bottom pressure torques being exerted on the fluid columns in a stratified ocean.

Where shelf width is comparable to the internal Rossby radius of deformation, resonant coupling between the first mode quasi-geostrophic wave and the non-geostrophic Kelvin wave is significant (Wang, 1975). With both stratification and depth variations typical of continental shelf and slope regions Allen (1975) found that barotropic shelf waves and baroclinic internal Kelvin waves are coupled. He concluded that the internal Kelvin waves can force barotropic motion which extends over both the shelf and slope and also that the dispersion curves of Kelvin and shelf wave modes exchanged dynamic properties and instead of crossing, instead 'kiss' (Fig 1.10).

Forcing of the barotropic mode by the baroclinic mode in regions of topography due to the barotropic mode 'feeling' the topography to a much greater extent was also found by Anderson (1981).

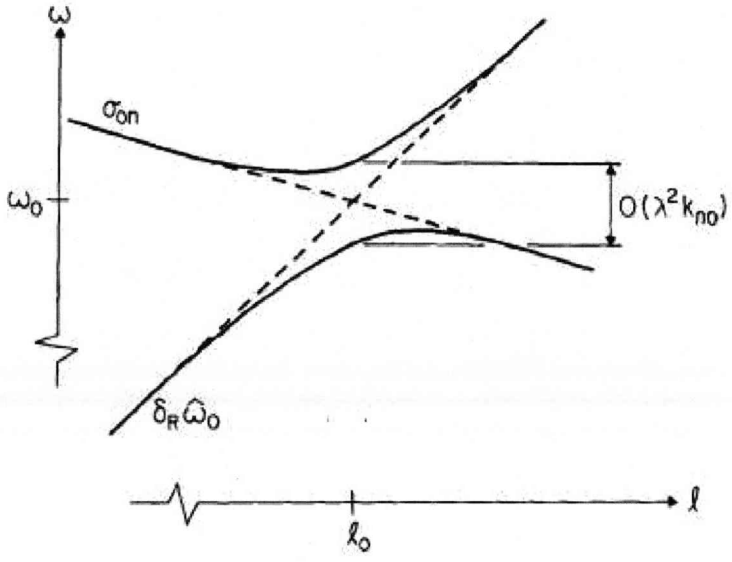

Figure 1.10: Schematic of the dispersion curves of the internal Kelvin and shelf wave modes near the point of apparent intersection (Allen, 1975)

Continuously stratified models such as Wang and Mooers (1976) and Huthnance (1978) are most realistic. The effect of increasing density stratification was found by Wang and Mooers (1976) to extend the influence of the coastal wall and to enhance the effect of bottom trapping. The phase speeds of the two wave modes were similar and the contributions to each wave mode from the competing effects of the coastal wall and bottom slope are comparable. Therefore, they suggest that the classification in terms of either a baroclinic Kelvin wave or a barotropic shelf wave is meaningless and this is shown by their mode 1 wave which is a topographic Rossby wave for small wavenumbers and a baroclinic Kelvin wave for large wavenumbers. Their first shelf profile did not exhibit the 'kissing' modes that appeared in Allen (1975).

Huthnance (1978) found that waves of sub-inertial frequency in a continuously stratified ocean and trapped over a continental shelf and slope form one infinite discrete sequence of modes with frequencies decreasing to zero - the mode frequencies increasing with stratification. In three formal asymptotic limits the waves adopt special forms;

- large longshore wavenumber (Rhines, 1970) bottom trapped waves.
- small stratification - barotropic continental shelf waves.
- large stratification - baroclinic internal Kelvin like waves.

For weak stratification the sloping floor is seen as a varying depth implying potential vorticity changes. In general both topographic and stratified elements of the situation are involved and are characterised by their degree of oscillation along the sloping sea floor. Huthnance (1978) did not find any evidence of the mode coupling phenomena described by Allen (1975) and Wang (1975) suggesting that this phenomenon was essentially due to the two-layer approximation of the basic continuous density profile usually observed in shelf-slope regions (Mysak, 1980).

In terms of propagation speed we could expect these hybrid waves to travel at speeds between that of the CSW, around 3 ms^{-1}, and the coastal Kelvin waves, of the order 30 ms^{-1} dependent on shelf depth, over shelf regions. Their speed will be dependent upon the topographic and stratification conditions present and could vary quite dramatically within the range suggested if such conditions vary considerably, as is possible in the realistic ocean.

1.4.5 Observational studies

As we have seen there have been many model studies carried out on the coastal trapped wave problem from the very idealised to the more realistic, however, can these coastal trapped waves, in their various forms, be observed in the real ocean?

It was Hamon (1962) who detected a time lag between adjusted sea level variations at two different points on the East Australian coast thus discovering the continental shelf wave. Robinson (1964) then followed this with a construction of their theory.

A number of studies looked at the continental shelf of the eastern Pacific and indeed, due to the narrow nature of the slope here, the CTW are detected to a greater extent than in locations elsewhere. When the modelled and observed longshore velocity were compared by Battisti and Hickey (1984) it was shown that, at low frequencies, greater than 80% of variance in the coastal subsurface pressure (SSP) was accounted for by the mode 1 CTW. In his study off the coast of Peru, Brink (1982a) also found that most of the observed sea level and alongshore velocity fluctuations in a 5-10 day period were due to free waves with little input from local winds. Both Clarke (1977) and Martinez and Allen (2004) agreed that the modelled coastal trapped wave theory was able to explain a wide range of coastal trapped, quasi-geostrophic motions.

A further large study, the Australian Coastal Experiment (ACE) was undertaken in the coastal waters of New South Wales (Church et al., 1986a,b; Church and Freeland, 1987; Freeland et al., 1986; McIntosh and Schahinger, 1994). They also agreed that CTW account for a significant percentage of the variance of the alongshore currents over shelf and slope regions. Church et al. (1986a) found the alongshore propagation of

CTW were at a similar phase speeds to theory. However, Freeland et al. (1986) found the observed waves were travelling faster than the theory would suggest but determined this was a consequence of contamination by local wind-forced waves.

A notable discovery of early ACE analysis was that the mode 2 wave carried a greater fraction of the CTW energy than mode 1 (Church et al., 1986a). Hsieh (1982) supported this finding. However, later analysis by McIntosh and Schahinger (1994) found that mode 1 had approximately twice the energy flux of the mode 2 wave. Both studies agreed that the use of the mode 3 wave could not be justified and was statistically insignificant. McIntosh and Schahinger (1994) also determined that mode 1 was not highly correlated with mode 2 suggesting the mechanism for the two modes was less strong than thought previously and there may not even be a common energy source for the two modes.

1.5 Forcing Parameters

1.5.1 Wind Forcing

Although I am largely interested in the buoyancy forcing of boundary waves it is also necessary to determine the effect of the local wind driven dynamics which may dominate the signal. The thermohaline circulation buoyancy forcing cannot be thought of as independent from the wind driven circulation (Wajsowicz and Gill, 1986).

Mysak (1967) proposed that the anomalous behaviour seen in the sea level may be the generation of shelf waves in resonance with pressure variations from Hamon (1966). However, Adams and Buchwald (1969) argued in their paper that the longshore component of the stress of the geostrophic wind can generate sufficient vorticity to explain many of the important features of the observations by Hamon (1966). It may be seen that the zero-divergence assumption leads to an equation in which the forcing terms due to pressure forcing are absent.

The equations of motion and continuity in the linearised, shallow-water wave theory, neglecting bottom friction and internal dissipative forces are;

$$\frac{\partial u}{\partial t} - fv = -g\frac{\partial \eta}{\partial x} + \frac{\tau_x}{h} \tag{1.1}$$

$$\frac{\partial v}{\partial t} + fu = -g\frac{\partial \eta}{\partial y} + \frac{\tau_y}{h} \tag{1.2}$$

$$\frac{\partial(hu)}{\partial x} + \frac{\partial(hv)}{\partial y} + \frac{\partial \eta}{\partial t} = 0 \tag{1.3}$$

considering an infinite straight coastline parallel to the y-axis where η is sea level. Let the depth h be a function of x so that all bottom contours are parallel to the coastline. For time and length scales involved, it is sufficient to assume that f is constant, and that the depth-integrated motion is horizontally non-divergent. Now it is possible to express u and v in terms of the streamfunction, ψ, by;

$$uh = -\frac{\partial \psi}{\partial y}, \; vh = \frac{\partial \psi}{\partial x} \tag{1.4}$$

Differentiating (1.1) with respect to y, (1.2) with respect to x, subtracting and using (1.4) , we obtain;

$$\boldsymbol{\nabla} \cdot (\frac{\boldsymbol{\nabla \psi}}{\boldsymbol{h}})_t + \boldsymbol{J}(\boldsymbol{\psi}, \frac{\boldsymbol{f}}{\boldsymbol{h}}) = \boldsymbol{k} \cdot \boldsymbol{\nabla} \times \left(\frac{\boldsymbol{\tau}}{\boldsymbol{h}}\right) \tag{1.5}$$

where $J(A, B)$ is the Jacobean $\frac{\partial A}{\partial x}\frac{\partial B}{\partial y} - \frac{\partial A}{\partial y}\frac{\partial B}{\partial x}$.

Adams and Buchwald (1969) concluded that because vorticity is a dominant feature of shelf waves, you would not expect pressure fluctuations to be a very efficient way of generating vorticity whereas for barotropic motion the stress of a wind parallel to the shelf is quite an efficient way of generating the necessary vorticity.

As mentioned previously boundary waves on the continental slope are not merely barotropic continental shelf waves or baroclinic Kelvin waves but a hybrid of both. Therefore, although wind forcing could largely account for the barotropic component this cannot adequately explain the wave signal as a whole, just as buoyancy forcing cannot either.

Gill and Schumann (1974) explained that the forcing effect is entirely dependent on the presence of a boundary as if there was no boundary the only effect of the wind would be to produce an Ekman flux in a thin layer near the surface. The deeper layers would not be affected. When the boundary is present, the Ekman surface flux is blocked and displacements of the free surface can be neglected and so continuity requires a flux of water in the deeper layers whose component normal to the coast exactly balances the normal Ekman flux, changing the vorticity, and so generating shelf waves.

Clarke (1977) showed that the linear, wind-forced quasi-geostrophic motion of stratified water over shelf topography can be described as a sum of modes, the amplitude of each of these modes satisfying a forced, first-order wave equation which Gill and Schumann

(1974) presented for the purely barotropic ocean. Clarke (1977) then presented analysis that suggested this forced wave equation can qualitatively explain a wide range of observational and numerical results. In the general case the forced first-order wave equation can be written;

$$\frac{\partial \phi}{\partial t} - c\frac{\partial \phi}{\partial y} = \frac{-bc\tau^y}{\rho_0 H_{mix}} = -\Upsilon c \tag{1.6}$$

where ϕ is the amplitude, as a function of y and t, of a given wave mode defined in terms of pressures as a function of x and z, found as the eigenvector of a two-dimensional problem. The other variables represented are t=time, y=longshore coordinate ($x = 0$ is the equation of the coastline), $\tau^y(y,t)$= the longshore component of the wind stress, ρ_0= representative density of the water, H_{mix}= the depth of the surface mixed layer, b and c are constants which differ for each mode. The Clarke (1977) solution is more realistic than Gill and Schumann (1974) as it includes the effects of both topography and stratification.

Battisti and Hickey (1984) found that at low frequencies a significant proportion of the variance in the longshore velocity on the Pacific northwest shelf was accounted for by a mode 1 wind forced coastal trapped wave. However, there is not the same strength of deep water formation in the Pacific so one must be cautious when evaluating such results.

Wind forcing, perhaps the most obvious driving mechanism for this kind of wave, has not been fully explained according to Brink (1982a). Therefore care must be taken when calculating the appropriate 'signal' of the coastal trapped wave and both buoyancy and wind forcing, especially on the local scale, should be considered.

1.5.2 The effect of a mean flow

From previous sections it has been determined that coastally trapped waves (CTW) propagate with the coast on their right. Therefore the waves travel southwards along the western boundary of the North Atlantic. However, in this region there are two ocean currents that may affect this propagation; the Gulf Stream which flows northwards along the continental slope from the Tropics and the Labrador Current which flows southwards from the Arctic (Fig 1.11).

Continental shelf waves in the presence of a barotropic coastal current are associated with variations in the background potential vorticity denoted by $\frac{(f+\zeta_0)}{h}$ where f is the Coriolis parameter, h is the fluid depth and ζ_0 is the vorticity of the mean current.

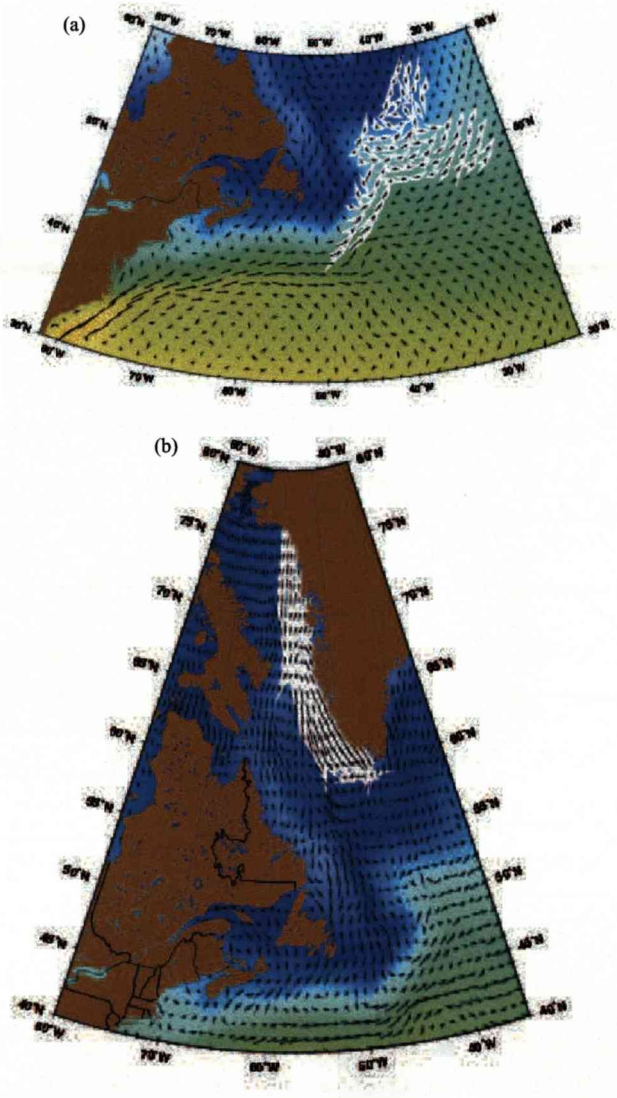

Figure 1.11: The Gulf Stream (a) and Labrador Current (b) represented by the Mariano Global Surface Velocity Analysis (*courtesy of University of Miami*) with the vectors representing the direction and magnitude of the current. The colours represent the ocean temperature from blue representing cold water through green to yellow representing warm water.

In the absence of a mean current (i.e ζ_0 is zero) it is well known that the CSW are uni-directional (Collings and Grimshaw, 1984).

When there is no mean current then Wilkin and Chapman (1987) analytical solution, for an exponential topography in a barotropic ocean, can be utilised;

$$\frac{\omega}{f} = \frac{bk}{(\frac{b^2}{4} + m_n^2 + k^2)}$$

where $m_n = bn\pi$ is the cross shelf wavenumber for mode n, k is the alongshore wavenumber and b is the topographic steepness factor.

If a uniform mean current is added, then the wave frequency becomes Doppler shifted and;

$$\omega = \omega_0 + Uk$$

where U represents the velocity scale.

When the mean current is sheared, the effective velocity which produces the Doppler shift is less than the maximum velocity of the mean current. However, only modes whose phase velocity (including the Doppler shift) is greater than the maximum velocity can propagate as discrete modes when the mean current is stable. Therefore the slowest waves (the highest modes) cannot propagate freely limiting the number of possible propagating modes. Modes are gradually lost as U increases due to varying shear. When the phase speed is equal to the mean current velocity at some point this location is called a critical layer (Yankovsky and Chapman, 1995).

According to Brooks and Mooers (1977) the CSW direction of propagation can be reversed by an opposing uniform mean current but in contrast, an opposing sheared mean current increases the tendency for propagation and produces a high wavenumber cut-off, at least for modes higher than the first. They found that particularly in western boundary currents, where the wave phase velocities of stable CSW and the current velocity are equal but opposed in direction, the contribution of the mean shear to the mean potential vorticity can significantly influence the dispersion characteristics of CSW. In their application of the barotropic model to the Florida Straits - Florida Current system they were concerned that the baroclinic structure of the Florida current may play a significant role in determining the topographically trapped wave characteristics. They did find that for wavelengths greater than 30km the barotropic model qualitatively reproduces the major features of the vertically stratified model.

Yankovsky and Chapman (1995) summarised that the mean current, which in this study is a sheared but stable current, typically eliminates the backward propagating waves and severely reduces the number of forward propagating modes. This could explain,

at least partly, the lack of observations of higher CTW along real coastlines and the success of simple, wind-forced, long-wave models such as Chapman (1983). The mean current need not be very strong to eliminate most of the propagating modes.

If propagating modes are not available, then evanescent modes may be excited which decay away from the region of current variations. If these evanescent modes aquire large amplitudes they may dominate the shelf dynamics in the vicinity of the scattering region appearing as compact, mesoscale features between the mean current and the shelf.

In their follow up paper, Yankovsky and Chapman (1996) showed that when the mean current was spatially varying in the alongshore direction the cross shelf profile of the basic state potential vorticity is changed. This alters the propagation characteristics and structure of the shelf waves thereby causing the excitation of additional modes.

Scattering of shelf waves is often considered as a mechanism by which shelf wave energy can be ultimately lost because the higher modes, which are excited by scattering, should be more susceptible to damping and distortion by bottom friction and other coastal processes. However, the results presented by Yankovsky and Chapman (1996) suggest that in the presence of a spatially varying mean current the scattering region with neighbouring mean currents may provide a source of energy for propagating shelf waves rather than a sink.

Narayanan and Webster (1987) also looked at the structure and propagation characteristics of CSW with a current flowing in the same direction as the shelf wave propagation such as would be the case in the Labrador Current (Fig 1.11). They determined that this current not only strongly modified the shelf waves but also supported energy propagating shear waves. For a sufficiently strong current, the decrease in shear wave wavenumber may cause the shear wave to coalesce directly with the forward propagating shelf waves thereby eliminating the possibility of backward energy propagation along the shelf altogether. Thus the presence of the shelf edge jet may be felt at all wavenumbers restricting the frequency range of the backward propagating shelf waves or may eliminate them altogether. It will also cause frequency shifts at low and high wavenumbers, and will allow shelf-shear evanescent modes to occur at wavenumbers comparable to those of the forward propagating ones at low frequencies. Narayanan and Webster (1987) determined that as the vertical decay length scale, for the case of the Labrador current, is calculated to be 400 m and the core of the current lies over the 500 m isobath, the shelf shear waves are at least partly barotropic.

All the models described in the previous sections have an array of limitations inherent within them. Yankovsky and Chapman (1995) suggested that including the interaction of the mean current with topography, which would alter both the mean current and change its effect on the free waves, would make for a more realistic model. In their

second paper Yankovsky and Chapman (1996) their emphasis of the role of the mean current as a scatterer by increasing the mean current velocity U resulted in the mean current becoming slightly unstable. They also suggested that the non-linear interaction between the mean current and the shelf waves may alter the scattering and/or lead to the growth of other dynamical features.

A major limitation mentioned in all the barotropic studies was the effect of neglecting stratification. Collings and Grimshaw (1984) describe the effects of density stratification: the stable waves wave frequency will be increased at all wavenumbers (Huthnance, 1978) and; there will be a new class of unstable waves due to the possibility of baroclinic instability.

1.6 Boundary conditions

1.6.1 The effect of changing shelf width

In addition to the question of which wave modes are supported by a sloping topography, changes in alongshore topography can result in scattering of CTW modes. Most real coastlines vary significantly over spatial scales which are much shorter than CTW length scales (Wilkin and Chapman, 1987). As CSW propagate along a shelf they encounter regions where the shelf and slope geometry varies strongly (Fig 1.12) over a comparitively small along-shelf distance (of the order of a shelf width or less). This can cause strong scattering of the wave energy into other modes as a consequence of mass and momentum conservation (Yankovsky and Chapman, 1995).

Studies by Allen (1976) and Hsueh (1980) found that when the cross-shelf momentum balance is assumed to be geostrophic scattering does not occur provided the shelf maintains the same relative (shelf similar) slope along its length (Webster, 1987).

Wilkin and Chapman (1987) used a barotropic model with a discontinuity in the shelf width using an exponential shelf profile and found that a CSW of frequency, ω, travelling along a shelf whose width changes abruptly from L_1 to L_2 at some point scatters into all allowable modes of that frequency. Other conclusions reached include:

1. The solution is relatively insensitive to the steepness of the exponential profile.
2. For a widening shelf, energy is readily transferred to higher modes.
3. For a widening shelf, there is a shadow zone of weak flow behind the coastline bend.

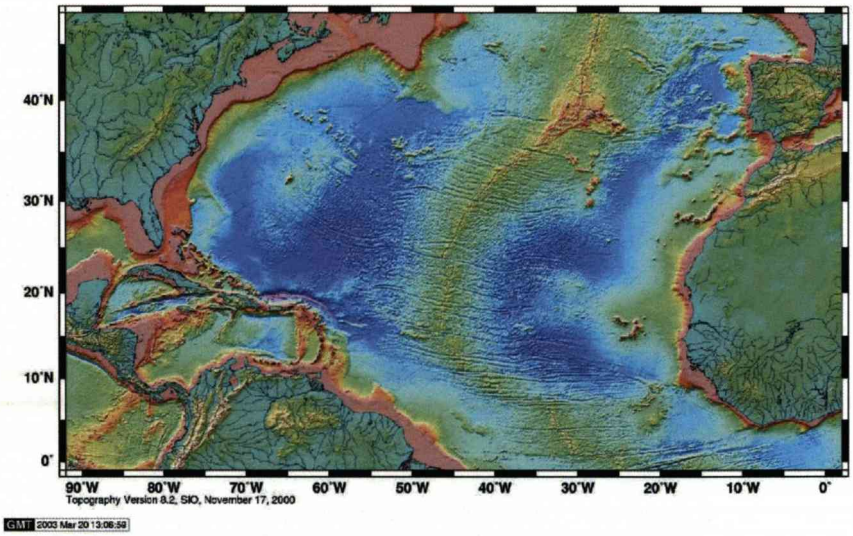

Figure 1.12: Bathymetry map with red indicating shallower ocean areas (the continental shelf) and dark blue representing the deepest areas. It can be seen that the shelf width is very variable on the western boundary of the North Atlantic (*courtesy of Scripps Institute of Oceanography*).

4. The scattered waves resulting from multiple incident waves of different modes can interfere to enhance the energy in some modes while reducing it in others.

Webster (1987) used a similar barotropic model with an exponential shelf profile but allowed the waves to be dispersive. He summarised that energy is scattered from the incident mode into a multiplicity of other modes, both propagating and evanescent. The degree of scattering depended not only on the strength of interaction between an incident waves and a topography varying in the along-shelf direction but also on how the scattered modes interfere with themselves. A degree of similarity was discovered between the scattering caused by narrowing and that of widening that at first seemed counter-intuitive. However, although the relative phases between the incident and transmitted waves for widening and narrowing shelves differ, their amplitudes and hence their energy fluxes remain the same.

Yankovsky and Chapman (1995) again used a barotropic model and found that as the shelf narrows, the adjustment to the changing geometry takes place through the excitation of evanescent modes which develop large amplitudes within and slightly outside the scattering region.

By including stratification, bathymetry and coastline variation into their model Wilkin and Chapman (1990) were aiming towards a more realistic model study. On both

widening and narrowing shelves there was generally a marked intensification of the flow within the scattering region and significant differences in the directions of the currents at points separated by a few tens of kilometres. This indicated that there were occurences of rapid variations in phase. On narrowing shelves, the influence of the scattering can extend upstream into the region of uniform topography even when backscattered free waves are not possible.

They concluded that the strength of the forward scattering into transmitted CTW modes is proportional to a topographic warp factor, which estimates the extent to which the topography departs from shelf-similarity. The scattering induced by non-shelf similar topographic variations is amplified by density stratification suggesting the baroclinic CTW wave structure will be altered to a greater extent than the barotropic CTW modes.

In their Australian observational study Church and Freeland (1987) determined that at low frequencies, long wavelength waves are not affected by relatively small gaps in the coastline but at higher frequencies, where the wavelength is smaller, such breaks become important. Therefore the length scales of the wave modes might result in preferential generation according to the topography of the coastline.

1.6.2 The effect of bottom friction

Very few of the model studies that have been discussed previously have included the dissipative effects of bottom friction. Brink and Allen (1978) looked at how bottom friction affects barotropic motion (continental shelf waves) over a continental shelf slope region. Three effects were determined:

1. It damps free waves.
2. It brings the directly forced component of the alongshore flow more nearly into phase with the local driving than with no friction.
3. It sets up cross shelf phase lags so that the flow nearshore leads that offshore with time. The greater frictional effect in shallow water (appearing as a larger local Ekman number) retards the flow preferentially near the coast. Vorticity development in shallow water leads that in deeper water where friction plays less of a role.

The presence of bottom friction in a barotropic study by Webster (1987) introduces alongshore decay and alters the structure of CSW particularly near to the coast. The wavelength of the CSW is principally dependent on the frequency whereas the decay

rate is dependent on the frequency, mode number and amount of bottom friction. With strong bottom friction set at $r = 0.1\ cms^{-1}$ Webster (1987) found substantial modification of the shelf wave structures on the inner part of the shelf and decay of wave forms in the direction of energy propagation. Mitsudera and Hanawa (1987) suggested that bottom friction was also likely to cause an increase in wave frequency as a result of elliptical motions in the bottom boundary layer.

Brink (1982b) used an approximate technique for including the effect of turbulent bottom friction in the forced first order wave equation governing long generalised coastal trapped waves in a stably stratified ocean. He found that the presence of stratification should decrease the effect of bottom friction, since the vertical motions which accomplish the spin-down process are inhibited.

Mitsudera and Hanawa (1988) suggested that the conclusion of Brink (1982b) may only apply to the first mode and that instead damping increases as stratification increases as a result of a change in wave characteristics. However, Clarke and van Gorder (1986) support the Brink (1982b) result despite the different approaches adopted in each of their studies. In a later work Brink (1990) points out that these two studies are only strictly valid for decay times that are long relative to the wave period.

The Mitsudera and Hanawa (1988) two layer study with topography also looked at the damping rates in the neighbourhood of a 'kissing' condition. Here the damping rates of the two adjacent modes intersect each other and are associated with a change in the properties of the wave from one family to another.

Barotropic continental shelf waves were found to be more susceptible to frictional decay than the baroclinic Kelvin waves, if all else is equivalent, by both Brink (1982b) and Mitsudera and Hanawa (1988). The cross shelf gradient of alongshore bottom stress was found to allow vertical and lateral phase shifts for both free and forced waves. Brink (1982b) did warn that the estimated damping coefficient he presented could not be used if the frictional effect was too large.

Observational evidence from ACE found that the CTW were heavily damped but despite this can carry energy over substantial distances, perhaps 1000 km or 2000 km (Church and Freeland, 1987). The higher modes were seen to be preferentially damped by friction.

1.7 Chapter summary

- The slowdown of the THC, and associated rapid climate change, has been identified as a low risk event; however, due to possibly disastrous impacts, monitoring of changes to North Atlantic forcing and the resulting adjustment are vital.
- A coherent signal has been detected, using altimetry data, over long distances along the continental slope of the western boundary which matches the propagation pathway of coastal trapped waves. However, altimetry does not allow for the modal structure or wave speed of the wave modes to be analysed.
- A number of idealised model studies have suggested a coastal trapped wave response to a change in forcing in the North Atlantic. JM02 found that such waves, in the form of baroclinic Kelvin waves in their vertical sidewalls basin, provided a rapid adjustment on a timescale of months. Their study did not include the effects of topography.
- Model studies incorporating realistic topography and stratification support the coastal trapped wave response theory and suggest that the barotropic mode may play a more important role than was previously thought.
- The large body of work on coastal trapped waves find that the introduction of topography allows a number of additional wave modes to be supported in addition to the baroclinic Kelvin waves found in a baroclinic vertical sidewall basin. In theoretical studies these coastal trapped modes are found to travel at higher wave speeds than the baroclinic Kelvin wave, and as such introduce shorter adjustment timescales.
- Observational studies of coastal trapped waves conclude that observed waves are generally well described by theory. Additionally a high degree of variance along continental slopes over long distances can be accounted for by the coastal trapped wave modes.
- In a stratified ocean, the topographic restoring mechanism is augmented by the stratification resulting in increased wave speeds.
- Coupling of the barotropic and baroclinic modes has been suggested in a number of studies particularly where there is rapid depth variations over the shelf break region.
- Changes in the Meridional Overturning Circulation have been shown to result in a change in sea level along the western boundary in the real ocean.

- Changes in shelf width cause scattering of coastal trapped wave energy into other modes and this is amplified by density stratification leading to greater modification of the wave structure of baroclinic coastal trapped waves than barotropic modes.
- Barotropic continental shelf waves are more susceptible to frictional decay than the baroclinic Kelvin waves. Higher wave modes are also seen to be preferentially damped in observational studies.

1.8 Thesis aims

How the signals of high-latitude forcing are communicated to the rest of the ocean, and the rate of the subsequent process, has important implications for the rapid climate change question. Marotzke and Klinger (2000) proposed an advective route whereas JM02 found a rapid coastal trapped wave response, in the form of baroclinic Kelvin waves. Therefore the first aim of this thesis is to determine which process is the most important for the adjustment of a topographic ocean.

The coastal trapped waves literature reviewed here demonstrates that the inclusion of topography results in a number of additional wave modes with higher wave speeds and corresponding shorter adjustment timescales. The role of the barotropic mode in ocean adjustment has also been suggested. The JM02 study did not address either of these questions.

In addition to determining the major rate-setting adjustment process in response to high-latitude forcing, there are a number of key questions we seek to answer in this thesis:

1. How are the detailed properties of coastal trapped wave modes affected by topography, both idealised and realistic?
2. Can the coastal trapped wave modes, calculated for the real ocean, explain the coherent signal observed along the western boundary of the North Atlantic?
3. Does the rapid adjustment conclusion of JM02 remain valid when the effects of topography are included?
4. How important is the barotropic mode to ocean adjustment in response to forcing in a topographic ocean?
5. How sensitive are the coastal trapped wave modes supported by the topography, and resulting adjustment patterns, to parameters such as shelf width, slope steepness and frictional influences?

6. In addition to the effect on the ocean boundary response how is the interior adjustment of the ocean affected by the inclusion of topography?

7. Finally, by addressing these questions can a theory for the adjustment pattern and speed in response to forcing be determined for the realistic Atlantic Ocean?

These questions will be addressed through analytical and numerical calculations of the coastal trapped wave modes initially on a profile by profile basis before moving onto a full basin idealised modelling study using the MIT General Circulation Model (MITgcm).

The structure of the thesis is described as follows:

Chapter 2 - Idealised wave mode studies: In this chapter we will first outline the analytical solution of rigid-lid barotropic continental shelf waves before calculating the wave properties of coastal trapped modes in the free surface barotropic and baroclinic limits over a number of idealised topographic profiles. A theory for the adjustment pattern and timescale for an ocean with idealised topography and stratification will be outlined according to the results of the wave calculations.

Chapter 3 - Realistic wave mode studies: Having determined the wave properties found over idealised topographies we shall then integrate a number of topographic profiles using depth data from an Atlantic Ocean data set to solve the free surface barotropic problem. Realistic stratification conditions will then be calculated and the wave modes of the free surface baroclinic solution analysed.

Comparisons between the idealised and realistic experiments will be outlined alongside the differences between the wave modes found in the barotropic and baroclinic solutions. The adjustment theory suggested in Chapter 2 will then be updated to take into account the results of these realistic experiments, and also suggest the relative importance of the barotropic mode.

Chapter 4 - Global idealised modelling: In order to analyse the large scale impacts of topography on an idealised Atlantic Ocean in response to change in forcing, and to determine whether a coastal trapped wave response is the most important adjustment process, the MIT General Circulation Model (MITgcm) was utilised.

The model was run with a number of idealised topographies, comparable to those used in the experiments of Chapter 2 and 3, to assess whether the conclusions concerning the predicted adjustment pattern and timescale developed from the detailed wave mode experiments are seen in our idealised model. The effects of changes in form of topography, location of topography and slope steepness on the adjustment pattern will be examined. Additionally the response of the ocean interior in a model ocean with

topography will be assessed to determine whether this longer timescale adjustment is also affected by the inclusion of topography.

Chapter 5 - Localised idealised modelling: This chapter will look in more detail at the response of the ocean to a change in forcing over the western boundary region. The theoretical behaviour that can be expected over a slope region in response to forcing is outlined and compared to the large scale results of Chapter 4. We then use the theory to explain how the ocean will react to a change in the location of the forcing region and compare this to the model results. The influence of friction, both lateral and bottom, is also assessed. Finally the variability in coastal sea level will be examined with reference to changing topography types and location of forcing.

Chapter 6-Synthesis and further work: The final chapter will provide an analysis of how the results of this thesis have addressed the key questions set out above and therefore provide a discussion of the overall implications of this study. Finally an indication of the further work motivated by our results is outlined.

Chapter 2

Idealised wave mode studies

2.1 Introduction

A major difficulty when investigating coastal trapped waves is the sheer complexity of modelling the full spectrum of waves present due to the great variation in topographic and stratification conditions along the western boundary of the North Atlantic.

A sensible first step is to investigate the purely barotropic situation thus eliminating the stratified and hybrid sections of the coastal trapped wave spectrum. By looking initially at the rigid-lid barotropic solution, in Section 2.2, we also eliminate the possibility of barotropic Kelvin wave modes (Fig 2.1). This approach is especially helpful as an analytical solution is possible in the case of an idealised topographic profile, as described by Buchwald and Adams (1968). This analytical solution can be compared against that obtained from a numerical solution and is used to test the solution method. Buchwald and Adams (1968) found propagation speeds of around 2.8 ms^{-1} for an idealised topography that could be compared to the continental shelf off New South Wales.

In Section 2.3 we will add a free surface condition to the barotropic solution and as such will include the barotropic Kelvin wave mode (Fig 2.1). The wave speed of the barotropic Kelvin wave is equal to $\sqrt{gH}$ where H is the water depth; in an ocean where $H = 3000\ m$ we would expect a deep ocean barotropic Kelvin wave to travel at 171.55 ms^{-1}. A coastal trapped Kelvin wave over a shelf with depth $H = 100\ m$ would travel at 31.32 ms^{-1}. Therefore we can expect wave modes representing the deep ocean barotropic Kelvin wave and coastal Kelvin wave in addition to the higher wave modes travelling at speeds around those of the continental shelf waves determined by Buchwald and Adams (1968).

Finally we will examine the free surface baroclinic coastal trapped wave solution (Section 2.4) using the BIGLOAD2 model developed by Brink and Chapman (1985). This model should allow us to analyse the full spectrum of coastal trapped waves (Fig 2.1) under idealised stratification conditions.

The results of all the experiments will be summarised in Section 2.5. The timescales of adjustment found using a number of idealised topographic and stratification profiles will be discussed with reference to the results of JM02. Additionally some predictions of what wave modes and adjustment timescales can be expected for the more realistic experiments of Chapter 3 will be outlined.

2.2 Rigid lid barotropic solution

2.2.1 Equations of motion

The derivation for the equation which represents the coastal trapped wave in a barotropic ocean begins with the equations of motion in the linearised shallow water theory;

$$\frac{\partial u}{\partial t} - fv = -g\frac{\partial \eta}{\partial x} \tag{2.1}$$

$$\frac{\partial v}{\partial t} + fu = -g\frac{\partial \eta}{\partial y} \tag{2.2}$$

and the equation of continuity;

$$\frac{\partial \eta}{\partial t} + \frac{\partial (hu)}{\partial x} + \frac{\partial (hv)}{\partial y} = 0 \tag{2.3}$$

where u, v = velocity in the x, y directions respectively in ms^{-1}, f = the Coriolis parameter, g = gravity in ms^{-2}, η = sea level in m and h = thickness of water column in m.

Two important assumptions are made at this point. Firstly that f is constant. It can be assumed that $\frac{\delta f}{\delta y} = \beta$ accounts for the variation of f with latitude. If length and time are appropriately small in comparison to variation in depth then the β terms can be neglected (Buchwald and Adams, 1968).

The second assumption is that the depth-integrated motion is horizontally non-divergent resulting in (2.4), replacing (2.3);

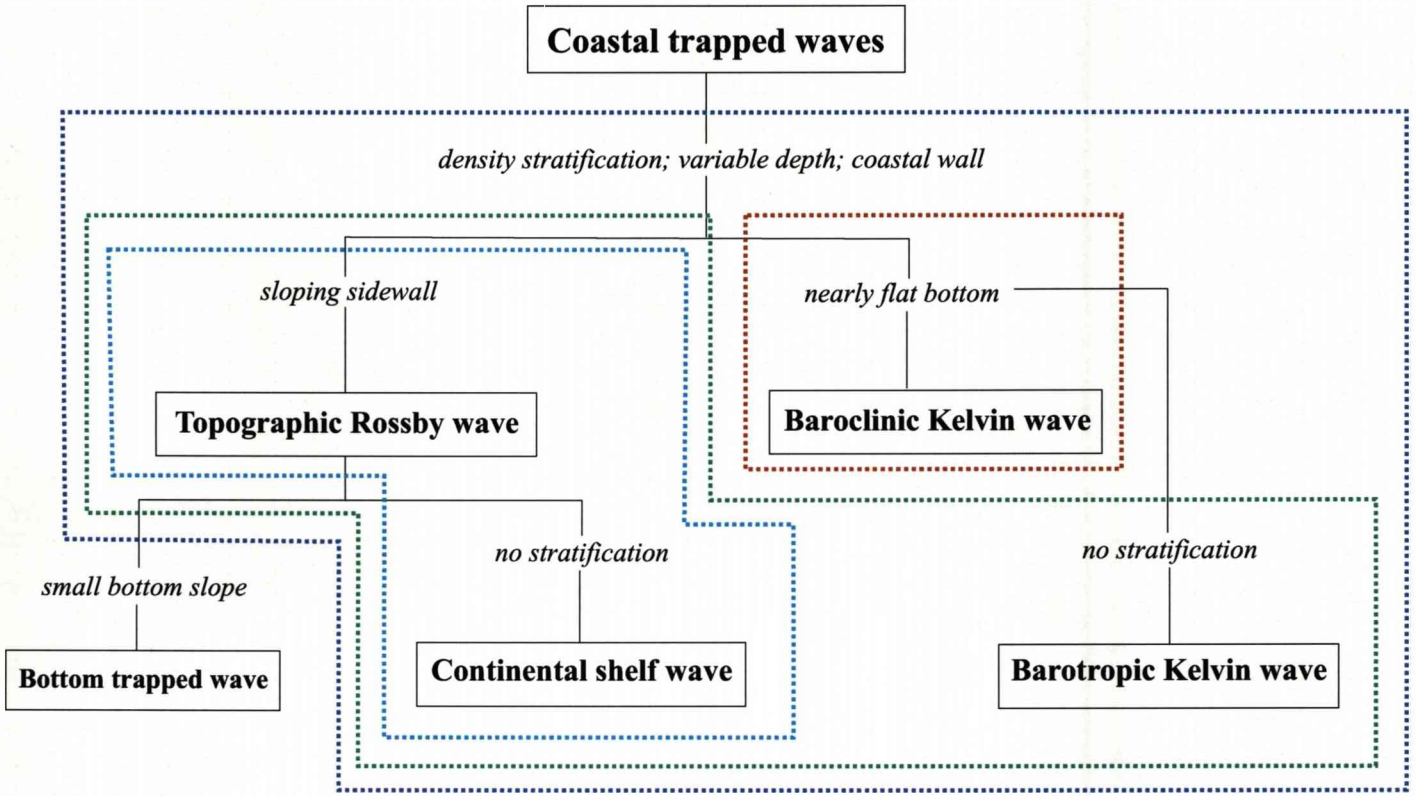

Figure 2.1: Coastal trapped waves classification diagram from (Wang and Mooers, 1976) identifying the wave type corresponding to differing conditions of topography and stratification. The rigid-lid barotropic solution (Section 2.2) solves for the continental shelf waves only (outlined in dashed cyan); the free surface barotropic solution (Section 2.3) solves for the continental shelf waves in addition to the barotropic Kelvin wave, both the deep ocean and shelf modes (outlined in dashed green) and; the free surface baroclinic solution (Section 2.4) should find the full spectrum of coastal trapped waves (outlined in dashed purple). The JM02 model only allowed baroclinic Kelvin waves (outlined in dashed red).

$$\frac{\partial(hu)}{\partial x} + \frac{\partial(hv)}{\partial y} = 0 \tag{2.4}$$

A streamfunction, ψ, is then introduced and u and v can then be expressed as;

$$uh = -\frac{\partial \psi}{\partial y} \tag{2.5}$$

$$vh = \frac{\partial \psi}{\partial x} \tag{2.6}$$

After partial differentiation of (2.1) with respect to y and (2.2) with respect to x, subtracting and using (2.5) and (2.6) the vorticity equation (2.7) below is obtained;

$$\nabla \cdot (\frac{\nabla \psi}{h})_t + J(\psi, \frac{f}{h}) = 0 \tag{2.7}$$

where $h = h(x)$.

For free waves along a straight coast, aligned along the y-axis, we assume that;

$$\psi(x, y, t) = \phi(x) e^{i(ky - \omega t)}$$

where k is the wavenumber and ω is the frequency.

This is then substituted into (2.7) to obtain;

$$(\frac{-\omega \phi_{xx}}{h} - \omega \phi_x (\frac{1}{h})_x + \frac{\omega \phi k^2}{h}) e^{i(ky - \omega t)} - k(\frac{1}{h})_x f \phi e^{i(ky - \omega t)} = 0$$

which simplifies to;

$$\phi_{xx} + \phi_x h (\frac{1}{h})_x + \phi(-k^2 + \frac{kf}{\omega} h (\frac{1}{h})_x) = 0$$

By setting $h(\frac{1}{h})_x = -\frac{h_x}{h}$ and $\sigma = \frac{\omega}{f}$, the resulting equation for barotropic continental shelf waves is;

$$\phi_{xx} - \frac{\phi_x h_x}{h} - \phi(k^2 + \frac{h_x}{h} \frac{k}{\sigma}) = 0 \tag{2.8}$$

2.2.2 The analytical solution

An analytical solution is possible in the case of an idealised exponential profile as described in Buchwald and Adams (1968). Starting with (2.8) a particular exponential form is chosen represented by;

$$h(x) = h_0 e^{2bx} \tag{2.9}$$

where h_0 is the depth at $x = 0$, x is the offshore distance and b is a topographic steepness parameter. From which $h_x = 2bh$ can then be substituted into (2.8) becoming;

$$\phi_{xx} - 2b\phi_x - \phi(k^2 + \frac{2bk}{\sigma}) = 0 \tag{2.10}$$

A solution is easily derived if we assume $\phi = Ae^{\alpha x}$ and thus (2.10) becomes;

$$\alpha^2 - 2b\alpha - (k^2 + \frac{2bk}{\sigma}) = 0$$

The solution to this quadratic is $\alpha = b \pm im$ where m is given by (2.11);

$$m^2 = -b^2 - k^2 - \frac{2bk}{\sigma} \tag{2.11}$$

Substitution of this value of α leads to the general solution (2.12);

$$\phi = A_1 e^{bx}(\cos mx + i \sin mx) + A_2 e^{bx}(\cos mx - i \sin mx) \tag{2.12}$$

2.2.3 Boundary conditions

The boundary conditions were set as described in Fig 2.2. At $z = 0$, $u = 0$ which requires that $\phi(0) = 0$. Substituting this condition in the general solution leads to $A_1 = -A_2$, and hence the particular solution is;

$$\phi = \phi_S = Ae^{bx} \sin mx \tag{2.13}$$

where subscript S = shelf.

From Fig 2.2, in the deep ocean $b = 0$ and therefore (2.8) becomes;

$$\phi_{xx} - k^2\phi = 0 \tag{2.14}$$

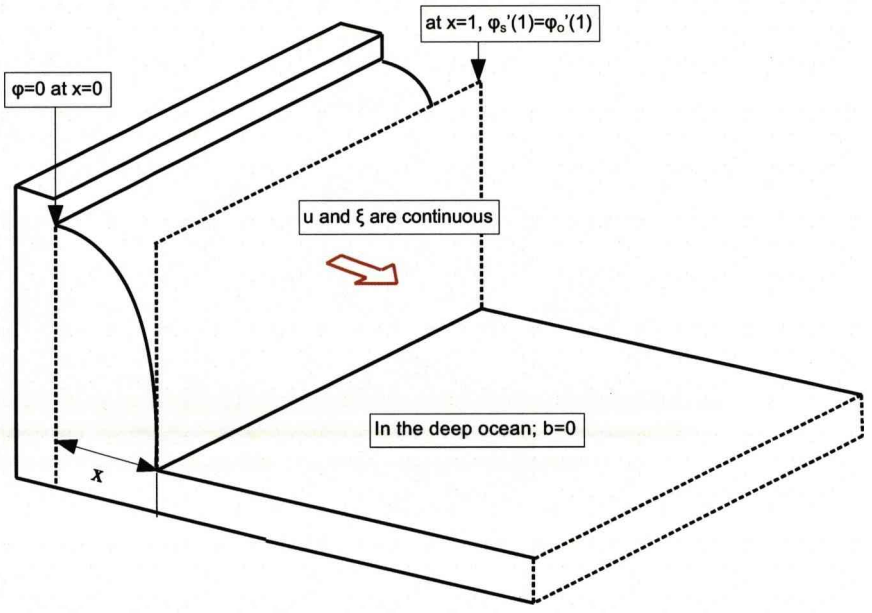

Figure 2.2: The barotropic model with an exponentially decaying topography and open boundary at $x = 1$.

Using $\phi = Be^{\alpha x}$ the appropriate solution of (2.14) representing the deep ocean is;

$$\phi_O = Be^{-kx}$$

where subscript O = ocean.

At the open boundary where $x = 1$ (thus defining the unit in which x is measured), η and u are continuous implying that;

$$\phi_S(1) = \phi_O(1) \tag{2.15}$$

leading to

$$Ae^b \sin m = Be^{-k} \tag{2.16}$$

and

$$\phi\prime_S(1) = \phi\prime_O(1) \tag{2.17}$$

leading to

$$Ae^{b}(b\sin m + m\cos m) = -kBe^{-k} \tag{2.18}$$

Together (2.16) and (2.18) can be solved (numerically) for m thus providing the relationship between σ and k using (2.11).

2.2.4 Numerical methods

To solve (2.10) numerically it was necessary to first rewrite the equation as;

$$\phi_{xx} - A\phi_x - Z\phi = 0 \tag{2.19}$$

where $A = 2b$ and

$$Z = k^2 + \frac{2bk}{\sigma} \tag{2.20}$$

This represents a two point boundary value problem where the boundary conditions at the starting point do not determine a unique solution to start with. A 'random' choice to satisfy incomplete starting boundary conditions will almost certainly not satisfy the boundary conditions at the other specified point (Press et al., 1986). There are two methods of solving such problems; the shooting method or relaxation methods. We can tell from the analytical result that the solution is oscillatory and as such the shooting method, with its variable stepwise adjustment, can adjust to the solution's peculiarities to a greater extent than relaxation methods.

An iterative value of Z was used to 'aim' the shot at the solution. The equation was then integrated forward, using finite differencing methods, from $x = 0$ to $x = 1$. In order to determine the value of Z which satisfies the boundary conditions at $x = 1$ a misfit, y, was calculated. The gradients at this point were then matched. As ϕ is continuous then B can be set as $\phi_S(1)$ and therefore from (2.15) and (2.17);

$$\phi\prime_O(1) = -k\phi_S(1)$$

and

$$y = \phi\prime_S(1) - \phi\prime_O(1)$$

To find the value of Z which satisfies the boundary conditions, Z_R, the point at which y is a minimum is found using bracketing and bisection routines (Press et al., 1986). The

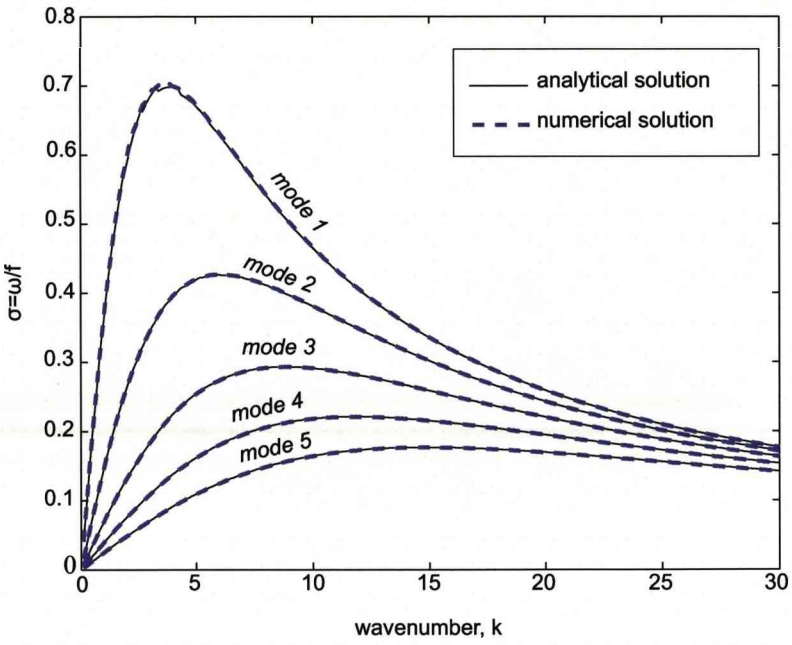

Figure 2.3: The dispersion relation for the first five continental shelf wave modes for an idealised exponential topography from the analytical solution (black line) and the numerical solution (magenta dashed line) for $b = 2.7$.

relationship between σ and k, the frequency relation, can then be found by rearranging (2.20) to give;

$$\sigma = |\frac{2bk}{Z_R - k^2}|$$

2.2.5 Comparison of analytical and numerical solutions

The frequency ratio from the numerical model using an exponential profile (Fig 2.3) compares favourably with the analytical solution shown by Buchwald and Adams (1968).

The frequency relation plot can be broken down into sections of each mode curve. Narayanan and Webster (1987) describe the three types of wave mode that are found in the barotropic solution:

1. The curve before (k_{max}, σ_{max}) are the long forward propagating shelf wave modes.

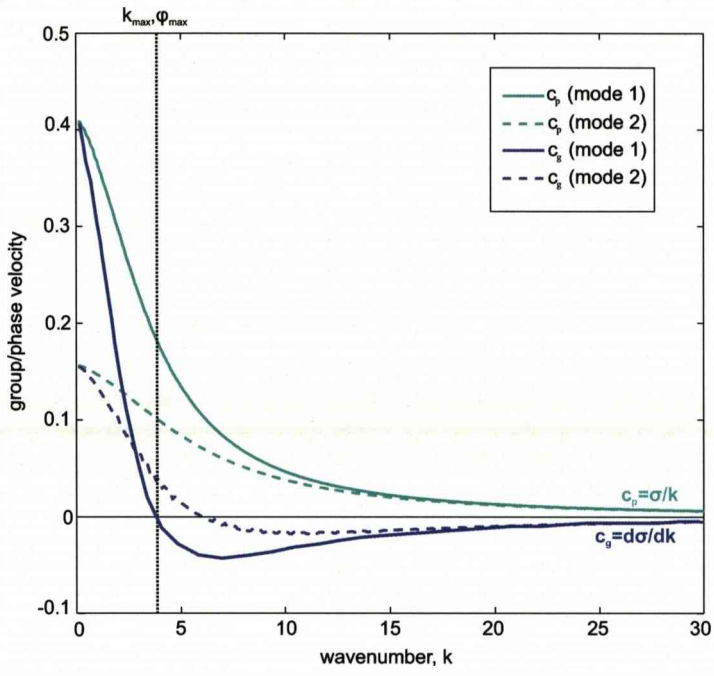

Figure 2.4: Phase speed, c_p (green line), and group velocity, c_g (purple line), as a function of wavenumber, k, for mode 1 (solid) and mode 2 (dashed) waves. Below k_{max} (black dashed) c_p and c_g have the same sign which is not the case for $k > k_{max}$.

2. The curve after (k_{max}, σ_{max}) are short shelf waves which are backward propagating, that is have negative group velocity although the phase velocity remains positive.

3. Finally as the frequency increases the forward and backward propagating modes coalesce becoming non-energy propagating evanescent modes.

Fig 2.4 shows that for values of $k < k_{max}$ the group velocity, c_g, and the phase velocity, c_p, are of the same sign whereas if $k > k_{max}$ then they are opposite signs. The modes that are of most interest to this study are the long forward propagating shelf wave modes which represent those barotropic coastal trapped waves that propagate southwards along the western boundary in the Northern hemisphere. We are therefore only interested in the lower end of the wavenumber range where $k < k_{max}$ and the wave mode speeds converge (Fig 2.4).

We are aware that by looking at long waves this contradicts the assumption that topography and f vary slowly over a wavelength. However, it is often the case that wave modes derived in this way provide a useful guide to dynamics and this is what we are seeking.

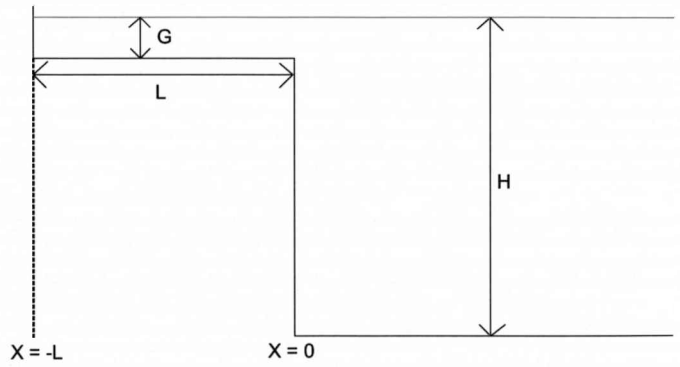

Figure 2.5: Shelf topography with width L, depth G and deep ocean depth H.

2.3 Free surface barotropic solution

2.3.1 Introduction

The rigid lid experiments allowed for an analytical solution and more simple numerical solution of the continental shelf wave modes; however, due to the rigid lid condition the barotropic Kelvin wave was not possible. By solving for a free surface condition, but remaining in a barotropic ocean, we can now analyse both the continental shelf wave and barotropic Kelvin wave section of the coastal trapped wave spectrum (see Fig 2.1). With the inclusion of both deep ocean and shelf barotropic Kelvin wave modes we would expect to find these modes with considerably higher wave speeds than the continental shelf waves of the rigid-lid barotropic solution.

2.3.2 Step topography solution

We look firstly at the solution for a single step topography with a shallow shelf of width, L, and depth, G, and a deep ocean depth of H (Fig 2.5).

The solution to the problem in shallow water is;

$$\eta = Ae^{\beta x} + Be^{-\beta x}$$

where

$$A = \frac{1}{2}(1 - \beta + \frac{(\beta^2 - 1)}{\alpha\beta})$$

$$B = \frac{1}{2}(1 + \beta - \frac{(\beta^2 - 1)}{\alpha\beta})$$

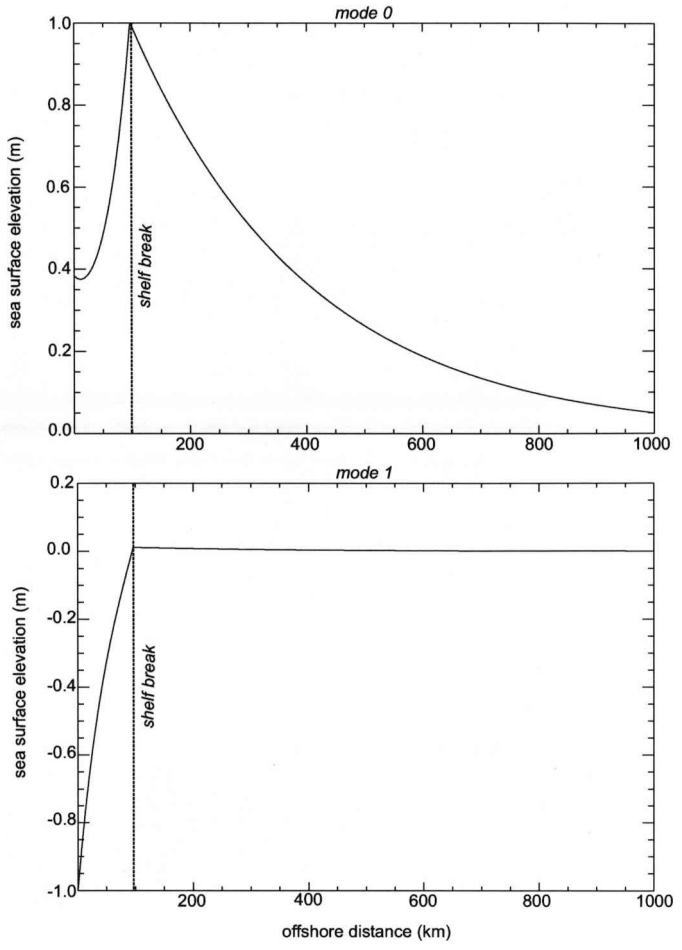

Figure 2.6: The mode 0 double Kelvin wave (top panel) and mode 1 coastal Kelvin wave (bottom panel), in terms of sea surface elevation, for the single step topography with $L = 0.32$ barotropic Rossby radii, $G = 100\ m$ and $H = 3000\ m$

with $\beta = \sqrt{\frac{H}{G}}$ and $\alpha = \frac{1}{2} \pm \sqrt{(\frac{1}{4} - D)}$ where $D = \frac{(1+\beta)(1-\beta)(1-e^{2L\beta})}{\beta^2((\beta-1)+(\beta+1)e^{2L\beta})}$ (see Appendix A for full solution). Here α is equal to the wave speed as a fraction of $c_0 = \sqrt{gH}$ so $\alpha_1 = \frac{1}{2} + \sqrt{(\frac{1}{4} - D)}$ and $\alpha_2 = \frac{1}{2} - \sqrt{(\frac{1}{4} - D)}$. Therefore $\alpha_1 + \alpha_2 = 1$ and the sum of the two wave speeds is equal to c_0.

H is the deep ocean depth and G is the depth of the shelf; set to 3000 m and 100 m respectively; L is measured in units of deep barotropic Rossby radius $R_0 = \frac{\sqrt{gh}}{f}$. Assuming a latitude of 25°N, the positive root of this solution represents the mode 0 pure double Kelvin wave, with a wave speed of 142.2 ms^{-1} and a maximum amplitude on the shelf break. The negative root corresponds to the mode 1 wave with a speed of 29.35 ms^{-1} (Fig 2.6), which in this case is a coastal Kelvin wave. Here, we are taking $L = 908\ km$, thus representing a wide shelf.

2.3.3 Varying shelf parameters

The shelf described in Section 2.3.2 becomes a control run from which to experiment varying a number of parameters such as shelf width (L), shelf depth (G), deep ocean depth (H) and latitude. For each of these experiments the input values were altered accordingly and the resulting wave speeds of the mode 0 (double Kelvin wave) and mode 1 (coastal Kelvin wave mode) are summarised in Table 2.1.

L (km)	G (m)	H (m)	*latitude* $(°N)$	c_0 (ms^{-1})	c_1 (ms^{-1})
227	100	3000	25	159.03	12.52
454	100	3000	25	149.93	21.62
908	100	3000	25	142.21	29.34
1816	100	3000	25	140.29	31.26
908	50	3000	25	149.52	22.02
908	200	3000	25	135.10	36.45
908	100	2000	25	110.68	29.39
908	100	5000	25	191.94	29.53
908	100	3000	5	160.45	11.09
908	100	3000	45	140.98	30.57

Table 2.1: Test values of shelf width, L, shelf depth, G, deep ocean depth, H, latitude and corresponding mode 0 and mode 1 wave speeds, c_0 and c_1 at reference latitude $25°N$.

The effect of varying the parameters are outlined below and are also summarised in Fig. 2.8;

- **Varying shelf width**: From the control run shelf width value of 908 km we reduced the shelf width to 454 km and 227 km and then increased the width to 1816 km while keeping all other variables constant. Fig 2.7 shows that as shelf width is increased the mode 0 wave speed decreases and the mode 1 wave speed increases. It is not a linear relationship, however, as the decrease and corresponding increase in the wave speeds is largest at the smaller end of the shelf width range. For example an increase by a factor of 2 from 227 km to 454 km results in an increase of 73% in the mode 1 speed whereas changing the shelf width from 908 km to 1816 km only results in a 6.5% increase in wave speed. Due to the lower wave speed values of the mode 1 waves their proportional increases/decreases are larger.

- **Varying shelf depth**: The shelf depth was reduced and increased by a factor of 2 to 50 m and 200 m respectively. A shallower (deeper) shelf depth results in an

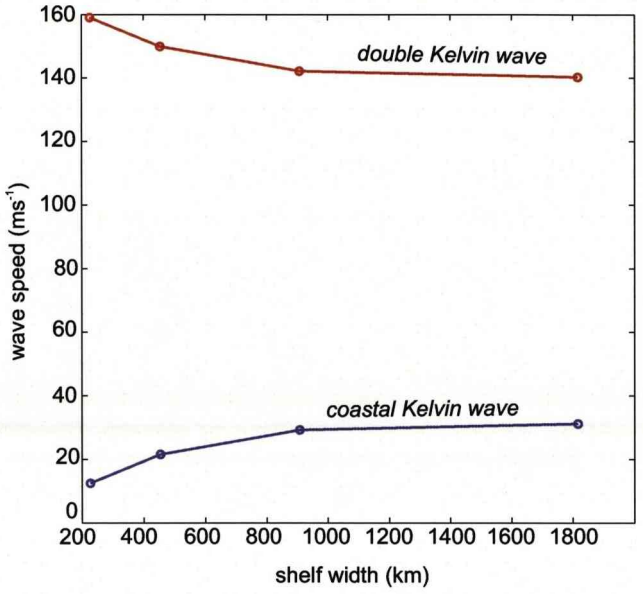

Figure 2.7: Wave speeds of the mode 0 double Kelvin wave (red line) and mode 1 coastal Kelvin wave (magenta line) corresponding to shelf width.

increased (decreased) mode 0 wave speed and decreased (increased) mode 1 wave speed.

- **Varying deep ocean depth**: Decreasing (increasing) the deep ocean depth to 2000 m (5000 m) resulted in a decreased (increased) Kelvin wave speed and increased (decreased) mode 1 wave speed.

- **Varying latitude**: Moving from the control run latitude of $25°N$ to $5°N$ ($45°N$) results in an increase (decrease) in mode 0 wave speed and decrease (increase) in mode 1 wave speed. At $5°N$ ($45°N$) the mode 0 wave speed is faster (slower) and the mode 1 wave mode is slower (faster) than at $25°N$.

If we look carefully at the wave speed values we notice that at all points the sum of the mode 0 and mode 1 wave speeds is equal to the deep ocean barotropic wave speed ($c = \sqrt{gH}$). Therefore any increase (decrease) in the mode 0 double Kelvin wave must be associated with a decrease (increase) in the mode 1 coastal Kelvin wave speed and this is clear from the experimental results.

Stratification results in the flow 'feeling' the topography to a lesser extent (Anderson and Killworth, 1977) resulting in the shelf break structure that the double Kelvin wave depends upon having less of an influence on the wave mode structure. However, in areas such as the Labrador shelf region the stratification is weak so, that even with rapid (but continuous) depth changes in the area north of the Grand Banks, the

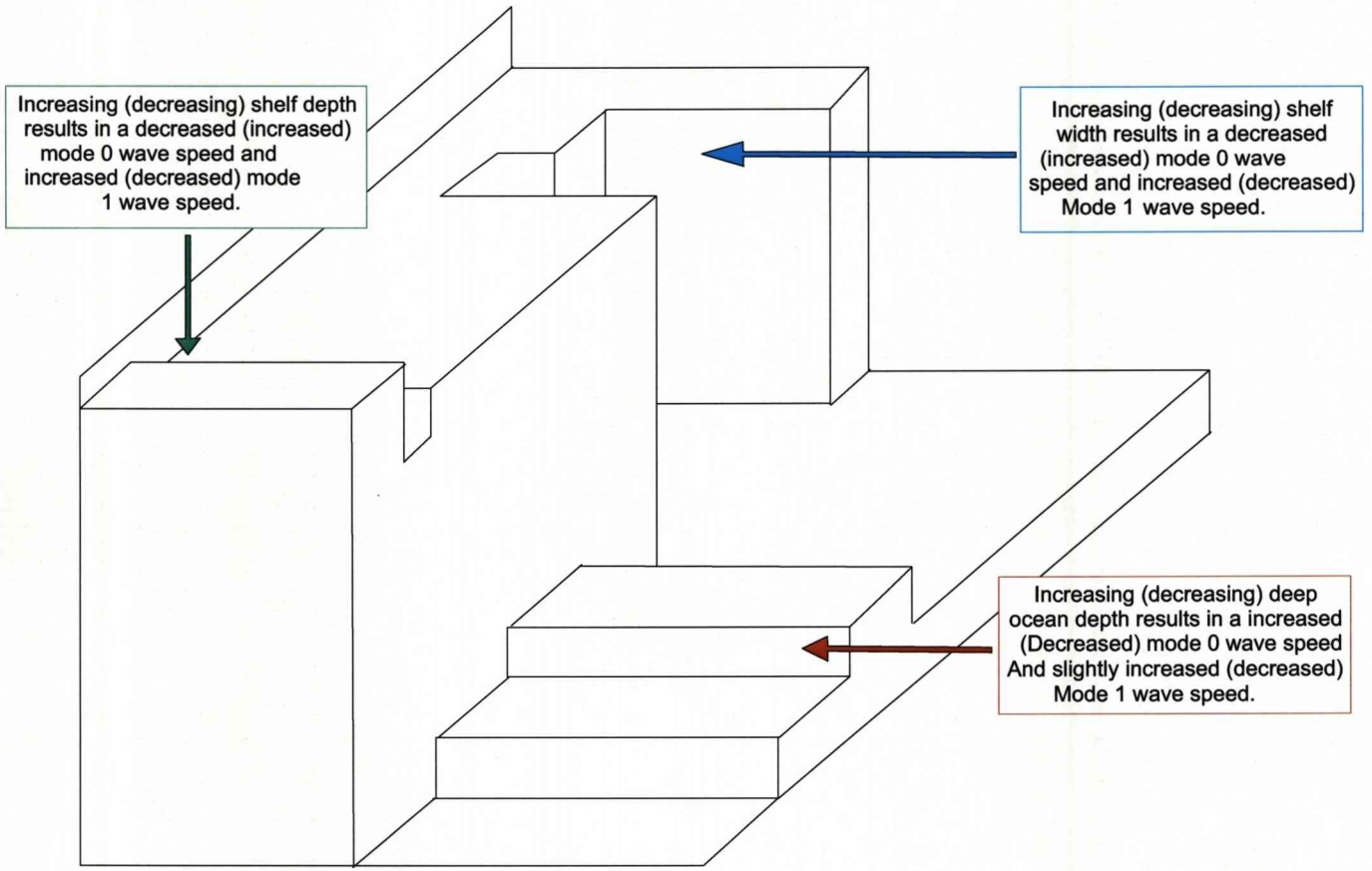

Figure 2.8: Annotated diagram outlining the effects of varying a number of shelf parameters on the mode 0 double Kelvin wave and mode 1 coastal Kelvin wave mode. The green box describes the effect of altering shelf depth, the red box describes the deep ocean depth effect and the blue box outlines the impact of a changing shelf width.

barotropic approximation may provide a reasonable approximation of the free waves there (Middleton and Wright, 1990) and allow for the presence of the double Kelvin wave.

2.3.4 Multiple step topography solution

In order to incorporate more complicated or realistic topographies a multiple step solution was required (Fig 2.9). The sea surface elevation in this case is again found from;

$$\eta = Ae^{\beta x} + Be^{-\beta x}$$

where this time;

$$A_{i-1} = \frac{\beta_{i-1}}{2Q_{i-1}}[A_i P_i(\frac{1}{\beta_i} + \frac{r}{{\beta_i}^2} + \frac{1}{\beta_{i-1}} - \frac{r}{{\beta_{i-1}}^2}) + \frac{B_i}{P_i}(\frac{1}{\beta_{i-1}} - \frac{r}{{\beta_{i-1}}^2} - \frac{1}{\beta_i} + \frac{r}{{\beta_{i-1}}^2})]$$

$$B_{i-1} = \frac{Q_{i-1}\beta_{i-1}}{2}[\frac{B_i}{P_i}(\frac{1}{\beta_i} - \frac{r}{{\beta_i}^2} + \frac{1}{\beta_{i-1}} + \frac{r}{\beta i - 1^2}) - A_i P_i(\frac{1}{\beta_i} + \frac{r}{{\beta_i}^2} - \frac{1}{\beta_{i-1}} - \frac{r}{\beta i - 1^2})]$$

with $P_i = e^{\beta_i X_i}$, $Q_i = e^{\beta_i X_{i+1}}$ and $\beta_i = \sqrt{\frac{H}{h_i}}$ where h_i is the depth on the level region, $r = \frac{c_0}{c}$ where $c_0 = \sqrt{gH}$ and X is the relevant offshore distance of the step. The full solution, utilising a backwards shooting method matching the solution at each of the steps and to the coastal boundary solution, is outlined in Appendix B

The solution can be calculated for as many modes as there are steps in the problem, however, for simplicity and clarity we will evaluate the sea level, η, and wave speed, c, for the first three modes only. Firstly we will analyse the solution over two different topographies, in addition to the shelf and vertical wall (*wideshelf*) profile, to determine the wave mode structures, corresponding wave speeds and basin wide picture (equator to $45°N$):

- An exponential slope with no shelf (*slope*);
- A wide shelf and exponential slope (*shelfslope*);
- A wide shelf and vertical wall (*wideshelf*);

The exponential slope is represented by the following equation;

$$h(x) = \alpha + \beta e^{b(\frac{x-x_1}{x_2-x_1}-1)}$$

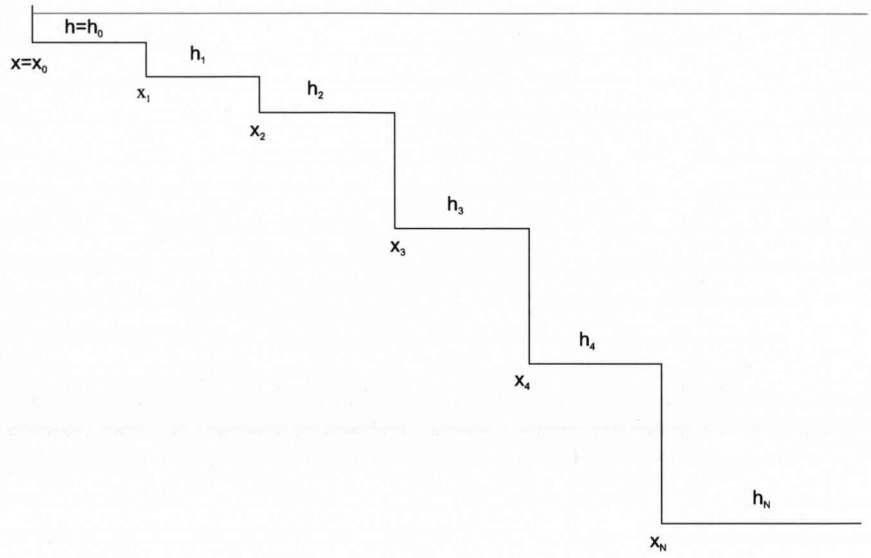

Figure 2.9: Multiple step topography with offshore distance, x, measured in units of R_0, and the depth, h, in m.

where $\alpha = B - \beta$ and $\beta = \frac{A-B}{e^{-b}-1}$ with A representing the depth of the shelf, B is the depth of the deep ocean, x_1 is the extent of the shelf and x_2 is the extent of the shelf and slope. Each unit in the x direction represent $0.2°$ of longitude; the wide shelf is $9°$ and the slope region is over $5°$. The topographic steepness factor b acts as a multiplying factor of the exponential; a higher b value results in a steeper exponential slope.

As with the shelf and vertical wall case the impact of a varying shelf width on the wave structure will be examined and finally the effect of a steepening slope will be assessed.

Mode structure over different topographies

The multiple step, free surface barotropic solution was solved for all latitudes from the equator to $45°N$ for the three topography types; *slope*, *shelfslope* and *wideshelf*. At each latitude the normalised sea surface elevation (normalised by division of all values by the mean sea surface elevation value) and wave speed was determined for the first three modes (Figs 2.11, 2.12, 2.13).

From Fig 2.11 we again see mode 0 is a double Kelvin wave and mode 1 is coastal Kelvin wave in the *wideshelf* case; at $45°N$ the mode 1 wave speed is 30.68 ms^{-1} which is very close to the shelf Kelvin wave speed of 31.32 ms^{-1}. As we approach the equator the mode 0 double Kelvin wave reaches towards the deep ocean barotropic Kelvin wave speed ($c = \sqrt{gH} = 171.55ms^{-1}$) and the mode 1 wave speed goes towards zero. This results from the findings of the single step solution where the two roots of the solution

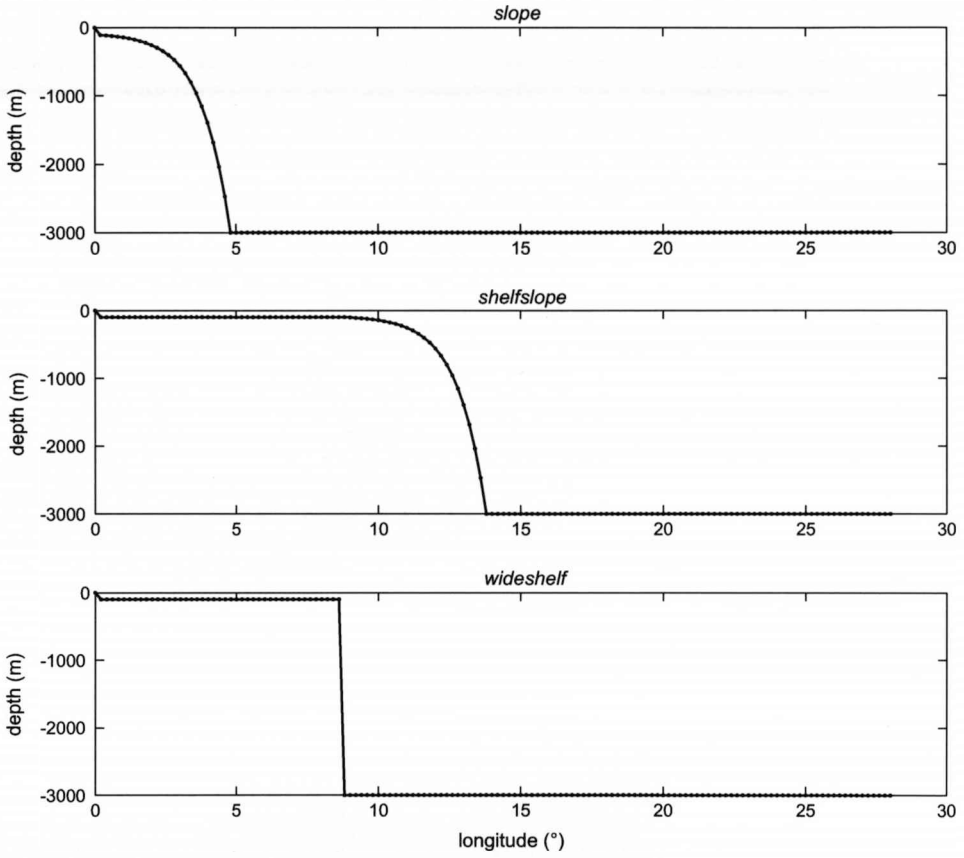

Figure 2.10: The three idealised topographic profiles utilised for all experimentation; *slope* (top), *shelfslope* (middle) and *wideshelf* (bottom).

sum to 1 and therefore an increase in mode 0 (double Kelvin wave) speed must be accompanied by a corresponding decrease in mode 1 (coastal Kelvin wave) speed.

In the *slope* case we find a mode 0 wave that appears equivalent to the deep ocean Kelvin wave but is affected, to some extent, by topography at higher latitudes. We see this mode, as in the *wideshelf* case, increasing from 143 ms^{-1} at $45°N$ to the deep ocean wave speed of 171.55 ms^{-1} at the equator. In a vertical sidewalls basin, the deep ocean Kelvin wave speed is equal to $\sqrt{gH}$ and as such is unaffected by the variation in f from high to low latitudes. Here, the influence of topography depends on how wide the slope is, as measured in units of $R_0 = \frac{c_0}{f}$. Near the equator, R_0 becomes large, and therefore the topography is seen as 'steep'.

The mode 1 wave in this case is again equivalent to a shelf or coastal Kelvin wave, as we can see from the horizontal structure (Fig 2.12). However, it is again modified by the topography as is evident from the wave speed; here we find a mode 1 wave speed of 17.75 ms^{-1} at $45°N$ decreasing to zero at the equator. The mode 2 wave exhibits a similar pattern in propagation speed from high to low latitudes as the mode 1 wave, however, it is travelling at a much slower speed; from 4.87 ms^{-1} at $45°N$ to zero at the equator closer to that of the continental shelf waves of Buchwald and Adams (1968).

In the case of the *shelfslope* topography the inclusion of a wide shelf results in a mode 0 wave with a structure (Fig 2.13) similar to the double Kelvin wave found in the *wideshelf* case (Fig 2.11). However, the presence of the *slope* topography in the shelf break region appears to modify the wave somewhat resulting in a lower wave speed of 125.36 ms^{-1} compared to the *wideshelf* value of 140.86 ms^{-1} at $45°N$. The *shelfslope* mode 1 wave very closely resembles the coastal Kelvin wave with a high latitude speed of 31.09 ms^{-1} which may have been expected given the distance of the coast to the topography in this example. It does, however, decrease rapidly over lower latitudes reaching zero at the equator as in the other two cases. The mode 2 wave is around 50% faster with *shelfslope* (7.42 ms^{-1}) rather than *slope* topography (4.88 ms^{-1}) but, again, displays the same decrease towards zero at the equator.

It is clear that in a topographic basin, in comparison to a vertical sidewalls, the modes supported by the topography result in a number of adjustment timescales. In a barotropic vertical sidewalls basin we would only find the mode 0 deep ocean barotropic Kelvin wave travelling at $\sqrt{gH}$ and providing a basin wide adjustment within days. In a vertical sidewalls basin in the one-and-a-half layer baroclinic limit (such as in JM02) we see only the baroclinic Kelvin wave, dependent on the stratification $g' = \frac{g(\rho_2-\rho_1)}{\rho}$ and equivalent depth $H_e = \frac{(h_1.h_2)}{(h_1+h_2)}$, travelling at $\sqrt{g'H_e}$ which in an ocean of 3000 m and $g' = 0.018\ ms^{-2}$, with $\frac{(\rho_2-\rho_1)}{\rho} = 1.85 \times 10^{-3}$, would equal 3.48 ms^{-1} and result in considerable slower adjustment of months.

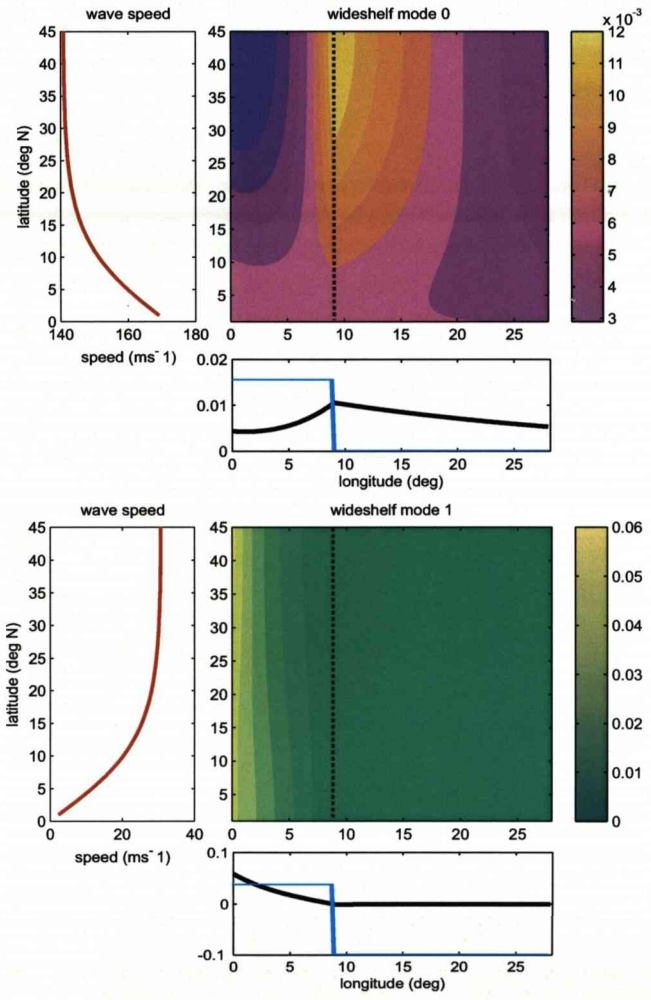

Figure 2.11: Wave structure plots for the mode 0 and mode 1 waves for the *wideshelf* case. In each case the contour plot shows the normalised sea surface elevation for the whole region; the wave speed plot indicates the speed of the wave mode at corresponding latitudes and; a cross section, taken at $25°N$, is shown in black with the topographic profile superimposed in blue.

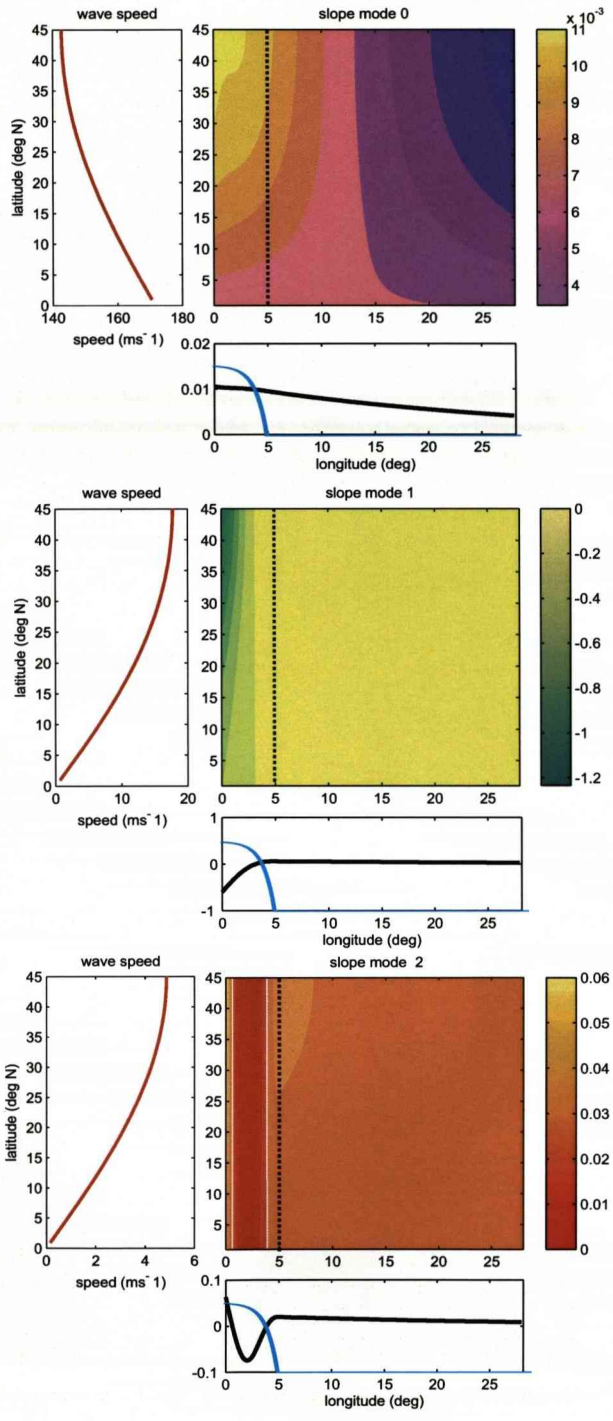

Figure 2.12: Wave structure plots for the mode 0, mode 1 and mode 2 waves for the *slope* case. In each case the contour plot shows the normalised sea surface elevation for the whole region; the wave speed plot indicates the speed of the wave mode at corresponding latitudes and; a cross section, taken at $25°N$, is shown in black with the topographic profile superimposed in blue.

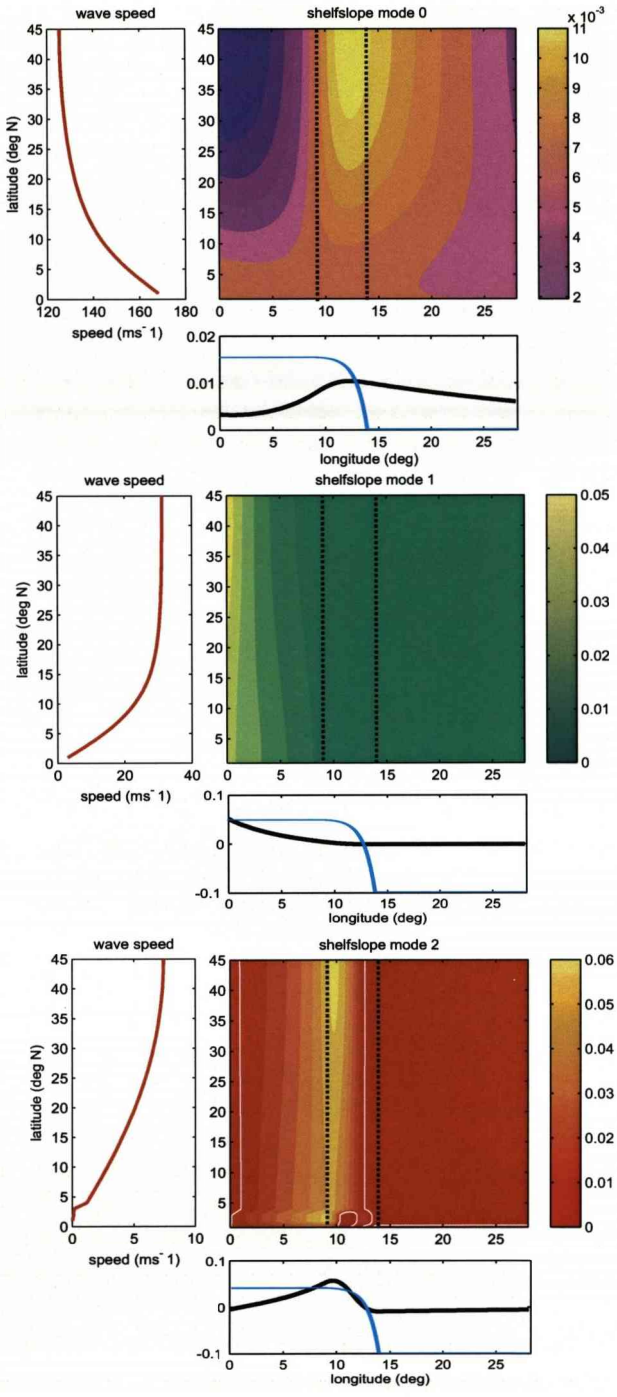

Figure 2.13: Wave structure plots for the mode 0, mode 1 and mode 2 waves for the *shelfslope* case. In each case the contour plot shows the normalised sea surface elevation for the whole region; the wave speed plot indicates the speed of the wave mode at corresponding latitudes and; a cross section, taken at $25°N$, is shown in black with the topographic profile superimposed in blue.

By including topography we find that in the barotropic limit solved for in this free surface barotropic solution a fast mode 0 deep ocean Kelvin wave type mode is still present which, although modified by the topography at high latitudes, travels round the ocean in a matter of days. The mode 1 wave generally in the form of coastal Kelvin wave provides a second relatively rapid adjustment mode; in the *shelfslope* and *wideshelf* it would travel around 2500 km per day and in the slope case around 1500 km per day with respect to the speeds at $45°N$. The mode 2 waves, supported over the topography, in the *slope* and *shelfslope* cases have speeds of 4 to 8 ms^{-1} away from the equator which is faster than the baroclinic Kelvin wave.

An interesting result of this solution is the behaviour of the three (or two in *wideshelf* case) modes in the low latitude region. As we approach the equator we find an acceleration of the mode 0 wave until it reaches the deep ocean Kelvin speed at the equator and the other mode wave speeds go to zero. The slow wave speeds of the mode 1 and 2 waves mean that the topographic 'restoring force' becomes less important for these modes near the equator. At some point, in the realistic ocean, stratification must become the more important factor, allowing these modes to couple to the baroclinic Kelvin waves at the equator. However, the mode 1 barotropic wave speed only becomes comparable to a baroclinic Kelvin wave speed within a few degrees of the equator, which suggests that nonlinear processes (or least non-WKB processes) may become important as the wave structure changes rapidly in this region.

The equatorial Kelvin waves are similar to the coastal or deep ocean Kelvin waves with the equator acting as a vertical sidewall and will travel at the same speed as the vertical sidewall Kelvin waves for all modes.

When the equatorial Kelvin wave reaches the eastern boundary, our findings suggest that as we move polewards along the eastern boundary the mode 1 and mode 2 waves will once again be excited and increase in speed while the mode 0 wave speed decreases as the effect of topography take hold (Fig 2.14).

Effect of a changing shelf width

In the single step solution we completed an analysis of the effect of a changing shelf width, amongst other variables, on the wave speed of the two modes and found that a wider shelf resulted in a decrease in the mode 0 double Kelvin wave speed and corresponding increase in the mode 1 coastal Kelvin wave speed. We shall now examine whether the same pattern is seen when we include slope topography and how the speed and wave structure changes as the shelf width is increased. The inclusion of the slope topography results in additional shelf wave modes.

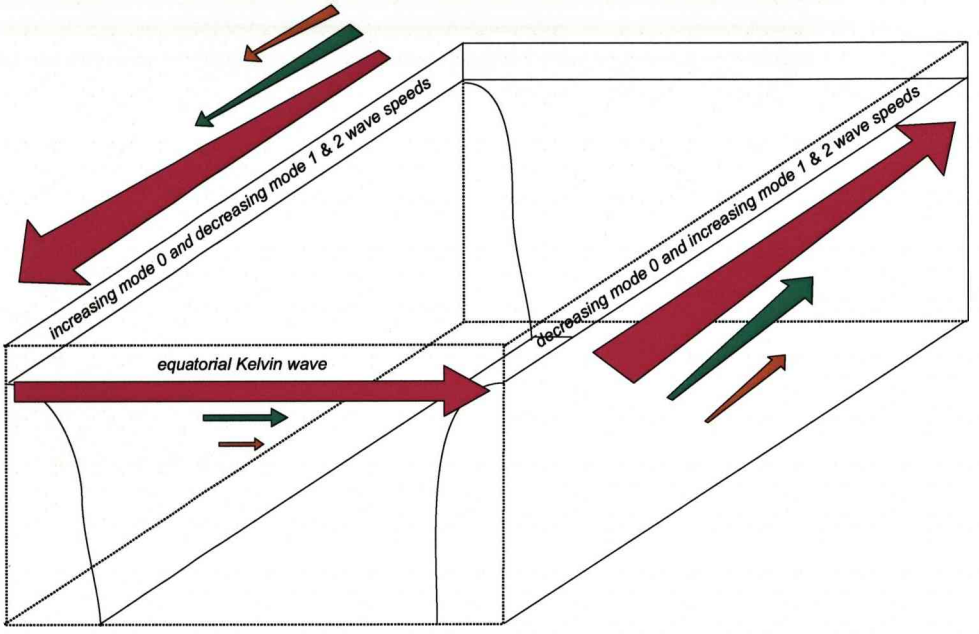

Figure 2.14: Basin schematic indicating the wave modes present on the western boundary, equator and eastern boundary. The mode 0 deep ocean barotropic Kelvin wave (magenta arrow) speeds up towards its theoretical value of 171.55 ms^{-1} at the equator. The mode 1 (green arrow) and mode 2 waves (orange arrow) both slow down and tend towards zero at the equator.

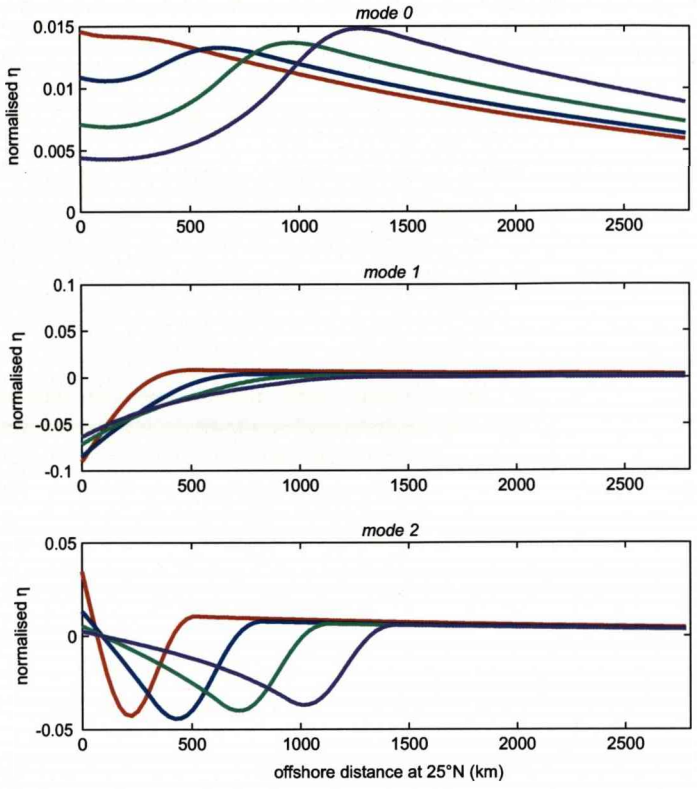

Figure 2.15: The normalised sea surface elevation is plotted for the mode 0, mode 1 and mode 2 waves relevant to the four shelf widths under investigation. *Slope* is shown in red, *shelf1* in blue, *shelf2* in green and *wideshelfslope* in magenta.

Again we have chosen $25°N$ as a control latitude where $R_0 = 2781\ km$. Four topographic profiles were tested:

- The slope topography, covering a distance of 504.45 km, with no shelf (*slope*);
- A shelf of 302.7 km and slope (*shelf1*);
- A shelf of 605 km and slope (*shelf2*) and;
- The wide shelf of 908 km and slope (*wideshelfslope*).

As we move from the *slope* topographic set-up to an increasingly wide shelf region the structure of the mode 0 wave changes from a deep ocean barotropic Kelvin wave like form to the recognisable double Kelvin wave structure we saw in the single step solution (Fig 2.15).

Table 2.2 shows the wave speeds for each of the modes. With an increasing shelf width we see a decreasing mode 0 wave speed and increases in both the mode 1 and mode

Profile	c_0 (ms^{-1})	c_1 (ms^{-1})	c_2 (ms^{-1})	c_{total} (ms^{-1})
slope	147.90	14.77	3.97	166.64
shelf1	136.19	24.08	5.52	165.79
shelf2	130.99	28.85	5.86	165.70
wideshelfslope	129.18	30.55	5.96	165.69

Table 2.2: The mode 0 (c_0), mode 1 (c_1), mode 2 (c_2) and total of the mode 1 to 3 wave speeds (c_{total}) for the four topographic profiles under investigation.

2 wave speeds as was the case in the shelf and vertical wall example. However, the mode 0 speed is somewhat lower than in the *wideshelf* example. When we compare equal shelf widths, the mode 1 speed is higher and there is the presence of the mode 2 wave. The inclusion of a slope in addition to the wide shelf appears to result in enhanced modification of the mode 0 wave by the topography. The mode 1 wave becomes increasingly like a pure coastal Kelvin wave as the topography becomes more remote from the coastal wall.

In Section 2.3.2 we saw that for the single step solution the sum of the two wave mode speeds were equal to c_0. It was interesting to check whether this would also be the case for the multiple step solution so that $\sum_{n=1}^{m} c = \sqrt{gH}$ where m is the total number of modes. From the c_{total} values for the first three modes in Table 2.2 this looks likely. Indeed when tested with m equal to the total number of steps in the solution the sum of all the modes was found to be exactly equal to $\sqrt{gH} = 171.55\ ms^{-1}$ and therefore provides an explanation to why the speed of the mode 0 wave decreases as the number of wave modes increases.

Effect of a steepening slope on wave modes

We shall now investigate how a steepening slope, and therefore decreasing topographic length scale Δx, affects both the wave mode structure and wave speed. Our previous results, from the single step experiment, suggest that we will find that a decreasing Δx will result in less modification, and therefore a smaller reduction in wave speed, of the mode 0 wave as the topography becomes more akin to the shelf and vertical wall form.

The same four topographic profiles were utilised as in the previous section (*slope*, *shelf1*, *shelf2* and *wideshelf*). The topographic length scale, represented by $\frac{1}{b}$ and relevant to $25°N$, was reduced from 100 km to 50 km, 34 km and finally 25 km. Fig 2.16 shows that, as we predicted, the mode 0 wave structure becomes increasingly like the *wideshelf* structure (Fig 2.6). The mode 1 coastal Kelvin wave structure remains rather constant while even with the smallest Δx we retain a mode 2 wave over the slope; this

mode 2 wave does not exist in the *wideshelf* case as it is supported by the presence of topography.

Fig 2.17 shows the variation in wave speed of each topographic profile over the Δx range. As expected we see a reduction in the mode 0 wave speed as Δx is increased from 25 km to 100 km for the *shelf1*, *shelf2* and *wideshelfslope* cases as the double Kelvin wave is increasingly modified by the topography. However, in the *slope* case we see a small increase as the topographic length scale is increased; in this case the mode 0 wave is more equivalent to the deep ocean Kelvin wave in the large Δx limit (Fig 2.12) whereas at lower Δx values where a shelf like feature appears we see the double Kelvin wave like structure emerge akin to the other topographic examples.

The mode 1 coastal Kelvin wave stays rather constant in the *shelf2* and *wideshelfslope* examples where the topography is more remote from the coastal wall and therefore any change in the steepness could be predicted to have less of an effect on this wave mode. In the *slope* and *shelf1* cases we see a decrease in the mode 1 wave speed as Δx increases bringing the modifying influence of the topography close to shore.

The mode 2 wave speed increases with an increasing Δx in all cases indicating the increasing influence of the slope, upon which the existence of this mode depends. The convergence of all cases at the lower end of the Δx suggests that this mode 2 wave depends on the topography over the slope and not on the width of the flat regions.

2.3.5 Free surface barotropic solution: summary of results

The introduction of a free surface allowed for explicit resolution of the fast mode 0 deep ocean barotropic Kelvin wave, or double Kelvin wave, and mode 1 coastal Kelvin wave modes which were not possible under the rigid lid conditions. Therefore three potential adjustment timescales, associated with each of the modes, were discovered:

1. The mode 0 deep ocean barotropic Kelvin wave or double Kelvin waves travel at speeds near to, and increase towards, the theoretical value of 171.55 ms^{-1} for an ocean of 3000 m depth. This mode would propagate around the basin in a matter of days.

2. The mode 1 wave travels at speeds near to the theoretical coastal Kelvin wave value of 31.32 ms^{-1} for a 100 m shelf before decreasing towards zero wave speed near to the equator. The adjustment timescale of this mode would be of the order of weeks, but with a slowing towards the equator leading to either nonlinear behaviour or coupling with baroclinic Kelvin waves in this region.

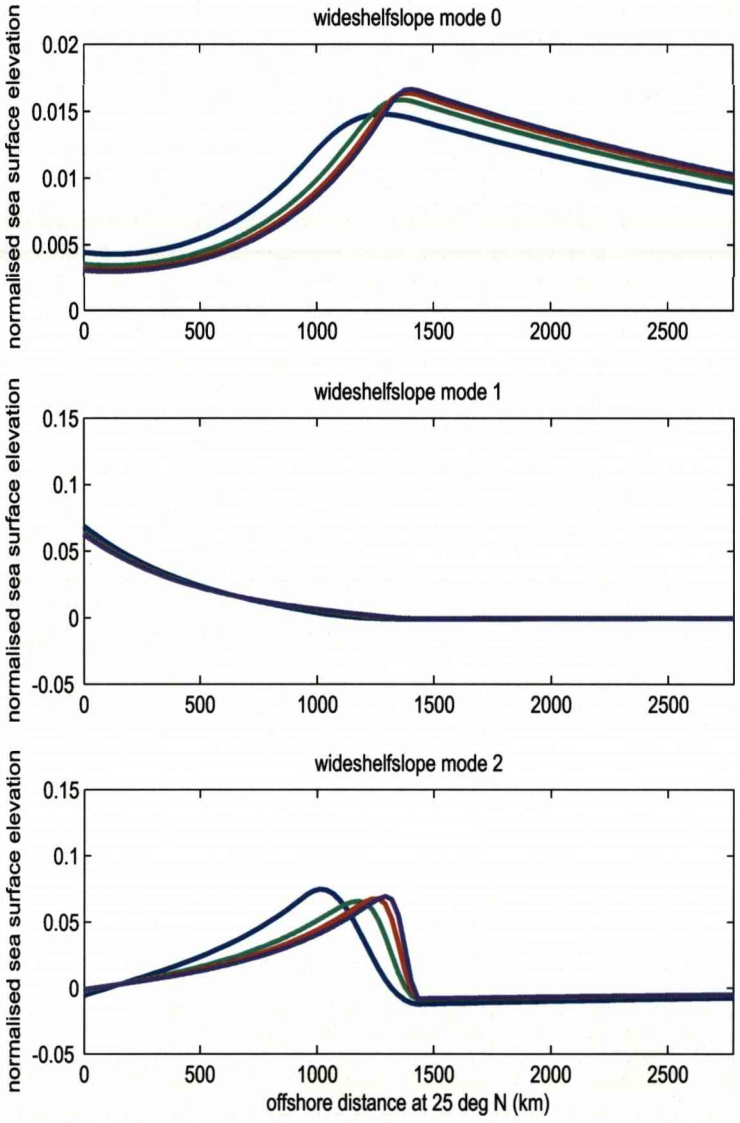

Figure 2.16: The mode 0 (top panel), mode 1 (middle panel) and mode 2 (bottom panel) wave structures for $\Delta = 100\ km$ (blue), $\Delta = 50\ km$ (green), $\Delta = 34\ km$ (red) and $\Delta = 25\ km$ (magenta).

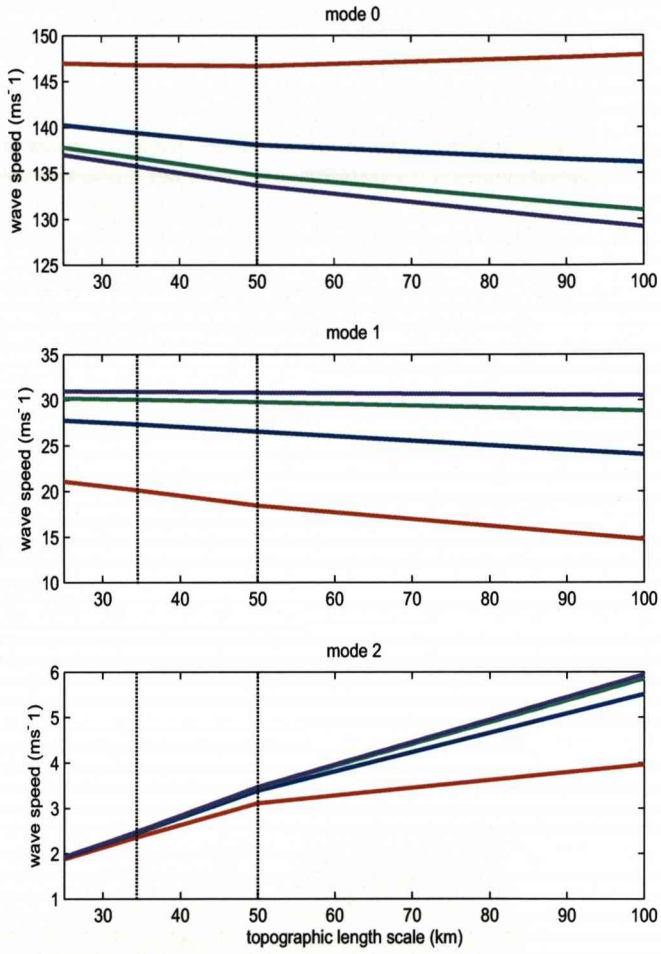

Figure 2.17: The variation in wave speed in relation to an increasing topographic length factor for the *slope* (red), *shelf1* (blue), *shelf2* (green) and *wideshelfslope* (magenta) topographies for mode 0 (top panel), mode 1 (middle panel) and mode 2 (bottom panel).

3. The mode 2 wave supported by the topography has wave speeds of around 5 to 8 ms^{-1} at high latitudes before also tending towards zero at the equator. This mode has an adjustment timescale of months.

It is clear that the wave modes found in this free surface barotropic experiment are considerably faster than the baroclinic Kelvin wave in the JM02 study. The change in wave speeds of the modes as they approach the equator is interesting as it suggests that the decreasing f value does not allow for the support of barotropic coastal trapped modes even in the presence of topography. We can suggest that the equatorial modes are all pure Kelvin waves but that when they arrive on the eastern boundary the additional coastal trapped modes are excited once more and will speed up along the eastern boundary with increasing f values.

Another notable result is that the mode 0 wave speed appears to be affected by the topography and particularly so when the shelf width is increased and the mode becomes more like a double Kelvin wave. The mode 1 wave is modified to a greater extent when the influence of topography is closer to the coastal wall whereas when it is remote the wave speed approaches the theoretical value. The mode 2 wave, supported by the topography, decreases in speed when the shelf width or the slope steepness is increased.

We can expect the free surface baroclinic solution, discussed in the next section, to provide similar mode 0 and mode 1 (away from the equatorial region) waves, however, the mode 2 wave is likely to be modified by the effects of stratification, as the topographic and stratification 'restoring forces', as measured by wave speed, are similar in this case.

2.4 Free surface baroclinic solution

We now want to investigate the behaviour of waves that occur in a more realistic free surface, baroclinic ocean. The BIGLOAD2 baroclinic model for coastal trapped waves with continuous stratification and topography, developed by Brink and Chapman (1985) was used to investigate the free surface baroclinic solution. This model will allow for the full spectrum of coastal trapped waves to be analysed (Fig 2.1).

The idealised model geometry can be seen in Fig 2.18. The depth at the coast must be non-zero but may be arbitrarily small. The model is solved on a fixed point grid, that is the same number of points at every depth, resulting in the vertical resolution being much greater closer to the shore, in shallow water. The model can be run with a rigid lid or a free surface; to allow for Kelvin waves we opt for the free surface option.

Rhines (1970) found that stratification reduces the influence of topography on wave modes which are not bottom-trapped. This may result in stratification taking over

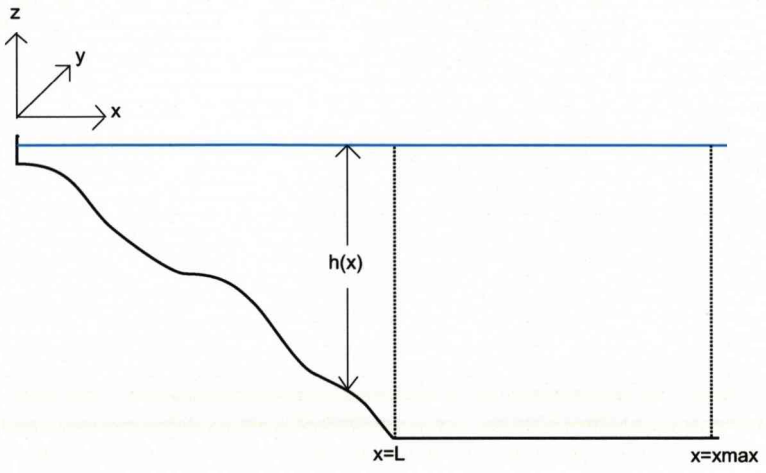

Figure 2.18: Model geometry for the BIGLOAD2 free surface baroclinic model.

from topography as the 'restoring force' for the coastal trapped wave, and a resulting increase in wave speed.

2.4.1 Background equations

The governing equations of motion for the baroclinic case in the bulk of the ocean are;

$$\epsilon u_t - fv = -\frac{1}{\rho_0} p_x \tag{2.21}$$

$$v_t + fu = -\frac{1}{\rho_0} p_y \tag{2.22}$$

$$0 = -p_z - g\rho \tag{2.23}$$

$$u_x + v_y + w_z = 0 \tag{2.24}$$

$$\rho_t + w\rho_{0z} = 0 \tag{2.25}$$

where u, v and w are the velocity components in the respective x, y and z directions. The Coriolis parameter is f, g is the acceleration due to gravity and the pressure is p. Density is defined as;

$$\hat{\rho}(x,y,z,t) = \rho_0(z) + \rho(x,y,z,t) \tag{2.26}$$

The Boussinesq approximation is made throughout. All variables vary as $e^{i(\omega t+ly)}$ so that the equations above reduce to (Brink and Chapman, 1985);

$$0 = p_{xx} + \frac{2f\beta}{(f^2-\epsilon\omega^2)}p_x - p[-\epsilon l^2 + \frac{l\beta}{\omega} - \frac{2f^2\beta l}{\omega(f^2-\epsilon\omega^2)} + (f^2-\epsilon\omega^2)(\frac{p_z}{N^2})_z] \tag{2.27}$$

where $\beta = \frac{df}{dy}$ subject to;

$p_z + \delta\frac{N^2}{g}p = 0$ at $z = 0$
$w + h_x u = 0$ at $z = -h(x)$
$u = 0$ at $x = 0$
$u_x = 0$ at $x = xmax$

The parameter δ decides whether the rigid lid or free surface conditions are used (Brink and Chapman, 1985) and the ϵ value is set as either the long-wave approximation (0) or general frequency and wavenumber (1). For all our experimentation we are solving for a free surface in the long-wave limit and therefore (2.27) reduces further to;

$$0 = p_{xx} + \frac{2\beta}{f}p_x - p[\frac{l\beta}{\omega} - \frac{2\beta l}{\omega} + f^2(\frac{p_z}{N^2})_z]$$

2.4.2 Model limitations

There are a number of limitations in this model which must be taken account of when analysing the model results (Brink and Chapman, 1985) ;

1. The barotropic Kelvin wave will generally have no zero crossings in pressure, the first coastal trapped wave will have one and so on. However, isolated pockets of reversed sign in p will exist; these extraneous crossings represent numerical error.

2. The program does not work well when the shelf-slope width is small relative to the first internal Rossby radius of the deep ocean.

3. The program's performance is suspect near $\omega = f$ as a spurious mode exists for $\beta = 0$ and $\omega = f$ which has $p = p_0 e^{-lx}$ with $p_z = 0$

4. For $\omega = f$ the inertia-gravity wave continuum is quantised by the offshore boundary condition and the results are useless.

5. The program has trouble finding the deep ocean barotropic Kelvin wave.

The limitation of the model in finding the deep ocean barotropic Kelvin wave means that the very fast adjustment timescale found for this wave mode in the barotropic limit is lost and this should be noted carefully.

2.4.3 Mode finding

In the case of BIGLOAD2 output the diagnostic which describes the mode most adequately is the pressure field. The mode 0 coastal trapped mode, the barotropic Kelvin wave, has no crossings in pressure, the mode 1 coastal trapped wave has a single zero crossing and so on. To obtain the wave speed relevant to each mode the solution had to be run at the frequency range relevant to that mode.

Early studies by Brink (1982a) and Battisti and Hickey (1984) found good comparisons with observations using single mode analysis, however, Clarke and van Gorder (1986) argued that seven or more modes were required for accuracy. In his study of hindcasting currents off Northern California Chapman (1983) found no improvement in results when more than three modes were used and Lopez and Clarke (1989) concluded that wave propagation becomes umimportant for higher modes.

Due to the difficulties involved in mode finding outlined above we shall largely restrict our results to the mode 1 wave over the full basin analysis; however, single profile analysis will be completed for the first three modes as in the barotropic experiments.

2.4.4 Idealised study: horizontal structure

As with the free surface barotropic experiments it is useful to carry out a number of idealised experiments to simplify the problem and allow for comparison with the previous experimentation. We will first look at a single profile at the control latitude of $25°N$ to investigate the detailed modal structure and propagation speed of the waves over the *slope*, *shelfslope* and *wideshelf* topography.

Stratification input

The BIGLOAD2 model requires a buoyancy frequency profile (N^2) as a stratification input. The N^2 value is calculated from the following equation;

$$N^2 = \frac{-g}{\rho}\frac{\delta\rho}{\delta z} \tag{2.28}$$

where g is the acceleration due to gravity and ρ is the potential density. The BIGLOAD2 setup requires a single N^2 input for each depth level at the offshore boundary. A N^2 value of $2.41 \times 10^{-4} s^{-2}$ was utilised for the single profile analysis at $25°N$; this value was extracted from full basin idealised stratification profiles used later in Section 2.4.5 that vary linearly from weaker stratification at high latitudes to stronger stratification at low latitudes.

Mode analysis

The first three modes were found for each of the topographic cases and their pressure field analysed (Figs 2.19, 2.20, 2.21). As described previously, the mode 1 coastal trapped wave will have one crossing in pressure, the second mode will have two crossings and so on. The mode 0 barotropic Kelvin wave would have no zero crossings in pressure but as the BIGLOAD2 model has problems finding this mode we do not expect to find it in our analysis. The normalised sea surface pressure for each mode (normalised by the division of all sea surface pressure values by the root mean square) was extracted and can be compared to the normalised sea surface elevation values in the barotropic experiments. The wave speeds relevant to each mode of the topographic cases were also calculated.

In all three cases we can see from the horizontal structure of the mode 1 wave that it is a coastal Kelvin wave. The *shelfslope* and *wideshelf* mode 1 wave speeds are indeed very close (30.30 ms^{-1} and 29.31 ms^{-1} respectively) to the coastal Kelvin wave speed of 31.32 ms^{-1} we would expect with a shelf depth of 100 m, and relative remoteness of the coastal wall from the topography. The *slope* mode 1 appears to have been modified by the slope region which has resulted in a reduced wave speed of 15.20 ms^{-1}. These results for the mode 1 wave compare closely to the mode 1 wave found in the free surface, barotropic experiment (slope mode 1 wave speed = 14.09 ms^{-1}) both in terms of wave structure and speed, for all the topographic cases.

The mode 2 wave of the free surface, baroclinic experiment is close to the mode 2 wave of the barotropic solution with a very similar horizontal structure (Fig 2.19 and 2.20). The wave speeds associated with this mode are somewhat higher in the baroclinic case, 4.87 ms^{-1} compared to 3.97 ms^{-1} for the *slope* case, suggesting that the inclusion of stratification allows the slope to support a faster mode 2 wave than in the barotropic limit. However, the modal pressure field plots show us that the wave modes retain a rather barotropic nature as the nodes do not deviate greatly from the vertical.

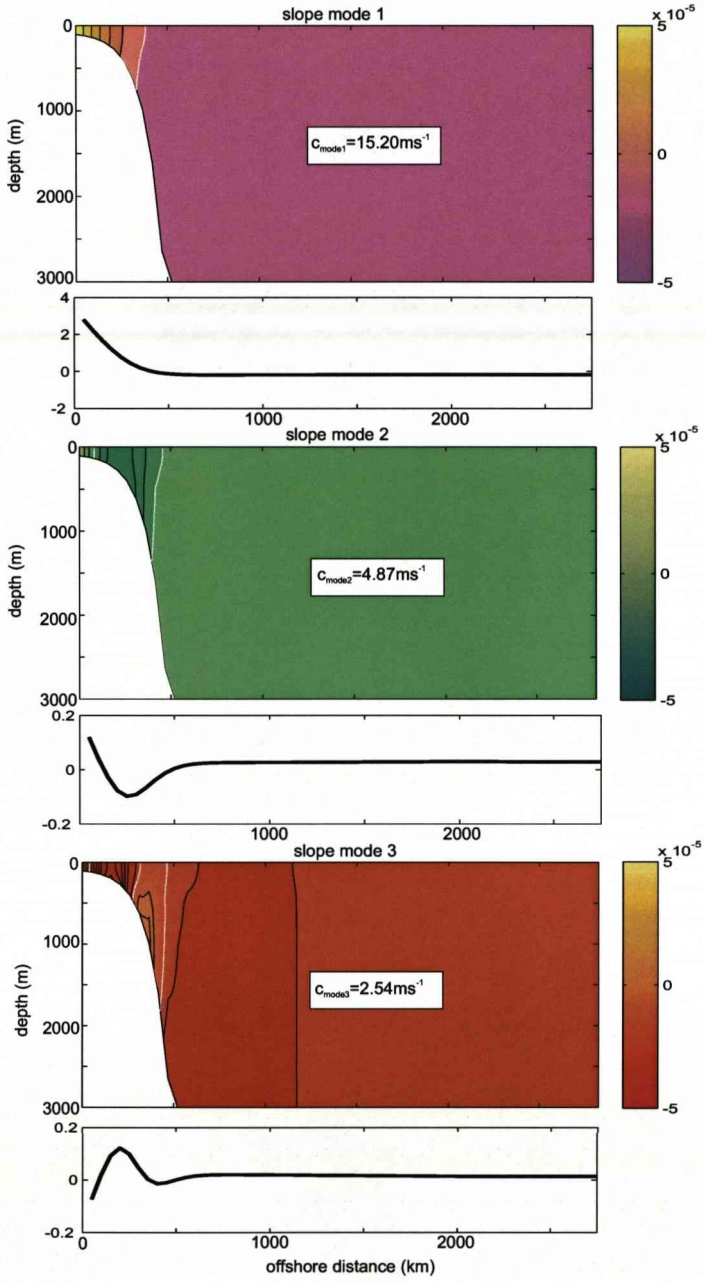

Figure 2.19: Pressure field (with arbitrary scaling) and normalised sea surface pressure for mode 1 (top), mode 2 (middle) and mode 3 (bottom) waves over the *slope* topography. The zero crossing in pressure is highlighted in white on each pressure field. The wave speed of each mode is superimposed on the pressure field in a white box.

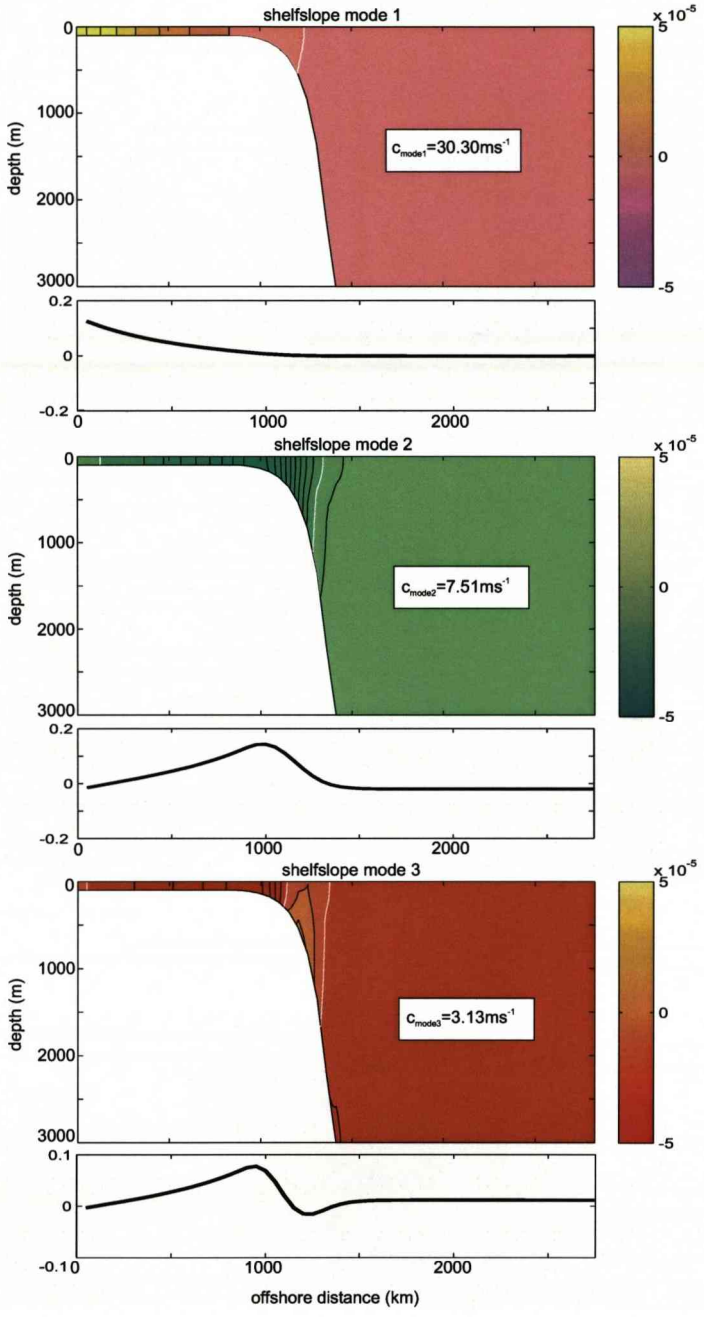

Figure 2.20: Pressure field (with arbitrary scaling) and normalised sea surface pressure for mode 1 (top), mode 2 (middle) and mode 3 (bottom) waves over the *shelfslope* topography. The zero crossing in pressure is highlighted in white on each pressure field. The wave speed of each mode is superimposed on the pressure field in a white box.

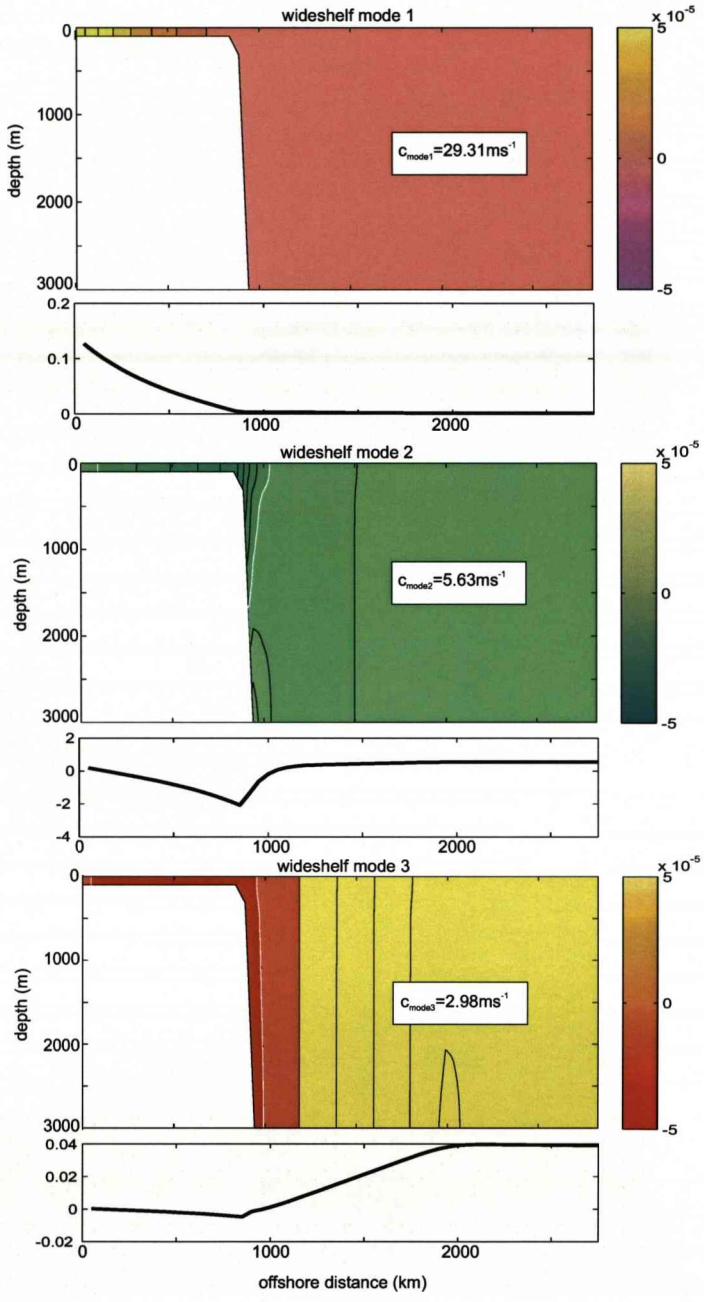

Figure 2.21: Pressure field (with arbitrary scaling) and normalised sea surface pressure for mode 1 (top), mode 2 (middle) and mode 3 (bottom) waves over the *wideshelf* topography. The zero crossing in pressure is highlighted in white on each pressure field. The wave speed of each mode is superimposed on the pressure field in a white box.

2.4.5 Full basin idealised modes

After gaining an insight into the modal wave structure at a single latitude we will now look at the wave speed profiles for the whole basin and compare these with the barotropic results. The outcome of the barotropic experiments was that the mode 0 barotropic Kelvin wave became faster towards the equator and the other modes tended towards zero. As this mode is not captured in this stratified experiment can we expect all of the available modes to tend towards zero at the equator?

Idealised stratification profiles were calculated up to $45°N$ with stronger stratification at the equator (maximum $N^2 = 3.5 \times 10^{-4} s^{-2}$) linearly decreasing to weaker stratification at high latitudes (minimum $N^2 = 1.5 \times 10^{-4} s^{-2}$). This idealised stratification was then run along with the *slope* topography and the first three wave modes located and their wave speeds extracted (Fig 2.22). It was not possible to locate any wave modes at latitudes below $5°N$, due to difficulties in locating the roots of the solution at these low f values, so those latitudes were excluded.

Fig 2.22 shows the propagation speed of the first three modes relevant to the *slope* topography and we can clearly see that all three modes slow down towards low latitudes although modes 2 and 3 at least do not appear to be tending to zero speed. It seems that in the region where it is difficult to find solutions is precisely the region where stratification is suspected to become the dominant factor. This means that, unfortunately, we cannot resolve the question of how the waves behave on approaching the equator, thus enhancing the suspicion that nonlinear processes are likely to become important.

Effect of a steepening topography in a stratified ocean

The results of the barotropic solution when tested with a variable topographic length scale Δx over the *slope* topography (at $25°N$) showed that the mode 1 coastal Kelvin wave slowed with a greater Δx whereas the mode 2 wave increased in speed. We could expect the difference in wave speed corresponding to a varying Δx to be reduced in the stratified model, as the wave speeds are partly governed by stratification.

The results for the mode 1 coastal Kelvin like wave are similar to the barotropic model (Fig 2.23) with a decreasing wave speed associated with an increase in Δx values. As expected the decrease in wave speed is around 20% less in the baroclinic ocean indicating the influence of the stratification restoring force.

Although the mode 2 wave speed does increase with increasing Δx at high latitudes this is not the case at lower latitudes. Equatorwards of around $20°N$ we see a reversal

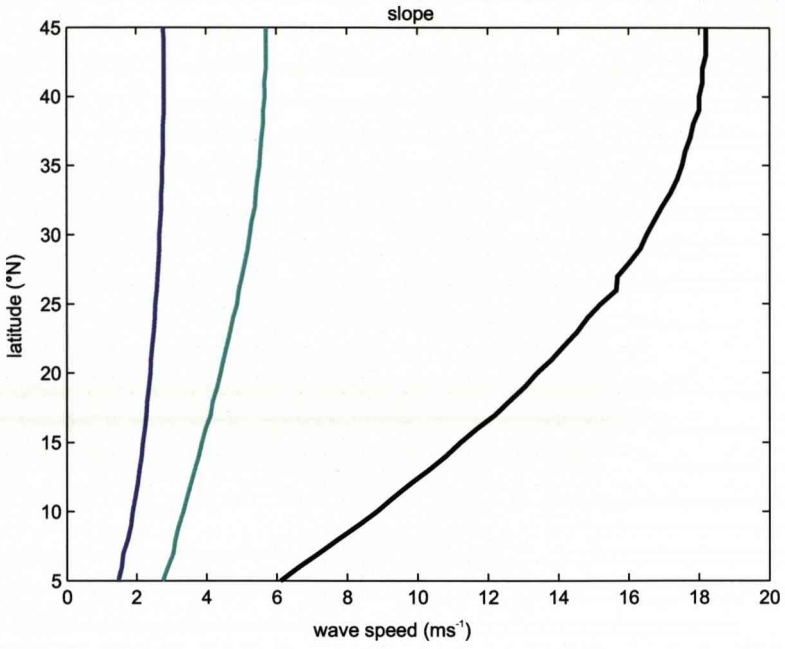

Figure 2.22: Propagation speed of mode 1 (black), mode 2 (cyan) and mode 3 (magenta) waves from $5°N$ to $45°N$ for the *slope* topography.

and wave speeds decreasing as the topographic length scale is reduced (Fig 2.23). We returned to the barotropic result and ran a full basin speed analysis for the mode 2 wave to determine whether this reversal occurs at lower latitudes in the barotropic ocean also; this was not the case with an increase in wave speed associated with increasing Δx for all latitudes.

This result suggests that in the baroclinic limit the stratification restoring force becomes dominant at latitudes less than around $20°N$. However, the effect of a decreasing f parameter does still appear to dominate within the equatorial region resulting in the wave speeds reducing. In the vertical sidewall case c is the Kelvin wave speed which varies in latitude only to the extent that the stratification varies.

2.4.6 Free surface, baroclinic solution: summary of results

The results found for the free surface baroclinic solution are very similar to those of the free surface barotropic experiment with the exception of the lack of the fast deep ocean or double Kelvin wave, which BIGLOAD2 has trouble finding. The mode 1 and mode 2 wave speeds were somewhat higher than the corresponding modes in the barotropic limit indicating the effect of the stratification restoring force. We could then expect these wave mode speeds to increase with stronger stratification nearer the equator but,

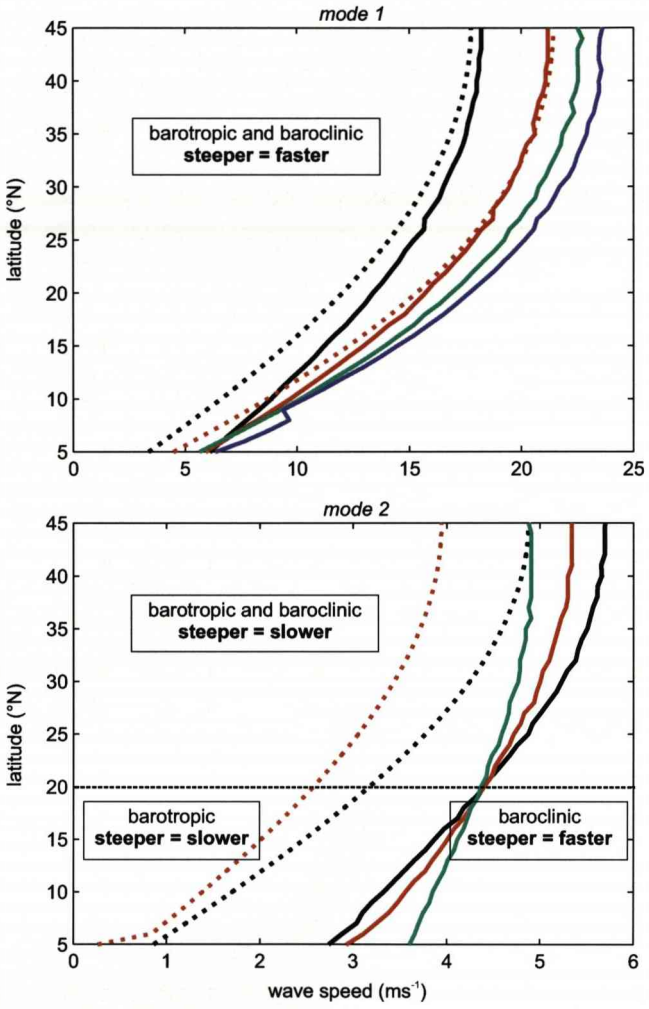

Figure 2.23: Propagation speed of the mode 1 (upper) and mode 2 (lower) waves for the *slope* topography for Δx (relevant to $25°N$) of 25 km (magenta), 34 km (green), 50 km (red) and 100 km (black). The corresponding barotropic wave mode speeds are superimposed (dotted lines). Note that solutions could not be found for $\Delta x = 34$ km and 25 km in the barotropic case for either mode or $\Delta x = 25$ km for the baroclinic mode 2. The steeper definition refers to the steepness of the slope.

for our parameters the effect of the decreasing f parameter dominates over the effect of increasing stratification in the regions where solutions can be found.

2.5 Chapter summary

The idealised experiments, both in the barotropic and baroclinic limit, have provided us with a great deal of insight into the mechanism of propagating coastal trapped waves in a model Atlantic Ocean and an estimation of adjustment timescales that we could expect within the real ocean. The key findings of the chapter are summarised:

- It is clear from these idealised studies that the inclusion of topography supports qualitatively different wave modes which travel at differing speeds: the mode 0 barotropic deep ocean or double Kelvin wave; the mode 1 coastal Kelvin wave on the shelf, and a number of higher coastal trapped modes supported by the presence of a sloping topography. A number of the modes found propagate significantly faster than the baroclinic Kelvin waves in JM02;
- The barotropic mode 0 wave would propagate around the ocean basin in a matter of days. The mode 1 and mode 2 waves would have adjustment timescales of weeks to months.
- The mode 1 and 2 coastal trapped wave speeds decrease towards the equator and to zero in the barotropic limit, to the extent where solutions can be found, suggesting that nonlinear processes may become important at low latitudes. This behaviour may result in a delay to the adjustment of the rest of the ocean. The barotropic mode 0 wave speed increases towards its theoretical maximum at the equator.
- A similar complicated coupling between equatorial Kelvin waves and predominantly barotropic CTW is likely to occur at the eastern boundary since part of the signal is carried by the barotropic mode.
- The inclusion of stratification appears to reduce the modifying effect on wave speed associated with proximity to, and steepness of, the topography. In addition, the restoring force associated with stratification allows for faster coastal trapped modes, especially at lower latitudes.
- The effect of stratification is, however, dominated by the effect of a decreasing f parameter, in regions where a solution can be found.

An estimation of the likely wave modes and associate adjustment timescales in an idealised topographic basin has been found and outlined above. The next chapter

will integrate realistic topographic and stratification profiles into both the barotropic and baroclinic models used in this chapter to determine whether similar wave mode structures and speeds are found under realistic conditions. A General Circulation Model (GCM) will then be utilised in Chapter 4 to investigate the response of an idealised topographic ocean to forcing and determine whether the wave modes found here can explain the adjustment patterns found.

Chapter 3

Realistic wave mode studies

3.1 Introduction

The idealised solutions of wave modes over a number of idealised topographies, and under idealised stratification conditions, provided a clear indication of the wave mode structures and speeds we could expect over regions of topography in both the barotropic and baroclinic limits. Given these findings we now seek to test the solutions given realistic values of topography and stratification extracted from Atlantic Ocean data sets. This will allow us to determine whether the theories of adjustment patterns and timescales suggested in Chapter 2 are feasible in the real ocean. As the rigid-lid barotropic solution does not allow for Kelvin waves it was deemed unnecessary to test the realistic scenario under the rigid lid conditions.

We will firstly describe the method used to extract a number of realistic topographic profiles from an Atlantic Ocean gridded topography data set in Section 3.2. A description of the profile processing, and resulting deviations from a true realistic picture, will also be outlined here along with an assessment of whether the idealised topographies of Chapter 2 are representative of the realistic profiles.

The free surface barotropic solution will then be solved over a number of the realistic profiles in Section 3.3 and the resulting wave modes compared to those determined in the idealised scenarios. We would expect to find broadly similar mode properties in terms of a very fast barotropic mode 0, fast coastal trapped mode 1 and slower topographic slope trapped mode 2. However, the more complicated topography of the realistic ocean could potentially result in greater modification of all wave modes especially in terms of their propagation speed. The behaviour of the wave modes at lower latitudes in the realistic ocean will be of particular interest to determine whether the same pattern of decreasing wave mode speed with a decreasing f parameter remains, with the exception of the mode 0 wave.

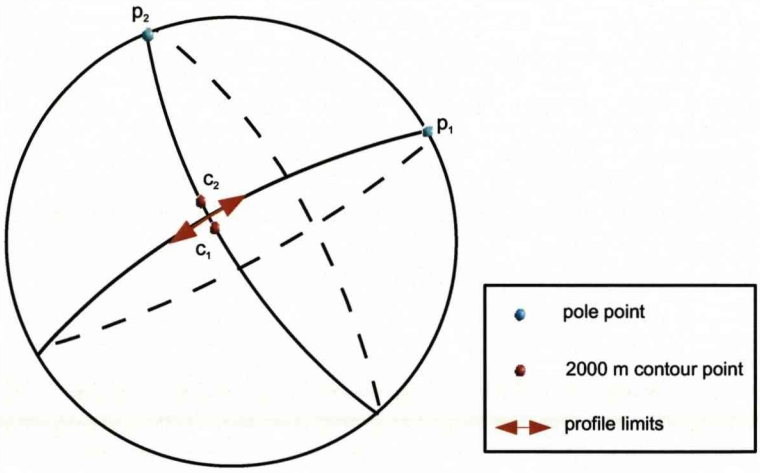

Figure 3.1: Diagram showing the two 2000m depth contour points, c_1 and c_2, along a great circle and the corresponding perpendicular great circle with pole points p_1 and p_2.

Finally, the free surface baroclinic solution, using the BIGLOAD2 model, will be calculated with realistic topography and stratification conditions (Section 3.4); the details of the calculation of realistic stratification and associated uncertainties will be outlined firstly. In Chapter 2 we concluded that stratification did appear to reduce the effect of topography, as well as providing an additional restoring force, and as such we can predict that this effect will be greater over more detailed and rougher topographic profiles. Single profile analysis, using the same profiles as for the barotropic experiment, will be carried out alongside an analysis over the full realistic domain to gain an insight into wave mode behaviour as we travel from north to south along the western boundary. Again the effect of a decreasing f parameter on the coastal trapped wave modes will be examined with interest.

The results of these realistic experiments, in both the barotropic and baroclinic cases, will be summarised in Section 3.5 and a suggestion of the adjustment patterns and timescales that could be expected in the real ocean will be outlined.

3.2 Method of extracting topographic profiles

A set of realistic topographic profiles at regular intervals down the western boundary was required to calculate wave modes relevant to realistic topographic profiles extracted along the western boundary of the Atlantic Ocean (Fig 3.2). This was achieved using a vector method for extracting points along the section of a great circle perpendicular to a great circle joining two initial points on the 2000 m depth contour (Fig 3.1).

Consider the vectors $c1$, $c2$, $p1$, $p2$ illustrated in Fig 3.1. These are vectors measured from the centre to points on the surface of a unit sphere. The pole point for the great circle between the two 2000 m depth contour points, $\mathbf{c_1}$ and $\mathbf{c_2}$ is;

$$\mathbf{p_1} = \frac{\mathbf{c_1} \wedge \mathbf{c_2}}{|\mathbf{c_1} \wedge \mathbf{c_2}|}$$

The pole point for the great circle perpendicular to the coast is $\mathbf{p_2}$ which is found from;

$$\mathbf{p_2} = \mathbf{c_1} \wedge \mathbf{p_1}$$

Any point on this second great circle is required;

$$|\mathbf{x}| = \mathbf{1}$$

$$\mathbf{x}.\mathbf{p_2} = \mathbf{0}$$

and therefore;

$$\mathbf{x} = \mathbf{c_1} \cos\lambda + \mathbf{o} \sin\lambda$$

where λ is the latitude, $\mathbf{o}$ is a vector perpendicular to $\mathbf{c_1}$ and perpendicular to $\mathbf{p_2}$ therefore $\mathbf{o} = \mathbf{p_1}$ and;

$$\mathbf{x} = \mathbf{c_1} \cos\lambda + \mathbf{p_1} \sin\lambda$$

Then for $\mathbf{x}$=$[x, y, z]$ the co-latitude (θ) and longitude (ϕ) values can be found as follows;

$$z = \cos\theta => \theta = \cos^{-1} z$$

$$x = \sin\theta \cos\phi => \phi = \cos^{-1}(\frac{x}{\sin\theta})$$

These co-ordinates are then used to extract the depth value at each point from a global one minute interval bathymetric grid (BODC, 2003); the resolution of the extracted profiles is 1.27 km. The extent of the extraction of the realistic profiles was limited by the increasing complexity of the bathymetry as indicated on Fig 3.2.

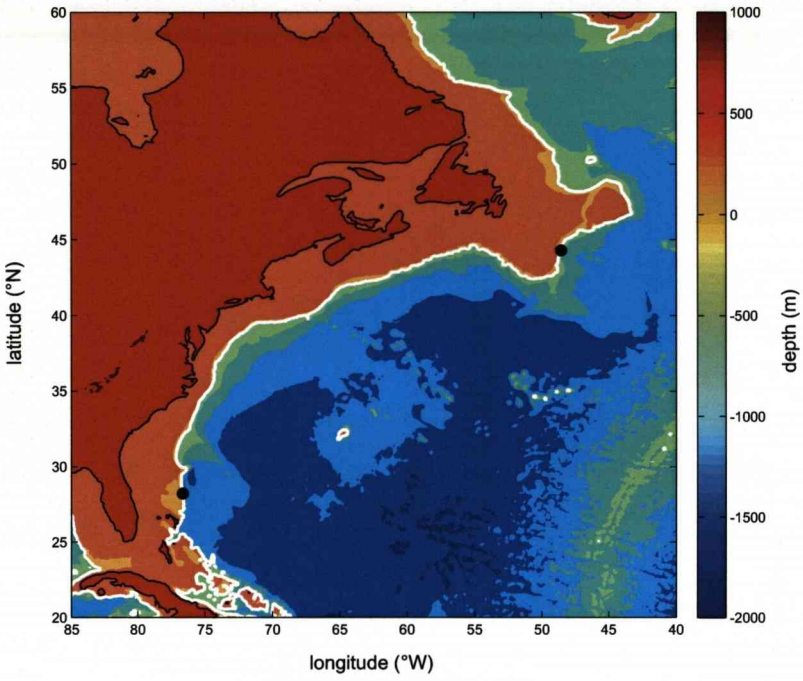

Figure 3.2: The Atlantic Ocean bathymetry data set (BODC, 2003) from which the realistic topographic profiles utilised in the realistic wave mode calculations were extracted. The $-2000\ m$ contour is highlighted in white and the maximum and minimum latitude points corresponding to the northern and southerly extent of the profiles are indicated by the two black dots.

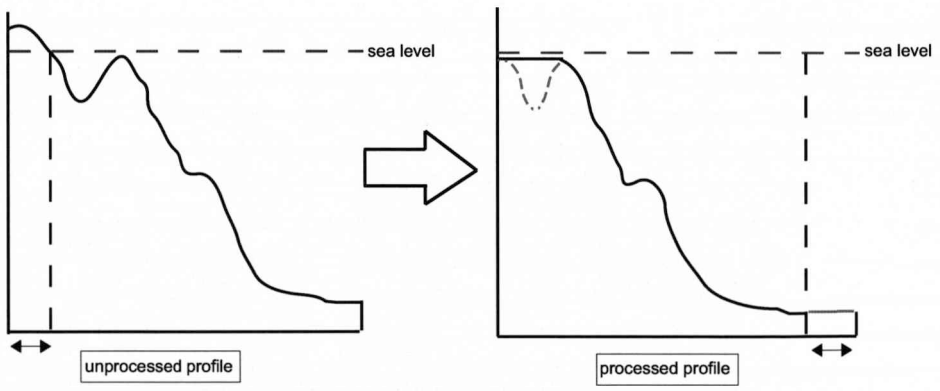

Figure 3.3: An illustration of unprocessed and processed profile where all values above sea level and any negative gradients removed.

3.2.1 Processing

In order for all the profiles to be of equal length in x and to eliminate any depth values above sea level some further processing was required. The number of values above sea level were counted and then this number of values added to the end of the profile. The additional values were then set to the depth value of the last point of the unprocessed profile (Fig 3.3). We also removed any negative gradients in the profiles in order to avoid channel like structures on the shelf region.

Around the mouth of the St Lawrence estuary and off Newfoundland, where the shelf is wide, a wall was inserted in order to extract the topographic profile as described above as the profile would otherwise never reach land while on the shelf. The maximum allowable distance of land from the 2000 m contour is limited to 446 km, that is half of the total profile length of 892 km with a horizontal resolution of 1.27 km. This was achieved by setting the first two values of each profile to a value above sea level. The estuary is thus ignored eliminating the possibility of trapped modes.

This additional processing does mean the resulting topographic profiles are not completely true to reality; however, it should allow for ease of numerical calculation and is necessary to fulfil the conditions assumed by the solution methods.

The processed profiles are plotted in three dimensions in Fig 3.4. There is a large degree of variation between the profiles in terms of shelf width, shelf depth and slope shape. As we determined in Chapter 2, changing shelf-slope properties, such as shelf width and depth, do result in modification of the wave mode characteristics. Therefore we can expect the variability in the realistic profiles to cause significant differences between the realistic wave modes.

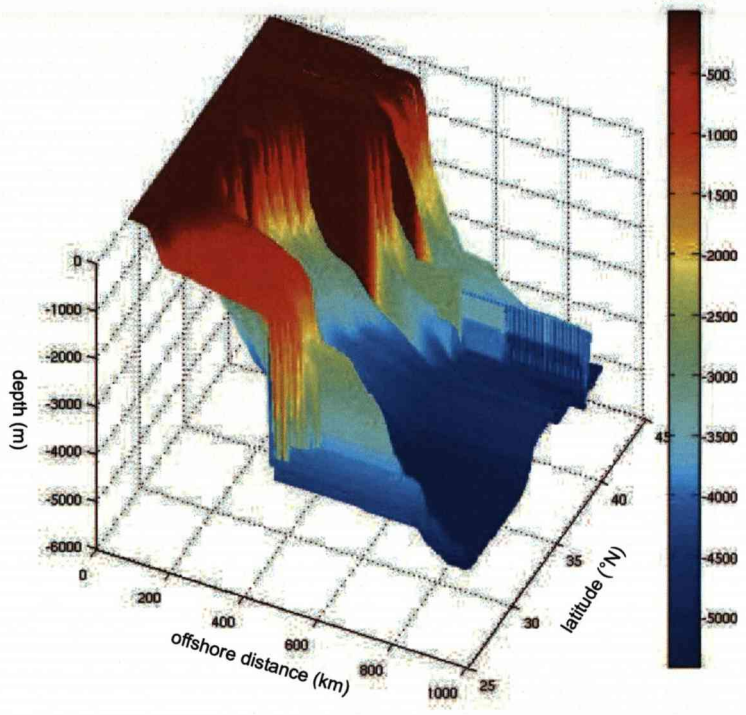

Figure 3.4: A three dimensional plot of the realistic profiles as a function of their midpoint latitude and offshore extent, which is equal for all profiles.

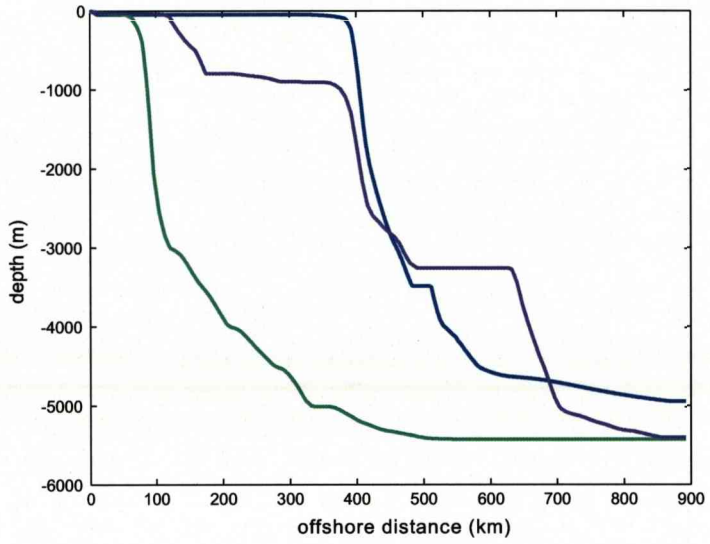

Figure 3.5: The three topographic profiles utilised for the single profile mode analysis in both barotropic and baroclinic solutions; *narrow shelf* (green line), *wide shelf* (blue line) and *three step* (magenta line).

3.3 Realistic, free surface, barotropic solution

3.3.1 Introduction

The free surface, barotropic solution does not allow for stratification resulting in the exclusion of the baroclinic Kelvin wave and hybrid coastal trapped waves that will exist in a realistic ocean. However, the results of Chapter 2 suggest the barotropic solution provides a good approximation of the mode 0 and mode 1 waves over idealised topography and allows for a simpler solution before moving directly to a fully realistic solution in terms of both topography and stratification.

3.3.2 Realistic single profile analysis

Three realistic profiles were chosen representing a *narrow shelf* at $34.36°N$, a *wide shelf* at $40.50°N$ and a more complicated *three step* profile at $30.95°N$ (Fig 3.5). The *narrow shelf* and *wide shelf* profiles have very similar slope shapes but differ greatly in terms of shelf width. The *narrow shelf* example can be compared to the *slope* example of Chapter 2 at the lower depth range and the *wide shelf* profile may be compared with the *shelfslope* profile utilised in Chapter 2. None of the idealised topographic profiles

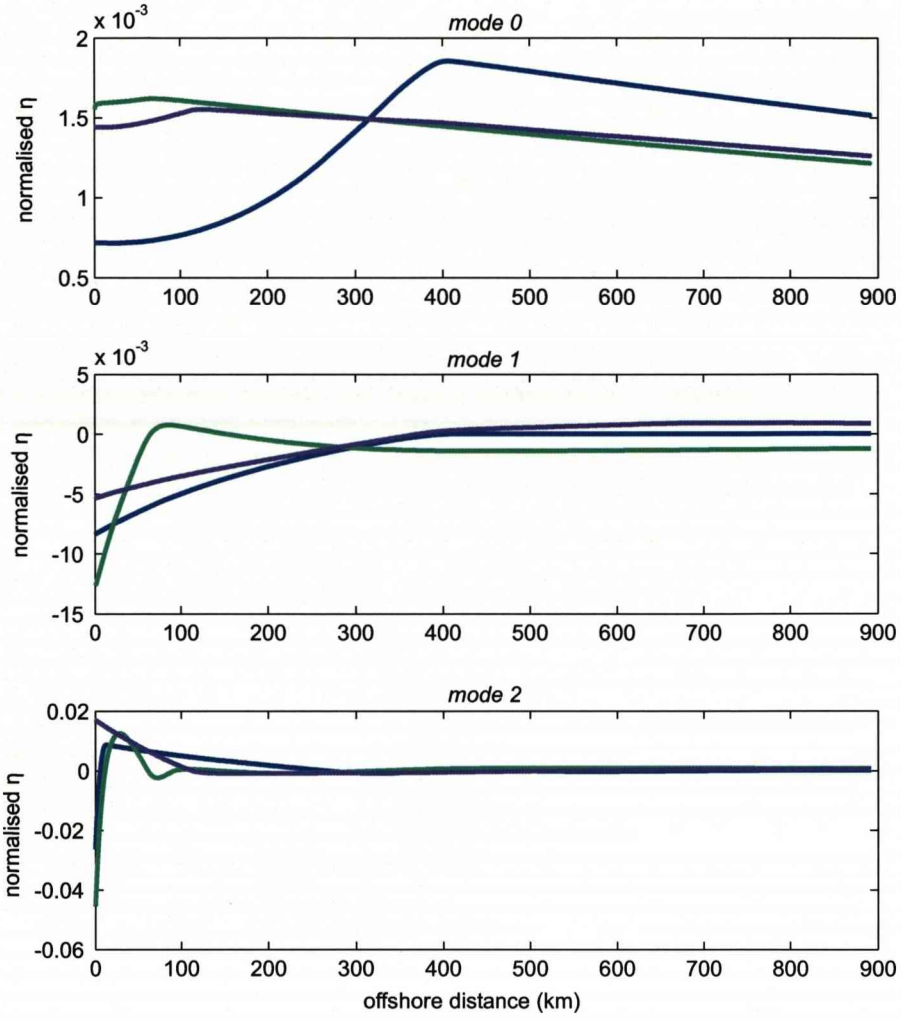

Figure 3.6: The normalised sea surface elevation, η, for all modes for each of the single profiles; *narrow shelf* (green line), *wide shelf* (blue line) and *three step* (magenta line).

can be compared to the *three step* profile in use here as a result of its rather complicated nature. The free surface barotropic solution was then run for each of these profiles.

The horizontal structure of the first three wave modes for the three test profiles is shown in Fig 3.6 and the corresponding wave mode speeds are shown in Table 3.1.

Narrow shelf wave modes

The *narrow shelf* mode 0 wave structure resembles a deep ocean Kelvin wave with a propagation speed of 216.89 ms^{-1}, compared to the theoretical value of 230.21 ms^{-1}, suggesting a relatively small modifying effect by the topography. The mode 1 wave

structure has similarities to that of a coastal Kelvin wave, however, modification has occurred and this is reflected in the wave speed of this mode. With the relevant shelf depth of 40 m the theoretical coastal Kelvin wave speed would be 19.81 ms^{-1}, however, the narrow shelf mode 1 wave speed is only 3.56 ms^{-1}. This suggests a large amount of modification due to proximity, and relative steepness, of the topography to the coastal wall.

Profile	c_0 (ms^{-1})	c_1 (ms^{-1})	c_2 (ms^{-1})
narrow shelf	216.89	3.56	0.52
wide shelf	191.63	18.15	0.39
three step	196.23	16.18	6.39

Table 3.1: The mode 0, mode 1 and mode 2 wave speeds (c_0, c_1 and c_2 respectively) corresponding to each of the single topographic profiles under analysis.

A similar result was found for the idealised *slope* example in the case of small shelf width and a steep slope although the reduction in mode 1 wave speed was not as large. The mode 2 wave in the realistic *narrow shelf* is also considerably smaller than in the idealised experiment possibly as the result of rougher topography modifying the wave modes to a greater extent.

Wide shelf wave modes

The mode 0 wave of the wide shelf profile has a clear double Kelvin wave structure with a speed of 191.63 ms^{-1} while the mode 1 wave is clearly a coastal Kelvin wave. The mode 1 wave speed, c_1, in this case is close to the theoretical value of 21.47 ms^{-1}, relevant to a shelf of depth 47 m as a result of the relative remoteness of the topography to the coastal wall; this pattern was also seen in the *shelfslope* example of Chapter 2. The slope of the wideshelf profile is steep and this may help explain the low wave speed of the mode 2 wave of only 0.39 ms^{-1} as the profile is close to approximating the wide shelf and vertical wall solution (*wideshelf* in Chapter 2) where only two roots exist, the mode 0 double Kelvin wave and the mode 1 coastal Kelvin wave.

Three step profile wave modes

Mode 0 of the more complicated *three step* topographic profile also has a double Kelvin wave like structure corresponding to the first shelf region. The mode 0 wave speed of 196.23 ms^{-1} is again approaching the theoretical value of 229.73 ms^{-1} suggesting relatively limited modification of the wave speed despite a much narrower shelf than is the case in the *wideshelf* example.

The mode 1 wave speed of 16.18 ms^{-1} is again close to the theoretical value of 19.81 ms^{-1} corresponding to the depth of the first shelf region and has a coastal Kelvin wave like structure. However, it appears to fill the shelf-slope region to the extent of the shelf break of the second shelf region where the theoretical coastal Kelvin wave would have a speed of 93.96 ms^{-1}.

The mode 2 structure is clearly unlike that of the slope trapped wave mode seen in the narrow shelf experiment and instead resembles a coastal Kelvin wave over the first shelf region. This allows for a faster mode 2 wave at 6.39 ms^{-1} than in the other examples. This would suggest that the more complicated topography associated with the realistic ocean may allow for additional coastal Kelvin wave-like modes travelling at greater speeds than modes supported over the topography.

3.3.3 Full realistic wave speed analysis

An interesting result of the idealised, free surface barotropic solution was the increase of the mode 0 wave speed and corresponding decrease of the mode 1 and mode 2 wave speeds with a decreasing f parameter. Therefore we calculated the first three wave modes for the extracted realistic topographic profiles (Fig 3.7) to determine whether this result remains true in the realistic ocean and additionally to assess the degree of variation that results from changes in the topography. Additionally the considerable differences in wave modes supported in each of the single profiles analysed in section 3.3.2 suggest that we will observe a high degree of variability over the full range of realistic profiles.

It is clear from Fig 3.7 that there is a great deal of variation in wave speed between profiles for all the wave modes as suspected. However, it is evident that the mode 0 wave consistently resembles a deep ocean or double Kelvin wave, with its associated high wave speed and very fast adjustment timescale, in the case of all the realistic profiles. The mode 1 and 2 waves cannot be as clearly differentiated in terms of coastal Kelvin or slope trapped wave modes as was the case in the idealised study. This is likely to be the result of the rougher realistic topography encouraging increased variation in the structure of these wave modes. Also the solution being unable to solve for the respective mode, and therefore finding a higher or lower mode, resulting in the 'spikiness' seen in Fig 3.7.

There would appear to be a weak increasing trend in the wave speed of the mode 0 wave with decreasing latitude as in the idealised experiments. However, the most pronounced increase in mode 0 wave speed, and subsequent decrease in mode 1 and 2 speeds, occurred at latitudes below the extent of the extracted realistic topographic profiles. Therefore it is reasonable that we should not expect a strong trend in the

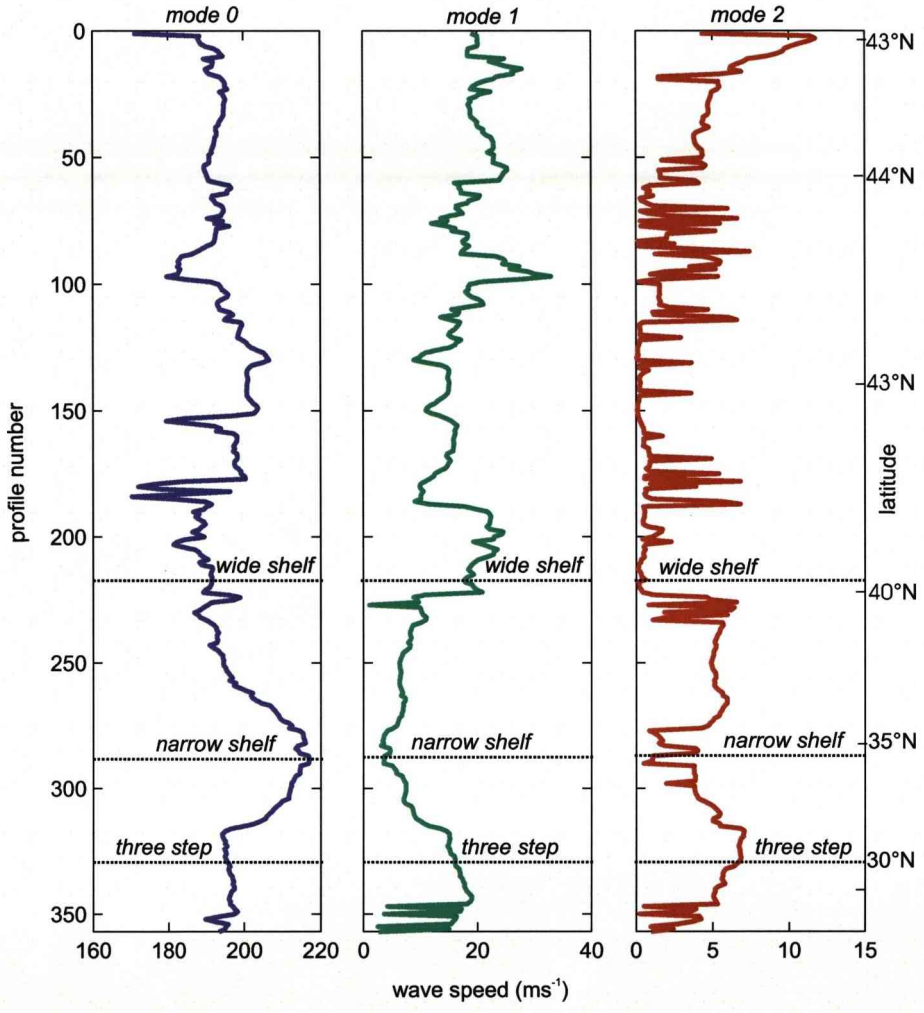

Figure 3.7: Wave speed as a function of profile latitude for the mode 0 (left-purple line), mode 1 (middle - green line) and mode 2 (right - red line) waves. The dashed black lines denote the relevant latitude of the profiles used in the single profile analysis.

realistic data; the effect of varying topography is clearly greater than the influence of f over realistic profiles.

3.3.4 Realistic barotropic solution summary

- The three wave modes identified in the idealised calculations; the mode 0 deep ocean or double Kelvin wave, the mode 1 coastal Kelvin wave and mode 2 slope trapped mode; are still found over the realistic profiles, however, a number of different modes are supported by the more variable realistic profiles.
- The mode 2 slope trapped wave modes are heavily modified in regions of steep topography resulting in significant attentuation of the mode wave speed.
- There is a great deal of variation in wave speeds between the realistic profiles suggesting the barotropic wave modes are afffected by detailed changes in the topography. However, the 'spikiness' we observe, particularly in the lower latitudes, of Fig 3.7 is likely due to the solution being unable to solve for the respective mode and therefore finding a higher, or lower, mode instead.

3.4 Free surface, baroclinic solution under realistic conditions

3.4.1 Introduction

The free surface baroclinic solution for coastal trapped wave modes can now be found using the BIGLOAD2 model (Brink and Chapman, 1985) with the realistic topographic profiles and a realistic representation of stratification conditions. The method of calculation of the stratification data is outlined firstly in Section 3.4.2. Single profile analysis will then be undertaken using the same profiles that were selected in the barotropic solution to allow for later comparison of the horizontal mode structure and wave speed.

From the idealised baroclinic experimentation of Chapter 2 we could expect a mode 1 coastal Kelvin like wave and two higher, slower, coastal trapped wave modes. In Chapter 2 we noted that the introduction of idealised stratification reduced the influence of the topography on the wave modes allowing for faster slope trapped mode 2 waves. Given the barotropic solution results of Section 3.3 showing that more realistic topography increasingly modifies the wave mode speeds we will examine whether the introduction of realistic stratification reduces the effect of topography in the realistic ocean to a greater extent than was evident in the idealised experimentation.

Finally a wave speed analysis of the full realistic topographic and stratification profile set will be undertaken for the mode 1 wave to determine whether the decreasing trend detected in the idealised experimentation is present. The results will also be compared with those of the realistic barotropic solution to evaluate the impact of stratification.

3.4.2 Calculation of stratification data

The BIGLOAD2 model requires the buoyancy frequency profile (N^2) as an input. The N^2 value is calculated from the following equation;

$$N^2 = \frac{-g}{\rho}\frac{\delta\rho}{\delta z} \tag{3.1}$$

where g is the acceleration due to gravity and ρ is the potential density.

It was therefore necessary to first calculate ρ at each level. The UNESCO (1983) algorithm was used to calculate the density of seawater given input values of temperature, salinity and pressure. This data was extracted from the Hydrobase2 database (Lozier et al., 1995) in the form of 1° annual gridded Atlantic data which has been fully interpolated and has also been through a single iteration of a smoothing filter.

The latitude, longitude and depth values along each of the topographic profiles were used to extract the corresponding stratification data. Further interpolation was required at this point largely due to the much reduced depth increment closer to shore. Any missing values were replaced with the closest real N^2 value.

The BIGLOAD2 setup requires a single N^2 input for each depth level at the offshore boundary. Therefore the N^2 value corresponding to the position of the final point of each profile for all depths was used.

3.4.3 Realistic single profile analysis

The free surface, baroclinic solution was calculated for the same three realistic topographic profiles utilised in the realistic barotropic single profile analysis. The resulting pressure fields and normalised surface pressure plots are shown in Fig 3.8, 3.9 and 3.10. The extraneous zero crossings in pressure are a result of numerical error and are noted as a limitation of the BIGLOAD2 model (Brink and Chapman, 1985). The introduction of realistic stratification alters the structure of wave modes which can no longer be clearly identified. In the idealised experiments the introduction of an idealised stratification did not result in such a pronounced modification of the mode structure.

Narrow shelf

In the *narrow shelf* example the first mode does still resemble a coastal Kelvin wave and is travelling at 16.61 ms^{-1} which is close to the theoretical value of 19.81 ms^{-1}. The barotropic solution comparable mode wave speed was heavily modified by the topography. Therefore the considerably less severe attentuation of mode wave speed in stratified case matches our expectation of stratification acting to reduce the influence of topography.

The mode 2 wave is also faster than in the barotropic limit further supporting this theory. The nodes of this mode are rather vertical and therefore suggest that this is a predominantly barotropic continental shelf wave mode. The mode 3 wave does not have a surface node and its structure is reminiscent of the baroclinic internal Kelvin like waves described by Huthnance (1978).

Wide shelf

The BIGLOAD2 model has not coped well with the wide, shallow shelf of the *wideshelf* example as shown by the numerous extraneous zero crossings in pressure over this region of the topography. As a result the mode 1 wave is not the coastal Kelvin wave that would be expected but is instead a higher coastal trapped mode that may be compared with the barotropic mode 2. In the barotropic case we found that the relatively steep topography of the wide shelf profile resulted in the first two wave modes approximating that of the single step topography and therefore a very slow slope trapped wave. The inclusion of stratification in the baroclinic case has reduced the influence of step like profile allowing for a number of higher, coastal trapped modes supported by the topography to be supported. The mode 1 coastal trapped wave speed at 5.13 ms^{-1} is considerably faster than the continental shelf mode 3 wave in the barotropic experiment.

The mode 2 and 3 waves, like the mode 3 wave of the *narrow shelf* example, are baroclinic internal Kelvin wave like modes and as such have lower wave speeds than more barotropic slope trapped wave modes in general. However, due to steep nature of the slope in this *wideshelf* example the slope trapped mode 2 wave was heavily modified in the barotropic experiment resulting in a very low wave speed. Therefore the inclusion of realistic stratification in this example has allowed a faster baroclinic mode to be supported over the steep topography.

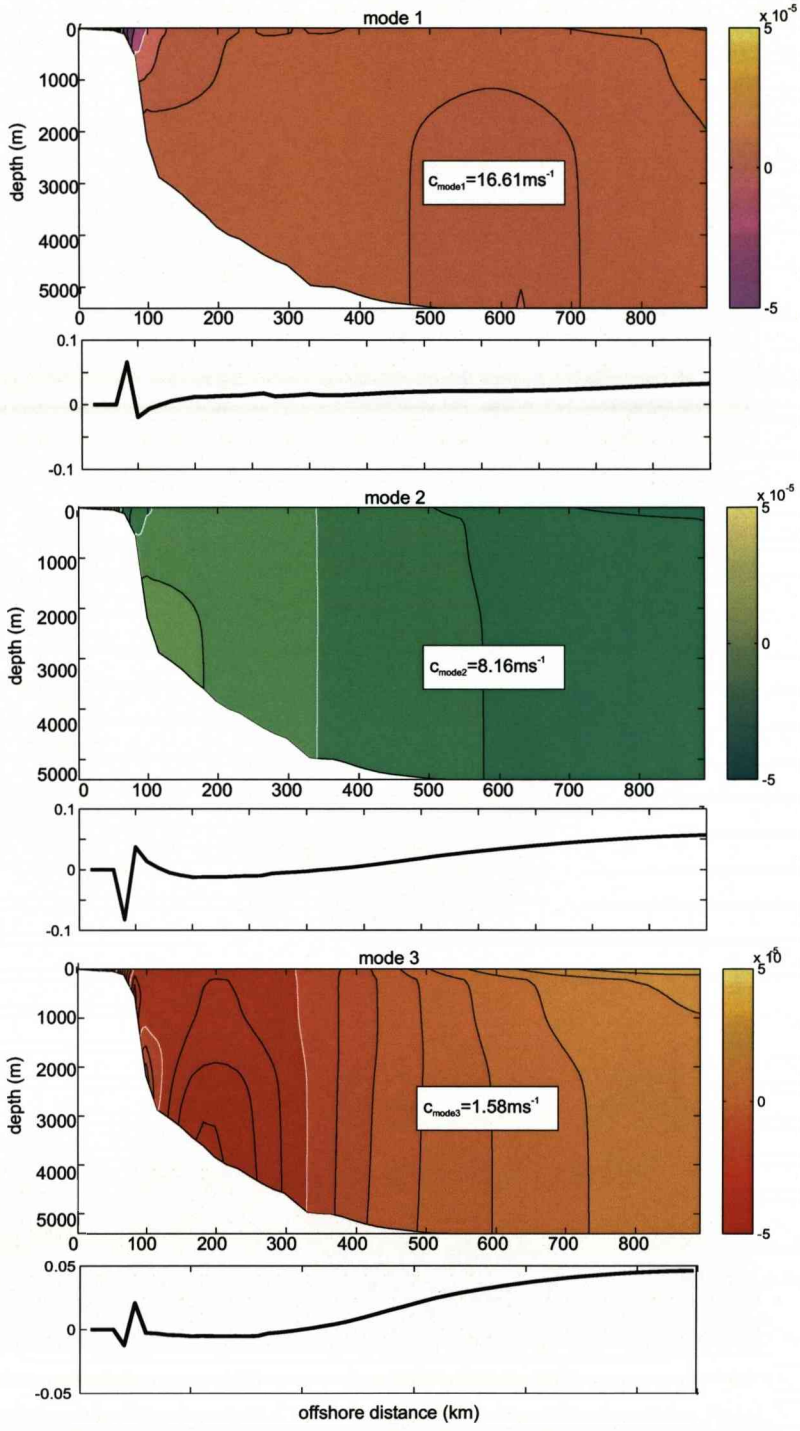

Figure 3.8: The pressure field (with arbitrary scaling) and normalised surface pressure for the mode 1 (top panel), mode 2 (middle panel) and mode 3 (bottom panel) waves with the *narrow shelf* profile at 34.36°N. The respective mode wave speed is superimposed on the pressure field relevant to each mode.

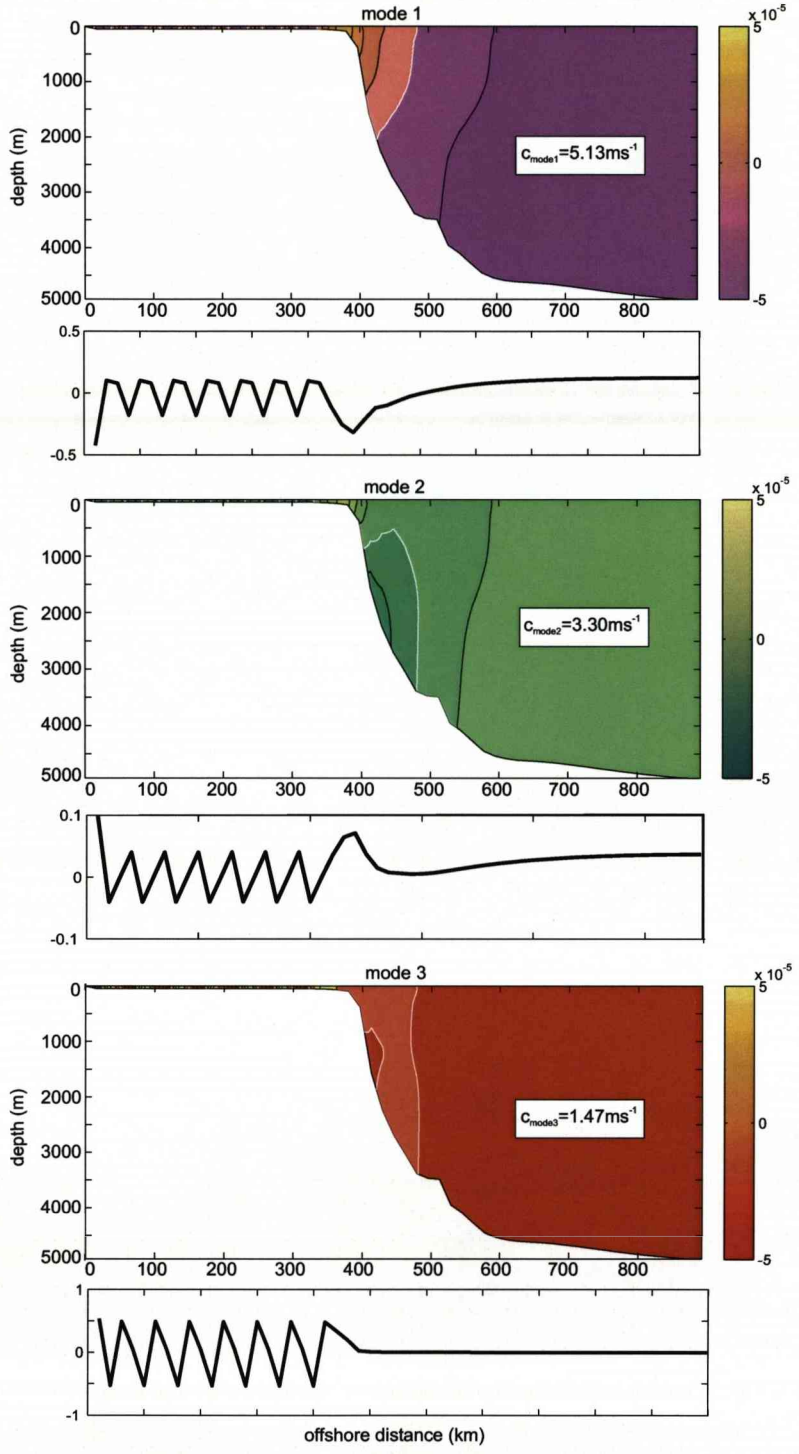

Figure 3.9: The pressure field (with arbitrary scaling) and normalised surface pressure for the mode 1 (top panel), mode 2 (middle panel) and mode 3 (bottom panel) waves with the *wide shelf* profile at $40.50°N$. The respective mode wave speed is superimposed on the pressure field relevant to each mode.

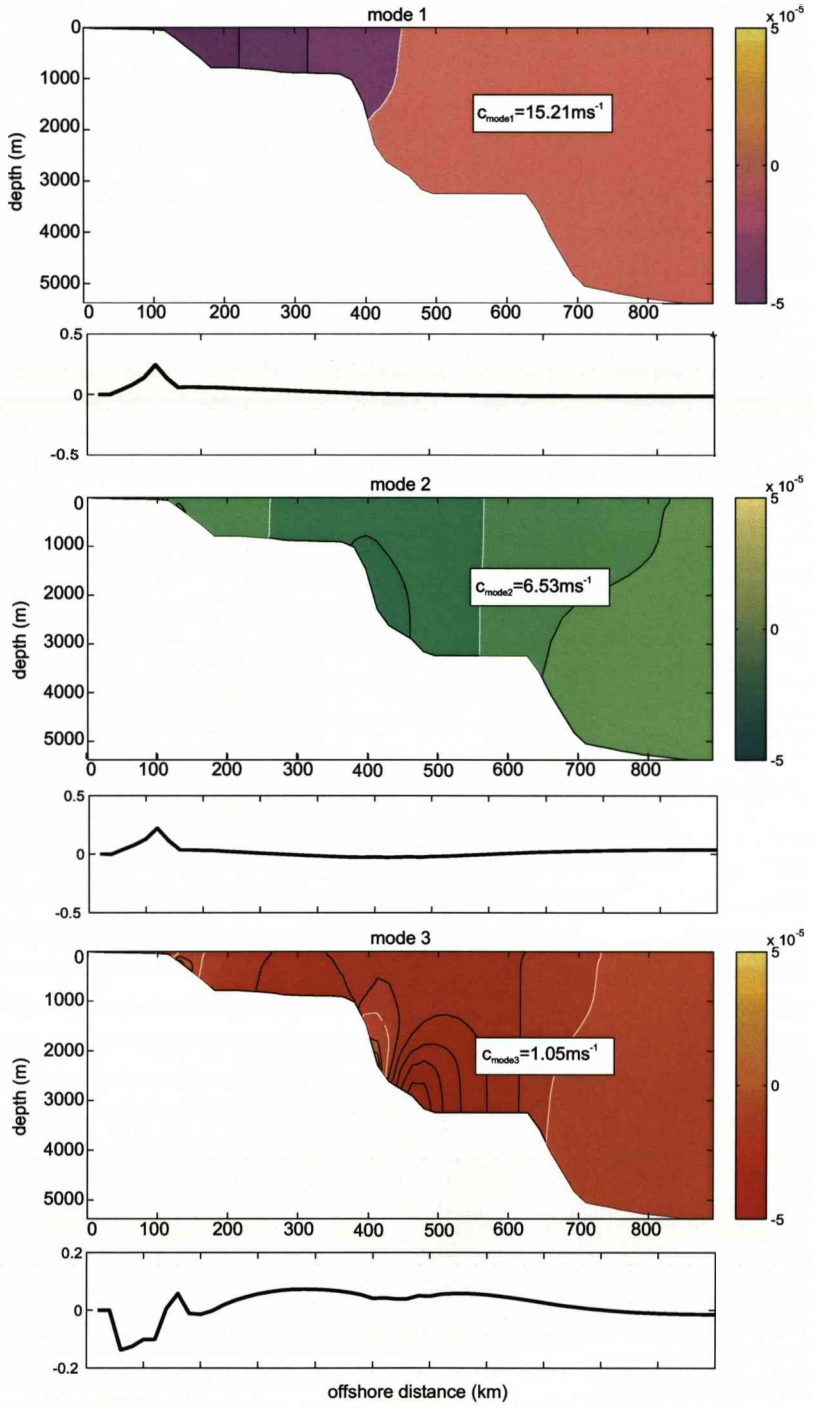

Figure 3.10: The pressure field (with arbitrary scaling) and normalised surface pressure for the mode 1 (top panel), mode 2 (middle panel) and mode 3 (bottom panel) waves with the *three step* shelf profile at $30.95°N$. The respective mode wave speed is superimposed on the pressure field relevant to each mode.

Three step topography

Again the shallow first shelf region of the *three step* profile has not been adequately solved for in the BIGLOAD2 model and as such we again do not see a mode 1 coastal Kelvin wave. Neither do we find the additional coastal Kelvin wave like mode over the secondary shelf region. The mode 1 coastal trapped wave is, however, travelling at 15.21 ms^{-1} and therefore considerably faster than the mode 2 slope trapped wave modes of the barotropic solution or the baroclinic Kelvin wave of the JM02 study.

The mode 2 wave appears very barotropic in nature, with very little deviation of the nodes from the vertical, and indeed the wave speed of this mode is very close to that of the mode 3 wave in the barotropic limit. The mode 3 wave is again an internal baroclinic Kelvin wave like mode supported over a region of steep topography.

We should note at this point that it is rather difficult to find a good solution due to the problems and limitations associated with the BIGLOAD2 model and as such the reliability of individual profile calculations is, at this point, questionable.

3.4.4 Full realistic solution

The mode 1 wave was solved for all realistic profiles in the baroclinic limit and its speed plotted as a function of latitude (Fig 3.11). From the differences observed between the profiles in the single profile analysis we can expect a significant amount of variation over the range of the realistic data set as was also the case in the barotropic full realistic solution.

The frequency range, where these modes are located, will alter according to the topographic and stratification conditions and may jump abruptly from one profile to the next. This represented a major obstacle while trying to obtain a full picture of the modal structure along the western boundary and resulted in a painstaking manual process of pressure field analysis to ensure the same mode was being followed.

There is indeed a significant amount of variation between the profiles and no clear separation of the wave modes that was seen in the idealised experiments. Instead the mode 1 wave appears to vary between a coastal Kelvin wave like mode travelling at speeds around 20 ms^{-1} and slower, higher mode coastal trapped wave modes with wave speeds of around $5 - 8$ ms^{-1}.

We can also note that the pattern in mode 1 baroclinic wave speed is similar to that observed in the mode 1 and 2 wave speeds of the realistic barotropic solution (Fig 3.12). This comparison emphasises our earlier suggestion that the baroclinic mode 1 wave varies between a coastal Kelvin wave like wave, akin to the barotropic mode 1

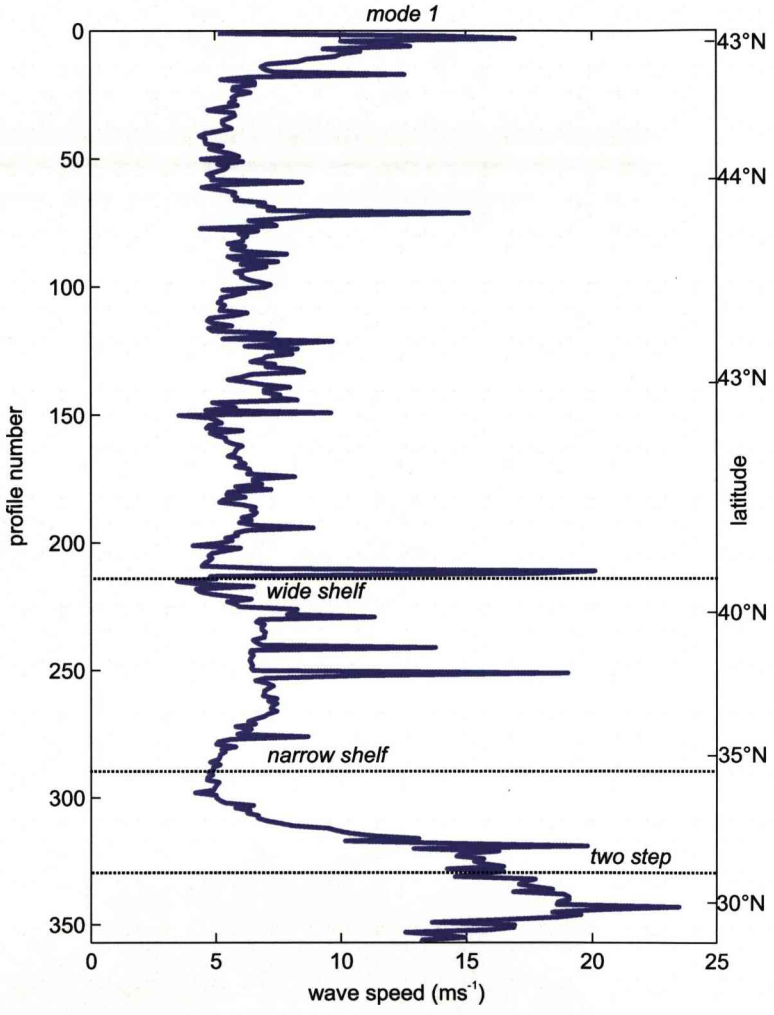

Figure 3.11: The realistic, baroclinic mode 1 wave speed as a function of latitude for all realistic profiles.

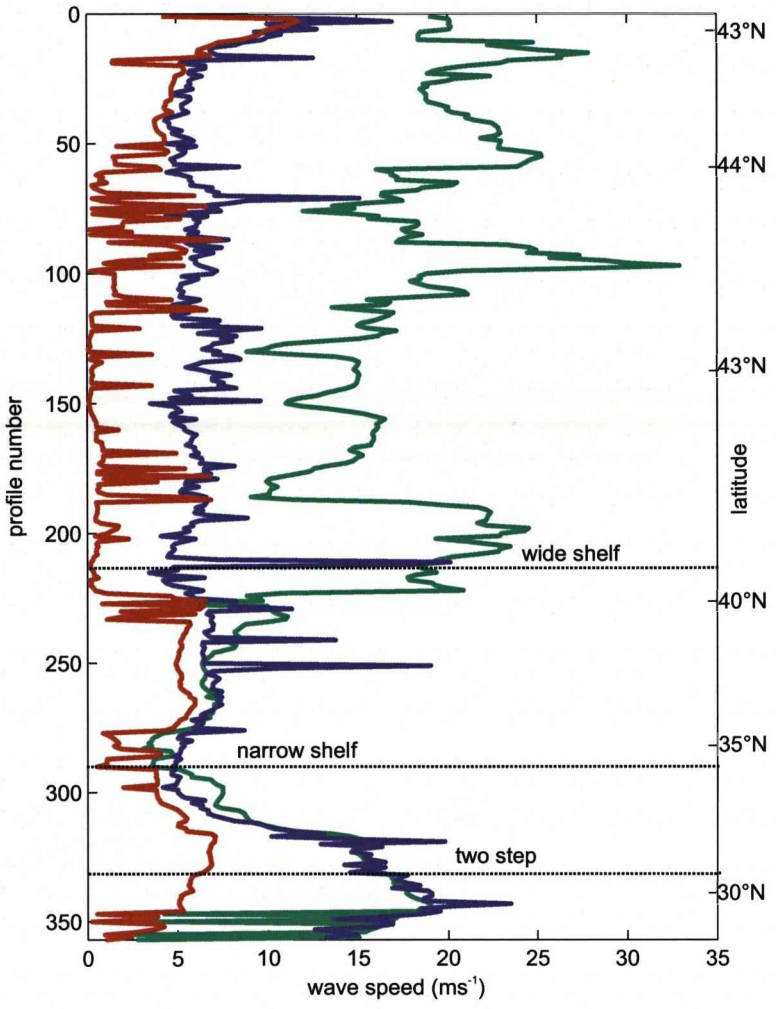

Figure 3.12: Comparative plot of the realistic, baroclinic mode 1 wave (magenta line) against the realistic, barotropic mode 1 (green line) and mode 2 (red line) wave speeds for all latitudes.

wave; where the depth of the shelf is sufficiently deep to allow BIGLOAD2 to solve for this mode; and a higher coastal trapped wave mode closer in speed to the barotropic mode 2 wave. At high latitudes where the coastal Kelvin wave is not solved for in the baroclinic case we see a very similar pattern between the mode 1 baroclinic and mode 2 barotropic wave albeit with a difference in magnitude which we can associate with the stratification increasing the effective restoring force. The similarities between the barotropic and baroclinic cases does restore our faith somewhat in the solutions provided by the BIGLOAD2 model.

We again observe a 'spikiness' in all the modes displayed in Fig 3.12 due to the mis-identification of modes in both the barotropic and baroclinic solutions.

These results could lead us to suggest that the barotropic solution provides a good approximation of the coastal trapped wave modes in the realistic ocean although the wave speeds of the mode 2 wave may be somewhat increased by the effects of stratification.

3.4.5 Realistic, baroclinic solution summary

- The introduction of stratification results in difficulty in finding some of the wave modes.
- Where we can identify particular wave modes it seems that the mode 2 wave is sped up by stratification, but the mode 0 and mode 1 waves are not greatly influenced.
- In the baroclinic limit, over regions of very steep topography, baroclinic internal Kelvin like wave modes are supported propagating at speeds of the order 1 to 3 ms^{-1}.

3.5 Chapter summary

The inclusion of realistic topography and stratification profiles has resulted in a number of effects on the wave modes we firstly examined over idealised topographies and stratification conditions in Chapter 2. The key findings of our realistic experimentation in both the barotropic and baroclinic limit are summarised below:

- The introduction of both realistic topographic and stratification profiles resulted in a high degree of variation, according to the offshore topography, suggesting that the properties of the wave modes supported are linked to detailed changes in the topography and stratification.
- The very fast barotropic response found in the idealised experiments remains consistent in the barotropic realistic solution. As BIGLOAD2 has difficulty solving for this mode we cannot determine whether it would be affected by the inclusion of stratification.
- The inclusion of stratification increases the effective restoring force and reduces the influence of topography on the wave modes resulting in an enhancement of mode wave speeds, particularly the mode 2 wave.
- In regions of very steep topography the mode 2 coastal trapped wave mode is heavily modified. However, in the stratified ocean, baroclinic internal Kelvin wave like modes are supported here.

- We did not find a pattern of decreasing mode 1 and 2 wave speed with decreasing f parameter in either the barotropic or baroclinic realistic scenarios. However, the realistic topography and stratification data was limited to latitudes greater than around $28°N$ whereas the most significant decrease in wave speed in the idealised experimentation was found at lower latitudes.

- As in the idealised experiments we find that the barotropic solution provides a good approximation of the mode 0 and 1 waves supported, and their associated properties, in the realistic ocean although the mode 1 wave speeds may be as slow as $3 - 5\ ms^{-1}$ in a regions with a very narrow shelf.

We conclude that although differences between the idealised and realistic experiments have been observed, as detailed above, the idealised solution of Chapter 2 will provide a good first approximation of wave modes supported and their associated timescales. The inclusion of realistic stratification does not alter the mode 1 wave significantly and we can therefore be assured that a simpler stratification, or indeed a barotropic ocean, can be useful in interpreting the ocean adjustment process.

Chapter 4

Idealised modelling: Global

4.1 Introduction

The detailed calculations of coastal trapped waves modes under free surface barotropic and baroclinic conditions allowed us to determine their structure and behaviour over a number of idealised and realistic topographies. Indeed, the inclusion of topography of any form allowed for coastal wave modes with largely barotropic properties to propagate at considerably higher speeds than those modes supported by the idealised baroclinic ocean of JM02. The coastal trapped wave modes were found to be significantly modified by the detailed changes over realistic topographic profiles.

These results would suggest that the presence of topography would considerably alter the ocean adjustment suggested by JM02. The presence of a substantial barotropic mode would allow for an even more rapid initial ocean adjustment. In addition the changes in wave structure found over topography may result in a reduction of the longer time scale adjustment of the interior ocean. For example, a change to the degree of trapping of waves at the eastern boundary. In order to test these hypotheses the MIT General Circulation Model (MITgcm) was utilised to carry out a number of idealised experiments. It is a numerical model designed to simulate fluid phenomena over a wide range of scales in the ocean.

In this chapter a number of idealised topographies were set up to analyse the large scale impact of the changes we observed in the topographic profile calculations of Chapter 2 and 3. These results can be compared to those of JM02 to determine whether their conclusions (see detailed description in Chapter 1) hold true for a topographic ocean.

A number of experiments were completed to assess:

1. The effect of the type of topography on the western boundary; the differences observed in the wave mode calculations would suggest that the impact of differing topographic types may result in faster adjustment and a less simple propagation pattern.

2. The effect of the location of topography within the domain on the initial and longer time scale adjustment including an analysis of signal behaviour on the eastern boundary, which is responsible for the propagation of information into the ocean interior. JM02 suggested that the eastern boundary coastal trapped signal did not amplify, as would be expected with increasing f, as the energy was instead propagated into the interior ocean as Rossby waves. This may no longer hold true when topography is present on the eastern boundary.

3. The adjustment pattern of the southern hemisphere; the very fast barotropic mode found in our wave mode calculations should theoretically result in adjustment in the southern hemisphere on a timescale of days.

4. The effect of including open boundaries to simulate a Southern Ocean; by ignoring the presence of a Southern Ocean in our idealised experiments the results may not be considered relevant to the realistic ocean. However, it is expected that the inclusion of open boundaries will only impact upon the adjustment of the model South Atlantic.

The set-up of the MITgcm and the topography types used are briefly described before the results of the above experimentation are presented. The conclusions reached and the questions that remain to be addressed are summarised at the end of the chapter.

4.1.1 Description and basic setup

For this study a two-layer, free surface set-up was initialised with the top 1000 m at $15°C$ and the bottom 2000 m at $5°C$ (Fig 4.1). There are 15 vertical layers, varying in thickness between 50 m and 1500 m, in total adding up to a deep ocean depth of 3000 m. The vertical resolution is highest around the depth of the interface. A constant salinity of 35 psu is maintained throughout. The model domain reaches from $50°S$ to $50°N$ and is 45° wide. Model resolution of 0.2° allows for the adequate resolution of Kelvin waves as it remains smaller than the baroclinic Rossby radius, $R_0 = \frac{\sqrt{g'H_e}}{f}$, for all values of latitude, ϕ.

Hsieh et al. (1983) found that the Kelvin wave speed is unaffected by model resolution when discretised on a C-grid, as is the case of the MITgcm; however, the wave structures and damping may be altered. Free-slip conditions are used throughout with

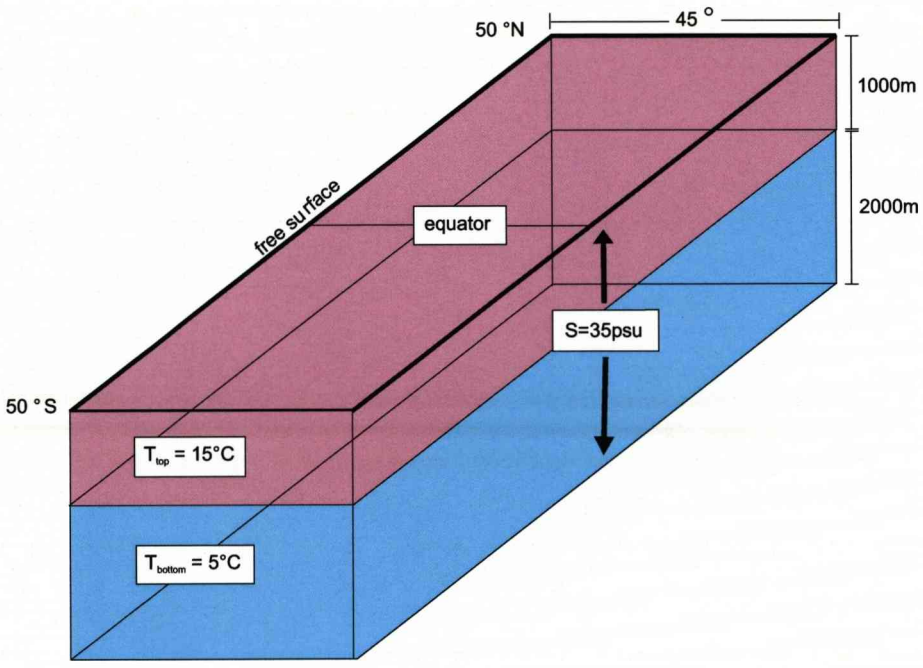

Figure 4.1: Basic MITgcm setup for idealised experimentation.

the exception of experimentation of changing bottom friction (see Chapter 5) that require no-slip conditions for the bottom boundary. Davey et al. (1983) determined that free-slip waves were generally less sensitive to lateral viscosity than no-slip waves particularly in regard to longshore phase speed. Computational stability often requires a large lateral viscosity which inhibits coastal trapped waves and therefore the use of free-slip reduces this effect.

4.1.2 Forcing methods

A change in deepwater formation, modelling a potential cause of change to the MOC, was simulated by conducting a temperature relaxation in the north west corner of the domain. The deepwater formation is simulated by cooling a prescribed volume of the surface warm layer to the temperature of the deep layer. The temperature field is relaxed in a three dimensional location over a 'source' area with a surrounding linearly decreasing sponge layer acting to prevent shocks to the system. For the temperature tracer, T, at every point the tendency is modified so that;

$$(\frac{dT}{dt})_{new} = (\frac{dT}{dt})_{old} - \frac{M_{rbc}}{\tau_T}(T - T_{rbc})$$

where M_{rbc} is a three dimensional mask with values varying between 0 and 1 with no time dependence. Where $M_{rbc} = 1$, the relaxing timescale is $\frac{1}{\tau_T}$ and where $M_{rbc} = 0$

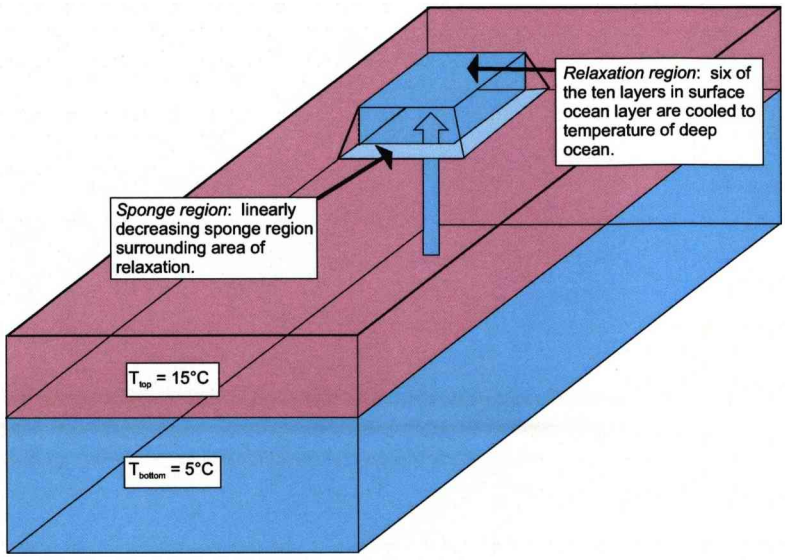

Figure 4.2: An illustration of the relaxation and sponge regions in the MITgcm experiment setup. The standard extent of the forcing region was 4° by 4° with sponge regions extending a further 4° along the eastern and southern boundary of the forcing region. In this region the water column up to 500 m depth is cooled to $5°C$ whereas in the rest of the ocean the water column down to 1000 m is at $15°C$.

there is no relaxation. T_{rbc} represents the temperature field the values are relaxed towards. The relaxation timescale, τ_T, is set at 30 days for the majority of runs unless stated otherwise. The detail of the location of the relaxation region is described in Fig 4.2.

4.2 Control run: comparison with JM02

Initially a vertical sidewalls run was completed to provide a comparison with JM02 and also ensure the model was simulating processes, such as Kelvin waves, correctly. With the conditions of vertical sidewalls, no bottom slope and two-layer stratification, only Kelvin waves will be present.

The sea surface elevation, η, field is shown at $t = 30$ days and $t = 300$ days alongside the surface layer thickness field of JM02 (Fig 4.3). The propagation pathway in both cases is clearly very similar and is easily distinguished as representing the pathway of baroclinic Kelvin waves travelling equatorwards along the western boundary before propagating across the equator as equatorial Kelvin waves. The theoretical baroclinic Kelvin wave speed was calculated as 3.48 ms^{-1} from the following equation;

$$c = \sqrt{g' H_e}$$

The reduced gravity value $g' = \frac{g(\rho_2 - \rho_1)}{\rho_2}$ and equivalent depth $H_e = \frac{h_1 h_2}{h_1 + h_2}$ where, in this case, $h_1 = 1000\ m$ and $h_2 = 2000\ m$.

Such a wave would reach the equator in around 17 days from the centre of the forcing region ($45°N$); the model wave reaches the equator in a comparable time to both this theoretical value and also that seen in JM02, allowing for the greater distance from the forcing region in JM02.

On reaching the eastern boundary the signal splits and propagates polewards symmetrically. As in JM02 the perturbation is transmitted westwards into the interior by Rossby waves thus preventing any significant re-amplification of the eastern boundary coastal trapped signal as it propagates poleward.

4.2.1 Differences between the control run and JM02

In the north-west corner of our model domain we observe wave forms (Fig 4.3) that are not seen in JM02. At first inspection these waves appear to be short barotropic Rossby waves. To confirm this supposition a cross section was taken at $35°N$ and analysed over a 300 day run period (Fig 4.4). For such short planetary waves the group velocity, c_g, acts in an eastwards directions, opposite to the phase velocity (Gill, 1982), and this is evident in Fig 4.4. We can calculate c_p and the zonal component of c_g, from the dispersion relation, as;

$$c_p = \frac{-\beta}{k^2 + m^2 + \frac{1}{R_0^2}}$$

$$c_g = \frac{\beta(k^2 - m^2 - \frac{1}{R_0^2})}{(k^2 + m^2 + \frac{1}{R_0^2})^2}$$

For short, barotropic waves we can ignore $\frac{1}{R_0^2}$ and assuming $k^2 >> m^2$ we find;

$$c_p = -\frac{\beta}{k^2}$$

$$c_g = \frac{\beta}{k^2}$$

Given a latitude of $35°N$ and an estimated wavelength of $\lambda \approx 900\ km$ we calculate an expected c_g of $0.38\ ms^{-1}$ for short barotropic waves from the equation. From Fig 4.4 we calculate a very rough estimate of c_g as $0.24\ ms^{-1}$. Phase speeds near the western boundary, c_p $(nearwest)$, and in the mid ocean, c_p $(midocean)$ were estimated as $0.15\ ms^{-1}$ and $0.45\ ms^{-1}$ respectively. We can therefore confirm that the waves

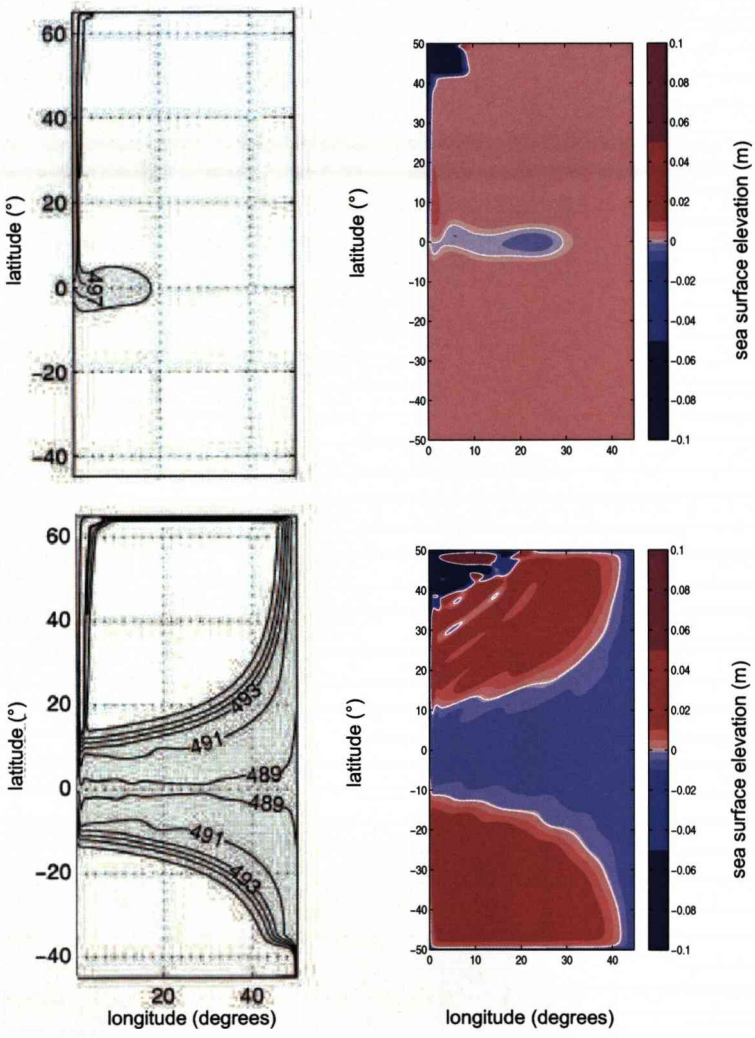

Figure 4.3: MITgcm sea surface elevation plots for $t = 30$ days and $t = 300$ days alongside plots of surface layer thickness from JM02.

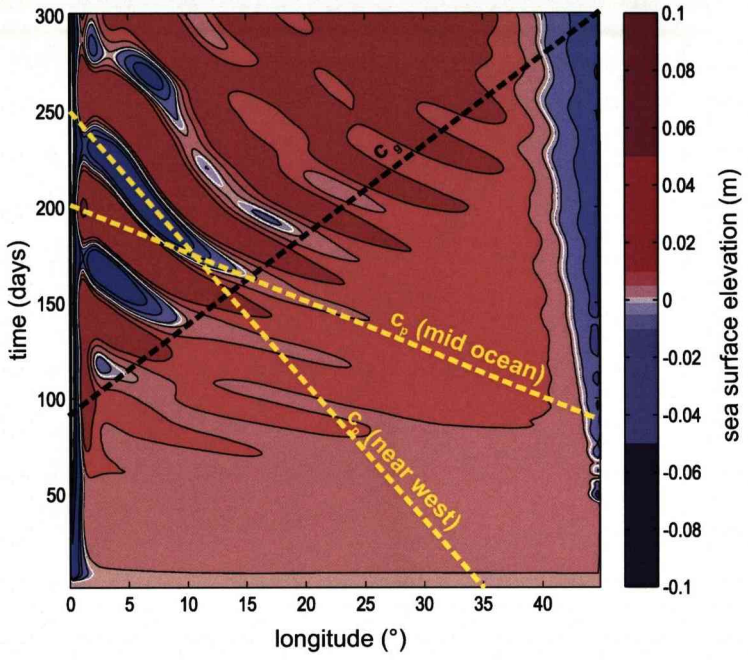

Figure 4.4: A Hovmueller plot along a latitudinal cross section at $35°N$ over the 300 day time period. Estimates of group speed, c_g (black dashed line), and phase speeds (yellow dashed lines) near the western boundary, c_p (*nearwest*), and in the mid ocean, c_p (*midocean*) confirm these wave forms as eastwards propagating short barotropic waves.

observed in the η fields of Fig 4.3 are indeed eastward propagating short barotropic waves.

There are a number of detailed differences between the JM02 model and the MITgcm used in this study. They use a reduced-gravity, shallow-water model with a moving surface layer of 500 m and an infinitely deep, motionless lower layer rather than a two layer set-up eliminating the presence of barotropic Kelvin waves. In addition, instead of a temperature relaxation forcing the model ocean, they prescribe an outflow from the surface on the northern boundary to represent deep water formation. Their model domain reaches farther north to $60°N$ and also $5°$ further longitudinally. Finally, their model is run under no-slip conditions whereas in this simulation free-slip conditions are used.

However, from the results of our control run these model differences do not appear to impact upon the fundamental dynamical response of the ocean to a change in forcing.

4.3 Topographic profile selection

In order to test the impact of topography on the large scale adjustment of the Atlantic Ocean a suite of topography types (Fig 4.5) were selected, in addition to the vertical sidewall case (vertical):

1. An exponential slope at all boundaries (*slope*).
2. A wide shelf and exponential slope on the western boundary with exponential slope at all other boundaries (*shelfslope*).
3. A wide shelf and vertical wall on the western boundary and vertical wall at all other boundaries (*wideshelf*).
4. An exponential slope on the western boundary only (*west*).
5. An exponential slope on the eastern boundary only (*east*).
6. Exponential slopes on western and eastern boundaries and vertical walls at the northern and southern boundaries (*westeast*).
7. An exponential slope at all boundaries but with open boundaries to represent the Southern Ocean (*open southern*).

All of the topographies described above, with the exception of the last example, are closed at all boundaries. The exponential slope is represented by the same equation as in Chapter 2;

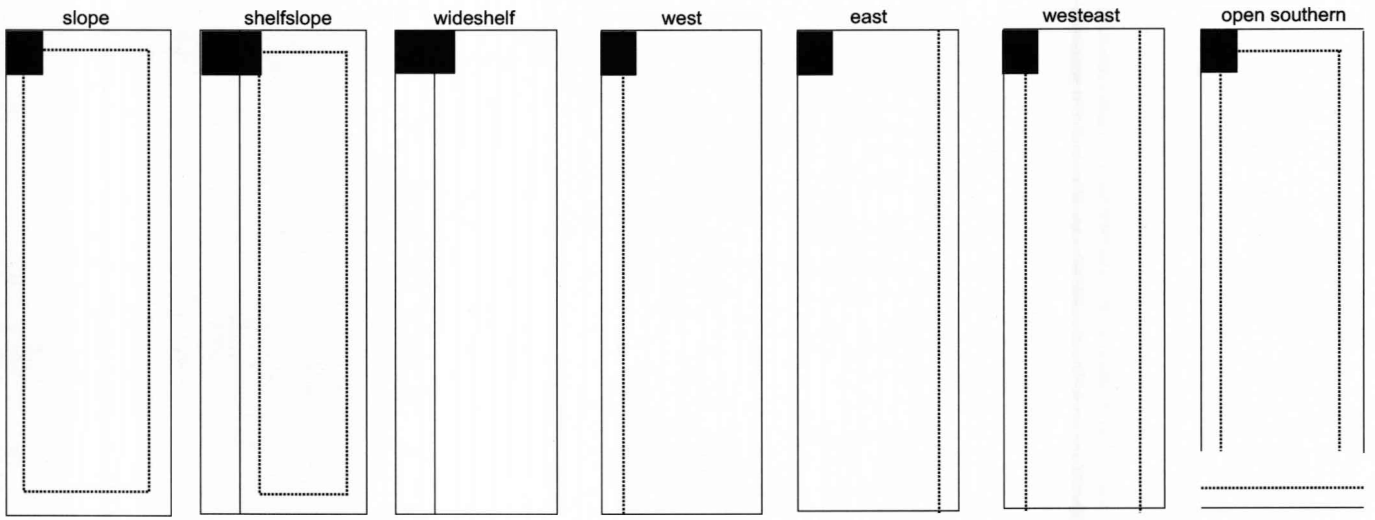

Figure 4.5: The seven different basin topographies utilised in the MITgcm experimentation. Vertical walls are represented by a solid line and the extent of exponential slopes as a dashed line. The forcing areas are represented by the filled black boxes.

$$h(x) = \alpha + \beta e^{b(\frac{x-x_1}{x_2-x_1}-1)}$$

where A is the depth of the shelf, B is the depth of the deep ocean, x_1 is the extent of the shelf, x_2 is the extent of the shelf and slope, and $\alpha = B - \beta$ where;

$$\beta = \frac{A-B}{e^{-b}-1}$$

The topographic steepness factor, b, has a standard value of $b = 5$. The values of A and B are 100 m and 3000 m respectively. The topographic length scale here is taken to be represented by $\frac{1}{b}$ and will vary with latitude; for example at $25°N$ the standard value represents a topographic length scale of around 100 km.

The inclusion of an idealised exponential topography at the northern boundary takes into account the almost continuous continental shelf in the realistic ocean.

Topography is represented by 'shaved cells' in the MITgcm (Adcroft et al., 1997). This is in comparison to the 'staircase' or 'step' topography, where steps are chosen to fit the model grid, commonly used in height coordinate ocean models which is only suitable for very high vertical and horizontal resolution studies. Terrain-following coordinates can also be used to represent topography, however, Haney (1991) found that hydrostatic consistency proved problematic in such models particularly above steep slopes. As experimentation on steep slopes will be carried out within this study (see Chapter 5) such a problem should be avoided. Adcroft et al. (1997) concluded that the shaved cell approach is clearly more accurate than the conventional staircase representation.

4.4 Effect of differing topography types

Firstly we look to investigate the effect of three different boundary topography types (*slope*, *shelfslope* and *wideshelf*) on the whole ocean adjustment (Fig 4.6). In the *slope* and *shelfslope* examples the northern, southern and eastern boundaries are exponential slopes whereas in *wideshelf* all other boundaries, apart from the western boundary, are vertical walls.

4.4.1 Initial adjustment

In *slope* the negative anomaly propagates equatorwards along the $\frac{f}{h}$ contours reaching the coast at around $30°N$ by $t = 30$ days. A positive anomaly is evident along the coast at high latitudes (greater than $30°N$). Along the equator we can see the

propagation of equatorial Kelvin waves and the anomaly then divides on reaching the eastern boundary travelling polewards. This pattern is symmetrical in the northern and southern hemisphere; although the signal appears weaker in the southern hemisphere we can already see the western boundary has been influenced. It should be noted that the magnitude of the signals outside of the western boundary region are very small, of the order of *mm*. Such rapid propagation can only be understood in terms of a barotropic adjustment associated with the very fast deep ocean or double Kelvin waves we identified in Chapter 2.

When a wide shelf is added along with an exponential slope, in the *shelfslope* example, we see that the perturbation behaves in the same manner over the slope region before flowing over the shelf region along the $\frac{f}{h}$ contours. The positive anomaly observed in *slope* also expands across the shelf region to the coast resulting in the same pattern of positive sea level north of $30°N$ with negative values equatorwards of this value.

In the *wideshelf* example the anomaly leaks onto the shelf almost immediately then expands across the shelf along the $\frac{f}{h}$ contours as in shelfslope. However, in this case as the anomaly reaches the shelf almost immediately the negative anomaly fills the whole shelf at all latitudes. This may also be in part due to the lack of slope topography on the other boundaries hampering the recirculation of the coastal trapped signal that is evident in the other two examples.

Propagation speed of waves along the western boundary

From the results of Chapters 2 and 3 we could expect to see a faster propagation of coastal trapped waves along the western boundary when topography is present; for example the coastal Kelvin wave travelling at around 31 ms^{-1}. This expectation cannot be conclusively proven from the $t = 30$ day; however, a Hovmueller plot along the western boundary for the first three months (Fig 4.7) clearly shows that the inclusion of topography allows for faster wave modes and resultant wave adjustment.

4.4.2 Longer scale adjustment

Examining the η field at timescales of longer than 30 days (Fig 4.8) we begin to see the larger scale adjustment of the ocean basin.

Western boundary region

In the *slope* case the negative coastal anomaly has built up. The positive anomaly in the north west corner moves progressively equatorwards through the time period and

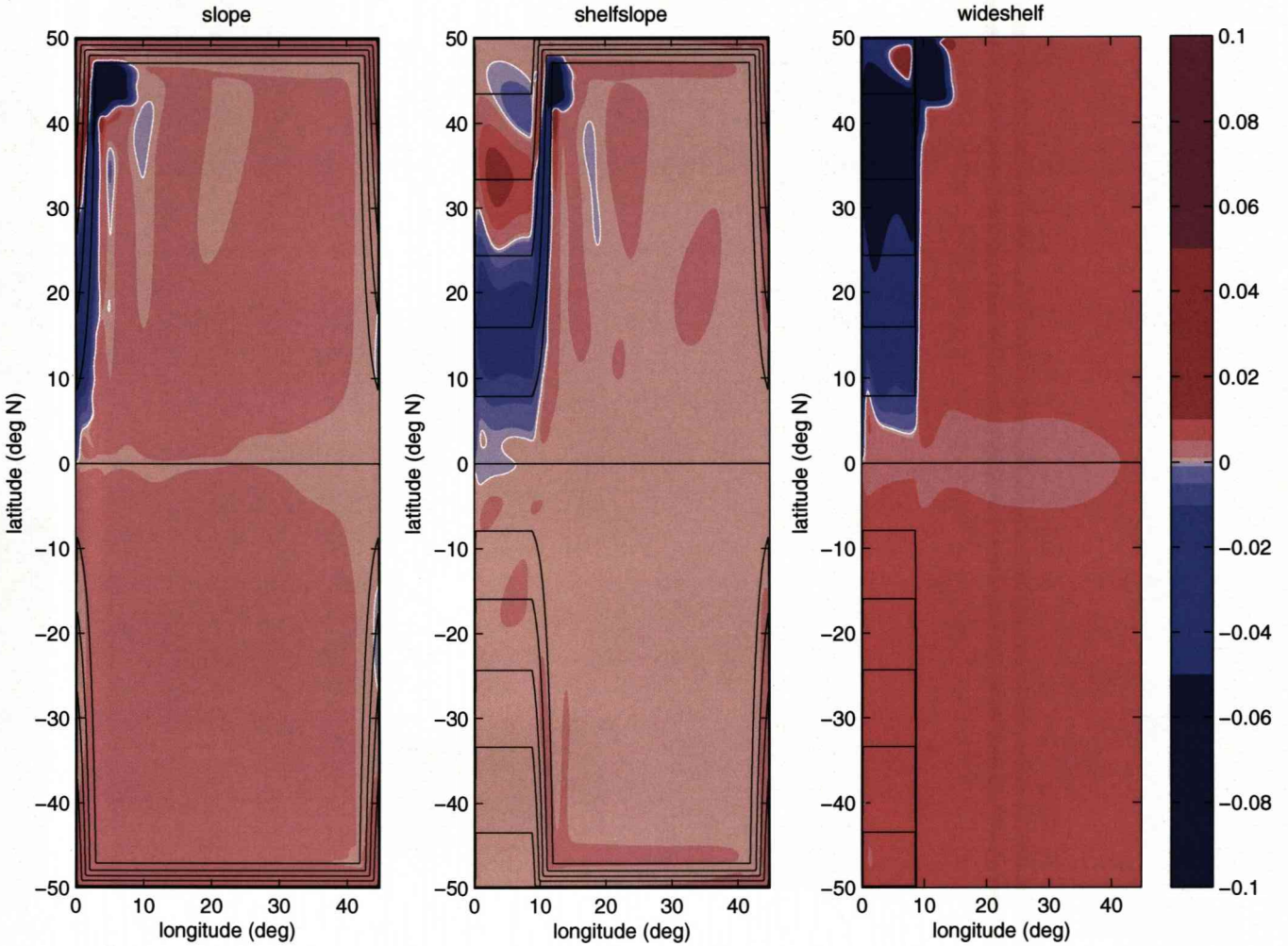

Figure 4.6: Sea surface elevation field (in metres) for *slope* (left), *shelfslope* (centre) and *wideshelf* (right) at t=30 days with $\frac{f}{H}$ contours shown in black.

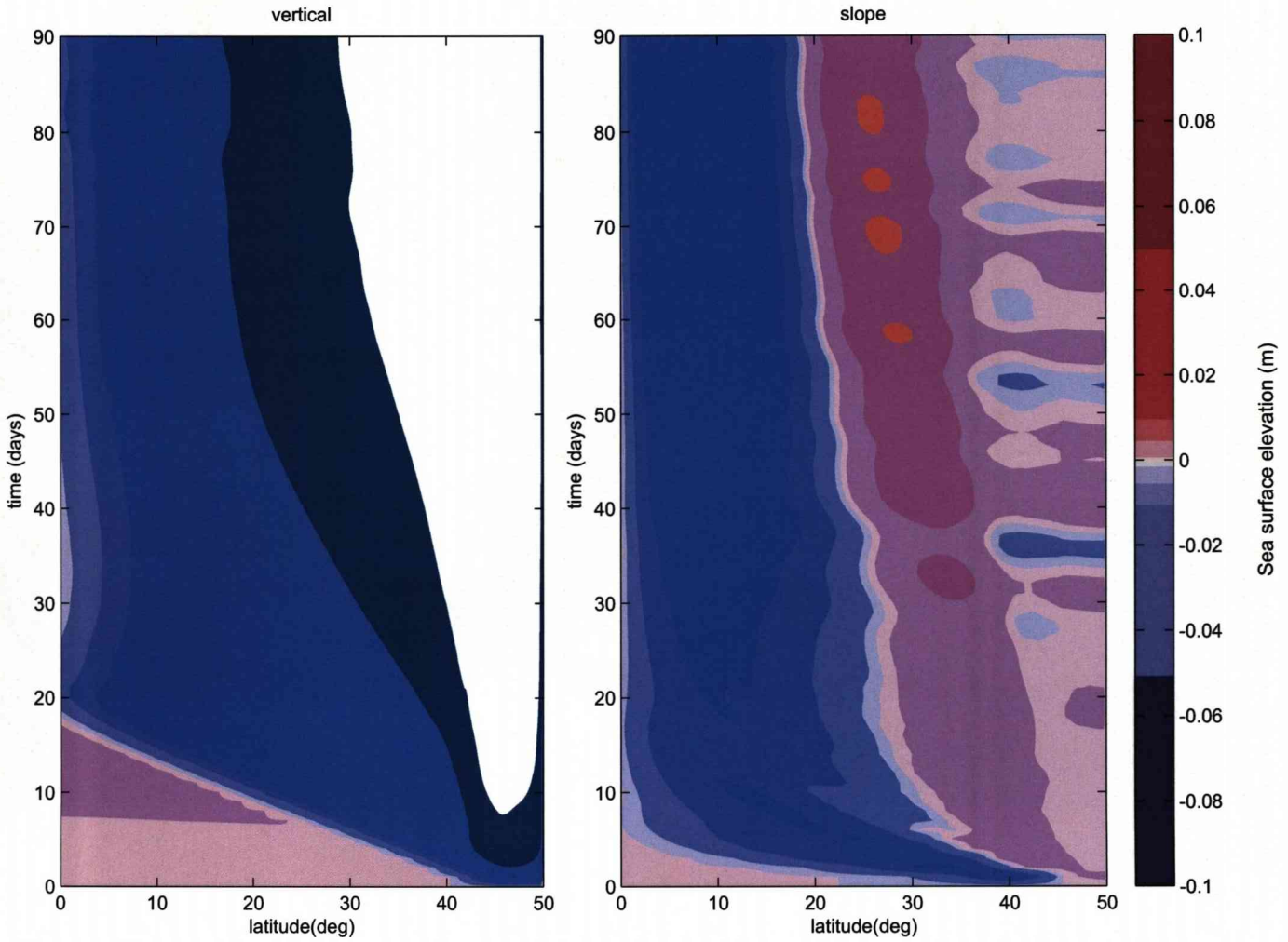

Figure 4.7: Hovmueller plots of sea surface elevation in metres along the western boundary for the *vertical* (left) and *slope* (right) topographic scenarios.

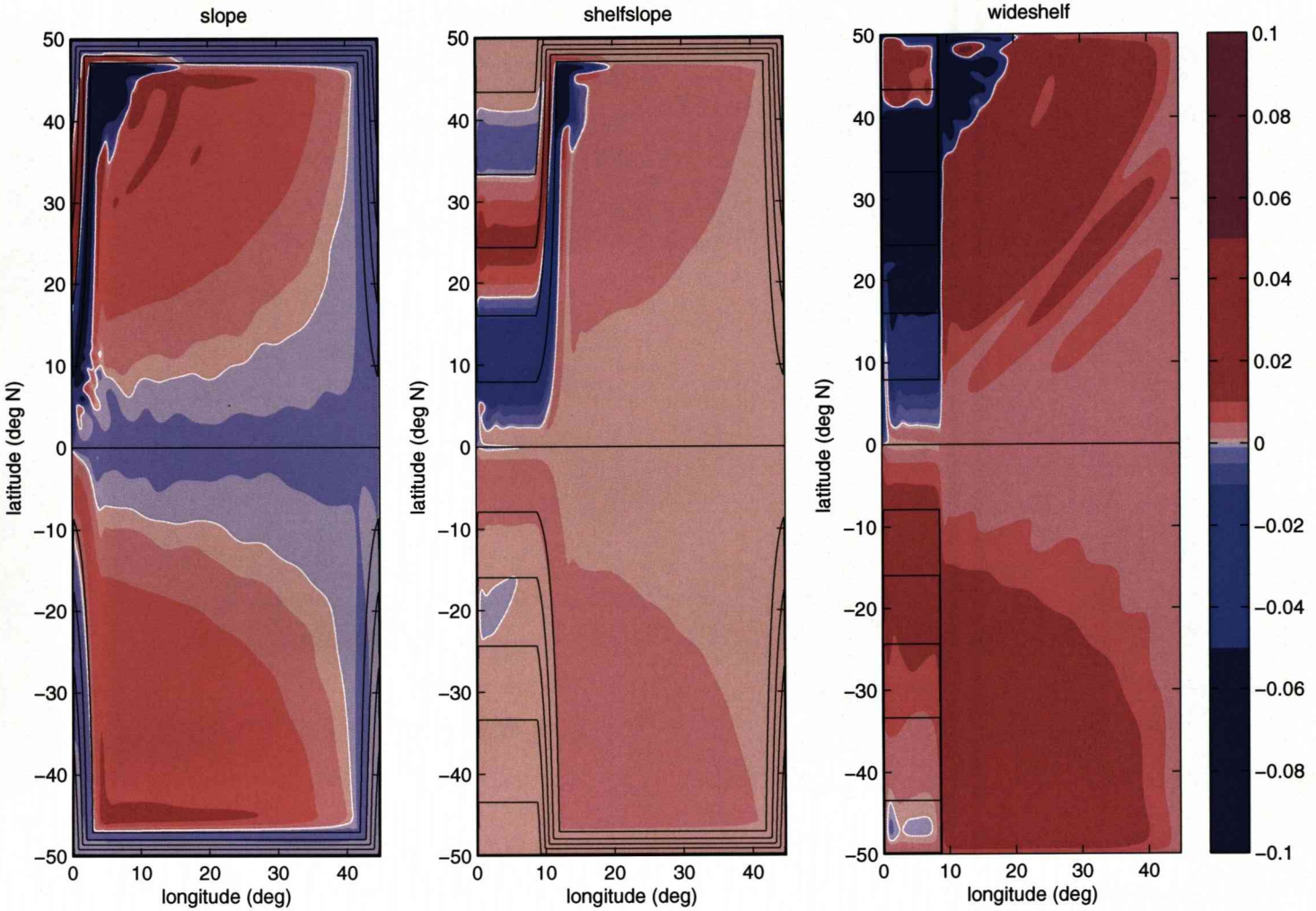

Figure 4.8: Sea surface elevation field (in metres) for an exponential *slope* (left), *shelfslope* (centre) and *wideshelf* (right) at $t = 360$ days with $\frac{f}{H}$ contours shown in black.

a negative anomaly builds to the north suggesting the coastal trapped perturbation is recirculating. We also see the positive anomaly in *shelfslope* has moved equatorwards allowing a negative anomaly to build at higher latitudes over the shelf region. The positive anomaly in sea surface elevation on the western boundary moves equatorwards much less quickly in the *wideshelf* case. This is likely to be due to the vertical boundaries, outwith the western boundary, resulting in a slower boundary signal, close to the baroclinic Kelvin wave speed of 3.48 ms^{-1}, rather than the faster wave speeds seen for coastal trapped waves of a more barotropic nature.

Eastern boundary and interior

The interior behaviour observed is quite different in each of examples. At first inspection it appears that there may be greater propagation of Rossby waves from the eastern boundary in *slope* and *wideshelf* than in the *shelfslope* example. A cross section of the sea surface elevation field was taken at $25°E$ for each of the examples and compared (Fig 4.9).

From this comparison we see that the interior signal in the *slope* and *wideshelf* cases are greater than than for the *shelfslope* example; indeed the *wideshelf* interior signal is considerably larger outwith the equatorial region. This may represent differences in the adjustment process near to the forcing region. Unlike JM02, we do not choose the strength of the overturning but instead allow the model to choose this by determining how quickly the density anomaly relaxes (or would relax in the absence of our continued 'relaxation' forcing). Perhaps it is the case that the overturning circulation is smaller in the *slope* and *shelfslope* cases as what JM02 term as forcing is smaller.

Another interesting feature of the interior cross section (Fig 4.9) is that, in comparison to *slope* and *shelfslope*, the *wideshelf* sea surface elevation pattern is not symmetrical in the northern and southern hemispheres. In the southern hemisphere we do not see the wave like structures that are apparent in the northern hemisphere *wideshelf* sea surface elevation. The presence of topography along the eastern boundary would therefore appear to result in greater similarity between the interior adjustment patterns of each hemisphere. The eastern boundary behaviour and its impact upon the adjustment of the interior will be analysed in greater detail in Section 4.6.1.

Regional anomaly magnitudes

The sea surface elevation fields presented here are somewhat deceptive on first inspection. The non-linear colour scale is useful for highlighting the smaller scale features of the adjustment, which may otherwise be lost. It does, however, create a false impression

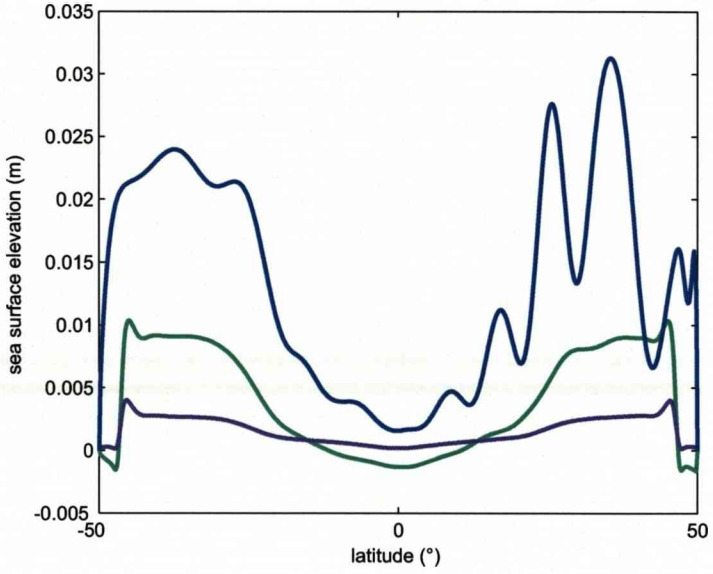

Figure 4.9: The sea surface elevation for *slope* (green), *shelfslope* (magenta) and *wideshelf* (blue) along the 25° longitudinal cross section at $t = 360$ days .

of the magnitude of the anomalies in the model basin. JM02 noted that the equatorial and eastern boundary signals are very much smaller than the western boundary signal. This is also true in our study as can be clearly seen in Fig 4.10 with the western boundary sea surface elevation anomaly being of the order of *cm* whereas the equatorial and eastern boundary signals are of the order of *mm*.

4.5 Location of topography within domain

In this second experiment we compared the adjustment pattern associated with topographies west, east and westeast (Fig 4.11) which differ in terms of location of the slope and can be compared with *slope*.

Western boundary region

A notable difference between *west*, *east*, *westeast* and *slope* is the absence of the positive anomaly alongshore at high latitudes allowing the negative anomaly to fill the entire western boundary in the northern hemisphere (Fig 4.11). This suggests that the positive anomaly occurs as the result of the presence of an exponential slope on the northern boundary. Indeed this may be due to frictional effects of the flow set up by the propagation of the barotropic mode around the boundaries within a matter

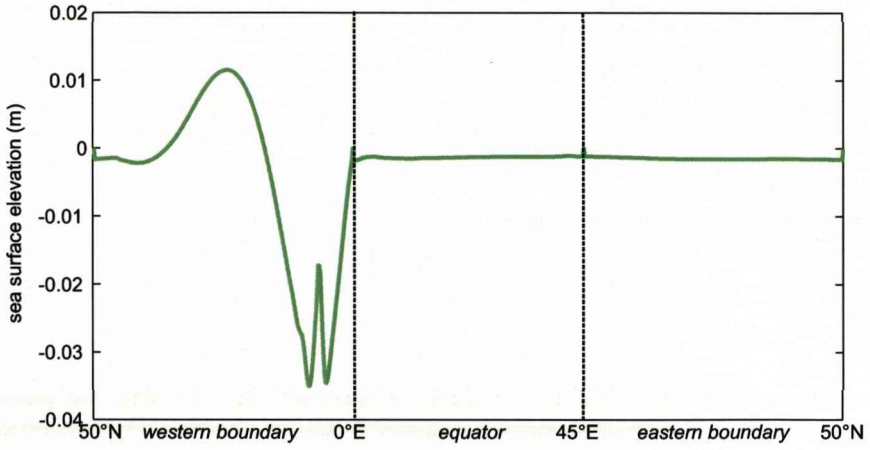

Figure 4.10: The sea surface elevation for *slope* along the western boundary, equator and eastern boundary clearly showing the much larger amplitude of the western boundary signal in comparison to that along the equator or western boundary.

of days. Where a northern exponential slope, or likely any bottom slope, exists there opens a propagation pathway for fast barotropic modes. As stated, where the northern boundary is represented by a vertical wall we do not see the positive anomaly.

Equatorial region

When there is no western boundary topography, as in *east*, the signal either appears to travel across the equator more quickly or the equatorial signal is of a larger amplitude. This is interesting as we would expect a faster signal along the western boundary when topography is present supporting the faster coastal trapped wave modes we identified in Chapters 2 and 3. We also determined that the coastal trapped wave speeds decreased towards zero at the equator. This behaviour in the equatorial region may result in less successful excitement of the equatorial Kelvin wave than is the case with the baroclinic Kelvin wave as the wave modes are less well matched.

Indeed, the comparison of the equatorial signal magnitude in the *slope*, *shelfslope* and *wideshelf* cases suggested that the more remote the wave nodes were from the density interface at the equator the smaller the equatorial signal. When we examine the sea surface elevation along the equator and eastern boundary for the *west*, *east* and *westeast* cases (Fig 4.13) we find that the equatorial signal is of a larger amplitude for *east* than either *west* or *westeast*, which are very similar, supporting this theory.

Therefore the inclusion of topography on the western boundary appears to result in a reduction in the signal magnitude communicated to the rest of the ocean due to less

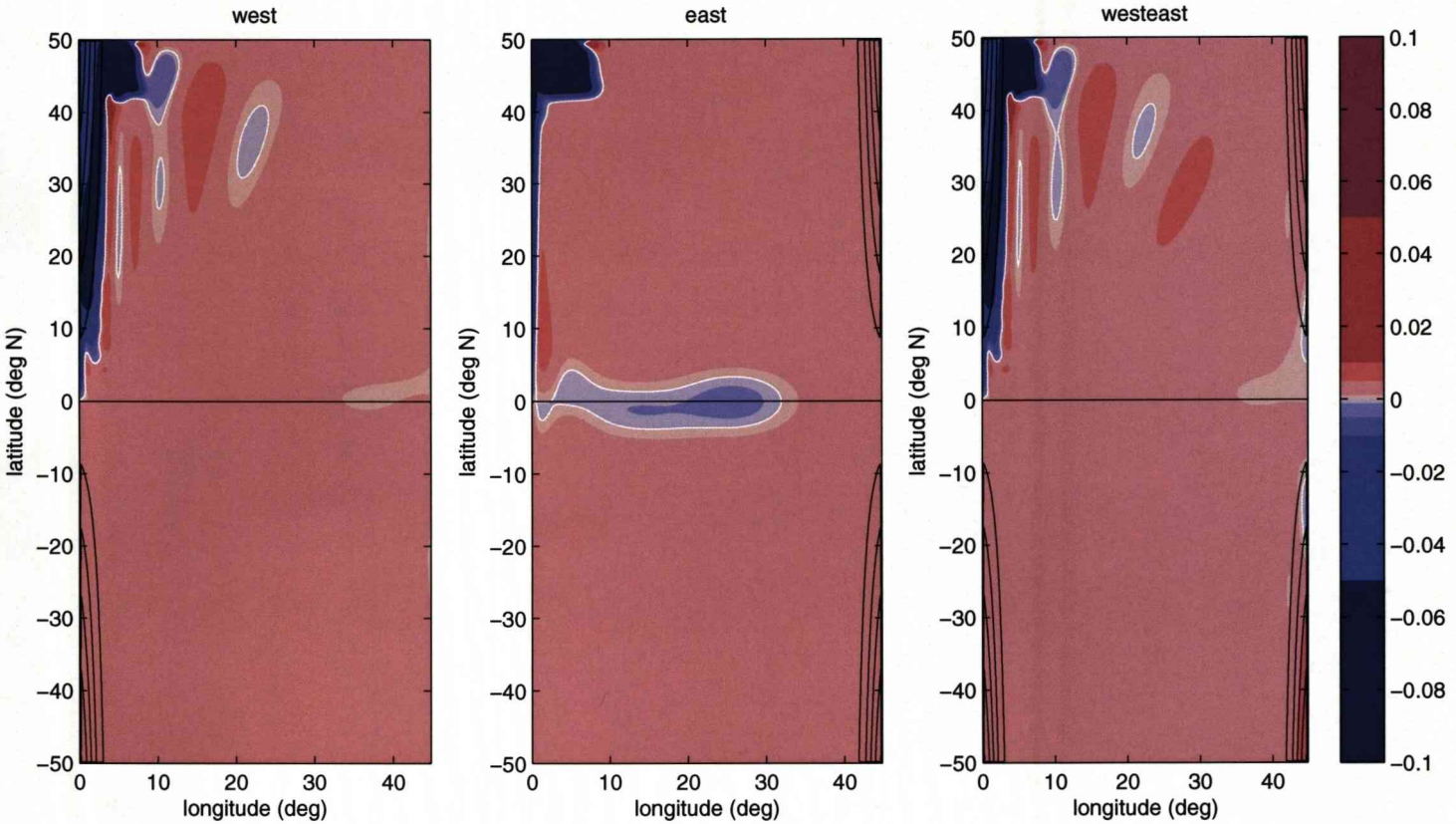

Figure 4.11: Sea surface elevation field (in metres) for *west* (left), *east* (centre) and *westeast* (right) at t=30 days with $\frac{f}{H}$ contours shown in black.

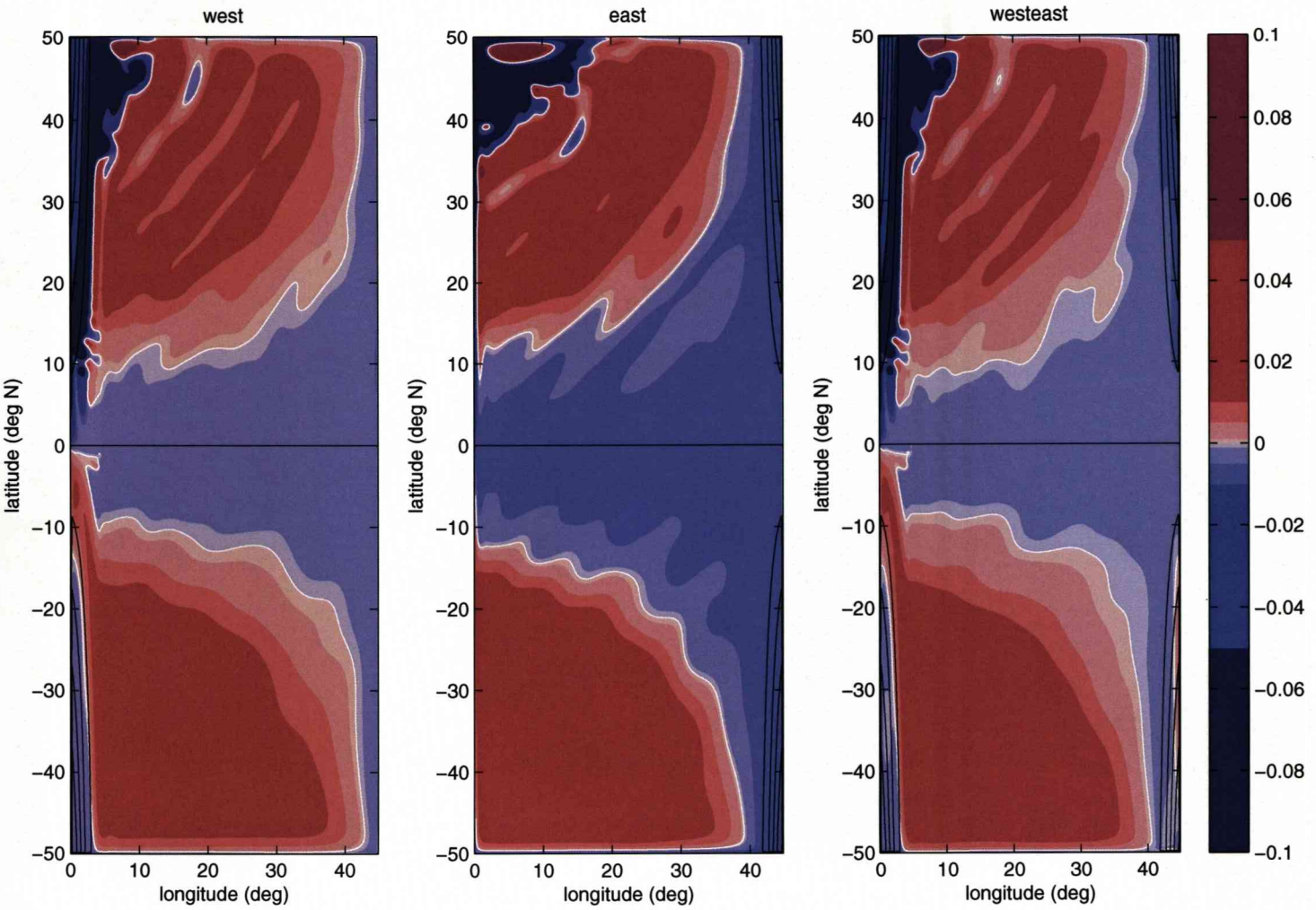

Figure 4.12: Sea surface elevation field for *west* (left), *east* (centre) and *westeast* (right) at t=360 days with $\frac{f}{H}$ contours shown in black.

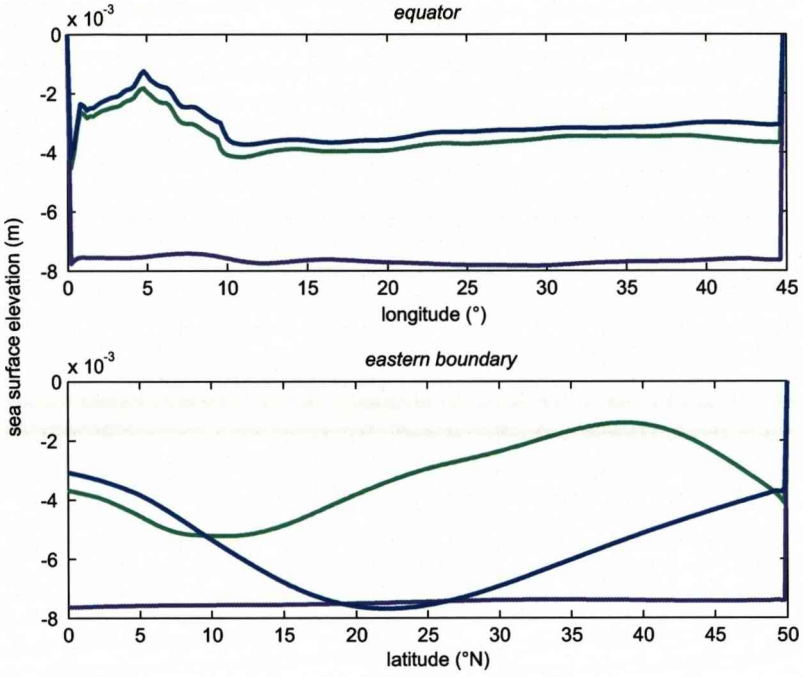

Figure 4.13: The sea surface elevation for *west* (green), *east* (magenta) and *westeast* (blue) along the equator (top panel) and eastern boundary (bottom panel) at $t = 360$ days.

effective excitation of equatorial Kelvin waves by the largely barotropic coastal trapped wave signal.

Eastern boundary and interior

In the *east* example, where the exponential slope is confined to the eastern boundary, the picture is very similar to the *vertical* case as we might expect in the initial adjustment process (Fig 4.11). We again analysed η values along the $25°E$ longitudinal line (Fig 4.14) and find that *west* and *westeast* cases are very similar. As in the *slope*, *shelfslope* and *wideshelf* cases we suggest the differences between the topographic examples are the result of differences in how quickly the density anomaly relaxes, which the model is free to choose in each case.

Looking at the longer timescale adjustment (Fig 4.12) there appears to be the greatest propagation of Rossby wave energy in *east* and the less so in *west* suggesting less trapping is occuring when there is a sloping eastern boundary. However, whether this observation of increased trapping is indeed valid or the result of the difference in forcing magnitude as previously suggested requires a more detailed analysis of the eastern boundary behaviour (see Section 4.6.1).

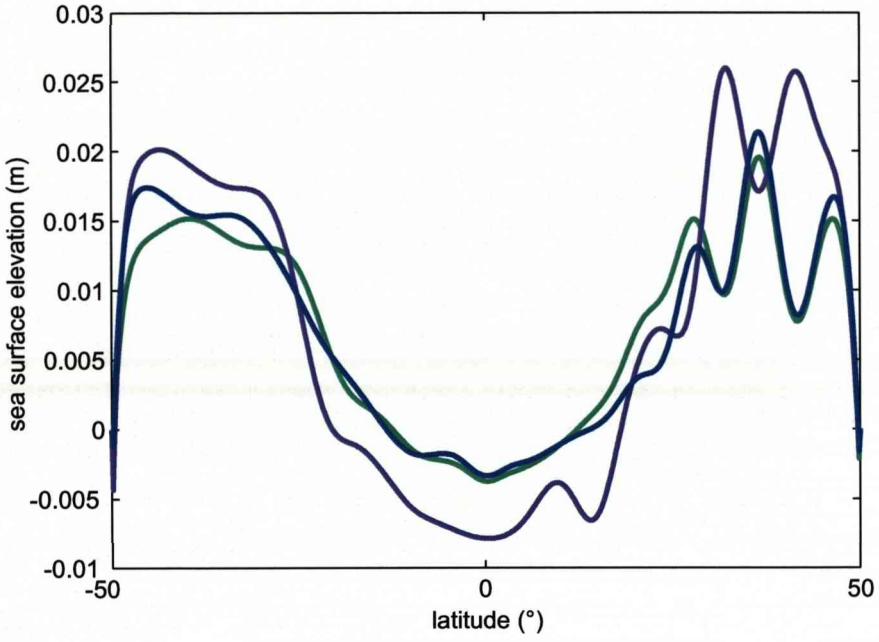

Figure 4.14: The sea surface elevation (in metres) for *west* (green), *east* (magenta) and *westeast* (blue) along the $25°E$ longitudinal cross section at $t = 360$ days.

Anderson and Killworth (1977) describe in their model that when stratification is included into a topographic basin the ocean responds by redistributing energy westwards in two ways. The barotropic Rossby mode is excited and rapidly carries information away from the eastern boundary. On a slower time scale the baroclinic response, in form of a westwards propagating Rossby wave fills the ocean. When they include topography on the western boundary they only find that the response in the eastern half of the basin is similar to the case without topography. With topography confined to the eastern half of the basin they found the western boundary region developed in a similar manner to the flat bottom case. These results are comparable to those found in this study.

4.6 Eastern boundary analysis

As discussed earlier, in JM02 the coastal trapped signal along the eastern boundary remained constant despite an increasing f value as energy was instead propagated westwards into the deep ocean as Rossby waves. However, this is only the case for low frequency Rossby waves as higher frequencies cannot propagate. Veronis (1966) concluded that the effect of bottom topography was shown to be very important in the

generation of Rossby waves and potentially more so than the β effect in some areas. We would therefore expect the pattern in our topographic examples to depart somewhat from the JM02 results.

We have a good idea of the wave mode structures and speeds we can expect to see over an eastern boundary slope region from the idealised wave mode calculations of Chapter 2. The mode 0 wave is a barotropic deep ocean or double Kelvin wave with speeds up to 171.55 ms^{-1} for this model ocean of depth 3000 m; the mode 1 wave is a coastal Kelvin wave, likely to be somewhat modified by the topography, ranging in speed from zero at the equator to around 18 ms^{-1} at high latitudes and; the mode 2 coastal trapped wave speed varies from zero at equator to around 5 ms^{-1} at high latitudes. Where the eastern boundary is represented by a vertical sidewall we would only expect the deep ocean barotropic and baroclinic Kelvin waves with wave speeds of 171.55 ms^{-1} and 3.48 ms^{-1} respectively.

In the equatorial region we determined that only Kelvin waves are supported but on reaching an eastern topographic boundary the additional coastal trapped modes would be excited once more. Therefore we do not expect the form of the western boundary topography to affect the wave modes supported on the eastern boundary.

4.6.1 Signal amplification

By examining the sea level at two latitudes ($10°N$ and $30°N$) over a 180 day period we can analyse whether topography has an impact on the propagation of Rossby waves. Fig 4.15 shows the sea surface elevation values at the two latitudes for the slope profile and also the same two time series when a calculated lag of two days has been applied to the $30°N$ data.

The amplitude of the waves at the two latitudes has been calculated and plotted as a function of their frequency (Fig 4.16). This allows for not only a first order estimate of the amplification of the eastern boundary signal as it travels polewards but a representation of the wave mode frequencies seen.

The vertical case, comparable to JM02, does show some amplification, however, it appears limited when compared to that seen in the other cases and likely due to the model differences described previously such as the absence of a barotropic Kelvin wave.

From the Rossby wave dispersion relation (Gill, 1982);

$$\omega = -\frac{\beta k}{k^2 + l^2 + \frac{1}{{R_0}^2}}$$

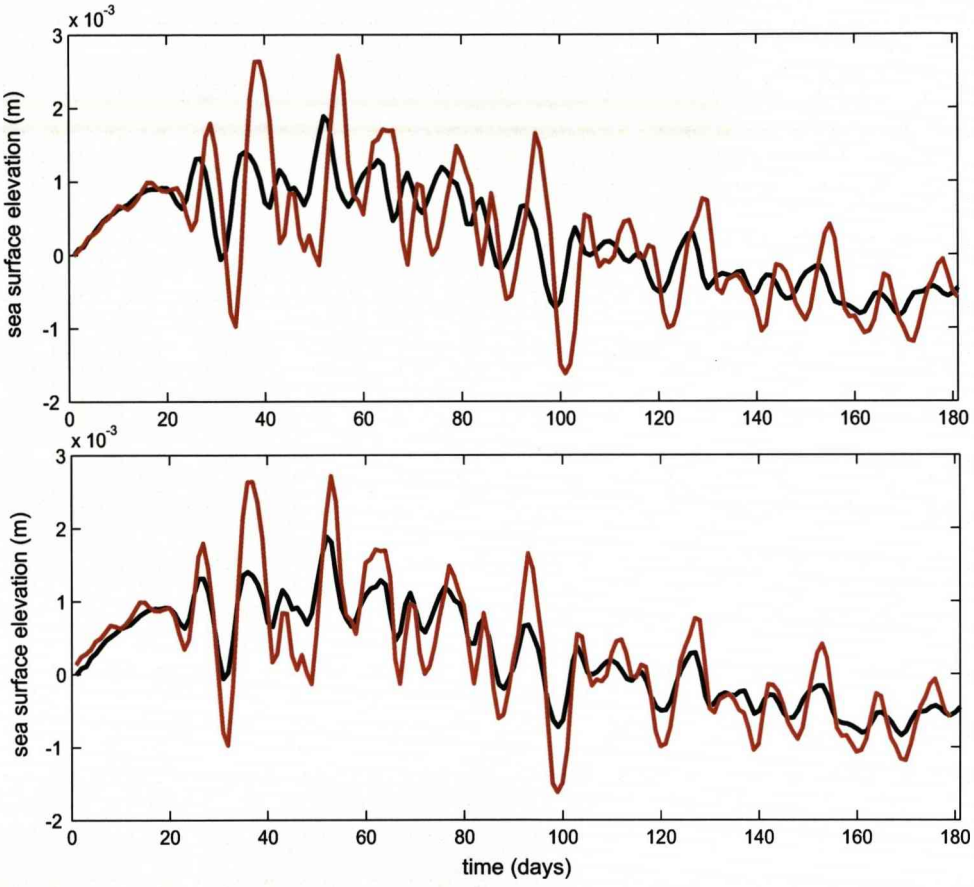

Figure 4.15: The sea surface elevation at $10°N$ (black line) and $30°N$ (red line) on the eastern boundary for the *slope* topography (top panel) and then when a two day lag has been applied to the $30°N$ data (bottom panel).

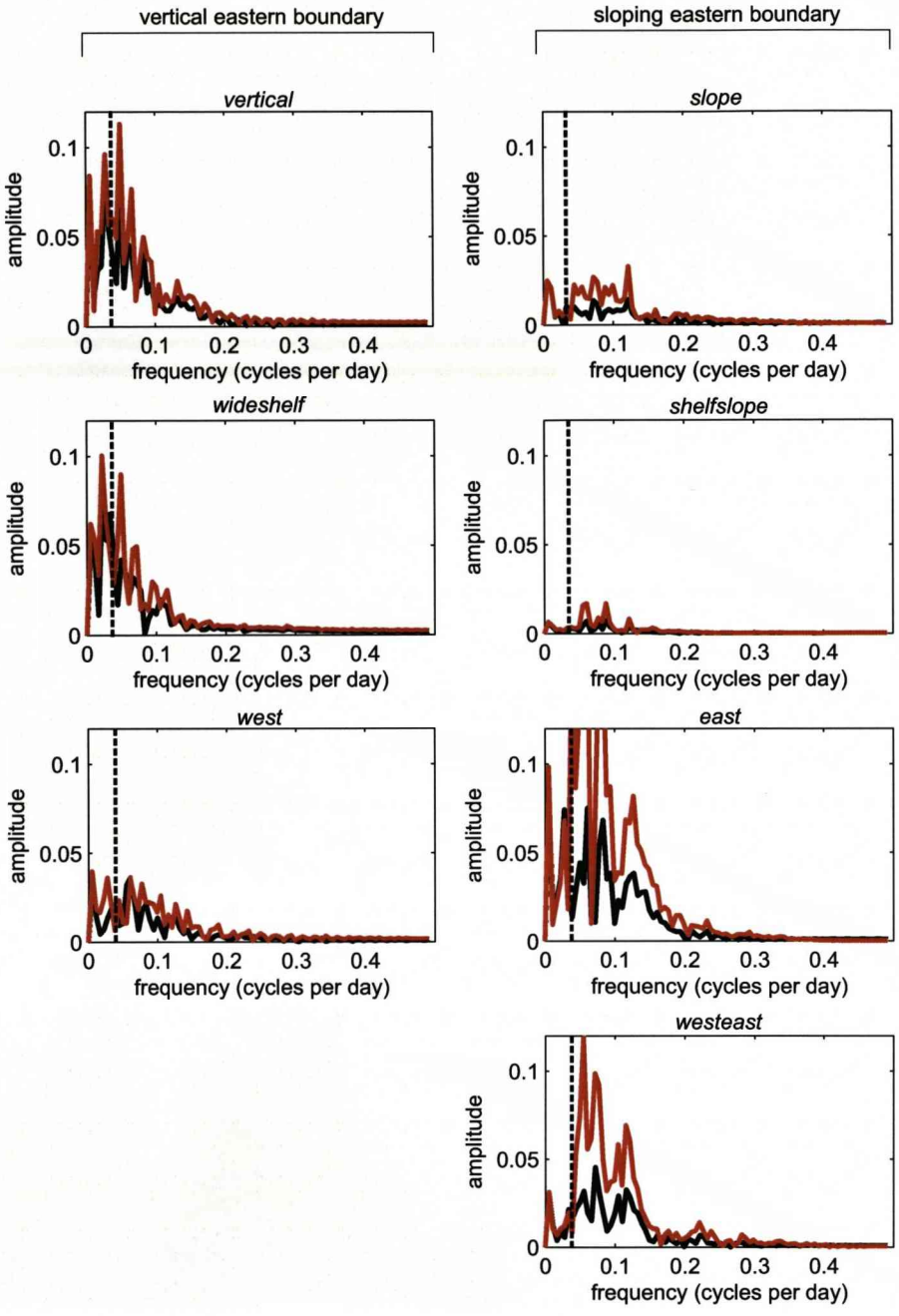

Figure 4.16: The amplitude has been plotted against the frequency for the sea level signal at $10°N$ (black line) and $30°N$ (red line). The maximum frequency for offshore propagation, ω_{max}, for the baroclinic case is superimposed (black dashed line). The cases with a vertical eastern boundary are found to the left and those with a sloping eastern boundary to the right.

assuming $l = 0$ and with $k = \frac{1}{R_0}$ we can find the maximum frequency for offshore propagation, ω_{max}, is;

$$\omega_{max} = \frac{\beta R_0}{2} \tag{4.1}$$

where $R_0 = \frac{c}{f}$ and $\beta = (\frac{2\omega}{r_e}) \cos\phi$. There is, of course, both a baroclinic and barotropic wave speed and therefore a baroclinic Rossby radius ($R_0 = \frac{\sqrt{g'H_e}}{f}$) and barotropic Rossby radius ($R_0 = \frac{\sqrt{gH}}{f}$). For frequency values less than ω_{max} the energy can be propagated westwards into the deep ocean by Rossby waves.

At the equator the Rossby wave spectrum becomes a set of discrete modes and the equation for ω becomes (from Gill (1982));

$$\omega = \frac{-\beta k}{k^2 + \frac{(2n+1)}{R_{eq}^2}}$$

where $R_{eq} = \sqrt{\frac{c}{\beta}}$, the equatorial Rossby radius. This gives the maximum frequency;

$$\omega_{max} = \frac{\beta R_{eq}}{2\sqrt{2n+1}}$$

If we now substitute for R_{eq}, and choose $n = 1$, we obtain;

$$\omega_{max} = \frac{1}{2}\sqrt{\frac{\beta c}{3}} \tag{4.2}$$

From 4.2 we can calculate the minimum period and maximum frequency at which the baroclinic Rossby wave can exist at any latitude. At the equator $\beta = 2.29 \times 10^{-11}$ and therefore the period $T_{min} = \frac{2\pi}{\omega} = 28.2$ days. From this we find the maximum frequency to be 0.035 $cycles\ day^{-1}$. Higher frequencies cannot be attenuated by baroclinic Rossby wave radiation so can be expected to amplify unless they attenuate by barotropic Rossby wave radiation. The corresponding maximum frequency for barotropic Rossby waves $\omega_{max} = 0.25\ cycles\ day^{-1}$. If re-amplification occurs as a result of an increasing f parameter, the amplification factor is calculated as;

$$AF = \frac{sin30°}{sin10°} = 2.88 \tag{4.3}$$

The amplification factor for the eastern boundary time series was calculated for the frequency ranges less than AF_1, or greater than AF_2 the maximum frequency for baroclinic Rossby waves but less than the barotropic ω_{max};

$$AF = \frac{\sqrt{amplitude(30°N)^2}}{\sqrt{amplitude(10°N)^2}}$$

Table 4.1 summarises the amplification factors, AF_1 and AF_2, calculated for the two frequency ranges. There is a clear pattern differentiating between the cases with a vertical eastern boundary and those with a sloping eastern boundary. With a vertical eastern boundary we observe a degree of amplification in both frequency ranges but AF_2 is greater than AF_1, except for the *west* example.

Topography	*eastern slope?*	AF_1	AF_2
vertical	no	1.21	1.48
wideshelf	no	1.16	1.47
west	no	1.54	1.24
slope	yes	1.00	2.16
shelfslope	yes	1.12	2.25
east	yes	1.01	2.78
westeast	yes	1.02	2.51

Table 4.1: Amplification factors, AF_1 and AF_2 calculated over the two frequency ranges for the seven topographies organised according to presence of a sloping eastern boundary.

In the cases where there is a sloping eastern boundary we see very little amplification, AF_1 values are close to 1, below the baroclinic ω_{max} suggesting very effective offshore radiation of baroclinic Rossby waves. This is perhaps somewhat surprising as it indicates that despite the coastal trapped signal, excited on the eastern boundary by the equatorial Kelvin wave, being largely barotropic it does indeed couple very well with baroclinic Rossby waves in the frequency range for which propagation is possible. Additionally the AF_2 values for these cases approach the theoretical AF value calculated in (4.3) indicating very little barotropic Rossby wave radiation, this is especially true of the *east* example.

When the eastern boundary is a vertical wall; as in *vertical*, *wideshelf* and *west*; we find some degree of amplification in both frequency ranges. The AF_1 values indicate somewhat less effective radiation of baroclinic Rossby waves and the AF_2 values are considerably less than the theoretical AF value indicating some degree of attenuation.

Our original suggestion of a sloping eastern boundary resulting in greater amplification of the polewards propagating signal than in the case of a vertical boundary therefore holds but not according to our original theory. Amplification according to theory does not result in a decrease in offshore propagation of baroclinic Rossby waves. Indeed a sloping eastern boundary is found to very effectively radiate baroclinic Rossby waves

at the low frequencies where propagation is possible and amplify at higher frequencies according to theory.

The eastern boundary behaviour along a vertical wall is initially puzzling; we would expect the baroclinic Kelvin waves supported here to couple very effectively with the baroclinic Rossby waves resulting in complete radiation at frequencies below the baroclinic ω_{max}; however, this was not the case. This result along with the apparent damping of expected amplification at higher frequencies leads us to suggest that friction may be responsible for the differences between the vertical and sloping boundary examples.

All of the MITgcm runs, at this point, have been completed with lateral friction corresponding to a Munk width ($\partial_M = (\frac{A_h}{\beta})^{\frac{1}{3}}$ of 92 km. The baroclinic Rossby radius ($R_0 = \frac{c}{f}$) relevant to our model ocean is equal to 137 km at $10°N$ and only 48 km at $30°N$; at latitudes greater than $15°N$ the Munk width is therefore greater than the baroclinic Rossby radius. This leads us to suggest that the lateral friction is attenuating the amplification of the coastal trapped signal resulting in the decreased AF_2. We also suggest that friction is responsible for the reduced effectiveness of offshore Rossby wave propagation at low frequencies.

When topography is present, it is the barotropic or shelf Rossby radius which is important. This is calculated as between 1236 km and 429 km over the latitude range in question and is therefore always larger than the Munk width thus reducing the frictional influence. The example with topography can then behave in a manner closer to the theoretical ideal.

4.6.2 Propagation speed analysis

From the lag values used in 4.6.1 we can calculate the corresponding wave speeds for all the topographic cases. For the examples with a sloping eastern boundary (*slope*, *shelfslope*, *east* and *westeast*) a two day lag was calculated representing a wave speed of 12.88 ms^{-1}. It is clearly evident from both the time series plots and our previous wave mode calculations that there is not a single wave mode but a number of modes travelling at different speeds. If we look back to our idealised wave mode calculations of Chapter 2 the wave speed calculated from the lag here is comparable to those found for the coastal Kelvin wave like mode 1 wave; this mode's wave speed at $10°N$ is 8.84 ms^{-1} and at $30°N$ is 16.52 ms^{-1} from the barotropic results of Chapter 2.

It is likely the mode 1 wave dominates the signal in the slope case as it is trapped against the coastal wall from where the data was extracted whereas the higher mode coastal trapped waves are supported further offshore over the slope. Where the eastern boundary is a vertical sidewall (*vertical*, *wideshelf* and *west*) a seven day lag is cal-

culated corresponding to a wave speed of 3.68 ms^{-1} which is close to the theoretical baroclinic Kelvin wave speed of 3.48 ms^{-1} we would expect here.

4.6.3 Eastern boundary conclusions

- At the low frequencies, where Rossby waves exist, the largely barotropic signal along a sloping eastern boundary couples very well with baroclinic Rossby waves as shown by the lack of amplification. We had anticipated that even long-period waves would reamplify with topography, but our results show quite clearly they do not.
- At higher frequencies the coastal trapped signal in the sloping boundary cases amplifies as expected.
- In the case of a vertical sidewall, with a Munk width greater than the baroclinic Rossby radius, the radiation of baroclinic Rossby waves and amplification of the eastern boundary signal is attenuated by the effects of lateral friction. In the sloping boundary case the relevant barotropic Rossby radius is always greater than the Munk width resulting in little frictional influence.
- Wave propagation on the eastern boundary is significantly faster when topography is present, as fast largely barotropic coastal trapped modes are excited, in agreement with the wave mode calculations of Chapter 2.

4.6.4 Southern hemisphere adjustment

In a number of the simulations we see rapid adjustment, within one month, in the southern hemisphere. Indeed a signal on the western boundary of the southern hemisphere becomes apparent within days of forcing commencing in the North Atlantic (Fig 4.17). In the deep ocean, the barotropic Kelvin waves travel at 171.55 ms^{-1} covering over 14800 km per day so we could expect the barotropic mode to be forcing such an adjustment on the timescale of days.

From the sea surface elevation field 5 days into the simulation (Fig 4.17) we can clearly see evidence of a signal on the western boundary of the southern hemisphere especially in the *shelfslope* and *wide shelf* cases. The results of Chapter 2 showed the deep ocean barotropic or double Kelvin wave speed being modified by the effects of the topography. However, the adjustment timescale of these mode 0 waves is still of the order of days as confirmed by Fig 4.17. The mode 1 coastal Kelvin wave and mode 2 slope trapped modes will take weeks or months to reach the southern hemisphere, and perhaps longer if delayed by processes within the equatorial region.

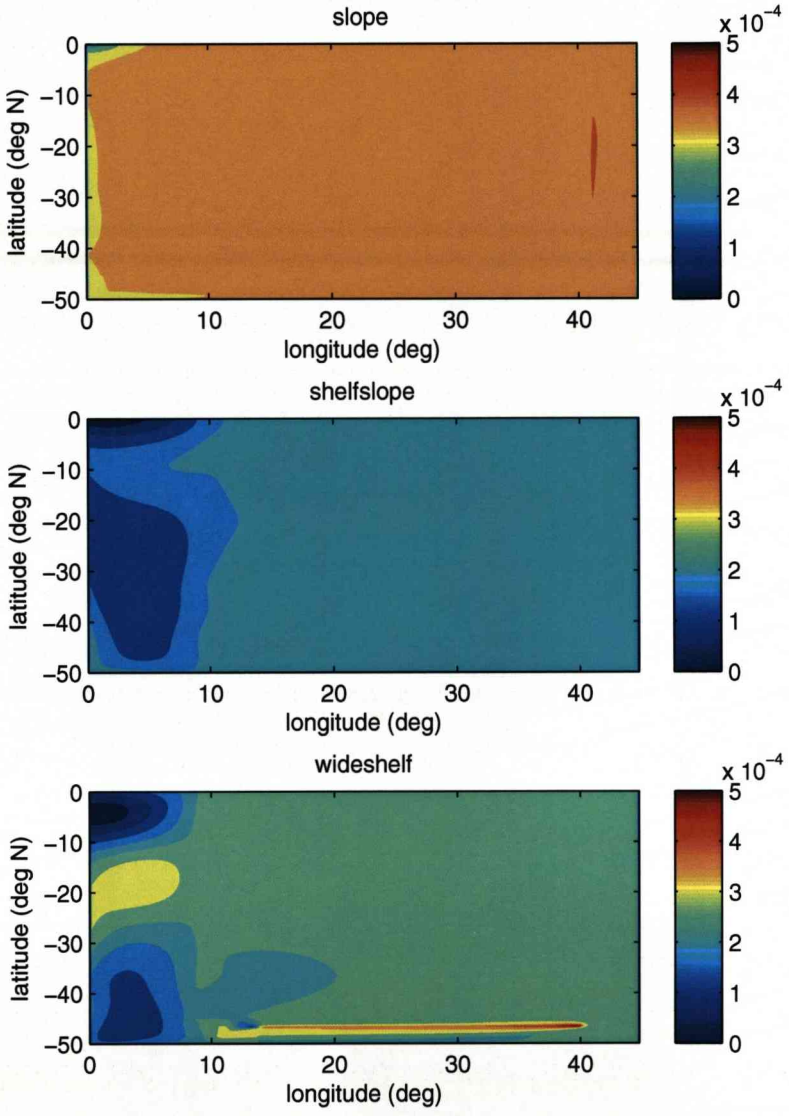

Figure 4.17: Sea surface elevation field (in metres) at t=5 days for *slope* (top panel), *shelfslope* (middle panel) and *wideshelf* (bottom panel) topographies. A signal is clearly seen on the western boundary of the southern hemisphere, albeit small in magnitude. The contour interval here is 5×10^{-5}.

This rapid southern hemisphere adjustment is not seen in JM02 but was identified in the isopycnic model study of Roussenov et al. (2008) using realistic topography. They suggested that the rapid adjustment was the result of the barotropic mode which propagates round the ocean basin within a matter of days and certainly before the arrival of coastal trapped waves. Our results also show such rapid propagation in the initial stage of adjustment. Roussenov et al. (2008) were concerned that the sponge layer at their southern boundary may have contibuted towards this effect; however, there is no such sponge layer in our study and a similar result is observed.

This result suggests that the barotropic mode provides a very fast full ocean response to forcing, as a result of density re-distribution; however, the amplitude of this response is small.

4.7 Open boundary in the Southern Ocean

In an attempt to make the idealised experiments more realistic, open boundaries in the Southern Ocean (a cyclic boundary condition in place of the eastern and western boundaries over a 5° latitude range north of the southern slope) were introduced (*opensouthern*) to represent the linking nature of the Southern Ocean. The forcing and topography setup of *opensouthern* in the basin is identical to slope and can therefore be compared directly to assess the impact of the open boundaries.

The inclusion of the Southern Ocean appears to make very little difference to the adjustment pattern in the model Atlantic in the timescale here of 30 days (Fig 4.18). The behaviour on the western boundary of the South Atlantic differs, but the extent of this difference is of the order of *mm*. The pattern in η evident over the North Atlantic is nearly identical to the closed boundary solution.

By $t = 360$ days the adjustment pattern over the western boundary region has remained almost identical in *opensouthern* and *slope*. Over the rest of the basin there is some difference; however, as we described earlier the magnitudes of the signal outwith the western boundary region are small.

From this result we can conclude that although including a Southern Ocean may appear to be a more realistic option, it does in fact make a minimal difference to the adjustment pattern especially in the North Atlantic which is the area of most interest. Therefore the use of closed boundaries in all other experimentation can be deemed valid. However, it should be noted that the real world ocean has three basins rather than the one represented in these MITgcm simulations and this impact has not been assessed here.

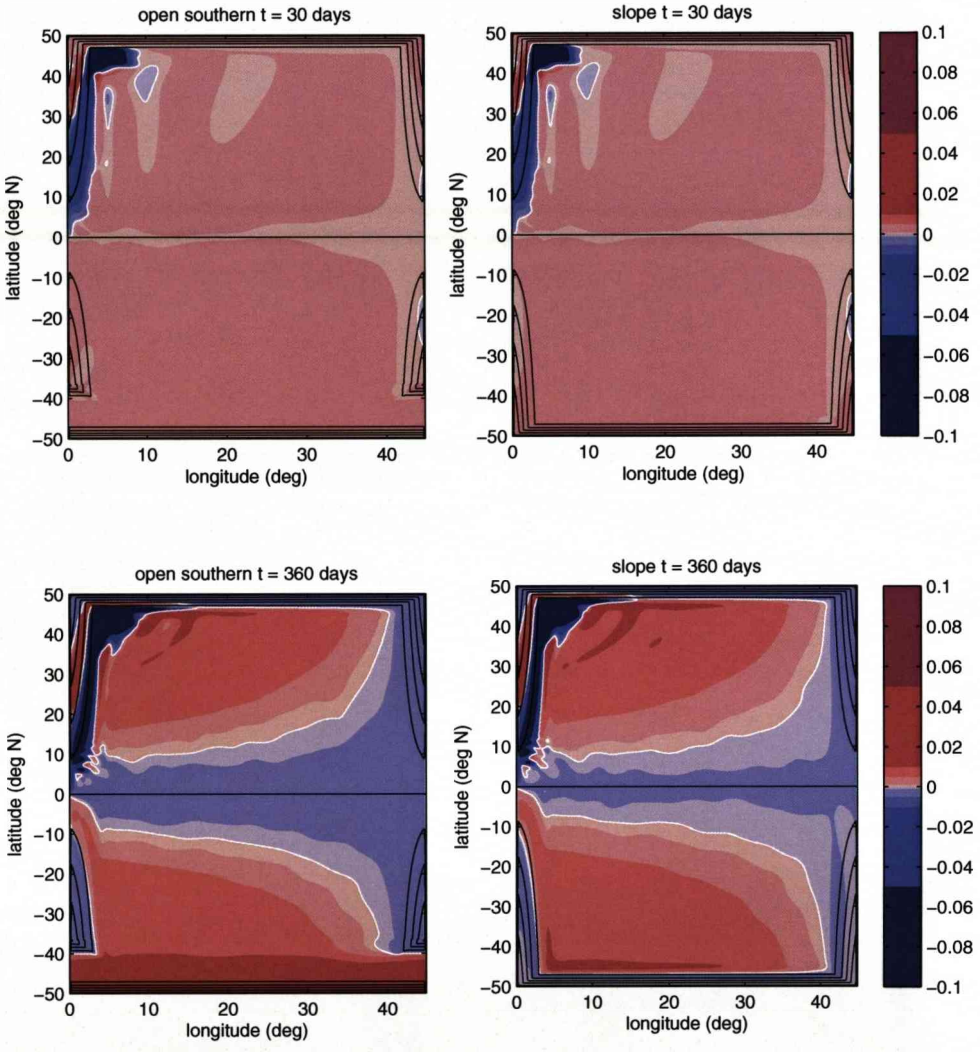

Figure 4.18: Sea surface elevation plots (in metres) at $t = 30$ (top) and 180 (bottom) days for example with *opensouthern* (left) and the closed boundary comparison slope (right) at $t = 30$ and 360 days. Contours of $\frac{f}{h}$ are superimposed onto the η field (black lines).

4.8 Chapter summary

The key findings of this chapter examining the whole Atlantic Ocean response to a change in North Atlantic forcing are summarised:

- It is clear that the coastal trapped wave response is the most important adjustment process in response to high-latitude forcing.
- The inclusion of topography into a model Atlantic basin has important implications for the adjustment pattern observed over the western boundary region of the North Atlantic. In a topographic basin the coastal trapped waves are modified resulting in a faster propagation of the perturbation due to the generally higher wave speeds of barotropic Kelvin waves and higher mode coastal trapped wave modes than baroclinic Kelvin waves.
- Although differences can be detected in experimentation with a variety of topographic basins, with the exception of the western boundary region of the North Atlantic, the magnitude of these differences are small.
- The sign of the sea level anomaly along the western boundary is not constant, as is the case in a vertical sidewalls basin, when there is topography present on the northern boundary.
- Fast moving barotropic coastal trapped waves initiate offshore propagation of barotropic Rossby waves allowing for rapid adjustment of the whole ocean basin on a shorter timescale than the purely baroclinic case in agreement with Roussenov et al. (2008). The amplitude of this signal is small and the higher coastal trapped modes are required to develop an overturning response to forcing.
- A sloping eastern boundary excites a largely barotropic coastal trapped signal. Although this might be expected to couple less well with baroclinic Rossby waves, and therefore to produce a coastal sea level signal that grows in amplitude with increasing f, we find that such amplification is confined to frequencies at which baroclinic Rossby waves cannot exist. These results show that western boundary topography does not act to strengthen the trapping of eastern boundary waves.
- The topography either reduces or delays the Rossby wave response, despite producing faster wave speeds. This may be as these coastal trapped wave modes do not match the equatorial Kelvin waves as effectively as the baroclinic Kelvin wave of the vertical sidewall case. Remoteness of the wave node from the density interface also appears to play a part.

- The inclusion of an open boundary to represent the Southern Ocean does not significantly affect the adjustment pattern over the western boundary region of the North Atlantic.

It is clear from the experiments contained in this chapter that the most important effect of topography, besides altering wave speeds, is on the pattern of flow and sea level in the western boundary region of the North Atlantic, with coastal sea level changing quite markedly between the various cases. In the next chapter we will investigate this variability of the western boundary region in more detail.

Chapter 5

Idealised modelling: Local

5.1 Introduction

The conclusions reached in Chapter 4 suggest that although topography had an effect on the whole ocean adjustment the most significant impact of its inclusion was over the western boundary region. The form of topography on the western boundary resulted in considerable differences in the adjustment pattern over this area. Therefore this chapter will analyse the response to forcing over the western boundary region in more detail.

Firstly we will discuss the theoretical behaviour, according to JEBAR (Joint Effect of Baroclinicity and Bottom Relief) principles, that would be expected over a slope region as a result of forcing. The model results of Chapter 4 can then be compared to this theoretical ideal to help us understand the physical processes that are underway.

A forcing location experiment will be analysed according to the theoretical understanding to determine whether we could expect only a localised response to a forcing limited to the shelf or deep ocean regions, compared to the non local response we observed when forcing took place over both the shelf and slope region. In addition, we will test a case of forcing over the northern boundary slope to determine whether the adjustment pattern also behaves as the theory would suggest.

A further analysis will be completed into how frictional forces, both bottom and lateral, affect the magnitude and propagation pattern of the flow on the shelf and slope region with reference to frictional theory, and also to results from previous studies. We could expect increasing friction to lead to the flow deviating from inviscid theory.

Whether the recirculation of the coastal signal, resulting in a positive anomaly in sea surface elevation along the western boundary, which was observed at high latitudes in

the presence of a northern slope, is related to the frictional input will also be investigated.

Finally, the effect of different topography types and forcing locations on coastal sea level will be analysed. The vertical sidewalls examples, such as JM02, result in a homogenous negative anomaly in sea level along the entire western boundary region. The large scale results of Chapter 4 show that this would not be the case in a topographic ocean, without significant frictional influence, with variation between positive and negative anomalies over the western boundary of the northern hemisphere, when the northern slope is included. Therefore a more detailed analysis was required as to the details of the topographic effect on coastal sea level due to the potential implications for the impacts of rapid climate change and for the suggestions of the use of sea level as a proxy of the strength of the Meridional Overturning Circulation (Bingham and Hughes, 2009).

Although the results of these idealised experiments can prove revealing, it is necessary to determine whether the conclusions reached are transferable to a more realistic ocean. As such a continuously stratified run was completed and will be analysed against the two-layer results to determine the validity of this study's results. The inclusion of continuous stratification is not expected to differ greatly from the more idealised scenario in agreement with the detailed wave mode calculation results of Chapters 2 and 3.

5.2 Slope behaviour theory

Firstly we shall look at the theory of how flow is likely to behave over topography and we can then compare this to the results of the idealised experimentation. A theoretical adjustment pattern may be explained according to JEBAR principles. For a steady, linear, inviscid flow with no wind stress, the following constraint relates bottom pressure anomaly to changes in stratification (Hughes, 2008):

$$J(p_b, \frac{h}{f}) = -J(E, \frac{1}{f}) = \frac{E_x \beta}{f^2} \tag{5.1}$$

$$J(p_b, \frac{h}{f}) = \frac{\partial p_b}{\partial s} | \bigtriangledown \frac{h}{f} |$$

where $E = g \int_{-h}^{0} \rho' z dz$, p_b is the difference of bottom pressure from its initial state, ρ' is the difference of ρ from the initial state, h is the depth and f is the Coriolis parameter. The distance s is measured along the $\frac{h}{f}$ contour from NE to NW to SW. In the relaxation region ρ' is positive and z is negative. Therefore E is negative in the relaxation region and $E = 0$ elsewhere.

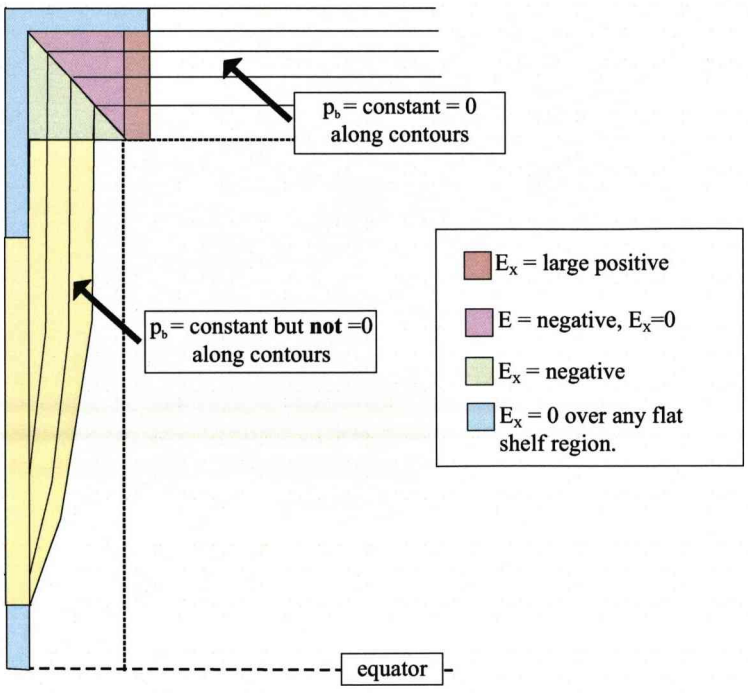

Figure 5.1: Annotated figure to explain the joint effect of baroclinicity and bottom relief (JEBAR) principles and can be related to the sea surface elevation patterns seen in the model runs.

(5.1) can then be written as;

$$\frac{\partial p_b}{\partial s} = \frac{E_x \beta}{|\bigtriangledown \frac{h}{f}| f^2}$$

Where E is constant, p_b is constant along $\frac{f}{h}$ contours. If along the northern boundary we assume $E = 0$ then p_b is constant and equal to zero along the contours. In the relaxation region E is negative and p_b is varying. On the western boundary, outside of the relaxation zone, p_b is again constant but not equal to zero. Near to the boundary p_b is small as $E = 0$ in shallow water (Fig 5.1).

Now we shall examine the sign we can expect the anomaly to have on the western boundary south of the relaxation region. If we look at Fig 5.2 in terms of an area integral we obtain;

$$\int J(p_b, \frac{h}{f}) dA = -\int J(E, \frac{1}{f}) dA$$

therefore

$$\oint p_b \bigtriangledown \frac{h}{f} . d\underline{s} = -\oint E \bigtriangledown \frac{1}{f} . d\underline{s} = \oint \frac{E}{f^2} \bigtriangledown f . d\underline{s}$$

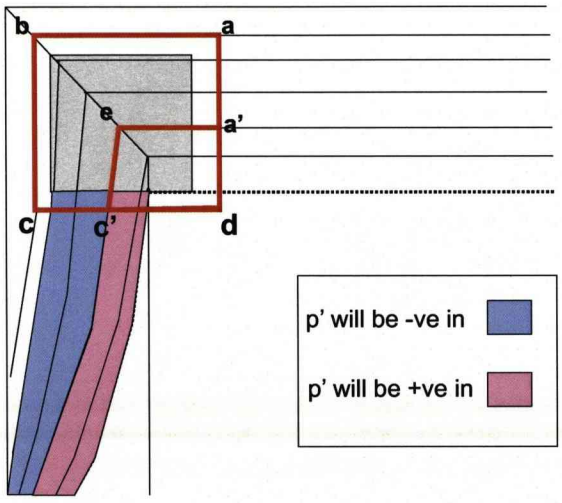

Figure 5.2: Annotated figure describing the area integral described in theory to calculate sign of anomaly along the western boundary. The black lines represent $\frac{f}{h}$ contours.

From Fig 5.1 we know that $E = 0$ outside of the grey shaded regions in Fig 5.2 and thus;

$$\oint_{abcda} \frac{E}{f^2} \bigtriangledown f.d\underline{s} = 0$$

therefore we can write;

$$\oint_{abcc'ea'a} \frac{E}{f^2} \bigtriangledown f.d\underline{s} = -\oint_{a'ec'da'} \frac{E}{f^2} \bigtriangledown f.d\underline{s} = \int_{c'}^{e} \frac{E}{f^2} \bigtriangledown f.d\underline{s} = \int_{c'}^{e} \frac{E\beta}{f^2} dy$$

This function is negative since E is negative here. If we now look at the problem in terms of pressure perturbation assuming $p_b = p_0 + p'$ where p_0 is equal to the value of the function of $\frac{h}{f}$ along da then around any circuit;

$$\oint p_0(\frac{h}{f}) \bigtriangledown \frac{h}{f}.d\underline{s} = 0$$

and

$$\oint p' \bigtriangledown \frac{h}{f}.d\underline{s} = \oint \frac{E}{f^2} \bigtriangledown f.d\underline{s}$$

and $p' = 0$ along da and outside the shaded regions. Therefore;

$$\frac{1}{f}\int_{c}^{c'} p' \bigtriangledown h.d\underline{s} = \int_{c'}^{e} \frac{E\beta}{f^2} dy = -ve = \frac{h(c') - h(c)}{f}\overline{p'} \tag{5.2}$$

where $\overline{p'}$ represents the vertical average between c and c' and

$$\frac{1}{f}\int_{c'}^{d} p' \bigtriangledown h.d\underline{s} = -\int_{c'}^{e} \frac{E\beta}{f^2}dy = +ve = \frac{h(d)-h(c')}{f}\overline{p'} \tag{5.3}$$

where, in this case, $\overline{p'}$ is the vertical average between c' and d.

From these expressions we find that $\overline{p'}$ must therefore change sign from negative in the shallower region (c to c') to positive in the deeper region (c' to d). If we choose c' to occur where $\overline{p'} = 0$ then $\overline{p'}$ will be negative in the shallow region (shaded blue in Fig 5.2) and positive in the deeper region (shaded red in Fig 5.2).

We can also describe the depth and zonally integrated geostrophic transport, T;

$$\begin{aligned} T &= \int_{h(c')}^{h(c)}\int_{west}^{east} \rho v_g dx dz \\ &= \frac{1}{f}\int_{h(c')}^{h(c)}\int_{west}^{east} \frac{\partial p}{\partial x}dx dz \\ &= \frac{1}{f}\int_{h(c')}^{h(c)} p_{east} - p_{west} dz \\ &= -\frac{h(c')-h(c)}{f}\overline{p'} \; if \; p_{east} = 0 \end{aligned}$$

Therefore the negative pressure anomaly corresponds to a northward flow over the upper slope with a southwards flow corresponding to the positive pressure anomaly in the deeper slope region.

Essentially if forcing occurs over non-zonal orientated $\frac{f}{h}$ contours, that is the green region in Fig 5.1, then the barotropic adjustment requires a rapid propagation of the bottom pressure anomaly with the structure shown by the red and blue regions in Fig 5.2.

5.2.1 Relationship with MOC

We can compare the flow patterns predicted by the theory with the Meridional Overturning Circulation. The temperature relaxation of our model study is designed to mimic convection, and the predicted response of the MITgcm runs represents an overturning brought about by a barotropic adjustment process. This is comparable to the single overturning cell found by Bingham et al. (2007) to dominate interannual MOC variability north of the Gulf Stream. Their OCCAM study shows a polewards upper layer above 1300 m and southwards lower layer between 1300 m and 3000 m, similar to the flow set up in our model basin in response to forcing (Fig 5.3).

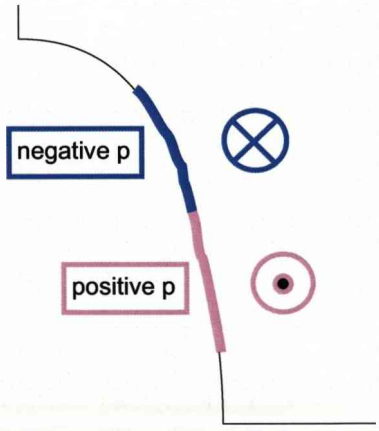

Figure 5.3: An illustration showing the negative anomaly on the shallower reaches of the slopes and the positive anomaly in the deeper regions and the resulting northwards and southwards flow, which can be compared to the single overturning cell described by Bingham et al. (2007).

5.2.2 Comparison with idealised experiments

Now we can compare this theoretical prediction of behaviour of an anomaly in a topographic ocean - with a shelf and exponential slope on the western boundary - to the results of the idealised experiments of Chapter 4 outside regions of significant density change. We can take the pressure perturbation p' to be equivalent to the sea surface elevation anomaly, η. It should be noted that it is the positive anomaly observed offshore, in deeper water, of the negative anomaly in η that is to be compared with the theoretical predictions of the propagation of anomalies in a topographic ocean.

Fig 5.4 shows that the negative perturbation does tend to largely follow the $\frac{f}{h}$ contours in line with the theory and the prediction of a negative anomaly in the shallower slope region and the positive anomaly on the deeper section. As the negative anomaly spreads equatorwards and up the slope there is some deviation away from the $\frac{f}{h}$ contours suggesting a frictional influence on the flow. The deviation from the contours would appear greater on the northern flank of the anomaly where the depth of the slope is shallower, and therefore a greater drag could be expected. We could also expect a second positive anomaly in very shallow water, which will not contribute strongly to the vertical integral in Fig 5.2, since it only exists over a small depth change.

Jackson et al. (2006) noted a similar pattern of flow along the $\frac{f}{h}$ contours of the western boundaries of both barotropic and baroclinic gyres in both the frictional and inertial limit. When friction was increased in the baroclinic solutions the stratification allowed for a weaker deep flow and as such the $\frac{f}{h}$ contours exerted less influence on the streamfunction (Fig 5.5). In their study the friction was found to control how the fluid moves

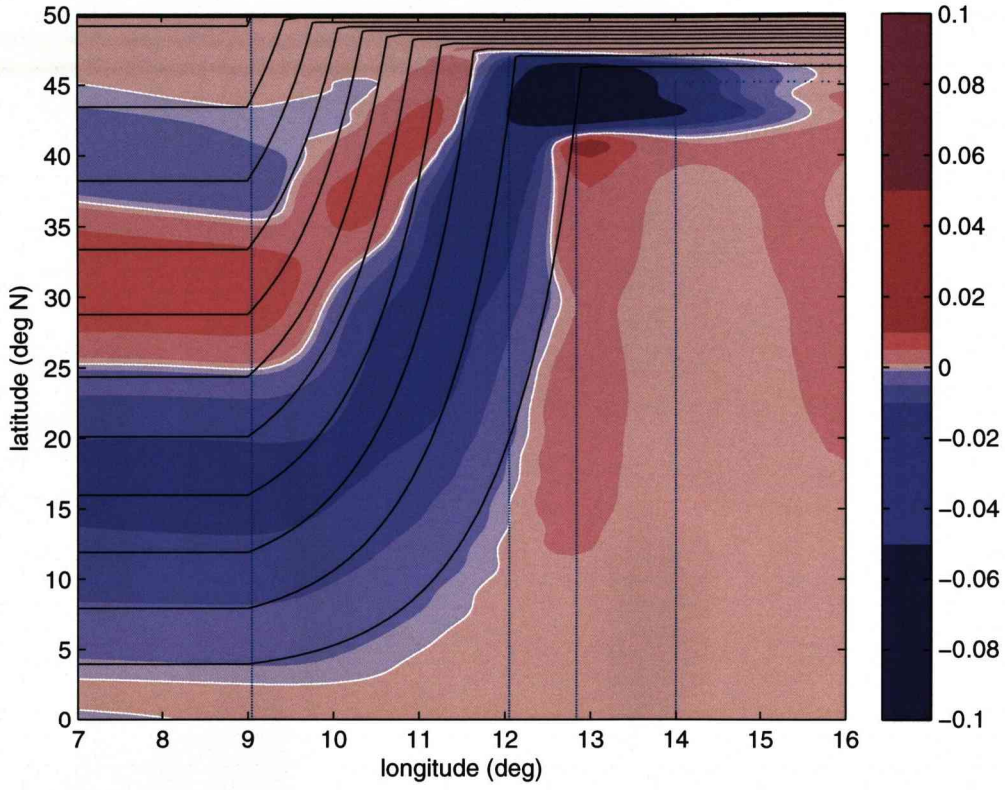

Figure 5.4: A close up of the forcing region in the *shelfslope* topographic experiment at t=30 days. The $\frac{f}{h}$ contours (black lines) and isobaths at 100 m, 500 m, 1000 m and 3000 m (blue dashed lines) are superimposed onto the η field.

across $\frac{f}{h}$ contours with higher (lower) friction forcing the fluid to higher (lower) $\frac{f}{h}$ contours.

Our experiment can be considered to be analogous to the classical two-gyre experiments, but with density (JEBAR) taking the place of the wind stress curl in driving the gyres. The forcing inside $a'ec'da'$ is analogous to a region of negative wind stress curl, and that inside $a'abcc'ea'$ is analogous to the positive wind stress curl, with $\frac{f}{h}$ contours taking the role played by f contours in the flat bottomed case.

In order to verify whether a similar effect of friction is relevant to the propagation of the anomaly along the western boundary in our study a frictional analysis has been completed (Section 5.4).

However, we will firstly carry out an analysis on the effect the location of the forcing region within the model basin has upon the adjustment pattern and then consider whether the results agree with the theory we have outlined in this section.

5.3 Location of forcing region

The importance of the location of the forcing region on the ocean adjustment pattern is now examined to determine whether the patterns we have observed over the slope region in previous experiments are still observed when the forcing region is relocated. Theory suggests that if forcing occurs over zonal $\frac{f}{h}$ contours, and therefore $dy = 0$, then we should not expect a rapid propagation of the anomaly away from the forcing region. To test this hypothesis, in addition to forcing acting over the shelf and slope region (*slope*, *shelfslope* and *wideshelf*), as in Chapter 4, we include three other forcing region locations (Fig 5.6): confined to the shelf region (*onshelfrelax*); confined to the deep ocean south of the northern boundary (*deepoceanrelax*); and over the central part of the northern boundary slope (*northsloperelax*).

5.3.1 Forcing over shelf and slope

There are pronounced differences in the sea surface elevation field depending on the location of the relaxation forcing region. In cases *slope*, *shelfslope* and *wideshelf* where the forcing region reaches over both the shelf and slope the response to the forcing is clearly nonlocal (Chapter 4: Fig 4.6). A response is also seen in the direction of propagation of boundary waves from the forcing region, along $\frac{f}{h}$ contours in *slope*. The perturbation travels southwards along the slope on the $\frac{f}{h}$ contours and spreads across the shelf, again along the $\frac{f}{h}$ contours which are constant in the longitudinal sense across

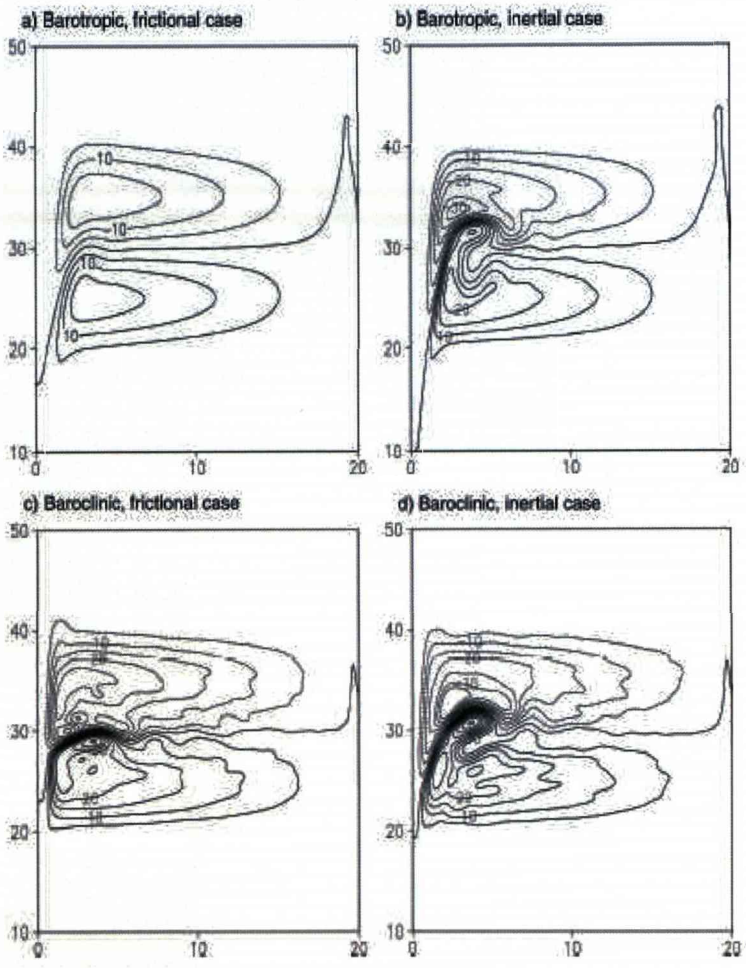

Figure 5.5: The streamfunction, ψ, for the following gyre integrations with sloping sidewalls: (a) barotropic frictional, (b) barotropic inertial, (c) baroclinic frictional, and (d) baroclinic inertial. The ψ pattern reveals a western jet running from the equator along the slope to the intergyre boundary, which remains broadly unchanged as the friction and stratification alters. The slope is typically 2° wide. From Jackson et al. (2006).

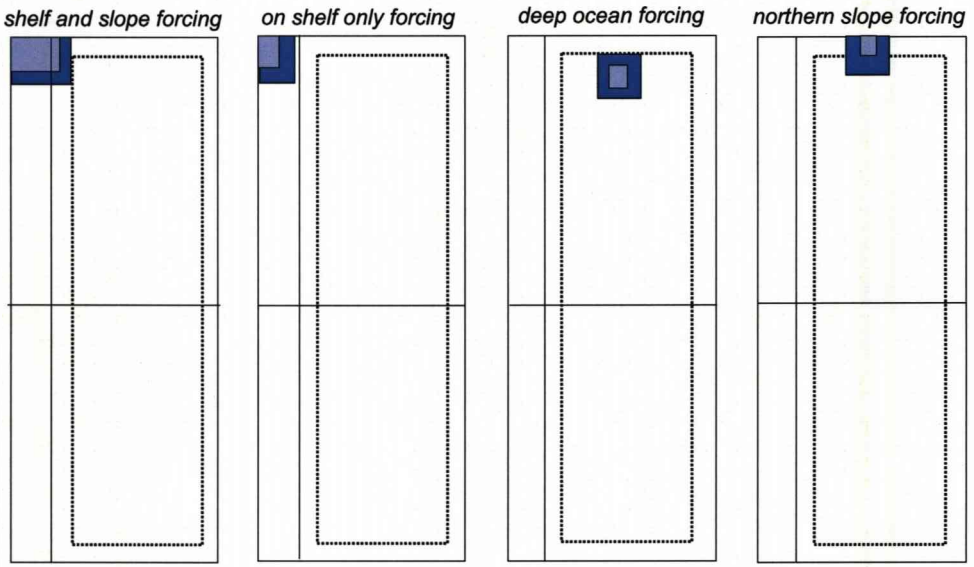

Figure 5.6: The four areas of temperature relaxation in the forcing experiments.

the shelf. In the case of *wideshelf* the negative anomaly leaks onto the shelf almost immediately and spreads across the shelf in the same manner as in *shelfslope.*

5.3.2 Forcing over shelf or deep ocean only

In the case of forcing being confined to the shelf region (*onshelfrelax*) or deep ocean (*deepoceanrelax*) there is a very small response away from the forcing region (Fig 5.7), confirming the importance of the slope region to the rapid propagation of influence away from the forcing region.

The location of the forcing region is clearly an important factor in whether the response of the forcing is local or non local and the speed at which the anomaly is propagated away from the forcing region. When forcing occurs over the shelf region or deep ocean away from any slope the short-term response is small and localised. In the case of forcing taking place over the slope region a non local response is clear alongside a rapid propagation of the anomaly away from the forcing region.

The theoretical explanation outlined at the start of this chapter has been shown to explain this behaviour over the slope. It can also provide the reasons for the limited response in these two other cases.

5.3.3 Forcing over the northern slope region

A third example was tested to examine whether the location of forcing within the slope regions affects the propagation pattern with an example with forcing taking place over the northern boundary slope region, away from either western or eastern slopes. This experiment resulted in rapid propagation (Fig 5.7), similar to that of forcing over the shelf and slope, which was not initially expected from the theory (Fig 5.8) as $dy = 0$ along $b'd'$, which is equivalent to $c'e$ in Fig 5.2, and therefore;

$$\int_{b'}^{d'} \frac{E\beta}{f^2} dy = 0$$

The negative and positive anomalies travel along the $\frac{f}{h}$ contours of the northern boundary and then follow them down the western boundary in a similar pattern, although slightly reduced in amplitude, to the *shelfslope* example (Fig 5.4). This leads us to suspect that the rapid propagation is therefore not only a process of barotropic adjustment but that the density anomalies in the relaxation zone initiate baroclinic processes resulting in propagation of the anomaly along the northern slope.

To further test the hypothesis that baroclinic processes are responsible for the propagation along the northern slope region an additional run was completed (*northrestrict*).

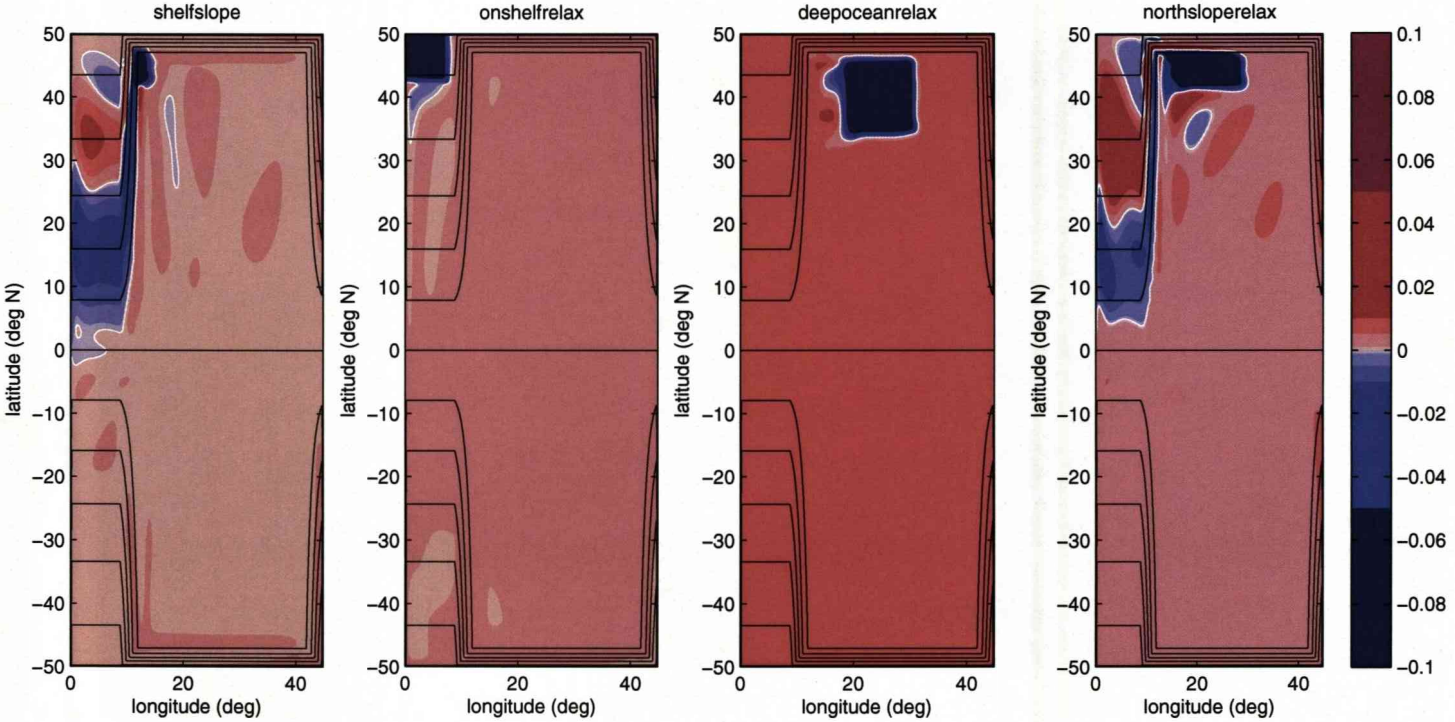

Figure 5.7: Sea surface elevation field (m) for examples *onshelfrelax* (left), *deepoceanrelax* (centre) and *northsloperelax* (right) at $t = 30$ days.

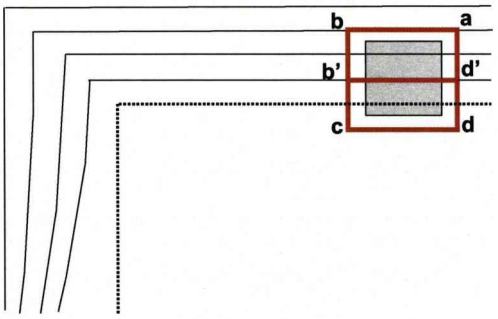

Figure 5.8: Diagram indicating the location of the forcing region over the northern exponential slope and the subsequent area integral relative to the JEBAR theory. The integral from b' to d' is equal to zero in this case as $dy = 0$ along this line. From the steady barotropic theory alone this would suggest only a limited localised response as was the case with shelf and deep ocean restricted forcing.

The density interface in the forcing region was relaxed in the same way as previous runs; however, the rest of the ocean was relaxed to the initial density field instead of being allowed to evolve as before. This should restrict the baroclinic processes, and therefore restrict the non local response along the western boundary, we observed in *northsloperelax* (Fig 5.7). The relaxation timescale was reduced to seven days to limit the baroclinic response as far as possible; any further reduction in the timescale of relaxation would likely result in numerical problems. The forcing region was moved eastwards for increased clarity but remained away from the influence of the eastern boundary.

We can see in Fig 5.9 that by restricting the baroclinic response in this way we do not observe the clear propagation pattern along the slope region as was the case in the initial northern slope forcing experiment. The disturbances seen over the shelf and interior regions are due to the hard relaxation forcing the fast barotropic modes around the basin. Interestingly when the baroclinic response has been restricted we can clearly see that the positive and negative anomalies along the western boundary are the result of the barotropic mode.

In *northsloperelax*, when the baroclinic processes are unrestricted and the forcing region is located closer to the slope, we see a skew on the westwards edge of the forcing region as the baroclinic flow propagates towards the slope. In *northrestrict* the restriction of the baroclinic response has resulted in an even greater skew of the whole forcing region as the baroclinic flow setup by the anomalies in the density field tries to escape as baroclinic Rossby waves (Fig 5.9). This skew reflects the fact that vertical velocities associated with the density anomaly (Fig 5.10) produce density changes which cause the

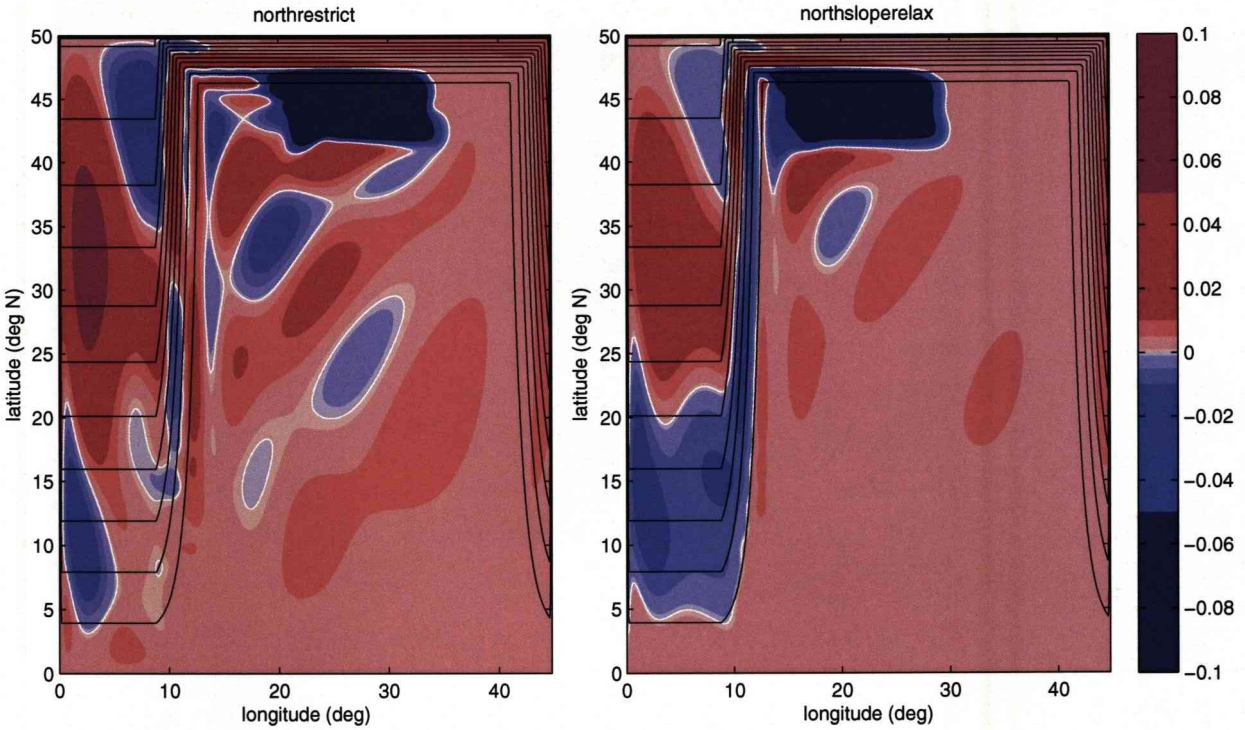

Figure 5.9: Sea surface elevation field (m) for the case where baroclinic processes are restricted outside of the forcing region, *northrestrict* (left), and the case where there is no restriction (*northsloperelax*). The forcing region in northrestrict has also been moved further away from the western boundary slope than is the case in *northsloperelax*.

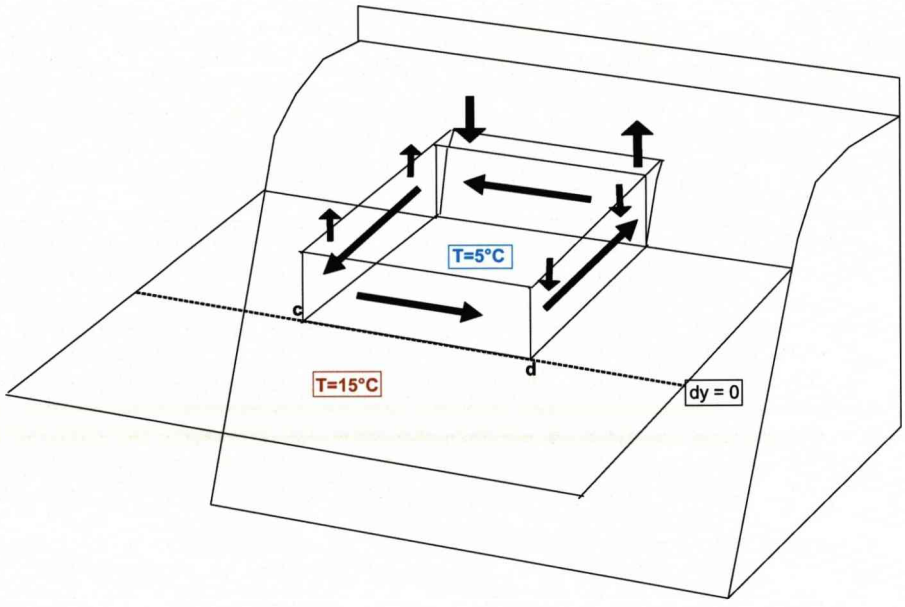

Figure 5.10: Circulation and upper layer velocities associated with a patch of raised density interface. The black lines represent the upper layer velocities initiated by the changes in density as a result of the temperature relaxation within the forcing region over the northern slope. Although we have attempted to hold the density anomaly close to constant by relaxation, the associated thermal wind flow implies large vertical velocities which are tending to modify the anomaly (in opposite senses at its eastern and western end), making it very difficult to maintain the symmetry required for the effect of the anomaly on bottom pressure to integrate to zero.

anomaly to propagate, making time dependence important. Strong relaxation prevents a coherent propagation resulting in a more complicated bottom pressure response.

We can therefore conclude that the theory set out in Section 5.2 does adequately explain the barotropic processes behind the pattern of signal propagation in slope regions with varying f. However, baroclinic processes must be taken into account in regions of constant f where forcing is occurring over a slope region: the density perturbation cannot be chosen arbitrarily as it will produce large local adjustment processes.

5.4 Frictional effects

As described in Section 5.2.2, Jackson et al. (2006) found that the effect of friction was to deviate the flow from the $\frac{f}{h}$ contours in their idealised study of ocean gyres with sloping sidewalls. In this section we will investigate how varying friction, both lateral and bottom, affects the propagation pattern on the western boundary and determine whether the Jackson et al. (2006) result is also found in this study. A classification

system was devised to assess the effect of either bottom or lateral friction on the propagation pathway in η by extracting the latitude of the point of minimum sea surface elevation, $\eta_{minimum}$, along the longitudinal value in the middle of the shelf region at $7°E$ at $t = 30$ *days*. A higher latitude value for the $\eta_{minimum}$ corresponds to a greater deviation from the $\frac{f}{h}$ contours. We approach this analysis in terms of length scales derived from frictional theory.

5.4.1 Frictional theory

We consider the effects of friction and nonlinearity that become important in a steady circulation, after some time (t_s) from spin up of the ocean in response to forcing, and may lead to a steady western boundary current of width $\delta = (\beta t_s)^{-1}$.

Taking the curl of the depth-averaged momentum equation, for a homogenous, flat-bottomed ocean, but retaining nonlinear terms and two forms of friction (both lateral and bottom), we come to the vorticity equation;

$$\frac{D}{Dt}\zeta + \beta v + r_b\zeta - A_h \bigtriangledown^2 \zeta - f\frac{\partial w}{\partial z} = 0 \tag{5.4}$$

where A_h is the lateral viscosity coefficient and r_b is the linear bottom drag function. The type of layer formed as the boundary thins is dependent upon whether the bottom friction, lateral friction or nonlinearity terms become important first (Gill, 1982).

Stommel's solution

If we look first at the case where lateral friction is ignored and only bottom friction is maintained (when $t_S = r_b^{-1}$), this corresponds to Stommel (1948) original model for western intensification. The boundary layer width under these conditions is;

$$\delta_S = \frac{r_S}{\beta}$$

where δ_S denotes the Stommel scale of boundary layer thickness for western intensification and r_S is the bottom friction.

Munk's solution

When lateral friction becomes important first, and bottom friction is ignored, we refer to the Munk (1950) model which describes the vertical average of a baroclinic ocean

with negligible bottom velocities (Pedlosky, 1996). Here t_S is of order $\frac{\delta^2}{A_h}$ which leads to a boundary, or Munk, layer width of;

$$\delta_M = (\frac{A_h}{\beta})^{\frac{1}{3}}$$

Fofonoff mode

The final possibility is that the nonlinear terms will become important initially allowing the free, nonlinear mode of motion discovered by Fofonoff (1954). The change in velocity component across the boundary layer will have the same magnitude U as that in the interior and t_S is of the order $\frac{\delta}{U}$ resulting in an inertial boundary layer width of;

$$\delta_I = (\frac{U}{\beta})^{\frac{1}{2}}$$

All of the models discussed above are relevant only to a barotropic ocean, however, a length scale analysis utilising the length scales found may provide an interesting insight into the importance of the barotropic response in the MITgcm experimentation. For this analysis we are using sea surface elevation, η, as a diagnostic from the model output and we therefore write (5.4) in terms of this variable, and integrate across the boundary current to obtain;

$$\frac{D}{Dt}\frac{\partial \eta}{\partial x} + r_b \frac{\partial \eta}{\partial x} - A_h \frac{\partial^3 \eta}{\partial x^3} + \beta(\eta - \eta_0(y)) = 0 \tag{5.5}$$

where $\eta_0(y)$ is the sea surface elevation at the outer edge of the boundary layer. We will use (5.5) to examine whether the impact of friction in the model simulations is comparable to what we would expect.

5.4.2 Varying bottom friction

In order to include the effects of bottom friction in the MITgcm the no-slip bottom boundary was initiated. Bottom drag is added in addition and is described as a stress, which is expressed as a linear or quadratic function of the mean flow in the layer above the topography. For simplicity, and in order to calculate δ_S easily, only the linear function of bottom drag was utilised, denoted by r_b, and the stress calculated from the following equations;

$$\tau_{13}^{bottomdrag} = (2A_v \frac{1}{\Delta r_c} + r_b)u$$

$$\tau_{23}^{bottomdrag} = (2A_v \frac{1}{\Delta r_c} + r_b)v$$

where A_v is the vertical viscosity coefficient and Δr_c is the vertical grid spacing between cell centres. The r_b value in the model is measured in ms^{-1} and is therefore not directly equivalent to the r_S value in the Stommel length scale equation, measured in s^{-1}. They can be related by $r_S = \frac{r_b}{H}$ where H is an average depth, set here as 1000 m, leading to a Stommel width, $\delta_S = \frac{r_b}{H\beta}$.

Two bottom friction scenarios were calculated with $r_b = 9.2 \times 10^{-4}$ and 3×10^{-3} ms^{-1} corresponding to $\delta_S = 92$ km (ds92noAh)and 300 km (ds300noAh) respectively. The length scale of the topography is around 900 km for the shelf plus an additional 550 km of slope region respective to a $25°N$ latitude. Each of these frictional scenarios was repeated with some lateral friction ($A_h = 500m^2s^{-1}$) to determine the extent of its effect in comparison to the effect of a changing bottom friction (ds92withAh and ds300withAh).

Veronis (1966) numerical study considered only the case of no bottom friction and a varying ratio of $\frac{\delta_I}{\delta_S}$. He found that at low values of $\frac{\delta_I}{\delta_S}$ the solution was equivalent to that of the Stommel solution. As the ratio is increased further (to 2, 4 and 8) the inertial effects become increasingly important until at $\frac{\delta_I}{\delta_S} = 8$ all east-west asymmetry was lost (Pedlosky, 1996).

5.4.3 Varying lateral friction

From the analytical solution of Munk (1950) when $x = \delta_M = (\frac{A_h}{\beta})^{\frac{1}{3}}$ the velocity has a maximum. Where $x = \pi.\delta_M$ the velocity is zero and the streamfunction has a maximum showing the width of the western boundary current to be $\pi\delta_M = \pi(\frac{A_h}{\beta})^{\frac{1}{3}}$. For numerical stability the MITgcm requires that δ_M is greater than the model resolution at low latitudes ($\approx$ 22 km). However, many people prefer to use $\delta_M = (\frac{A_h}{\beta})^{\frac{1}{3}}$ as a length scale with at least two grid points representing δ_M as this leads to a better representation of the western boundary current and less numerical noise.

A further stability criteria requires limitation in the lateral friction variable, A_h, according to a maximum value set by the horizontal Laplacian friction stability parameter described by;

$$S_l = 4\frac{A_h \delta t_v}{\Delta x^2}$$

The upper limit for stability of S_l is 0.3. As $\Delta x \approx$14 km at $50°N$ and the time step, δt_v, is equal to 800 seconds the maximum A_h value is $\approx 1.8 \times 10^4$ m^2s^{-1}. If we consider

Scenario	Stommel width (km)	Munk width (km)
nofric	0	0
ds92noAh	92	0
ds300noAh	300	0
ds92withAh	92	92
ds300withAh	300	92
dm92	0	92
dm300	0	300

Table 5.1: The Stommel width, δ_S, and Munk width, δ_M, corresponding to each of the frictional scenarios under examination.

the minimum value of δ_M representing at least two grid squares then the Munk width is limited to between approximately 44 km and 300 km.

In order to provide comparison with the bottom friction effects δ_M was also set at 92 km (dm92) and 300 km (dm300), both values being within the calculated limits described. The lower value corresponds to an A_h value of 500 $m^2 s^{-1}$. The idealised experiments of Chapter 4 were carried out with no bottom friction and an A_h value of 500 $m^2 s^{-1}$ ($\delta_M = 92$ km).

5.4.4 Results and Analysis

The MITgcm was run with the six scenarios described in the previous two sections plus a run without the influence of lateral or bottom friction (nofric) to provide a basis for comparison. These seven frictional scenarios are outlined in Table 5.1.

Effect of bottom friction

The inclusion of bottom friction has a significant impact on the adjustment pattern along the western boundary shelf-slope region of the domain. This is seen in the forcing of the propagating negative anomaly up onto the shelf across a number of $\frac{f}{h}$ contours, in a similar way to the effect of a decreasing topographic length scale. When compared to the non-frictional case the point of minimum η crossing moves from 26°N to 38.5°N with $\delta_s = 92$ km and to 40.5°N when $\delta_S = 300$ km for the lowest topographic length scale value (Fig 5.15). There is not a substantial difference between the two δ_S cases, despite the increase from 92 to 300 km (Fig 5.12), given the large deviation from the initial case of no frictional influence (Fig 5.11).

The inclusion of bottom friction slows and attenuates the coastal trapped signal. A notable result of the decrease in speed and magnitude of the coastal trapped signal is the almost complete absence of the shallow positive anomaly in sea surface elevation clearly

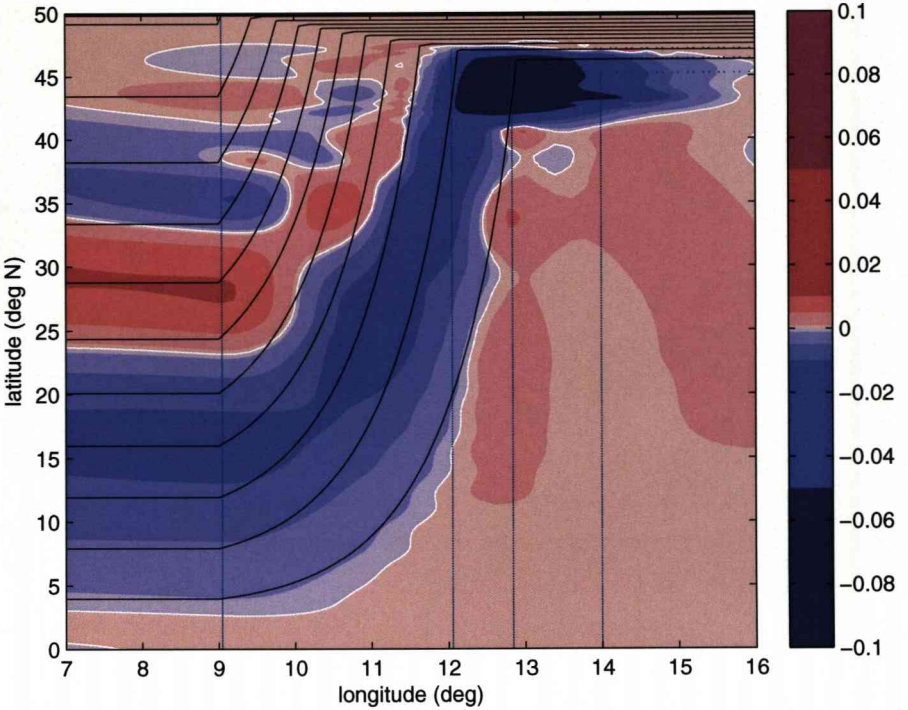

Figure 5.11: Sea surface elevation (m) with overlaid topography (blue dash) and $\frac{f}{h}$ contours (black line) for the case of no lateral or bottom friction at $t = 30$ days.

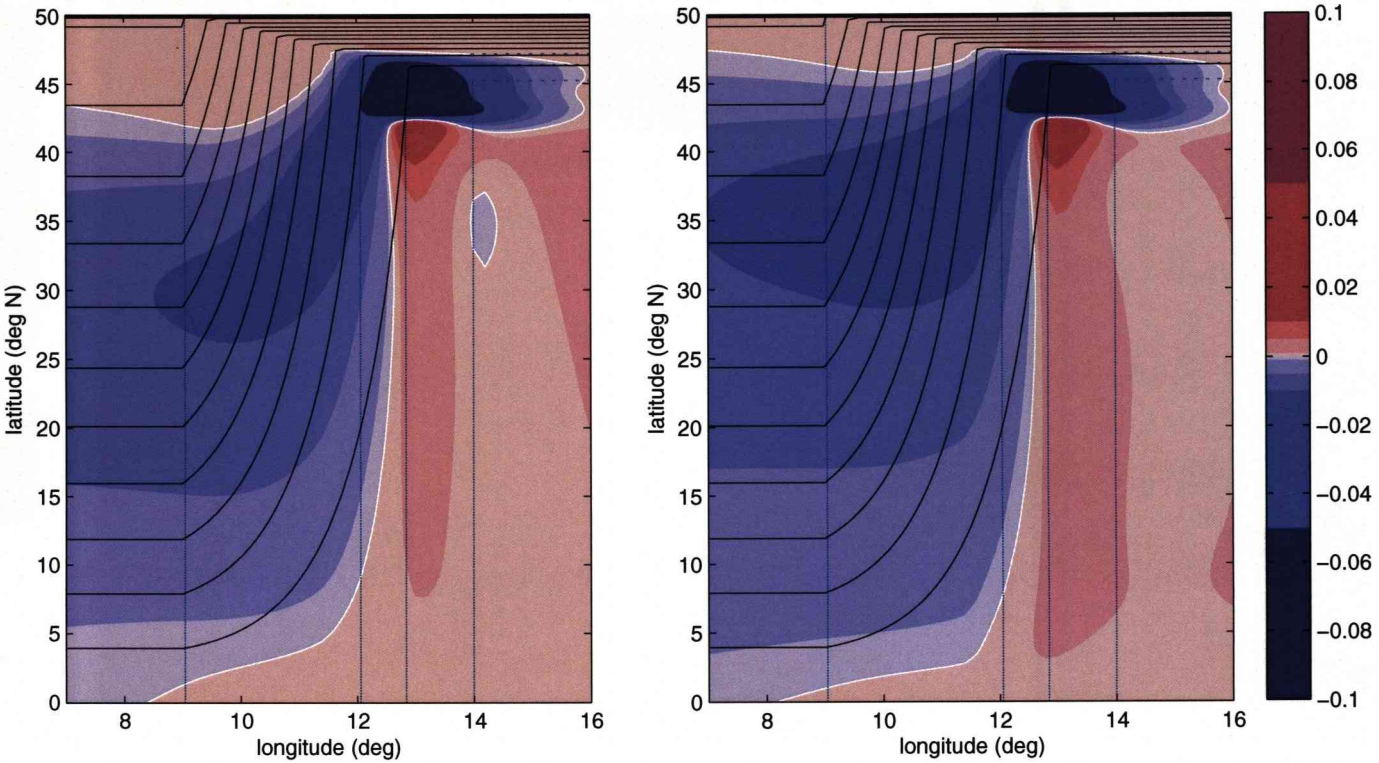

Figure 5.12: Sea surface elevation (m) with overlaid topography (blue dash) and $\frac{f}{h}$ contours (black line) for $\delta_S = 92\ km$ (left) and $\delta_S = 300\ km$ and inclusion of $\delta_M = 92\ km$ at $t = 30$ days.

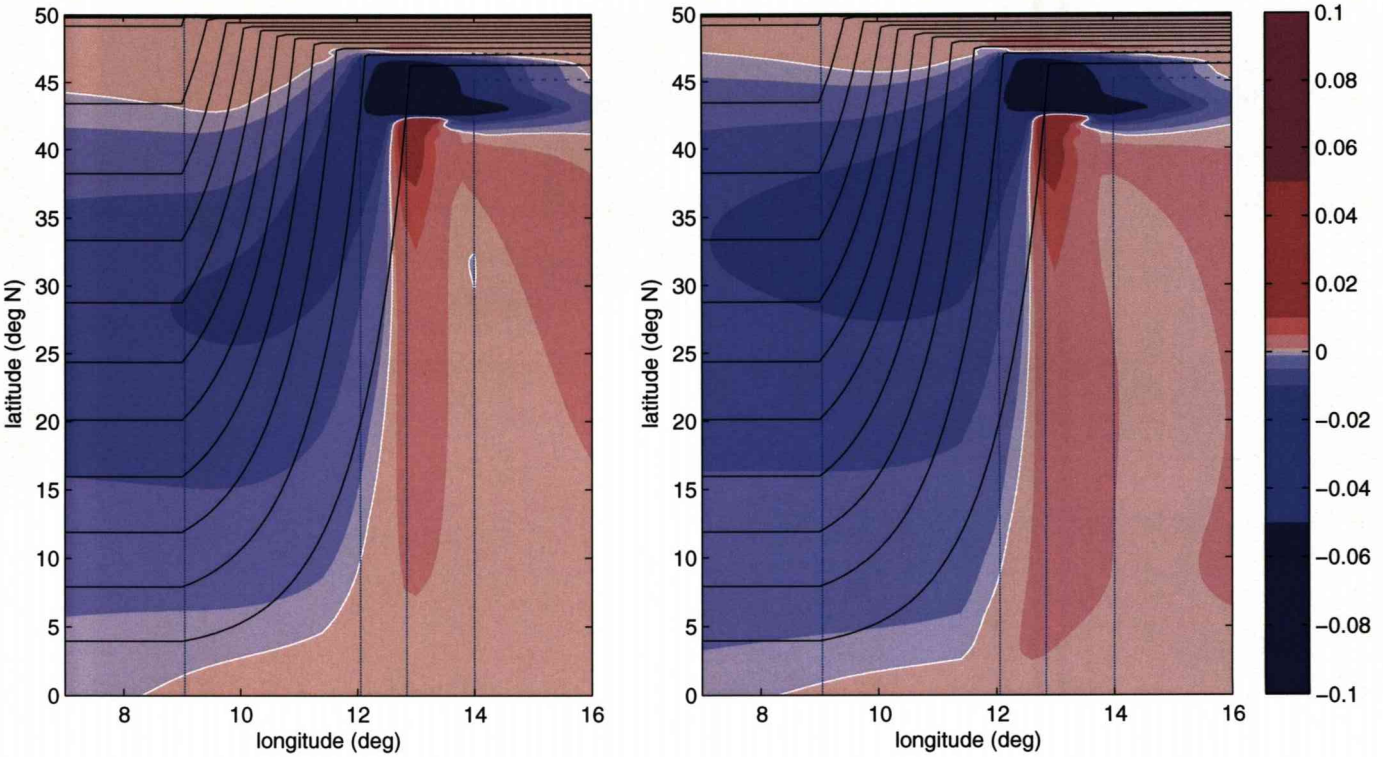

Figure 5.13: Sea surface elevation (m) with overlaid topography (blue dash) and $\frac{f}{h}$ contours (black line) for $\delta_S = 92\ km$ and $\delta_S = 300\ km$ with no lateral friction at $t = 30$ days.

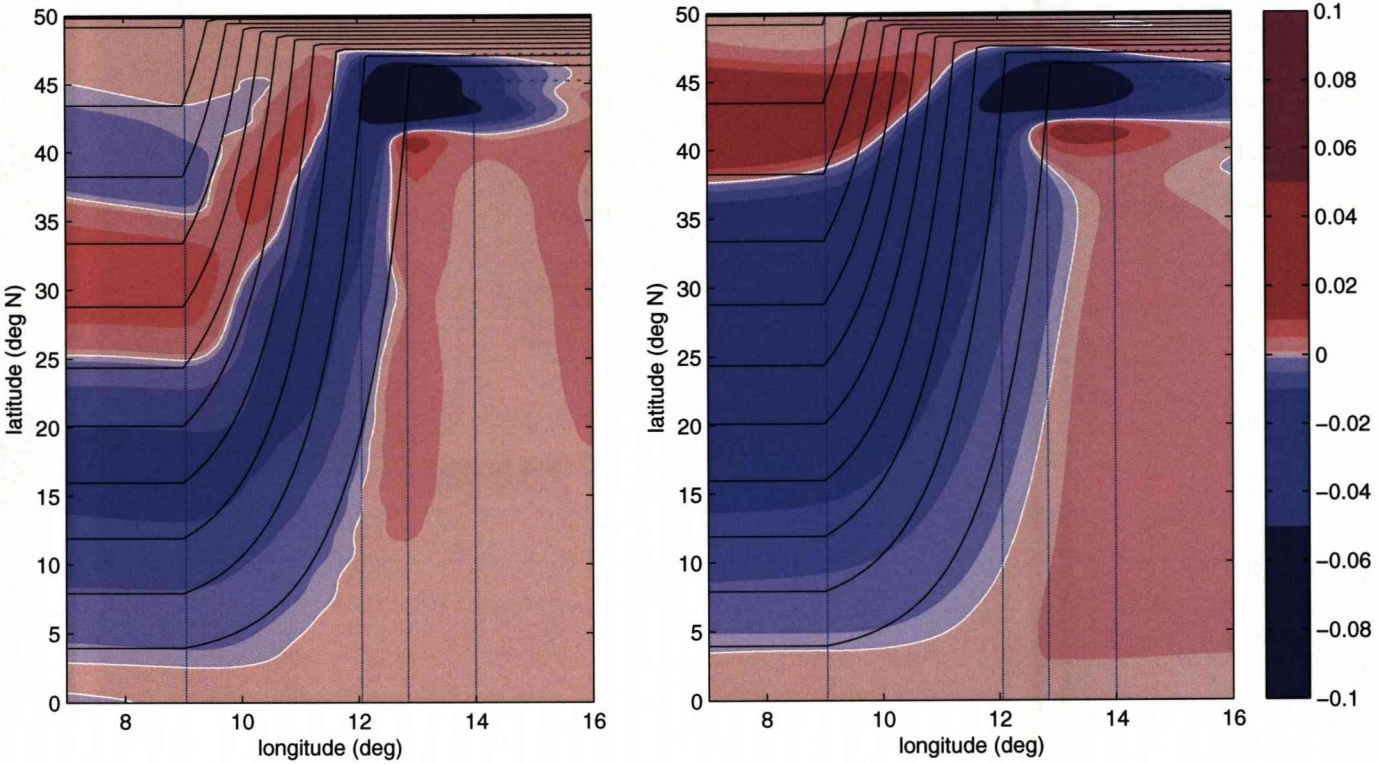

Figure 5.14: Sea surface elevation (m) with overlaid topography (blue dash) and $\frac{f}{h}$ contours (black line) for $\delta_M = 92\ km$ and $\delta_M = 300\ km$ with no bottom friction at $t = 30$ days.

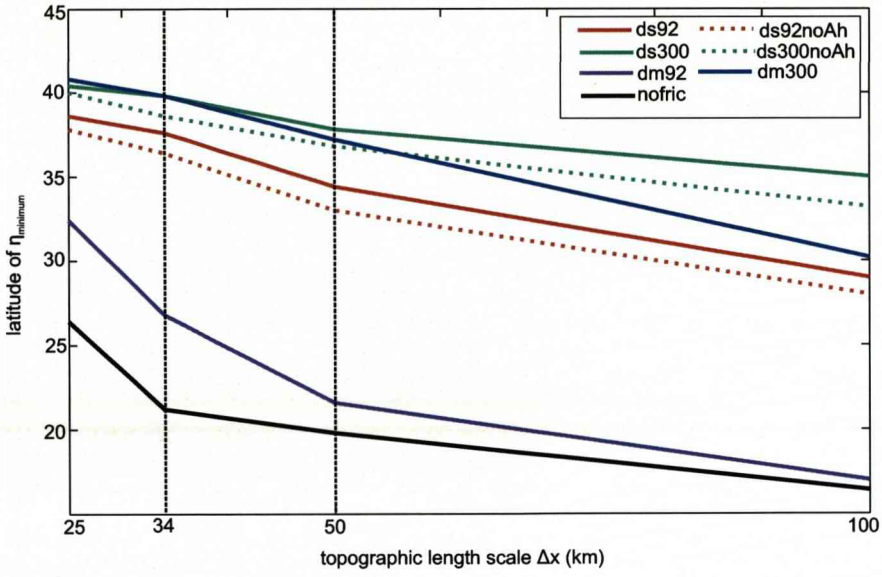

Figure 5.15: Comparison line graphs showing the latitude where the point of minimum η, $\eta_{minimum}$ contour crosses $7°E$ for all frictional scenarios over the varying topographic length scales.

observed in nofric (Fig 5.11), and the experiments presented in Chapter 4, propagating equatorwards along the western boundary shelf region. In addition to the attenuation of the coastal trapped wave modes, the increased deviation from $\frac{f}{h}$ contours results in the negative anomaly reaching the shelf region at higher latitudes (Fig 5.15) thus preventing any weak recirculating signal from propagating southwards.

Effect of lateral friction

The addition of lateral friction appears to have a less significant effect on the propagation pattern of the sea surface anomaly with the negative anomaly more closely following the $\frac{f}{h}$ contours along the slope before reaching the shelf region much closer to the equator than is the case in the bottom friction scenarios. If we compare the $\delta_M = 92\ km$ case (Fig 5.14) to that where there is no frictional influence (Fig 5.11) we see that the adjustment pattern is similar. When a lateral friction component corresponding to a Munk width of 92 km was added to both the δ_S cases there was a negligible difference to the adjustment pattern and classification results indicating the dominance of bottom friction.

There is, however, a greater difference between the adjustment pattern observed in the $\delta_M = 92\ km$ and $\delta_M = 300\ km$ cases than in the δ_S cases (both with and without

inclusion of lateral friction). This, however, could be expected when looking at the corresponding change in A_H and r_b values;

$$\Delta A_H = \beta(\frac{\Delta\delta_M}{\pi})^3$$

$$\Delta r_b = H\beta\Delta\delta_S$$

From these equations it can be seen that although there is an equal change in δ_M and δ_S, this results in a Δ^3 change in A_H and subsequent increase in lateral stress component which is not the case for the bottom drag parameter, r_b.

Due to the more limited impact of the inclusion of lateral friction on the speed and magnitude of the coastal trapped signal we again observe a positive anomaly in sea surface elevation propagation equatorwards along the western boundary shelf region (Fig 5.14). Where δ_M has been increased to 300 km the positive anomaly cannot propagate as far southwards, however, the magnitude of the anomaly is increased.

Response to steepening slope under frictional influence

In Chapter 4 we saw two regimes of propagation: firstly where the anomaly propagates southwards as a jet on the slope along the $\frac{f}{h}$ contours until they reach the shelf; and the second regime where the perturbation leaks almost instantly onto the shelf before propagating southwards. Further runs were then completed to determine how steep the slope must be before there is a shift from one regime to the other. Firstly no additional friction, either lateral or bottom, was added to this set of runs in order to see the effects of decreasing topographic length scale (Δx) more clearly. Our length scale starting point is that used throughout the experimentation in Chapter 4 of $\Delta x = 100$ km, assuming an example latitude of $25°N$. A further three, increasingly steep, profiles were tested with Δx of 50 km, 34 km and 25 km respectively.

As Δx decreases the degree of deviation from the $\frac{f}{h}$ contours becomes greater and increasingly like the pattern seen in the wideshelf example of Chapter 4.

With $\delta_S = 92$ km we find that a decreasing Δx results in the anomaly being deviated further from the pattern of $\frac{f}{h}$ contours up onto the shelf (Fig 5.16). In Chapter 2 we found the mode 2 wave speed increased with an increasing Δx which would appear to correspond to a lessened deviation of the negative anomaly from $\frac{f}{h}$ contours. Taking the mode 2 wave speeds at $25°N$ (1.93 ms^{-1}, 2.46 ms^{-1}, 3.47 ms^{-1} and 5.96 ms^{-1}) and using the spin down times corresponding to the relevant Stommel or Munk layer width we can calculate a distance over which the mode 2 wave has travelled during the spin down period for each Δx value (Table 5.2).

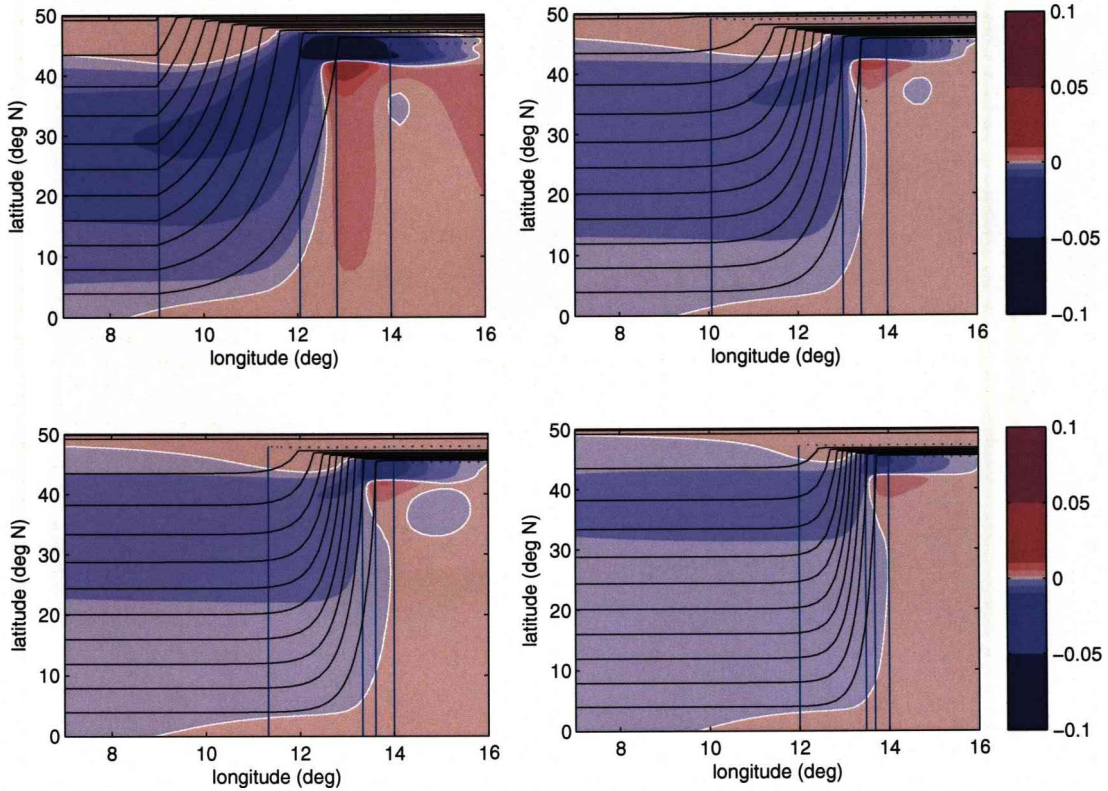

Figure 5.16: Sea surface elevation (m) with overlaid topography (blue dash) and $\frac{f}{h}$ contours (black line) for $\Delta x = 100\ km$ (top left), $50\ km$ (top right), $34\ km$ (bottom left) and $25\ km$ (bottom right) at $25°N$ for case with $\delta_S = 92\ km$ at $t = 30$ days.

Scenario	$\Delta x = 25\ km$	$\Delta x = 34\ km$	$\Delta x = 50\ km$	$\Delta x = 100\ km$
ds92noAh	2104	2681	3782	6497
ds300noAh	643	819	1156	1985
dm92	9.81×10^5	1.25×10^6	1.76×10^6	3.03×10^6
dm300	2.72×10^4	3.47×10^4	4.90×10^4	8.41×10^4

Table 5.2: Distance in m travelled by the mode 2 wave during the spin down period for each of the frictional scenarios and for each of the Δx values.

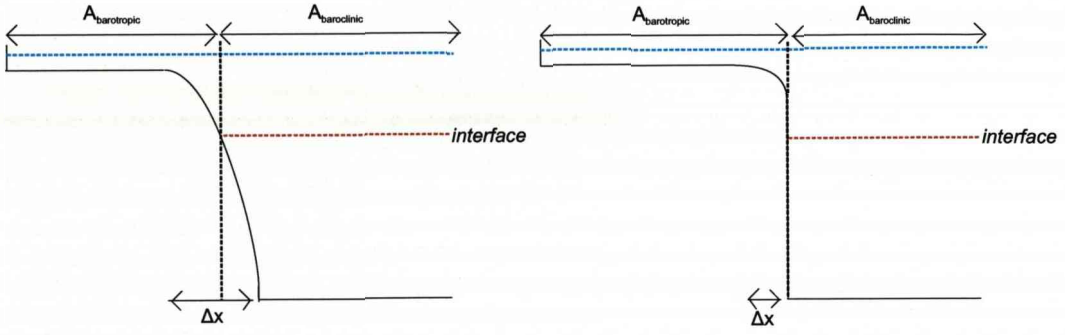

Figure 5.17: Cross sections illustrating the changing proportion of barotropic, $\Delta A_{barotropic}$, and baroclinic, $\Delta A_{baroclinic}$, influence in respect to the change in topographic length scale Δx

We can see the considerable difference between the effect of lateral and bottom friction; in the lateral friction scenarios the mode 2 waves can propagate over very large distances within the spin-down time whereas bottom friction reduces the distance the waves could be expected to travel considerably. The distance from the forcing region to the shelf along the $\frac{f}{h}$ contours could be estimated at approximately 4500 km. With the exception of scenario ds92 with $\Delta x = 100\ km$ this value is greater than the spin-down distance. Therefore the anomaly crosses the $\frac{f}{h}$ contours to reach the shelf region within the spin-down time.

If we look at the change in the area under barotropic or baroclinic influence this may also help to provide an explanation for the pattern seen. From Fig 5.17 we can see that as the topographic length scale (Δx) decreases, the barotropic area $A_{barotropic}$ increases, and the baroclinic area $A_{baroclinic}$ decreases. Brink (1982b) suggested that stratification inhibits the effect of bottom friction as the vertical motions which accomplish the spin up process are inhibited and also that barotropic CSW are more susceptible to frictional decay than baroclinic Kelvin waves. In this example the baroclinic influence in the slope region is reduced as Δx decreases. This results in greater deviation from the $\frac{f}{h}$ contours which was also seen when the bottom friction was increased supporting the assertion of Brink (1982b).

Mitsudera and Hanawa (1988) did suggest that this theory is only true for the mode 1 wave and that in fact damping increases as stratification becomes stronger as a result of a change in wave characteristics. However, Clarke and van Gorder (1986) show that the conclusions of Brink (1982b) remain true despite the different approach taken in their two sets of calculations. It should be noted that both the Brink (1982b) and Clarke and van Gorder (1986) results are only strictly valid for decay times long relative to the wave period (Brink, 1990).

5.5 Western boundary sea level fluctuations

In Chapter 4 we saw how the topography type, and particularly the inclusion of a northern exponential slope, affected the sea level pattern along the western boundary of the domain and this will now be discussed in more detail. Such an effect has important real world implications in terms of climate change mitigation and adaptation planning and also should be considered in the event of sea level, measured from tide gauges, being used as a measurement or proxy for the strength of the MOC as in Bingham and Hughes (2009).

5.5.1 Impact of topography type and location

The sea surface elevation along the western boundary of the model North Atlantic was plotted as a function of time (Fig 5.18) to determine the evolution of the sea level pattern after the initiation of forcing. In the vertical sidewalls case the negative anomaly fills the western boundary coast, on the timescale of a baroclinic Kelvin wave, with an increasing negative anomaly travelling equatorwards. The picture for both the *slope* and *shelfslope* cases is of a rapidly propagating negative anomaly along the western boundary closely followed by a positive anomaly which reaches around $17°N$ by three months and then stabilises at this latitude. After stabilisation occurs the anomalies become larger in respective magnitudes as time goes on.

As we saw in Chapter 4 when there is an exponential slope on both the western and eastern boundaries, but not at the northern and southern boundaries, the positive anomaly observed in the *shelf* and *shelfslope* cases is not found and as such negative sea level values are found at all latitudes (Fig 5.18). The inclusion of a northern slope opens up a propagation pathway for the coastal trapped signal, travelling at greater wave speeds than the baroclinic Kelvin wave along a vertical sidewall, allowing for re-circulating waves and a resultant positive sea level anomaly. In the realistic North Atlantic there is an almost continuous continental shelf along the northern North Atlantic leading us to suggest that there will be some degree of recirculation.

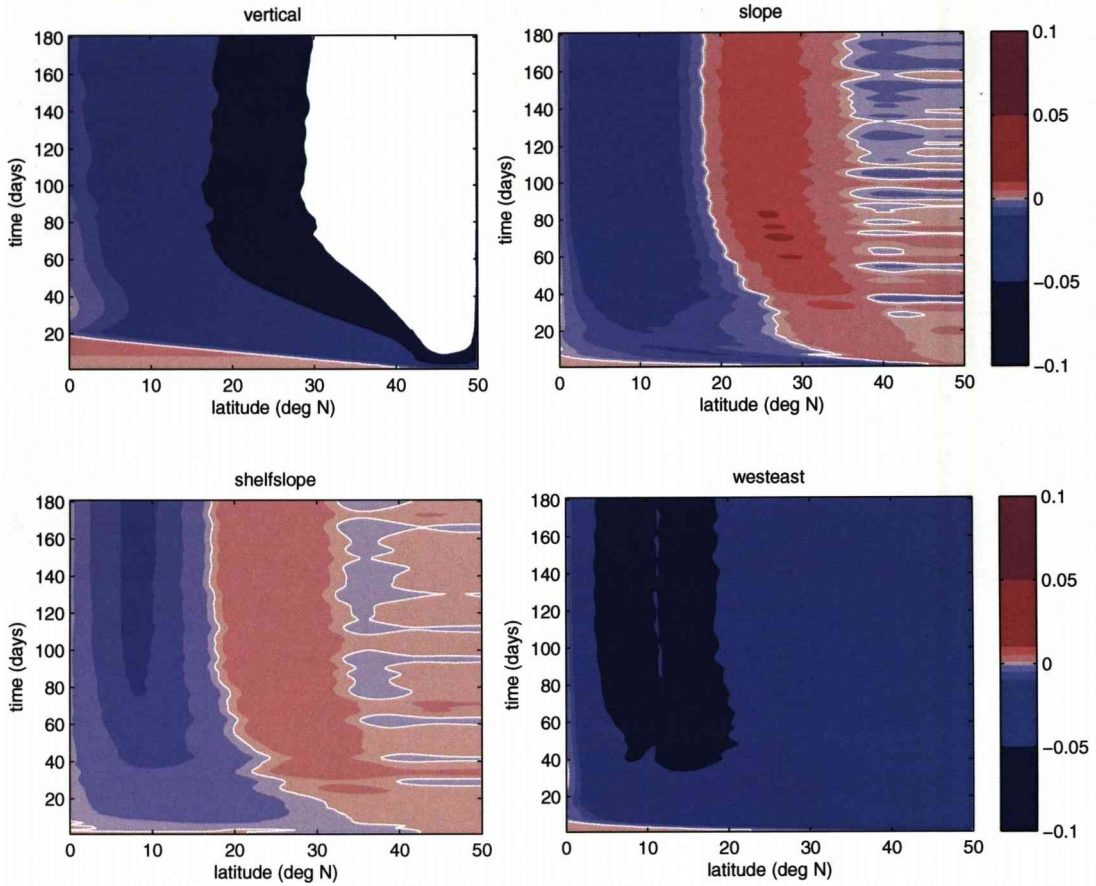

Figure 5.18: Hovmueller plots of the western boundary sea level for the first six months of the model simulation for *vertical* (top left), *slope* (top right), *shelfslope* (bottom left) and *westeast* (bottom right) topographies. Areas in white represent negative anomalies less than $-0.1\ m$.

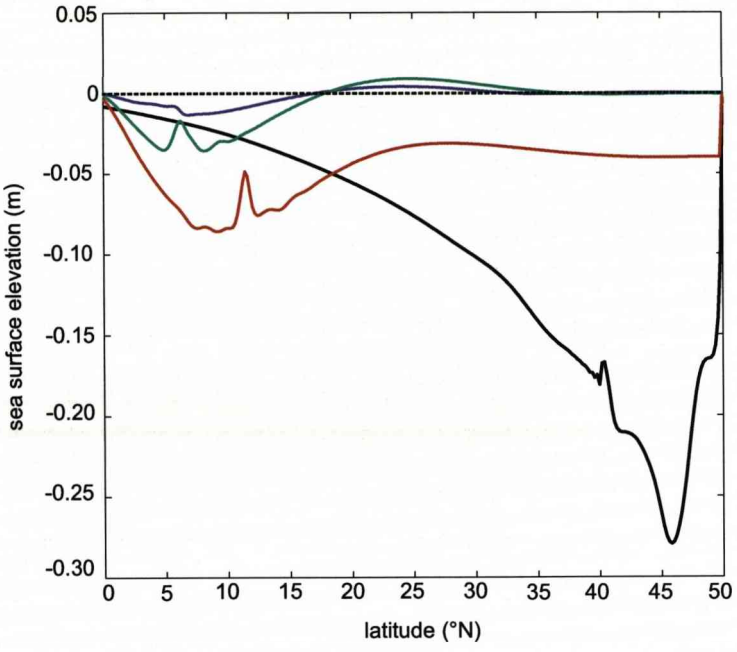

Figure 5.19: Line graph showing the sea surface elevation in m along the western boundary for *vertical* (black line), *slope* (green line), *shelfslope* (magenta line) and *westeast* (red line) at $t = 180$ days.

We now examine the relative magnitudes of the sea level anomalies corresponding to each of the topography types mentioned (Fig 5.19). It is clear that the negative sea level anomaly, outside of the forcing region itself, is much larger, of the order of tens of *cm* in the *vertical* example than in the other cases. When topography is introduced on the western boundary we firstly find a reduction in the magnitude of the anomaly and especially so for the two cases (*slope* and *shelfslope*) where slopes are also included at all boundaries. Indeed the positive or negative sea level anomalies of the *shelfslope* case are of the order of *mm* and in the *slope* case, a few *cm*.

Therefore it would seem that, in an ocean with topography the absolute sea level anomaly at any point along the western boundary is minimised compared to a vertical sidewalls basin. However, a sloping northern boundary results in both a positive (higher latitudes) and negative (lower latitudes) sea level anomaly. In short, details of topography and friction can lead to much more complicated coastal sea level signals than in the vertical sidewall case.

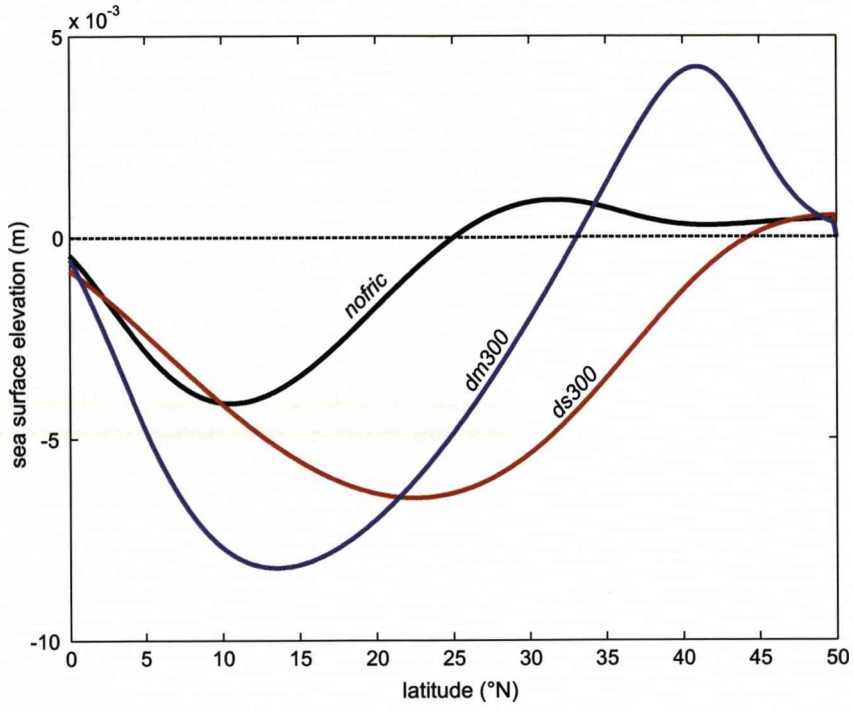

Figure 5.20: Line graph showing the sea surface elevation in m along the western boundary for the no friction (black line), $\delta_S = 300\ km$ (red line) and $\delta_M = 300\ km$ (magenta line) at $t = 30$ days for the slope topography.

5.5.2 Impact of frictional effects

In Section 5.4.4 we noted the change in the sea level anomaly along the western boundary under varying frictional influences. Increased bottom friction ($\delta_S = 300\ km$) resulted in an almost complete eradication of the positive anomaly in sea surface elevation along the western boundary for the slope topography. Increased lateral friction ($\delta_M = 300\ km$), without any bottom friction, prevented propagation of the anomaly equatorwards somewhat but the magnitude was increased. The differences due to the varying frictional influences is clearly demonstrated in Fig 5.20.

5.6 A continuously stratified example

A number of interesting results have been found through the course of our idealised modelling study, however, up to this point a two layer stratification profile has been used in all experimentation. A further run was completed with a more realistic continuous stratification profile to verify that the conclusions reached so far carry across to this more realistic scenario.

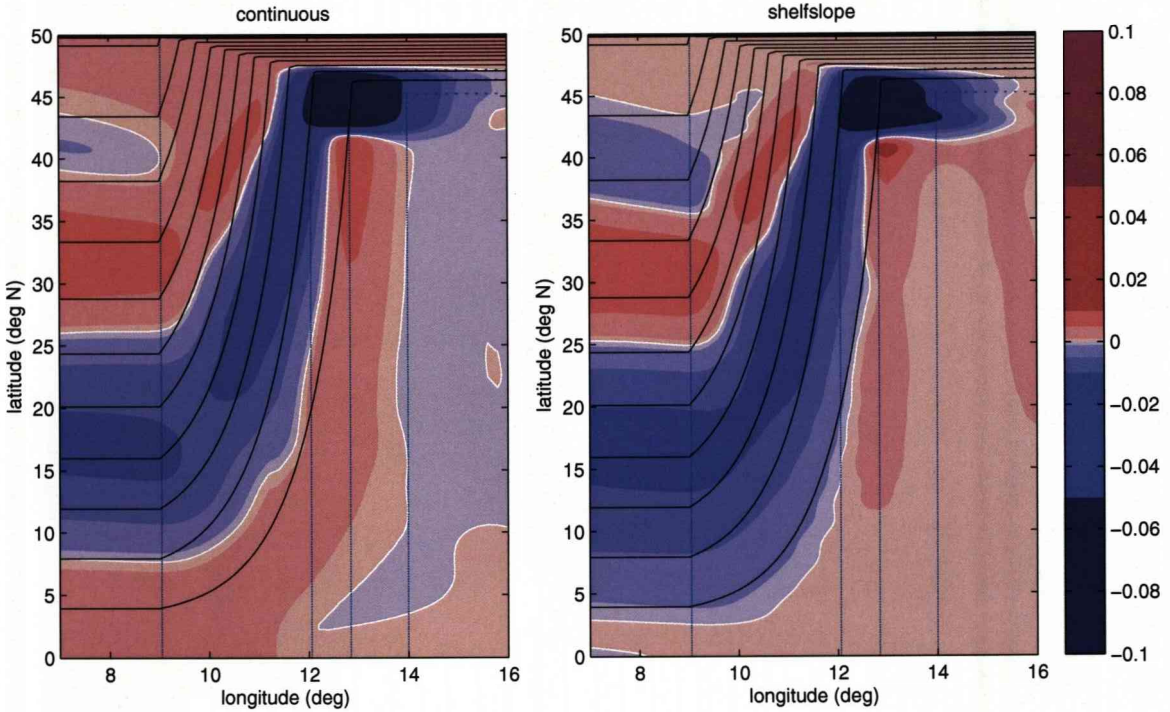

Figure 5.21: Sea surface elevation field for *shelfslope* topography under continuous stratification conditions at $t = 30$ days for the continuously stratified case (left) and the two layer case (right). Isobaths at 100 m, 500 m, 1000 m and 3000 m (dashed blue line) and $\frac{f}{H}$ contours (black line) are superimposed.

We can see for the comparitive sea surface elevation field plots (Fig 5.21) that the propagation pattern for the continuously stratified case is very similar to that of the two layer case. The difference in magnitude of anomalies is likely due to the reduced temperature change involved in the temperature relaxation in the continuous case; the magnitude of the anomaly depends on the change in T and therefore an equivalent T change will result in an equivalent magnitude of anomaly.

5.7 Chapter summary

This chapter has outlined the theoretical expectation of response to a temperature relaxation forcing in a model basin according to JEBAR principles and also to frictional theory. This theory appears to explain the general pattern of propagation, however, it is clear that in some cases there are additional physical processes taking place. The conclusions reached are summarised:

- The slope behaviour theory outlined in this chapter explains the basic mechanism for the response of a model basin to forcing, particularly for the case of the forcing region occurring over the north west corner of the domain. It also provides an adequate explanation of the limited response observed where forcing is restricted to the shelf or deep ocean regions.
- When the forcing region occurs over the northern boundary slope the theory would suggest only a limited, local response will be seen, however, this is clearly not the case. Our further investigations suggest that baroclinic processes within the forcing region initiate rapid propagation along the northern boundary slope in line with the JEBAR theory.
- The influence of friction results in the anomaly propagation deviating from the $\frac{f}{h}$ contours, as does a steepening topographic profile. Increasing bottom friction has a much more significant effect on the extent of this deviation than an increase in lateral friction.
- The location of the forcing region, the form of the topography and frictional influences have a significant impact on the sea level at the western boundary which may have implications for the use of western boundary sea level as a proxy for strength of the MOC. Continuous slope topography around the model ocean basin allows for a positive sea level anomaly to pervade the western boundary at high latitudes. When the forcing is confined to the shelf a positive anomaly is found at all latitudes outside the forcing region. The addition of bottom friction, even with all sloping boundaries, attenuates the coastal trapped signal and as a

result prevents the occurrence of a positive sea level anomaly along the western boundary.

- Experimentation with a continuously stratified case shows that the two-layer approximation is not a special case as far as the general pattern of response is concerned.

Chapter 6

Synthesis and further work

How the signals of high-latitude forcing are communicated to the rest of the ocean, and the rate of this process, is an important part of addressing the rapid climate change question. This thesis firstly sought to determine whether the advective route, proposed by Marotzke and Klinger (2000), or the rapid coastal trapped wave response, suggested by JM02, was the major rate-setting adjustment process. Our results clearly find the coastal trapped wave response to be the most important process of communicating high-latitude forcing to the rest of the ocean.

However, the exclusion of topography from the idealised model of JM02 did not allow for the full spectrum of coastal trapped waves (see Fig 6.1); only baroclinic Kelvin waves were supported. Existing literature suggested that the coastal trapped waves supported by topography have significantly higher wave speeds and also that the barotropic mode 0 may play an important role in how the ocean responds to forcing.

In Chapter 1 we set out a number of questions that we aimed to address. Here we describe the results of this thesis in terms of these questions (Section 6.1) and outline a theory for the adjustment process of a topographic ocean in response to forcing (Section 6.2). We then outline the simplifications made in our study (Section 6.3) before indicating potential future work (Section 6.4).

6.1 Addressing the thesis aims

How does topography affect the detailed properties of CTWs?

The inclusion of topography, and representation of the barotropic mode, allows for a number of wave modes, many of which travel at speeds considerably higher than the baroclinic Kelvin waves of JM02. Over idealised topography and stratification we find the following modes: a very fast mode 0 deep ocean barotropic or double Kelvin wave

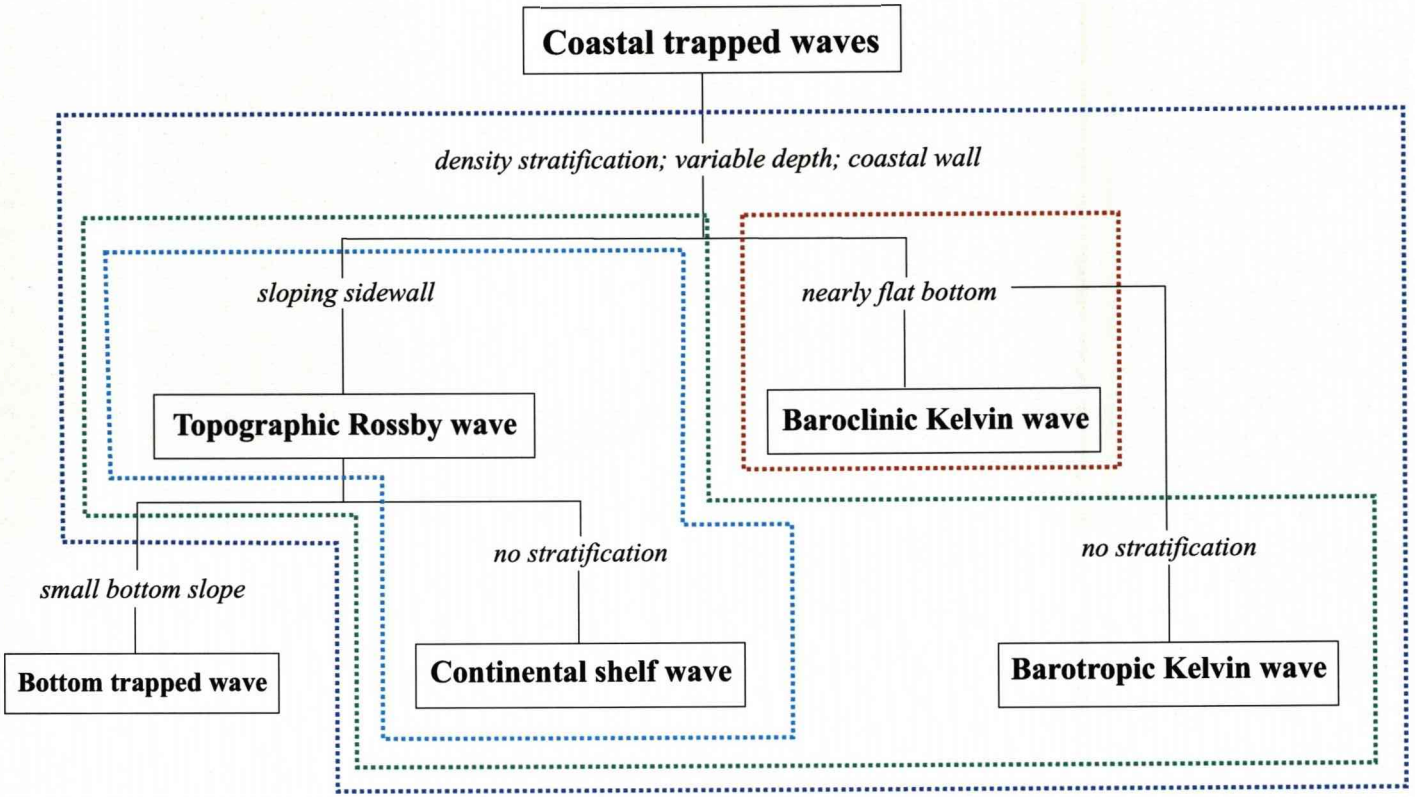

Figure 6.1: Coastal trapped waves classification diagram from (Wang and Mooers, 1976) identifying the wave type associated corresponding to differing conditions of topography and stratification. The rigid-lid barotropic solution (section 2.2) solves for the continental shelf waves only (outlined in dashed cyan); the free surface barotropic solution (section 2.3) solves for the continental shelf waves in addition to the barotropic Kelvin wave, both the deep ocean and shelf modes (outlined in dashed green) and; the free surface baroclinic solution (section 2.4) should find the full spectrum of coastal trapped waves (outlined in dashed purple). The JM02 model only allowed baroclinic Kelvin waves (outlined in dashed red).

with an adjustment timescale of days; a fast mode 1 coastal trapped Kelvin wave-like mode and; a number of slower slope trapped wave modes.

When realistic topography was included we found that the properties of the wave modes supported were linked to detailed changes in the offshore topography. However, we continued to find modes with varying wave speeds and corresponding adjustment timescales albeit with varying degrees of modification.

As expected the introduction of stratification, over both idealised and realistic topographies, resulted in an enhancement of the mode 2 wave speeds. Additionally, over areas of very steep topography, where continental shelf wave modes were modified considerably, the inclusion of realistic stratification allowed for the development of internal baroclinic Kelvin wave like modes with speeds greater than the severely modified continental shelf wave modes.

An interesting result of our idealised wave mode calculations was the increase in mode 0 deep ocean barotropic or double Kelvin wave speed, and the corresponding decrease of higher coastal trapped wave mode speeds, at low latitudes suggesting that non-linear processes may become important in the region of equatorial influence.

We suggest that as the higher coastal trapped wave modes supported by the topography do not match the equatorial Kelvin wave well at low latitudes the equatorial wave signal is somewhat delayed; the extent of this delay is not yet clear. This behaviour would not be seen in JM02 as the baroclinic Kelvin wave matches the equatorial Kelvin wave perfectly.

However, when the equatorial Kelvin wave reaches the eastern boundary we expect it to initiate coastal trapped wave modes over the topography which will increase in speed as they travel polewards along the eastern boundaries.

Can CTW explain the coherent signal along the western boundary?

Although we found there to be considerable variability in the wave modes linked to detailed changes in the topography, there remained a very fast mode 0 wave accompanied by higher modes of varying speeds according to the degree of modification by the topography. In particular, the mode 1 wave has speeds between around 5 ms^{-1} and 30 ms^{-1}, which is significantly faster than the baroclinic Kelvin wave of the vertical sidewall case.

The effect of topography and the resulting form of CTW, clearly affects the type of response over large distances, showing that the waves have an influence over long distances rather than dissipating over around 1000 km. This long range influence is consistent

with the fast wave speed for mode 1, and with the suggestion that CTW may account for the coherences seen in altimetry data.

Do the conclusions of JM02 remain valid in a topographic ocean?

We conclude that the fundamental dynamical view of JM02 remains broadly valid for a topographic ocean where waves rapidly communicate high-latitude anomalies along the western boundary. By allowing for barotropic Kelvin waves the very fast mode 0 wave can propagate around the basin in days; however, the amplitude is small and on its own is not important to the development of an overturning circulation response to forcing. Our mode 1 wave is also fast but may be delayed at the equator as topography appears to make the link between the CTW and equatorial Kelvin waves more complicated. Therefore although topography results in a faster response along the western and eastern boundaries the degree of delay in the equatorial region is not yet clear.

The most important effect of topography, besides altering wave speeds, was on the pattern of flow and sea level in the western boundary region of the North Atlantic. Interesting effects were also observed outside this region, but as was the case in JM02, the magnitudes of the signals were small in comparison to those on the western boundary.

The location of the forcing region is vital to how the forcing is communicated over the basin. If the forcing is confined to either the shelf or deep ocean regions, propagation of the anomaly is seriously curtailed. However, when the forcing takes place over the slope region, either along the western or northern boundary, we see a clear non-local response and rapid propagation of influence away from the forcing region.

The JEBAR theory outlined in Chapter 5 adequately explains this response when forcing occurs over the western boundary slope. In the case of forcing occuring over the northern boundary slope we find that predominantly baroclinic processes in the forcing region allow propagation of the anamoly along the $\frac{f}{h}$ contours of the northern boundary in accord with the JEBAR theory of barotropic adjustment.

How important is the barotropic mode to ocean adjustment?

The deep ocean barotropic Kelvin wave provided a very fast initial adjustment on a timescale of days around the ocean boundaries. In addition to the coastal response these waves also result in the initiation of offshore propagation of barotropic Rossby waves, which provide a rapid adjustment of the whole ocean basin on a much shorter timescale than in the purely baroclinic case. Rapid adjustment to high-latitude forcing in the northern hemisphere was also detected in the southern hemisphere, in agreement with Roussenov et al. (2008). The barotropic mode also appeared to be important to setting up the positive anomalies in sea surface elevation along the western boundary, which had significant effects on the sea level at the western boundary.

However, the amplitude of this mode 0 adjustment is small and is the consequence of density redistribution. The higher modes, equivalent to the baroclinic Kelvin wave of JM02, are required to develop an overturning circulation response to forcing.

How sensitive are CTW modes to slope parameters and friction?

The CTW modes are sensitive to changes in the topography, such as changing shelf width and slope steepness. We found that an increased shelf width allowed an increase in the mode 1 coastal Kelvin wave speed as the modifying influence of the topography became more remote from the coastal wall. In the cases where there was a negligible shelf region this mode 1 coastal Kelvin wave was quite heavily modified.

The coastal trapped modes supported over a sloping topography were increasingly attenuated by the effects of a steepening slope. In the case of a combined shelf and vertical wall profile we find only the double Kelvin wave and coastal Kelvin wave. Therefore as the slope becomes increasingly steep the solution becomes ever closer to this case.

We analysed the frictional influence on the response of the model ocean to forcing in the idealised MITgcm runs and found that friction acts to deviate the anomaly propagation from the $\frac{f}{h}$ contours onto shallower regions at higher latitudes. Increasing bottom friction had a much more significant impact on the extent of this deviation than lateral friction. This picture is in accord with estimates of the distance of mode 2 propagation over a spin-down time.

Is the interior ocean response affected by topography?

Topography appears to affect the interior ocean response as the Rossby wave response was reduced or delayed when topography was included despite the increased speed of the coastal wave response. As we have described only Kelvin waves are supported within the equatorial region, even in the presence of topography. Therefore we suggest that as the coastal trapped waves over topography are not baroclinic Kelvin waves they do not match, or excite, the equatorial Kelvin wave to the same extent. Indeed the topographic cases where the coastal trapped nodes were most distant from the density interface in the equatorial region resulted in a reduced equatorial signal thereby reducing or delaying the Rossby wave response in the model ocean.

A sloping eastern boundary supports a largely barotropic coastal trapped signal. Although this might be expected to couple less well with baroclinic Rossby waves, and therefore to produce a coastal sea level signal that grows in amplitude with increasing f, we found that such amplification was confined to frequencies at which baroclinic Rossby waves cannot exist. These results show that topography did not act to strengthen the

trapping of eastern boundary waves or reduce the offshore propagation of baroclinic Rossby waves.

The choice of lateral friction within the model did have an effect in the case of a vertical eastern boundary. The offshore radiation of baroclinic Rossby waves at low frequencies, and amplification of the coastal signal at higher frequencies, was attenuated as the baroclinic Rossby radius is less than the model Munk width for much of the latitude range. The lateral friction did not impact upon either of these mechanisms in the sloping boundary case as the relevant shelf barotropic Rossby radius is greater than the Munk width for all latitudes.

Coastal sea level signals

A further interesting finding of the idealised modelling study was the impact of topography on coastal sea level along the western boundary. In JM02 a consistent sign of anomaly was observed due to the coastal trapped wave response being limited to a baroclinic Kelvin wave; however, this was not the case when topography was introduced. With a continuous slope topography around the model basin, a positive sea level anomaly pervaded the western boundary at high latitudes resulting in a change in sign of sea level along the western boundary.

The inclusion of friction, however, did result in an attenuation of the coastal trapped signal, which resulted in the disappearance of the positive sea level anomaly along the western boundary. The sea level is also sensitive to the location of forcing; when forcing was restricted to the shelf region a positive anomaly was found at all latitudes outside the forcing region.

Relevance of topography to MOC adjustment

In Chapter 5 we found the overturning brought about by the theoretical barotropic adjustment process represented a northwards flow in the upper layers and a southward flow in the lower layer as in Bingham et al. (2007). A similar flow pattern was set up in our topographic model basin in response to forcing. If we compare the sea surface elevation pattern at $35°N$ (Fig 6.2), with negative values representing a northwards flow and positive values representing a southwards flow, for the *vertical* and *shelfslope* runs we can clearly see that the overturning circulation is only evident in the *shelfslope* case. Over the timescale of our study (one year) we find that an overturning circulation, akin to that of Bingham et al. (2007), is only evident in a topographic ocean.

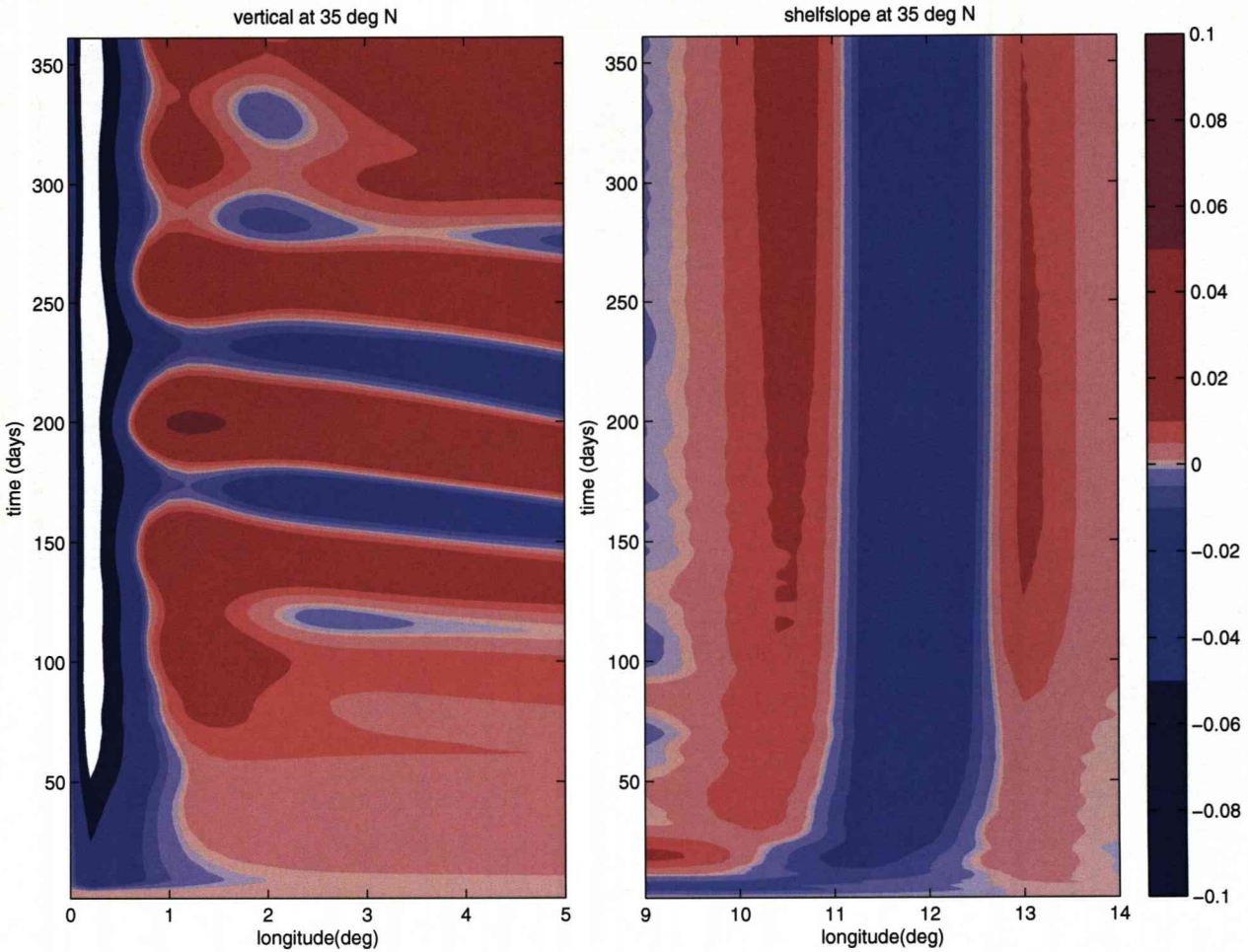

Figure 6.2: Hovmueller plots of sea surface elevation at $35°N$ for the *vertical* and *shelfslope* model runs.

6.2 A theory for the adjustment of a topographic Atlantic Ocean

Given the results of our detailed wave mode calculations and idealised modelling studies we suggest that the adjustment of the Atlantic Ocean with topography proceeds in the following manner. If forcing occurs over the slope region we see a rapid coastal trapped wave response on a number of timescales (Fig 6.3). Firstly the mode 0 deep ocean barotropic or double Kelvin wave propagates around the basin within days, initiating westwards propagating barotropic Rossby waves from the eastern boundary and, thus, provides a very fast full ocean response.

Next we find a number of higher coastal trapped wave modes travelling at speeds up to that of the coastal Kelvin wave at mid to high latitudes with adjustment timescales of weeks to months. These higher coastal trapped wave modes leave behind them an adjusted state in which sea level and bottom pressure signals follow the $\frac{f}{h}$ contours and as such travel further and further up the slope as they propagate equatorwards. Friction will act to deviate the response from the $\frac{f}{h}$ contours and attenuate the waves. At low latitudes the mode 1 and 2 wave speeds decrease (in the barotropic case, to zero at the equator), resulting in a rather sudden switch of mode structure to match the equatorial Kelvin wave. We suggest that this sudden switch is likely to result in nonlinear interactions between modes.

Due to the complicated behaviour we have discovered at the equator, possibly as the result of non-linear processes, the rate of adjustment of the rest of the ocean remains unclear.

When the equatorial Kelvin wave reaches the eastern boundary slope, the largely barotropic coastal trapped wave signals are once more excited and accelerate as they travel polewards once more. As in JM02, the coastal trapped signal along the eastern boundary will initiate westwards propagating baroclinic Rossby waves, which will transmit the signal to the ocean interior. There is some degree of amplification of the polewards propagating coastal trapped signal at frequencies above the maximum Rossby wave frequency, but topography does not enhance the trapping and amplification as might be suspected. Unless attenuated by friction the signal then continues to propagate along the northern boundary before travelling equatorwards once more along the western boundary.

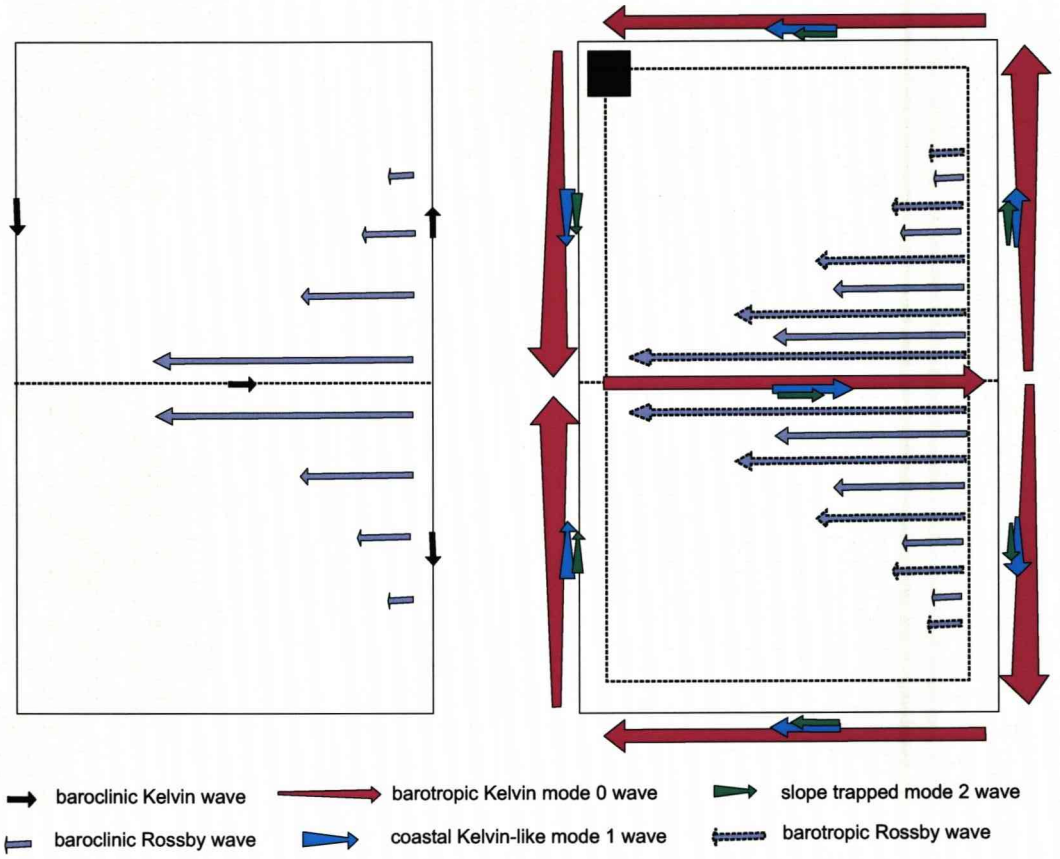

Figure 6.3: A comparison of the JM02 adjustment theory (left) and the proposed adjustment theory for an ocean with idealised topography (right) in response to forcing in the north west corner (black square). The size of the arrows provides an indication of wave speed showing the very fast mode 0 wave, fast mode 1 wave and slower mode 2 wave. The width of the arrows indicates an increase (mode 0) or decrease (modes 1 and 2) towards the equator.

6.3 Simplifications made in the study

A number of simplifications were made during the course of this study. Although we addressed both the general effects of topography and stratification, the detailed realism of these parameters was sometimes restricted. The chosen topographic profiles did not represent the full extent of the western boundary, being confined to between around $28°N$ and $44°N$, and as such the behaviour of the coastal trapped wave modes at low latitudes in the realistic ocean was not calculated. Therefore we could not determine how the stronger stratification at low latitudes affected the realistic wave modes.

For ease of numerical solution the topographic profiles were smoothed to an extent resulting in a reduction of the complexity of the realistic ocean being portrayed in the wave mode calculations. The realistic stratification profiles, utilised in the BIGLOAD2 model of the free surface baroclinic solution, were restricted to a single value at each depth level and therefore did not vary with x.

The difficulties involved with mode finding, and in finding solutions over shallow shelf regions, in the BIGLOAD2 model resulted in less comprehensive testing than was ideal. However, despite the limitations of this model the comparisons with the free surface, barotropic solution it provided increased our confidence in the results of the realistic experimentation. These comparisons suggested that the barotropic solutions provided a good approximation of the mode 0 and mode 1 waves; however, the mode 2 wave was modified to a greater extent by stratification.

Wind forcing, and the effects of a mean flow, were not incorporated into the idealised modelling experiments. Additionally the limited time period of the model runs does not allow for the presence of a fully spun-up ocean; however, the results of Roussenov et al. (2008) suggest that this is unlikely to have a significant impact on the outcome of our study.

We have also assumed in our wave mode calculations that topography and f remain constant with changing y, over large distances compared to wavelength. A full investigation would involve modes that are not sinusoidal in y, meaning two-dimensional barotropic and three-dimensional baroclinic structure has to be solved for, allowing for the appearance of spatially localised modes.

Despite the number of simplifications made during the course of this study we feel that the key outcomes hold true. Indeed our results have suggested that a great deal of information and insight can be gained from barotropic models using idealised topography which are considerably less expensive to run.

6.4 Further work

We find that the topography does not fundamentally alter the coastal trapped wave response, but instead allows for a less uniform and even faster response to a change in forcing. By conducting experiments using idealised topography we gained a cleaner picture of the topographic ocean's response to forcing.

JM02 determined that the lead time of predictability in the North Atlantic in response to thermohaline forcing was given by how long it took a Kelvin wave to propagate from the forcing region, down the western boundary and across the equator; such baroclinic Kelvin wave propagation would take place over a couple of months. Our idealised experimentation suggests that the very fast mode 0 barotropic wave would result in forcing being 'felt' over the whole Atlantic in a number of days although the amplitude of this adjustment is small.

The higher coastal trapped modes in a topographic ocean would travel faster than the baroclinic Kelvin wave on the western and eastern boundaries. However, although they would reach the equatorial region on a shorter timescale, the complicated behaviour we have observed near the equator may delay the adjustment outside the western boundary. Therefore further investigation into the wave mode behaviour as they approach the equator is required; such as whether mode 1 can merge smoothly into the first baroclinic Kelvin wave. This will help to provide a full picture of the adjustment of a topographic Atlantic Ocean.

Additionally, further understanding of the pattern and structure of the anomaly set up by the propagating coastal wave modes will be important for the use of western boundary sea level as a proxy for strength of the Meridional Overturning Circulation.

Appendix A

Free surface, barotropic solution: single step

Details of solution for the free surface, barotropic mode over a single step shelf topography (*pers. comm. C. Hughes*).

$$\eta_{XX} + \eta_X(\frac{h_X}{h}) - \eta(\frac{H}{h} - \frac{c_0}{c}\frac{h_X}{h}) = 0$$

where $c_0 = \sqrt{gH}$ and $X = \frac{x}{R_0} = \frac{xf}{c_0}$

On the flat; $\eta_{XX} - \eta\frac{H}{h} = 0$

When X is positive;

$$\eta = e^{-X}$$

$$\eta_X = -e^{-X}$$

$$\eta^+ = 1$$

$$\eta_X^+ = -1$$

and when X is negative;

$$\eta = Ae^X\sqrt{\tfrac{H}{G}} + Be^{-X}\sqrt{\tfrac{H}{G}}$$

$$\eta = Ae^{X\beta} + Be^{-X\beta}$$

$$\eta_X = \beta(Ae^{X\beta} - Be^{-X\beta}$$

$$\eta^- = A + B$$

$$\eta_X^- = \beta(A - B)$$

where $\beta = \sqrt{\frac{H}{G}}$ and $\beta > 1$ and where superscripts $+$ and $-$ refer to values adjacent to $x = 0$ (the position of the step) on the side of positive and negative x respectively.

Jump conditions: η is continuous therefore;

$$A + B = 1 = P \tag{A.1}$$

$$(h\eta_X)_X - \eta(H - \frac{c_0}{c}h_X) = 0$$

$$[h\eta_X] + \frac{c_0}{c}[h] = 0$$

$$H\eta_X^+ - G\eta_X^- + \frac{c_0}{c}(H - G) = 0$$

$$-H - \beta G(A - B) + \frac{c_0}{c}(\beta^2 - 1) = 0$$

$$-\beta^2 - \beta(A - B) + \frac{c_0}{c}(\beta^2 - 1) = 0$$

$$A - B = \frac{c_0}{c}\frac{(\beta^2 - 1)}{\beta} - \beta = Q \tag{A.2}$$

and $\frac{c_0}{c} = \frac{1}{R}$ and $R < 1$

The boundary condition at $X = -L$ can then be found;

$$f\eta + c\eta_x = 0$$

$$\eta_x = \frac{1}{R_0}\eta_X = \frac{f}{c_0}\eta X$$

$$\eta + \frac{c}{c_0}\eta_X = 0$$

$$Ae^{-L\beta} + Be^{L\beta} + \frac{c}{c_0}\beta(Ae^{-L\beta} - Be^{L\beta}) = 0$$

$$Ae^{-L\beta}(1 + \frac{c}{c_0}\beta) + Be^{L\beta}(1 - \frac{c}{c_0}\beta) = 0$$

$$A = (\frac{A+B}{2}) + (\frac{A-B}{2})$$

$$B = (\frac{A+B}{2}) - (\frac{A-B}{2})$$

or

$$\frac{(P+Q)}{2}e^{-L\beta} + \frac{(P-Q)}{2}e^{L\beta} + \frac{c\beta}{c_0}(\frac{(P+Q)}{2}e^{-L\beta} - \frac{(P-Q)}{2}e^{L\beta})$$

$$= \frac{P(e^{-L\beta} + e^{L\beta})}{2} + \frac{Q(e^{-L\beta} - e^{L\beta})}{2} + \frac{c\beta}{c_0}\frac{P(e^{-L\beta} - e^{L\beta})}{2} + \frac{Q(e^{-L\beta} + e^{L\beta})}{2}$$

$$= PcoshL\beta - Qsinh\beta + \frac{c}{c_0}\beta[QcoshL\beta - PsinhL\beta]$$

Therefore

$$\frac{c}{c_0} = \frac{1}{\beta}\frac{QsinhL\beta - PcoshL\beta}{QcoshL\beta - PsinhL\beta} = R \tag{A.3}$$

However, from A.1 $P = A + B = 1$ and from A.2 $Q = A - B = \frac{c_0}{c}\frac{(\beta^2-1)}{\beta} - \beta = \frac{\beta^2-1}{R\beta} - \beta$ and therefore;

$$R\beta = \frac{(\frac{\beta^2-1}{R\beta} - \beta)sinhL\beta - coshL\beta}{(\frac{\beta^2-1}{R\beta} - \beta)coshL\beta - sinhL\beta}$$

$$(\beta^2 - 1 - R\beta^2)coshL\beta - R\beta sinhL\beta = (\frac{\beta^2 - 1}{R\beta} - \beta)sinhL\beta - coshL\beta$$

$$-R^2(\beta^2 coshL\beta + \beta sinhL\beta) + R(\beta^2 coshL\beta + \beta sinhL\beta) + \frac{1-\beta^2}{\beta}sinhL\beta = 0$$

$$R^2 - R + \frac{(\beta^2 - 1)sinhL\beta}{\beta^2(\beta coshL\beta + sinhL\beta)} = 0 \tag{A.4}$$

writing $D = \frac{\beta^2-1}{\beta^2}\frac{sinhL\beta}{\beta coshL\beta + sinhL\beta} = \frac{\beta^2-1}{\beta^2}\frac{e^{2L\beta}-1}{(\beta-1)+(\beta+1)e^{2L\beta}}$

hence A.4 becomes $R^2 - R + D = 0$ and so

$$R = \frac{1}{2} \pm \sqrt{\frac{1}{4} - D} \tag{A.5}$$

given R, solution is then found from A.1 and A.2: $A = \frac{P+Q}{2}$, $B = \frac{P-Q}{2}$

$$A = \frac{1}{2}(1 + \frac{\beta^2 - 1}{\beta R} - \beta) \tag{A.6}$$

$$B = \frac{1}{2}(1 - \frac{\beta^2 - 1}{\beta R} + \beta)$$

In the limit as L goes to infinity, D goes to $\frac{\beta^2-1}{\beta^2}\frac{1}{\beta+1} = \frac{\beta-1}{\beta^2}$ and $\sqrt{\frac{1}{4} - D}$ goes to;

$$\frac{1}{\beta}\sqrt{(\frac{\beta}{2})^2 - \beta + 1} = \frac{1}{\beta}\sqrt{(\frac{\beta}{2} - 1)^2} = \pm(\frac{1}{2} - \frac{1}{\beta})$$

And R therefore goes to $\frac{1}{2} \pm (\frac{1}{2} - \frac{1}{\beta} = \frac{\beta-1}{\beta}$ (positive root) or $\frac{1}{\beta}$ (negative root). Substituting into A.6 gives us;

$$A^+ = \frac{1}{2}(1+\beta+1-\beta) = 1$$

$$B^+ = \frac{1}{2}(1-(\beta+1)+\beta) = 0$$

and

$$A^- = \frac{1}{2}(1+\beta-1-\beta) = \frac{\beta(\beta-1)}{2}$$

$$B^- = \frac{1}{2}(1-(\beta-1)+\beta) = \frac{(1+\beta)(2-\beta)}{2}$$

where the negative A and B represent the solution for the pure double Kelvin wave and the positive A and B represent the solution for the first continental shelf wave mode.

Appendix B

Free surface, barotropic solution: multiple step

Details of the long wave barotropic solution for a multiple step topography (*pers. comm. C. Hughes*).

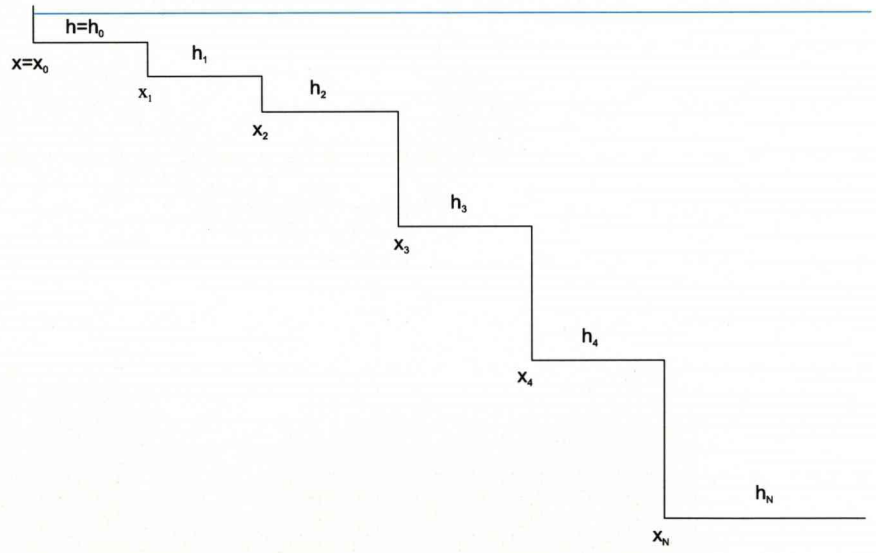

Figure B.1: Multiple step topography with offshore distance, x, measured in units of R_0 and the depth, h, in m.

The solution on level region, h_i is;

$$\eta = A_i e^{\beta_i X} + B_i e^{-\beta_i X}$$

$$\eta_X = \beta_i (A_i e^{\beta_i X} - B_i e^{-\beta_i X})$$

Jump conditions: at $X = X_i$

$$[\eta] = 0 = (A_i e^{\beta_i X_i} + B_i e^{-\beta_i X_i}) - (A_{i-1} e^{\beta_{i-1} X_i} + B_{i-1} e^{-\beta_{i-1} X_i})$$

$[h\eta_x] + r[h\eta] = 0$ therefore

$$h_i \beta_i (A_i e^{\beta_i X_i}) + r h_i (A_i e^{\beta_i X_i} + B_i e^{-\beta_i X_i})$$

$$= h_{i-1} \beta_{i-1} (A_{i-1} e^{\beta_{i-1} X_i} - B_{i-1} e^{-\beta_{i-1} X_i}) + r h_{i-1} (A_{i-1} e^{\beta_{i-1} X_i} + B_{i-1} e^{-\beta_{i-1} X_i})$$

or

$$A_i (\frac{e^{\beta_i X_i}}{\beta_i} + \frac{r e^{\beta_i X_i}}{{\beta_i}^2}) - B_i (\frac{e^{-\beta_i X_i}}{\beta_i} - \frac{r e^{\beta_i X_i}}{{\beta_i}^2})$$

$$= A_{i-1} \frac{e^{\beta_{i-1} X_i}}{\beta_{i-1}} (1 + \frac{r}{\beta_{i-1}}) - B_{i-1} \frac{e^{-\beta_{i-1} X_i}}{\beta_{i-1}} (1 - \frac{r}{\beta_{i-1}})$$

$$= \frac{A_i e^{\beta_i X_i}}{\beta_i} (1 + \frac{r}{\beta_i}) - \frac{B_i e^{-\beta_i X_i}}{\beta_i} (1 - \frac{r}{\beta_i})$$

Writing $P_i = e^{\beta_i X_i}$, $Q_i = e^{\beta_i X_{i+1}}$ and $Q_{i-1} = e^{\beta_{i-1} X_i}$

$[\eta] = 0$ therefore;

$$A_i P_i + \frac{B_i}{P_i} = A_{i-1} Q_{i-1} + \frac{B_{i-1}}{Q_{i-1}} \tag{B.1}$$

$[h\eta_x] + r[h\eta] = 0$ therefore;

$$\frac{A_i P_i}{\beta_i} (1 + \frac{r}{\beta_i}) - \frac{B_i}{P_i \beta_i} (1 - \frac{r}{\beta_i}) = \frac{A_{i-1} Q_{i-1}}{\beta_{i-1}} (1 + \frac{r}{\beta_{i-1}}) - \frac{B_{i-1}}{Q_{i-1} \beta_{i-1}} (1 - \frac{r}{\beta_{i-1}}) \tag{B.2}$$

We integrate in from offshore and find A_{i-1}, B_{i-1} given A_i, B_i. Eliminate $A_{i-1} Q_{i-1}$ from B.2 by substitution from B.1:

$$(A_i P_i + \frac{B_i}{P_i} - \frac{B_{i-1}}{Q_{i-1}})(1 + \frac{r}{\beta_{i-1}}) \frac{1}{\beta_{i-1}} - \frac{B_{i-1}}{Q_{i-1} \beta_{i-1}} (1 - \frac{r}{\beta_{i-1}}) = \frac{A_i P_i}{\beta_i} (1 + \frac{r}{\beta_i}) - \frac{B_i}{P_i \beta_i} (1 - \frac{r}{\beta_i})$$

therefore;

$$-\frac{B_{i-1}}{Q_{i-1}} (\frac{1}{\beta_{i-1}} + \frac{r}{\beta i - 1^2} + \frac{1}{\beta_{i-1}} - \frac{r}{\beta i - 1^2})$$

$$= A_i P_i(\frac{1}{\beta_i} + \frac{r}{{\beta_i}^2} - \frac{1}{\beta_{i-1}} - \frac{r}{\beta i - 1^2}) - \frac{B_i}{P_i}(\frac{1}{\beta_i} - \frac{r}{{\beta_i}^2} + \frac{1}{\beta_{i-1}} + \frac{r}{{\beta^2}_{i-1}})$$

and thus;

$$B_{i-1} = \frac{Q_{i-1}\beta_{i-1}}{2}(\frac{B_i}{P_i}(\frac{1}{\beta_i} - \frac{r}{{\beta_i}^2} + \frac{1}{\beta_{i-1}} + \frac{r}{\beta i - 1^2}) - A_i P_i(\frac{1}{\beta_i} + \frac{r}{{\beta_i}^2} - \frac{1}{\beta_{i-1}} - \frac{r}{\beta i - 1^2})) \tag{B.3}$$

Eliminate $\frac{B_{i-1}}{Q_{i-1}}$ from B.2 by substitution from B.1: $\frac{B_{i-1}}{Q_{i-1}} = A_i P_i + \frac{B_i}{P_i} - A_{i-1}Q_{i-1}$

$$\frac{A_{i-1}Q_{i-1}}{\beta_{i-1}}(1 + \frac{r}{\beta_{i-1}})$$

$$= \frac{A_i P_i}{\beta_i}(1 + \frac{r}{\beta_i}) - \frac{B_i}{P_i \beta_i}(1 - \frac{r}{\beta_i}) + (A_i P_i + \frac{B_i}{P_i} - A_{i-1}Q_{i-1})\frac{1}{\beta_{i-1}}(1 - \frac{r}{\beta_{i-1}})$$

therefore;

$$\frac{A_{i-1}Q_{i-1}}{\beta_{i-1}}(1 + \frac{r}{\beta_{i-1}} + 1 - \frac{r}{\beta_{i-1}}) = \frac{2A_{i-1}Q_{i-1}}{\beta_{i-1}}$$

$$= A_i P_i(\frac{1}{\beta_i} + \frac{r}{{\beta_i}^2} + \frac{1}{\beta_{i-1}} - \frac{r}{{\beta_{i-1}}^2}) + \frac{B_i}{P_i}(\frac{1}{\beta_{i-1}} - \frac{r}{{\beta_{i-1}}^2} - \frac{1}{\beta_i} + \frac{r}{{\beta_{i-1}}^2})$$

and thus;

$$A_{i-1} = \frac{\beta_{i-1}}{2Q_{i-1}}(A_i P_i(\frac{1}{\beta_i} + \frac{r}{{\beta_i}^2} + \frac{1}{\beta_{i-1}} - \frac{r}{{\beta_{i-1}}^2}) + \frac{B_i}{P_i}(\frac{1}{\beta_{i-1}} - \frac{r}{{\beta_{i-1}}^2} - \frac{1}{\beta_i} + \frac{r}{{\beta_{i-1}}^2})) \tag{B.4}$$

Boundary condition at coast: $h\eta_X + rh\eta = 0$ and $\eta_X + r\eta = 0$

Therefore;

$$\beta_0 A_0 e^{\beta_0 X_0} - \beta_0 B_0 e^{-\beta_0 X_0} + r A_0 e^{\beta_0 X_0} + r B_0 e^{-\beta_0 X_0} = 0$$

$$A_0 e^{\beta_0 X_0}(1 + \frac{r}{\beta_0}) + B_0 e^{-\beta_0 X_0}(\frac{r}{\beta_0} - 1) = 0$$

$$\frac{A_0 e^{2\beta_0 X_0}}{B_0} = \frac{1 - \frac{r}{\beta_0}}{1 + \frac{r}{\beta_0}}$$

$$(\frac{1 + \frac{r}{\beta_0}}{1 - \frac{r}{\beta_0}})\frac{A_0}{B_0}e^{2\beta_0 X_0} = 1$$

or

$$(\frac{1 - \frac{r}{\beta_0}}{1 + \frac{r}{\beta_0}})\frac{B_0}{A_0}e^{-2\beta_0 X_0} = 1$$

Bibliography

Adams, J. and V. Buchwald, 1969: The generation of continental shelf waves. *Journal of Fluid Mechanics*, **35**, 815–826.

Adcroft, A., C. Hill, and J. Marshall, 1997: Representation of topography by shaved cells in a height cordinate ocean model. *Monthly Weather Review*, **125**, 2293–2315.

Allen, J., 1975: Coastal trapped waves in a stratified ocean. *Journal of Physical Oceanography*, **5**, 300–325.

Allen, J., 1976: Continental shelf waves and alongshore variations in bottom topography and coastline. *Journal of Physical Oceanography*, **6**, 864–878.

Allen, J. and R. Romea, 1980: On coastal trapped waves at low latitudes in a stratified ocean. *Journal of Fluid Mechanics*, **98**, 555–585.

Anderson, D., 1981: Cross-equatorial waves, with application to the low-level East-African jet. *Geophysical and Astrophysical Fluid Dynamics*, **16**, 267–284.

Anderson, D., K. Bryan, A. Gill, and R. Pacanowski, 1979: The transient response of the North Atlantic: Some model studies. *Journal of Geophysical Research*, **84**, 4795–4815.

Anderson, D. and P. Killworth, 1977: Spin up of a stratified ocean, with topography. *Deep Sea Research*, **24**, 709–732.

Battisti, D. and B. Hickey, 1984: Applications of remote wind-forced coastal trapped wave theory to the Oregon and Washington coasts. *Journal of Physical Oceanography*, **14**, 887–903.

Bigg, G., T. Jickells, P. Liss, and T. Osborn, 2003: The role of the oceans in climate. *International Journal of Climatology*, **23**, 1127–1159.

Bindoff, N., et al., 2007: *Observations: Oceanic Climate Change and Sea Level. In: Climate Change 2007: The Physical Science Basis. Contribution of Working Group I to the Fourth Assessment Report of the Intergovernmental Panel on Climate Change [Solomon, S., D. Qin, M. Manning, Z. Chen, M. Marquis, K.B. Averyt, M. Tignor*

and H.L. Miller (eds.)]. Cambridge University Press, Cambridge, United Kingdom and New York, NY, USA.

Bingham, R. and C. Hughes, 2008: Determining North Atlantic meridional transport variability from pressure on the western boundary: A model investigation. *Journal of Geophysical Research*, **113**, doi:10.1029/2007JC004 679.

Bingham, R. and C. Hughes, 2009: Signature of the Atlantic meridional overturning circulation in sea level along the east coast of North America. *Geophysical Research Letters*, **36**, doi:10.1029/2008GL036 215.

Bingham, R., C. Hughes, V. Roussenov, and R. Williams, 2007: Meridional coherence of the North Atlantic meridional overturning circulation. *Geophysical Research Letters*, **34**, doi:10.1029/2007GL031 731.

BODC, 2003: *CD-ROM: Centenary Edition of the GEBCO Digital Atlas published on behalf of the Intergovernmental Oceanographic Commission and the International Hydrographic Organisation as part of the General Bathymetric Chart of the Oceans.*

Brink, K., 1982a: A comparison of long coastal trapped wave theory with observations off Peru. *Journal of Physical Oceanography*, **12**, 897–912.

Brink, K., 1982b: The effect of bottom friction on low frequency coastal trapped waves. *Journal of Physical Oceanography*, **12**, 127–133.

Brink, K., 1990: On the damping of free coastal-trapped waves. *Journal of Physical Oceanography*, **20**, 1219–1225.

Brink, K. and J. Allen, 1978: On the effect of bottom friction on barotropic motion over the continental shelf. *Journal of Physical Oceanography*, **8**, 919–922.

Brink, K. and D. Chapman, 1985: Programs for computing properties of coastal-trapped waves and wind-driven motions over the continental shelf and slope. *WHOI Technical Report*, **WHOI-85-17**, 1–45.

Broecker, W., 1995: Chaotic climate. *Scientific American*, **273**, 62–69.

Broecker, W., 1998: Paleocean circulation during the last deglaciation. *Paleoceanography*, **13**, 119–121.

Brooks, D. and C. Mooers, 1977: Free, stable continental shelf waves in a sheared barotropic boundary current. *Journal of Physical Oceanography*, **7**, 380–388.

Bryden, H., H. Longworth, and S. Cunningham, 2005: Slowing of the Atlantic meridional overturning circulation at 25N. *Nature*, **438**, 655–657.

Buchwald, V. and J. Adams, 1968: The propagation of continental shelf waves. *Proceedings of the Royal Society A*, **305**, 235–250.

Cane, M., 1989: A mathematical note on Kawase's study of the deep ocean circulation. *Journal of Physical Oceanography*, **19**, 548–550.

Chapman, D., 1983: On the influence of stratification and continental shelf and slope topography on the dispersion of subinertial coastally trapped waves. *Journal of Physical Oceanography*, **13**, 1641–1652.

Church, J., 2007: Oceans: A change in circulation? *Science*, **317**, 908–909.

Church, J. and H. Freeland, 1987: The energy source for the coastal-trapped waves in the Australian coastal experiment region. *Journal of Physical Oceanography*, **17**, 289–300.

Church, J., H. Freeland, and R. Smith, 1986a: Coastal-trapped waves on the East Australian continental shelf. Part I: Propagation of modes. *Journal of Physical Oceanography*, **16**, 1929–1943.

Church, J., N. White, A. Clarke, H. Freeland, and R. Smith, 1986b: Coastal-trapped waves on the East Australian continental shelf. Part II: Model verification. *Journal of Physical Oceanography*, **16**, 1945–1957.

Clarke, A., 1977: Observational and numerical evidence for wind-forced coastal trapped waves. *Journal of Physical Oceanography*, **7**, 231–247.

Clarke, A. and S. van Gorder, 1986: A method for estimating wind-driven frictional, time-dependent, stratified shelf and slope water flow. *Journal of Physical Oceanography*, **16**, 1013–1028.

Collings, I. and R. Grimshaw, 1984: Stable and unstable barotropic shelf waves in a coastal current. *Geophysical and Astrophysical Fluid Dynamics*, **29**, 179–220.

Davey, M., 1983: A two-level model of a thermally forced ocean basin. *Journal of Physical Oceanography*, **13**, 169–190.

Davey, M., W. Hsieh, and R. Wajsowicz, 1983: The free Kelvin wave with lateral and vertical viscosity. *Journal of Physical Oceanography*, **13**, 2182–2191.

Dickson, B., I. Yashayaev, J. Meincke, B. Turrell, S. Dye, and J. Holfort, 2002: Rapid freshening of the deep North Atlantic Ocean over the past four decades. *Nature*, **416**, 832–837.

Fofonoff, N., 1954: Steady flow in a frictionless homogenous ocean. *Journal of Marine Research*, **13**, 254–262.

Freeland, H., et al., 1986: The Australian coastal experiment: A search for coastal-trapped waves. *Journal of Physical Oceanography*, **16**, 1231–1249.

Gent, P., 2001: Will the North Atlantic Ocean thermohaline circulation weaken during the 21st century? *Geophysical Research Letters*, **28**, 1023–1026.

Gill, A., 1982: *Atmosphere-Ocean Dynamics*. Academic Press.

Gill, A. and A. Clarke, 1974: Wind induced upwelling, coastal currents and sea-level changes. *Deep Sea Research*, **21**, 325–345.

Gill, A. and E. Schumann, 1974: The generation of long shelf waves by the wind. *Journal of Physical Oceanography*, **4**, 83–90.

Gregory, J., et al., 2005: A model intercomparison of changes in the Atlantic thermohaline circulation in response to increasing atmospheric CO_2 concentration. *Geophysical Research Letters*, **32**, L12 703.

Grimshaw, R. and J. Allen, 1988: Low-frequency baroclinic waves off coastal boundaries. *Journal of Physical Oceanography*, **18**, 1124–1143.

Hamon, B., 1962: The spectrums of mean sea level at Sydney, Coff's Harbour, and Lord Howe Island. *Journal of Geophysical Research*, **67**, 5147.

Hamon, B., 1966: Continental shelf waves and the effects of atmospheric pressure and wind stress on sea level. *Journal of Geophysical Research*, **68**, 4635.

Haney, R., 1991: On the pressure gradient force over steep topography in sigma coordinate ocean models. *Journal of Physical Oceanography*, **21**, 610–619.

Hsieh, W., 1982: Observations of continental shelf waves off Oregon and Washington. *Journal of Physical Oceanography*, **12**, 887–896.

Hsieh, W., M. Davey, and R. Wajsowicz, 1983: The free Kelvin wave in finite-difference numerical models. *Journal of Physical Oceanography*, **13**, 1383–1397.

Hsueh, Y., 1980: Scattering of continental shelf waves by longshore variations in bottom topography. *Journal of Geophysical Research*, **85**, 1147–1150.

Hughes, C., 2008: A form of potential vorticity equation for depth-integrated flow with a free surface. *Journal of Physical Oceanography*, **38**, 1131–1136.

Hughes, C. and M. Meredith, 2006: Coherent sea-level fluctuations along the global continental slope. *Philosophical Transactions of the Royal Society A*, **364**, 885–901.

Huthnance, J., 1975: On trapped waves over a continental shelf. *Journal of Fluid Mechanics*, **69**, 689–704.

Huthnance, J., 1978: On coastal trapped waves: Analysis and numerical calculation by inverse iteration. *Journal of Physical Oceanography*, **8**, 74–92.

Jackson, L., C. Hughes, and R. Williams, 2006: Topographic control of basin and channel flows: The role of bottom pressure torques and friction. *Journal of Physical Oceanography*, **36**, 1786–1805.

Johnson, H. and D. Marshall, 2002: A theory for the surface Atlantic response to thermohaline variability. *Journal of Physical Oceanography*, **32**, 1121–1132.

Kaijura, K., 1974: Effect of stratification on long period trapped waves on the shelf. *Journal of the Oceanographic Society of Japan*, **30**, 271–281.

Kawase, M., 1987: Establishment of deep ocean circulation driven by deep water production. *Journal of Physical Oceanography*, **17**, 2294–2317.

Keigwin, L., G. Jones, S. Lehmann, and E. Boyle, 1991: Deglacial meltwater discharge, North Atlantic deep circulation and abrupt climate change. *Journal of Geophysical Research*, **96**, 16 811–16 826.

Latif, M., E. Roeckner, U. Mikolajewicz, and R. Voss, 2000: Tropical stabilization of the thermohaline circulation in a greenhouse warming situation. *Journal of Climate*, **13**, 1809–1813.

LeBlond, P. and L. Mysak, 1978: *Waves in the Ocean.* Elsevier Scientific Publishing Company.

Lopez, M. and A. Clarke, 1989: The wind-driven shelf and slope water flow in terms of a local and remote response. *Journal of Physical Oceanography*, **19**, 1091–1101.

Lozier, M., W. Owens, and R. Curry, 1995: The climatology of the North Atlantic. *Progress in Oceanography*, **36**, 1–44.

Manabe, S. and R. Stouffer, 1993: Century scale effects of increased atmospheric carbon dioxide on the ocean atmosphere system. *Nature*, **364**, 215–218.

Marotzke, J. and B. Klinger, 2000: The dynamics of equatorially assymetric thermohaline circulations. *Journal of Physical Oceanography*, **30**, 955–970.

Martinez, J. and J. Allen, 2004: A modeling study of coastal-trapped wave propagation in the Gulf of California. Part I: Response to remote forcing. *Journal of Physical Oceanography*, **34**, 1313–1331.

McDermott, D., 1996: The regulation of northern overturning by southern hemisphere winds. *Journal of Physical Oceanography*, **26**, 1234–1255.

McIntosh, P. and R. Schahinger, 1994: Coastal-trapped wave mode fitting: Reanalysis of the Australian coastal experiment. *Journal of Physical Oceanography*, **24**, 949–965.

Middleton, J. and D. Wright, 1990: Coastally trapped waves in a stratified ocean. *Journal of Physical Oceanography*, **20**, 1521–1527.

Miles, J., 1972: Kelvin waves on oceanic boundaries. *Journal of Fluid Mechanics*, **55**, 113–127.

Mitsudera, H. and K. Hanawa, 1987: Effects of bottom friction on continental shelf waves. *Continental Shelf Research*, **7**, 699–714.

Mitsudera, H. and K. Hanawa, 1988: Damping of coastal trapped waves due to bottom friction in a baroclinic ocean. *Continental Shelf Research*, **8**, 113–129.

Munk, W., 1950: On the wind-driven ocean circulation. *Journal of Meteorology*, **7**, 79–93.

Mysak, L., 1967: On the theory of continental shelf waves. *Journal of Marine Research*, **25**, 205–227.

Mysak, L., 1980: Topographically trapped waves. *Annual Review of Fluid Mechanics*, **12**, 45–76.

Narayanan, S. and I. Webster, 1987: Coastally trapped waves in the presence of a barotropic shelf edge jet. *Journal of Geophysical Research*, **92**, 9494–9502.

Pedlosky, J., 1996: *Ocean Circulation Theory*. Springer.

Press, W., B. Flannery, S. Teukolsky, and W. Vetterling, 1986: *Numerical Recipes: The Art of Scientific Computing*. Cambridge University Press.

Rahmstorf, S., 1995: Bifurcations of the Atlantic thermohaline circualtion in response to changes in the hydrological cycle. *Nature*, **378**, 145–149.

Rhines, P., 1970: Edge-, bottom-, and Rossby waves in a rotating stratified fluid. *Geophysical Fluid Dynamics*, **1**, 273–302.

Robinson, A., 1964: Continental shelf waves and the response of sea level to weather systems. *Journal of Geophysical Research*, **69**, 367–368.

Roussenov, V., R. Williams, C. Hughes, and R. Bingham, 2008: Boundary wave communication of bottom pressure and overturning changes for the North Atlantic. *Journal of Geophysical Research*, **113**, doi:10.1029/2007JC004 501.

Schiller, A., U. Mikolajewicz, and R. Voss, 1997: The stability of the North Atlantic thermohaline circulation in a coupled ocean-atmosphere general circulation model. *Climate Dynamics*, **13**, 325–347.

Schmittner, A., C. Appenzeller, and T. Stocker, 2000: Enhanced Atlantic freshwater export during El Niño. *Geophysical Research Letters*, **27**, 1163–1166.

Schmitz, J., W.J., 1996: On the world ocean circulation: Volume 1 some global features/ North Atlantic circulation. *WHOI Technical Report*, **WHOI-96-03**.

Stocker, T. and A. Schmittner, 1997: Influence of carbon dioxide emission rates on the stability of the thermohaline circulation. *Nature*, **388**, 862–865.

Stommel, H., 1948: The westward intensification of wind-driven ocean currents. *Transactions of the American Geophysical Union*, **29**, 202–206.

Suginohara, N. and M. Fukasawa, 1988: Set up of deep circulation in multi-level numerical models. *Journal of the Oceanographic Society of Japan*, **44**, 315–336.

Vellinga, M. and R. Wood, 2002: Global climatic impacts of a collapse of the Atlantic thermohaline circulation. *Climatic Change*, **54**, 251–267.

Vellinga, M. and R. Wood, 2007: Impacts of thermohaline shutdown in the twenty-first century. *Climatic Change*, **91**, 43–63.

Veronis, G., 1966: Rossby waves with bottom topography. *Journal of Marine Research*, **24**, 338–349.

Wajsowicz, R., 1986: Adjustment of the ocean under buoyancy forces. Part 2: The role of planetary waves. *Journal of Physical Oceanography*, **16**, 2115–2136.

Wajsowicz, R. and A. Gill, 1986: Adjustment of the ocean under buoyancy forces. Part 1: The role of Kelvin waves. *Journal of Physical Oceanography*, **16**, 2097–2114.

Wang, D., 1975: Coastal trapped waves in a baroclinic ocean. *Journal of Physical Oceanography*, **5**, 326–333.

Wang, D. and C. Mooers, 1976: Coastal trapped waves in a continuously stratified ocean. *Journal of Physical Oceanography*, **6**, 853–863.

Webster, I., 1987: Scattering of coastally trapped waves by changes in continental shelf width. *Journal of Physical Oceanography*, **17**, 928–937.

Wilkin, J. and D. Chapman, 1987: Scattering of continental shelf waves at a discontinuity in shelf width. *Journal of Physical Oceanography*, **17**, 713–724.

Wilkin, J. and D. Chapman, 1990: Scattering of coastal trapped waves by irregularities in coastline and topography. *Journal of Physical Oceanography*, **20**, 396–421.

Wright, D. and Z. Xu, 2004: Double Kelvin waves over Newfoundland shelf-break. *Atmosphere-Ocean*, **42**, 101–111.

Yang, J., 1999: A linkage between decadal climate variations in the Labrador Sea and the tropical Atlantic Ocean. *Geophysical Research Letters*, **26**, 1023–1026.

Yankovsky, A. and D. Chapman, 1995: Generation of mesoscale flows over the shelf and slope by shelf wave scattering in the presence of a stable, sheared mean current. *Journal of Geophysical Research*, **100**, 6725–6742.

Yankovsky, A. and D. Chapman, 1996: Scattering of shelf waves by a spatially varying mean current. *Journal of Geophysical Research*, **101**, 3479–3487.